CRANFIELD UNIVERSITY

ROBIN STANFIELD

INFLUENCE OF FLIGHT-PATH VARIABILITY OF CONDITIONS UPON IN-FLIGHT ICING

SCHOOL OF ENGINEERING

EngD THESIS

CRANFIELD UNIVERSITY

SCHOOL OF ENGINEERING

EngD THESIS

Academic Year 2007–2008

ROBIN STANFIELD

Influence of Flight-Path Variability of Conditions Upon In-Flight Icing

Academic Supervisor: Dr. David W. Hammond

Management Supervisor: Mr. Stephen Carver

Industrial Supervisor (2003-2005): Mr. Paul Spooner

October 2008

This thesis is submitted in partial fulfillment of the requirements for the degree of Engineering Doctorate.

Abstract

In design and development of aircraft, standard practice uses 'the icing design envelopes' to select atmospheric conditions for modelling icing encounters. Over the duration of these encounters, atmospheric conditions are assumed to be constant and to exhibit no variability. In reality variability exists, to an extent where it may adversely affect the severity of ice accretions beyond that identified by ground-based modelling. Similarly, certain tools and systems employed by industry may sacrifice efficiency & effectiveness in neglecting the variability that exists.

This project considered what operational and safety benefits might be derived from an enhanced knowledge of ice accretion under more realistic, variable conditions; in contrast with a reference case identified to have equivalent constant conditions. In doing so, variable encounters were modelled experimentally in an icing tunnel to compare against a constant-condition reference; aerodynamic penalty was assessed numerically using CFD, allowing a comparison to be made between variable and constant-condition profiles; and desk-research considered variable conditions in the context of existing and emerging technology.

Considerable differences were observed between variable profiles themselves and with the reference profile, with aerodynamic penalty being considerably enhanced for 25% of variable cases, and considerably reduced for a further 25%.

Desk-research suggests that in understanding variability, to reduce costs asso-

ciated with aircraft icing, more realistic ground-based modelling capabilities could reduce the need for natural flight-testing in the long term, though this would require substantial enhancement to current numerical prediction capabilities. Similarly, the power applied to ice protection systems could be tailored more specifically to demand, enhancing efficiency. On the basis of current instrumentation, this would first require development of more accurate and robust LWC measurement systems.

It was therefore recommended that specialists in meteorology, icing physics, ice protection systems and aerodynamics; conduct more extensive research towards understanding variability and assessing its potential to enhance flight-safety, whilst simultaneously reducing cost.

Acknowledgements

In completing this project, I would like to thank a number of people.

Firstly I'd like to thank Dr David Hammond for all of his support and guidance throughout this project.

Experimental work can be a chore, but it's not too bad when you're helped, cajoled and cursed along the way by a good technician. In that respect I was fortunate that Brian Stapleton was assigned to the icing tunnel.

I'd like to acknowledge the contribution made by my management supervisor, Steven Carver, whose relentless pursuit of my commercial acumen ensured the commercial relevance of the project was (nearly) ever present in my thoughts.

Thank you to Professor Kevin Garry of Cranfield University and Professor Ken Badcock of the University of Liverpool for numerous hours support in assessing how to perform the aerodynamic assessment of those infernal ice accretions. Together they made the aerodynamic side of the project possible.

I'd like to thank Roger Gent, Nick Dart, Malcolm Sutton and Paul Spooner who were all members of the project's industrial steering committee, and whose feedback proved invaluable.

Thanks to my learning team for all their support and a lot of fun during my year on the MBA - Richard, Peta, Martin, Nick and Cyrille. I'd also like

to thank EngD friends and colleagues, particularly Jason, Karl, Chris, Will, Kevin, Adam and Dermot. Specifically, I'd like to thank Kevin and Adam for their help and humour in the office, and apologise to Dermot for the three of us being such a distraction for the last year of his doctorate.

Finally I'd like to acknowledge the support of all friends and family, especially Samantha, for everything.

Contents

This page has been left intentionally blank.

List of Figures

This page has been left intentionally blank.

List of Tables

This page has been left intentionally blank.

Nomenclature

Abbreviations

AppendixC FAR 14 CFR Part 25 Appendix C - the icing design envelopes

CFD Computational fluid dynamics

$CIRT$ Cranfield Icing Research Tunnel

FL Freezing limit identified by Trajice2 (non-dimensional chordwise distance)

LWC Liquid water content (g/m^3)

MED Median effective diameter (μm)

MVD Median volumetric diameter (μm)

$RefIS$ Reference ice shape

ROC Rate of climb (ft/min)

SLD Supercooled large droplet

TWC Total water Content (g/m^3)

UAV Unmanned/uninhabited aerial vehicle

Greek Letters

α Aerofoil angle of attack (°)

ϕ_{lower} Lower horn growth vector angle (°)

ϕ_{upper} Upper horn growth vector angle (°)

$\rho(H)$ Density at altitude, H (kg/m^3)

ρ_{ice} Density of ice (g/m^3)

θ Temperature variability mode phase difference (°)

θ_{lower} Lower horn angle (°)

θ_{upper} Upper horn angle (°)

Roman Letters

c Aerofoil chord length (m)

C_D Drag coefficient (dimensionless)

C_L Lift coefficient (dimensionless)

C_P Pressure coefficient (dimensionless)

$C_{D_{CFD}}$ Drag coefficient predicted using CFD (dimensionless)

$C_{D_{Experiment}}$ Drag coefficient predicted by experiment (dimensionless)

$C_{L_{CFD}}$ Lift coefficient predicted using CFD (dimensionless)

$C_{L_{coarse}}$ Lift coefficient predicted using CFD with a coarse grid (dimensionless)

$C_{L_{Experiment}}$ Lift coefficient predicted by experiment (dimensionless)

$C_{L_{fine}}$ Lift coefficient predicted using CFD with a fine grid (dimensionless)

$C_{P_{lower}}$ Pressure coefficient on the lower surface (dimensionless)

$C_{P_{upper}}$ Pressure coefficient on the upper surface (dimensionless)

D Drag (N)

E Total collection efficiency (dimensionless)

GR Growth Rate (mm/min)

GR_{max} Maximum growth rate (mm/min)

h_{lower} Lower horn thickness (mm)

h_{upper} Upper horn thickness (mm)

L Lift (N)

l/s Lower surface

L_{lower} Lower surface freezing limit (mm)

L_{upper} Upper surface freezing limit (mm)

m Mass (kg)

n Freezing fraction (dimensionless)

$P(H)$ Standard pressure at altitude, H (Pa)

$P_A(H)$ Available power at altitude, H (kW)

$P_A(SL)$ Available power at sea-level (kW)

p_w Absolute water pressure (psi)

P_0 Standard pressure at sea level (Pa)

p_{w-0} Water pressure with system off (psi)

p_{w-g} Gauge water pressure (psi)

s Distance around ice profile from leading edge (m)

s/c Non-dimensional chordwise distance around ice profile from leading edge (dimensionless)

T Outside/ambient air temperature ($^\circ C$, $^\circ F$ or K)

t or $Time$ Encounter or icing blade measurement duration ($minutes$)

$T(H)$ Standard temperature at altitude, H ($^{\circ}C$)

T_A Available Thrust (N)

T_R Required Thrust (N)

T_0 Standard temperature at sea level ($^{\circ}C$)

T_{ave} Calculated encounter-averaged working section temperature ($^{\circ}C$)

t_{c-l} Centre-line ice thickness (mm)

t_{ice} Icing blade measurement thickness (mm)

T_{probe} Probe-measured working-section temperature ($^{\circ}C$)

T_{RPC} Temperature displayed by refrigeration plant controller ($^{\circ}C$)

u/s Upper surface

V Flight velocity (m/s)

V_{ws} Working section velocity (m/s)

W Weight (N)

W_c Critical water content (g/m^3)

x/c Horizontal position, proportional to aerofoil chord length (dimensionless)

y/c Vertical position, proportional to aerofoil chord length (dimensionless)

y^+ Non-dimensional first cell height

Chapter 1

Introduction

1.1 In-Flight Icing

In-flight icing is one of the many hazards of the flight environment. Flight within the atmosphere exposes the aircraft and particularly the external surfaces to whatever conditions mother nature chooses to introduce, and one element of those conditions is supercooled liquid water.

Supercooled liquid water exists in very small droplets; the majority of these droplets are of the order of microns in diameter, from $15\mu m$ to $40\mu m$. Since temperature reduces with altitude above sea-level, there comes a point where atmospheric temperature falls beneath $0°C$. At ground-level such droplets would ordinarily freeze at this, and lower temperatures. Yet this does not necessarily occur at altitude. In order to freeze (in the temperature range -40°$C \leq$ T $\leq 0°C$) solidification can only occur if there are small particles for the crystal structure to form around. These particles, known as cloud droplet freezing nuclei, are common at ground level but their presence at altitude is reduced. So at altitude these water droplets remain as supercooled liquid water unless either (a) the temperature drops to around -40°C where spontaneous freezing occurs without needing a cloud droplet freezing nucleus nucleus, or (b) the droplet encounters a cloud droplet freezing nucleus.

Now whilst an aircraft might be something of a large cloud droplet freezing nucleus it serves the purpose described above by providing an object onto which water droplets can freeze should the two collide. As and when this occurs ice deposits on the aircraft, and the resultant phenomenon is known as ice accretion, the physical process summarised by the term icing.

Ice accretion on aircraft is problematic primarily for safety reasons. The ice can accrete in critical regions of the aircraft and cause vital parts of the vehicle to suffer a dangerous reduction in performance capability. This reduction can be so severe as to cause a fatal crash. Much less severe are performance losses that reduce the efficiency of the aircraft and hence increase fuel consumption and cost. To mitigate against these possibilities aircraft manufacturers are required to demonstrate adequate performance capabilities for safe flight into known icing conditions.

Many instances of ice accretion exhibit growth characteristics known as either rime or glaze icing. The nature of ice accretion during an icing encounter can frequently be either wholly rime, or wholly glaze, but it is also common for the accretion to be a mixture of the two.

These two main types of ice growth generally occur at different extremes of the temperature range, and these are dependent upon the aircraft and its operation (size, shape, altitude, airspeed and attitude) and the properties of the icing environment expected to be encountered during that operation.

These factors determine how much of the total impinging water freezes, and how quickly it freezes. This process is dependent upon the overall thermal equilibrium, and is therefore dependent upon temperature and the heat fluxes involved in the icing process. The primary heat fluxes are the latent heat of fusion released upon freezing and the convective heat transfer. The latent heat of fusion is the energy released when the water changes state from liquid to solid. The convective heat transfer is the rate at which any heat present is lost to the ambient surroundings. The presence of rime or glaze ice accretion

is dependent upon how much of the energy generated upon freezing is lost through convection. If the convective heat flux is great enough then instantaneous freezing will occur, however if it is not and the latent heat dominates, then only part of the impinging water will freeze and the remainder will run backwards on the surface.

Rime icing normally occurs in parts of the atmosphere where the temperature is colder. Within these colder areas there is generally a relatively low amount of water present, where a low LWC produces less heat upon freezing. Upon impact with the aircraft this combination of factors leads to instantaneous freezing. The rapid nature of the freezing process means that the gaps between droplets contain trapped air, and this leads to a rough, opaque and brittle ice accretion. In addition immediate freezing at the impact location results in ice accretions under rime conditions that conform to the general shape of the underlying surface.

Glaze icing normally occurs in parts of the atmosphere where the temperature is less cold. Within these warmer areas there is a higher amount of LWC. In warmer scenarios where there is enough water, the convective heat transfer removes insufficient thermal energy released upon freezing for all particles to be frozen instantaneously. Consequently, whilst part of the water is frozen shortly after impingement, a certain proportion runs aft, until a further proportion of water can be frozen, or until the water runs off the trailing edge. The amount and distribution of water that is frozen around the leading edge varies depending upon the balance of heat fluxes, and the warmest region is in the stagnation region. As a result, less water freezes in the stagnation region and runs back to locations further aft. Over a period of time this difference in the freezing distribution causes the shape of the ice accretion to deviate more significantly from the shape of the aerofoil. Initially ridges appear above and below the stagnation region and these ridges develop into horns that grow outwards and often forwards into the airflow. These glaze ice shapes are far less opaque because very little air is trapped over the course of the freezing process. Moreover, less air within the ice re-

sults in denser, and subsequently stronger accretions, that are able to remain attached to the aircraft despite the large aerodynamic loads that would be expected to cause more brittle accretions to break off.

Rime and glaze accretions form the two main types when categorising by shape and appearance. They also have particularly different aerodynamic characteristics. Rime ice accretions generally conform to the aerofoil surface and so have a relatively small impact upon the aerodynamic performance. The accretion does however deviate from the original aerofoil design so will ordinarily cause some sort of change to the designed lifting capability. The additional roughness associated with a rime ice accretion is more detrimental to drag, adding to the overall viscous contribution. The horn shaped protrusions associated with glaze ice shapes are far more damaging to the lifting capability of the aerofoil because they promote boundary layer separation at significantly reduced angles of attack. Separation can be localised or it can dominate much of the aerofoil chord, depending upon the size and shape of the ice accretion. Such a damaging effect on lifting capability can significantly increase the stall speed and reduce the stall incidence of the aircraft, resulting in a disastrous loss of aerodynamic performance and stability/control. This huge penalty for lift has a further and comparable impact upon the drag, which is increased significantly due (primarily) to sizable quantities of separated flow and the associated turbulent wakes.

In conjunction with the terms rime and glaze, which are used to describe the ice growth process and accretion type, ice growth is often classified as either dry or wet. Dry ice growth refers to icing scenarios where instantaneous freezing occurs, with none of the water running aft beyond the impingement location. Wet ice growth refers to icing scenarios where instantaneous freezing does not occur, and some proportion of unfrozen water runs aft of the impingement location. Evidently then, dry ice growth is generally synonymous with rime icing, whilst wet ice growth occurs during accretion of glaze ice shapes. When both wet and dry growth regimes occur during the ice growth process, mixed ice accretions result, with a combination of both

opaque, rime ice and clear, glaze ice types present.

To differentiate between dry and wet ice growth regimes, several measures have been introduced over recent decades, including the well known freezing fraction and the Schumann-Ludlum limit. Both of these measures allow estimation of the ice growth regime, whether wet or dry, using input conditions that include the three primary atmospheric variables of liquid water content, temperature and droplet size. Their existence also highlights the importance of atmospheric parameters within the icing process and how, in combination with other factors, their values define the nature of the growth regime, and how changes in these parameters over the course of an encounter have the potential to drastically alter the nature of the growth regime and the severity of the ice accretion that results.

The responsibility of those who either engage in or assist in the manufacture, certification or operation of aircraft is to make every effort to ensure accidents and incidents attributable to aircraft icing are minimised, if not completely eliminated. Doing so requires a large array of activities associated with aircraft and ice protection design, encounter simulation and operational procedures. These activities can be extremely expensive and so continuing efforts towards enhanced safety in aircraft icing are interested in providing that safety efficiently as well as effectively.

1.2 Research Project

In undertaking ice protection design activities and encounter simulation activities it is necessary to be able to determine the kinds of conditions that might be encountered in operation. This is so that any simulations are able to describe the worst case scenario in terms of ice accretion, and so that any design of the aircraft and its ice protection system is adequate to ensure safe operation.

In ascertaining the expected worst case icing conditions, aircraft manufacturers utilise a standard tool known as the Appendix C icing envelopes, where Appendix C is short for Federal Aviation Regulations 14 CFR Part 25, Appendix C. This tool allows engineers to determine the maximum expected average LWC for a particular droplet size, temperature and encounter duration (cloud horizontal extent) for their aircraft and as such, allows them to determine sets of candidate conditions for the 'worst case'. Following simulations one or more sets of these conditions are determined to be the 'critical' conditions for particular phases of flight and these conditions, the ice accretion growth behaviour and the resultant 'critical' ice accretion are utilised in designing, developing and certifying the aircraft and its ice protection system for flight into known icing conditions.

This project has its origins in the assumption commonly made in applying the Appendix C icing envelopes to design, manufacture and operation of aircraft and ice protection systems. This assumption is, essentially, that the icing environment and its effects on aircraft are adequately captured by the values suggested in the icing envelopes; where those values describe the conditions throughout a spatially extensive icing encounter, and those values do not change.

Glancing skywards allows a simple examination of the validity of such an assumption. In doing so, how often does one observe patches of clouds that if flown through, would provide an encounter with constant levels of cloud water? Similarly with such a diverse weather environment, is it acceptable to consider temperature variation a negligible factor in a process heavily dependent upon its value? In truth neither the cloud liquid water content nor the ambient air temperature have been shown to be constant within the atmosphere, and it is in recognition of this fact where this project lies.

The ice accretion process has been shown to be heavily dependent upon the balance of thermal energy, or heat. Loss of heat through convection; heat gain upon freezing; increase in energy due to droplet kinetic energy; and heat gain

due to evaporative cooling, are some of the heat fluxes whose value depends upon temperature and LWC, and that impact the ice accretion process and the resultant shapes that cause aircraft to encounter difficulties. Certainly the existence of the threshold between wet and dry ice growth described by the freezing fraction and Schumann-Ludlum limit, confirm the suggestion that variable conditions have the potential to produce notably different ice accretions to that observed under assumed constant conditions. On this basis, it must be worthwhile to question if LWC and temperature conditions can change within an icing encounter, and perhaps change the outcome of the encounter itself, whether an assumption of unchanged icing conditions is acceptable any longer.

In addressing this question, it is also necessary to acknowledge that the Appendix C envelopes may be adequate. Such an assertion could certainly be expected from many within the aerospace industry, whose aircraft have been certified against conditions defined using the Appendix C standard. Given its years of service, and use in the development of ice protection systems and practises that have allowed successful flight through known icing encounters, Appendix C is an effective tool. Furthermore on the majority of occasions, Appendix C is conservative, accounting for combinations of variables that would create a severe icing encounter, but which would be expected to occur infrequently. Conversely though, Appendix C has already been proven inadequate in one major way, in failing to account for supercooled large droplets (SLD). On more than one occasion, SLD icing has been the cause of a fatal aircraft accident, illustrating tragically, that circumstances can arise where conditions can occur, that introduce a level of severity that is not accounted for by the combinations of LWC, temperature and droplet size described by Appendix C. Correspondingly, whilst Appendix C may be otherwise adequate, and the assumption of spatially constant conditions may yet prove to be valid, identifying that the variability of icing conditions could introduce a level of severity that is not accounted for by Appendix C, is sufficient alone to justify the current research.

So this is, in essence, the purpose of the project described within this document. Is an assumption of continuous, unchanged icing conditions acceptable? Finding out required two activities. The first involved the experimental simulation of ice accretions. Some of these accretions were generated under constant conditions as defined using the Appendix C envelopes. Others were generated using variable conditions that when averaged over the encounter, were equivalent to the constant conditions defined using the Appendix C envelopes. This activity resulted in ice accretions representative of constant conditions and others representative of variable conditions. The second activity comprised assessment of the aerodynamic penalties imposed by each of the ice accretion profiles generated. The outcome of this activity provided the means to assess whether or not there was any notable difference in ice accretion aerodynamic performance penalty for each variable-condition ice accretion, in comparison with a constant-condition ice accretion. Therefore this research programme allowed determination of whether or not the variability of icing conditions should be considered as part of the design/certification procedure for aircraft.

The industrial relevance of the project as described above, is present because of its focus on in-flight safety. The project developed further relevance by assessing the potential for cost reduction in design, development and operation of in-flight ice protection systems; by using an understanding of variability effects on ice accretion with an appreciation of existing and emerging technologies for use in these various stages.

The project refers to several different areas within aircraft icing and consequently, there is a great deal of theory not directly introduced within this document. However excellent publications in existing literature include Wagner et al. (1997) and a web-based tutorial by Politovich (1998), and these will provide a good initial knowledge of aircraft icing for anyone interested.

1.3 Document Structure

The purpose of this document is to present the ideology behind the research work and to convey its relevance to industry, before describing the different activities that led to its completion, the results of those activities and the conclusions.

In subsequent chapters the Literature Review describes how current procedures in aircraft icing developed and why it might be of benefit to acquire a better understanding of the impact of flight-path variability of icing conditions. The Research Methodology describes the implementation of the key activities required for completion of the research project. The Commercial and Technical Results chapters present the outcomes from the project's various activities with an accompanying narrative designed to highlight the most pertinent aspects. Discussion of these results, along with conclusions and recommendations for future work follow, with supporting material in appendices at the end of the document.

This page has been left intentionally blank.

Chapter 2

Project Scope - Industrial Relevance of Variability

2.1 Introduction

Within the aerospace industry, the challenges presented by aircraft icing and associated topics like ice accretion simulation, performance degradation and ice prevention/protection all arose through necessity. Were it not for the presence of icing conditions within the flight envelope; and the damaging susceptibility of aircraft to these conditions, it is unlikely that the discipline would exist. Activities undertaken in tackling aircraft icing have therefore emerged as a direct result of safety considerations for those undertaking air travel, whether passengers or crew.

Whilst driven by necessity the identification of and mitigation against icing conditions within aircraft flight has now become a lucrative stream of income generation for some and a source of cost for others. Operation in icing conditions requires manufacturers, regulators and operators to address a huge spectrum of interrelated activities. This spectrum of activities can be grouped into the following areas:

1. Icing certification;
2. Ground-based de/anti-icing (ice-prevention);

3. In-flight de/anti-icing (ice prevention/protection);
4. Runway & taxi-way de-icing and snow removal;
5. Icing effects on aircraft performance;
6. Icing physics;
7. Numerical simulation of icing and ice prevention/protection;
8. Experimental simulation of icing and ice prevention/protection;
9. Meteorological studies of icing;
10. In-situ measurement of icing conditions - tools, systems and instrumentation.

Each of the areas listed above provides numerous organisations with sources of cost and others with opportunities for income generation. Consequently many organisations may have an interest in the research described in this document. This chapter exists to describe the activities and interests of those involved in in-flight icing and to consider the commercial relevance of the research work, before outlining the aims for the commercially-oriented research undertaken in conjunction with the technical work.

2.2 Stakeholders within the Icing Community

In undertaking the project the driver behind consideration of variability was enhanced safety. The question 'is it good enough?', variants of which are found commonly in recent icing based literature, was applied to the use of constant conditions for simulations of icing encounters. This question was rooted within the 'safety case'; the case that queries how wise it is to fly an aircraft in icing conditions that are variable in nature, when the aircraft was certified considering predominantly constant conditions. Alternately the

safety case queries how wise it is to certify aircraft for flight using constant conditions for an environment which is potentially notably variable in its nature.

So one of the drivers of the investigation is safety. Yet in this day and age, safety considerations alone are not necessarily sufficient to bring about change. Aircraft icing is part of one of the world's most capitally-intensive and competitive industries and change is sometimes difficult to instigate. In considering the research project the overarching theme for investigation was variability. The safety case initiated a project that had the purpose to look at variability and see what it showed. The purpose of the commercial case was to look at variability and see what it was worth and to whom. By addressing the safety question and by identifying potential commercial opportunities associated with variability, the research project had scope to make a notable contribution within aircraft icing and aerospace.

Addressing the safety case was achievable, at least in theory: identify whether or not variable-condition icing encounters can prove more hazardous than constant-condition icing encounters. The commercial case was less clear cut. It was decided, therefore, to look to the icing community itself to see where knowledge of variability (and its exploitation) might provide scope for future commercial benefit.

To do this it was first necessary to identify the key stakeholders within aircraft icing. Those stakeholders would ordinarily be organisations involved in aerospace and with particular prominence in aircraft icing. Such organisations would be identifiable, therefore, by their involvement in the activities listed as 1-10 in this section.

In September 2007, the Society of Automotive Engineers held their Aircraft & Engine Icing International Conference; an event promoted for the progression of icing related technology, with some focus upon promotional of technological capabilities within (a) Aircraft Ground Operations and Deic-

ing, (b) Aircraft In-Flight Icing/Deicing, and (c) Meteorology. The technical programme covered the areas listed as 1-10 above, and organisations that were represented can be found in appendix A of this document. Of the long list, the majority of organisations represented fall into one of the following categories:

- Accident Investigation;
- Government Research Body;
- Regulator;
- Fixed Wing Aircraft Manufacturer (Large Civil Airliner, Jetliner, General Aviation, Commuter Aircraft);
- Helicopter Manufacturer;
- Aircraft Engine Manufacturer;
- Airline;
- Airport Services;
- Ice Protection System Manufacturer/Supplier;
- Academic Research Institution;
- Atmospheric Research;
- Software Provider (Aircraft Icing);
- Technological Consultancy.

Organisations that operate within the airport services category are unlikely to register significant interest in a project dealing specifically with in-flight icing. This is because airport services for icing consist of snow/frost removal from the runway and snow/frost/ice removal from aircraft whilst stationed at an airport. Ground-based ice protection can affect flight performance if there is any fluid residue on the aircraft following de/anti-icing, but this is a

relatively tenuous link between operations that are otherwise quite different. Removal of Airport Services from the categories of organisations that would likely be interested in the research leaves a list of twelve. A description of each category's role and reasons for interest follows.

Accident Investigation It is the role of accident investigators to examine evidence that is available relating to an aircraft accident, to attempt to determine the cause(s) and thereby make recommendations for preventative measures that aim to combat those cause(s). Those working in accident investigation are unlikely to have a great interest in the effect of variability unless it appears to have been influential in a previous accident. They would, however, be likely to support appropriate preventative measures suggested to them.

Government Research Bodies Organisations within this category exist to undertake research into a specific field or area of interest considered important by national governments. The progression of the field is likely to be considered worthwhile because of a national interest. A specific government department is likely to be responsible for the funding of the organisation. Within aircraft icing such organisations will work primarily towards safeguarding & enhancing safety; and towards the improvement of efficiency and effectiveness of products, systems and services involved in the field. Consequently organisations within this category should take an interest in research investigating variability of icing conditions; especially as it looks to (a) appraise a heavily utilised standard icing methodology and (b) to highlight areas where expertise in variability could further effectiveness/efficiency. Such organisations might also stand to benefit from any projects that might result should variability in icing to prove worth investigating further.

Regulator Within aerospace regulators exist primarily to promote safety standards within the industry. Regulators have the authority to stipulate the certification requirements for aircraft manufacturers and provide guidance to manufacturers on the steps to follow for certification.

Regulators also accept feedback from industry on various topics. The effect of variability of icing conditions should therefore be of notable interest to regulators.

Fixed Wing Aircraft Manufacturers Organisations in this category manufacture fixed wing aircraft of all types, from wide-body and narrow-body jets, to regional airliners and commuter aircraft. Aircraft manufacturers make money by designing, building and selling aircraft. In doing so the costs associated are very large and the certification requirements for flight into known icing conditions are one source of cost. Loss of aircraft, passengers and crew is another cost the manufacturer must take into account. Whilst, in the event of an accident, the airline and manufacturer will be insured; loss of aircraft sales and negative publicity would be extremely undesirable. Therefore the influence of variability of icing conditions should be of interest to aircraft manufacturers for the interests of safety and cost. However the type of interest may be expected to differ from company to company. Manufacturers of large airliners, for example, sell aircraft that predominantly fly above icing conditions and are relatively insusceptible to aircraft icing; yet their aircraft are regulated by the same rules as smaller aircraft that more regularly fly through icing conditions and are far more susceptible to its effects. It may therefore be anticipated that whilst larger manufacturers would naturally have an interest in the safety aspects of the research, their enthusiasm for any initiatives aimed at tangible cost reduction would be somewhat greater. Smaller aircraft manufacturers might be expected to more wholeheartedly embrace research into both safety and efficiency/effectiveness of their aircraft in icing conditions. The safety aspect of the research might receive particular attention from companies who have suffered at the hands of icing in the past.

Helicopter Manufacturers The certification for helicopters for flight into known icing conditions is much less common than for fixed wing aircraft, because of more problematic ice protection methods associated with rotors, engines and sensors. The level of interest in icing condi-

tions for this category is difficult to predict, however considering the restriction of rotorcraft flight envelopes that has historically been present because of icing, the potential for interest exists.

Aircraft Engine Manufacturers Organisations in this category manufacture propulsion units for aircraft of all types. Their income is often generated by sale of engines, associated services and maintenance. Engine manufacturers are interested in aircraft icing for two main reasons. Firstly ice accretion can affect the performance and condition of the engine. Ice can accrete in different locations ahead of and inside the engine causing a loss of performance and a potential for shed ice fragments to be ingested where they can damage internal components. Secondly many aircraft are reliant upon the engine as the source of an anti-icing capability in bleed-air systems. Extraction of bleed air from the compressor reduces the efficiency of the engine and introduces a direct cost of operating such a system in icing conditions. The cost of reduced efficiency is exerted upon fuel consumption. It is therefore likely that engine manufacturers will take interest in research work discussing efficiency.

Airlines Airlines purchase or lease aircraft and engines from aircraft and engine manufacturers, and make money by charging customers for their air travel service. Icing affects airlines in that they have to operate in icing conditions according to the manufacturer's instruction and the regulator's rules. Current development of aircraft generally experiences greater restrictions on the energy available for ice protection. Consequently the choice of IPS has implications for power and operational cost, and can therefore have some influence upon the type of aircraft an airline might choose to use. It is possible therefore that airlines could show an interest in any results of research that discusses safety in icing and the implications of variability for IPS design, power usage and associated cost.

Ice Protection System Manufacturer/Supplier Ice protection system

manufacturers design and sell systems for preventing the build-up of ice on critical aerodynamic surfaces or removing ice that has built up on those surfaces in flight. Associated suppliers sell numerous products associated with ice protection like wing coatings, novel materials and de/anti-icing fluids. These organisations generate income by developing solutions that protect aircraft from in-flight icing. The influence of variability would likely stir interest from such companies, though interest might be mixed. Some companies might consider knowledge of variability and the associated icing effects to be advantageous in tailoring system design. Others might consider it an unnecessary hurdle in certification for flight in icing that is obstructive to their product's success.

Academic Research Institution Universities who choose to undertake research and consultancy work within aircraft icing choose to do so because they consider it to be a novel, interesting topic of study; they consider it a topic worthy of study; and they consider it an area where they will be able to build and sustain an income & develop a successful reputation. Research work that is likely to prompt further projects in icing will likely receive positive interest from such institutions, unless of course the results disagree with those from associated projects at such institutions. Institutions with capabilities in experimental and numerical simulation, ice protection system design and assessment and other topics would no doubt be very keen to be involved in any projects were variability in icing to prove worth investigating further.

Atmospheric Research Organisations undertaking atmospheric research exist to ascertain the behaviour of the atmosphere and how it interacts with society. Organisations within this category will often be government bodies or a collective of like-minded groups (e.g. universities) working to further understanding of atmospheric science. Such organisations will also collaborate with others working in areas where atmospheric expertise is necessary. Consequently the topic of variability would likely be of significant interest to those within this category since

any projects resulting would benefit from some degree of atmospheric or meteorological expertise. Furthermore a more in-depth assessment of the variable nature of the icing atmosphere would be a project of particular value, and would be attractive to many within this sector.

Software Provider (Aircraft Icing) One of the key goals for those working within aircraft icing is to be able to certify their aircraft for flight into known icing conditions as quickly and cheaply as possible. To do this the best step would be a significant reduction in the amount of flight testing that is required. The ultimate goal therefore is to have ground based tools' capability enhanced over time to the point where they can be considered sufficiently competent, user friendly and reliable to be the main tools in design and certification. Advanced software already exists for many applications including airflow prediction, ice accretion analysis and ice protection system assessment; and many organisations (featuring in numerous other categories mentioned here) are involved in this area. Over time, and as computing power continues to grow, software capabilities in icing will get better and better, and whilst in the immediate future these tools will not replace flight testing; such an idea is not that far fetched. Consequently this is a valuable market contested by many in icing. Should variability prove sufficiently important within the ice accretion process, these organisations will have to develop a variability function within their product for it to remain competitive.

Technological Consultancy Organisations in this category operate in areas they consider financially lucrative, appropriate for their portfolio of activities and feasible for their operation. Within the field of aircraft icing, a huge number of commercial opportunities exist for such companies who can decide upon their areas of interest. Experimental work, software development, fundamental research and equipment design are all likely targets. It is therefore likely that such organisations would look to be involved within projects looking into variability, considering both safety-oriented and commercial opportunities.

2.3 Objectives of the Commercial Research

Having identified the stakeholders within the icing community the commercial research sought to identify the impact an understanding of flight-path variability might provide, considering the direct implications for safety and also more indirect opportunities for commercial benefit. The project has no specific sponsor and so a certain freedom existed to consider numerous areas where the research could be of use. An optimistic view might consider that the icing community would welcome recommendations from the safety case because all parties want enhanced safety. More realistically any safety-based recommendations could be received differently from various categories of stakeholder and it was considered wise to identify the views of an industrial sample on this topic. It was at least as important to supplement this information with views on where any commercial benefits might be found and how such benefits could support any safety based recommendations. Consequently the following objectives were developed for the commercial research:

- Create and distribute a questionnaire designed to examine the likelihood of the icing community supporting any safety-oriented recommendations for encounter modelling to incorporate variability.
- Conduct follow up discussions with targeted industry representatives to consider further the positions of differing organisations within the industry.
- Investigate (via literature and other methods) any areas where icing variability could be exploited for commercial opportunity.

Completion of these objectives would identify how the research work could be utilised in future with different members of the icing community to make a positive contribution. This work is reported in further sections of this document, featuring in the literature review, research methodology, results, discussion and conclusion sections.

Chapter 3

Literature Review

The origins of this research project stem from investigations that took place in the mid-20th century. These investigations and the application of the recommendations that followed have led to the standard approach for determining the critical ice shape, and subsequent choices in the design and implementation of ice protection systems.

This project investigates whether it is worth altering the way icing encounters are treated within aircraft design. It considers what operational and safety benefits might be derived from an enhanced knowledge of ice accretion under realistic conditions. More specifically it is concerned with the adequacy of today's use of Appendix C to determine conditions that model flight in icing as a constant-condition encounter; and with identifying how addressing variability could lead to ultimately better performing and more cost effective systems. This chapter therefore exists to introduce the origins of the research project and to identify areas where an enhanced knowledge of ice accretion in flight could prove beneficial to the aircraft industry.

3.1 Measurement of the Icing Atmosphere

3.1.1 A Historical Perspective - Development of Appendix C

The development of the Appendix C icing envelopes was begun with atmospheric flight research undertaken by staff of the Ames Aeronautical Laboratory of the National Aeronautical Advisory Committee (NACA). This investigation was described as follows:

"In order to establish a rational basis for the efficient design of thermal ice-prevention systems for airplanes, the Ames Aeronautical Laboratory of the National Advisory Committee for Aeronautics has undertaken an experimental investigation of the meteorological conditions conducive to the formation of ice on aircraft." (Lewis, 1947).

Over the course of several winters the investigation involved atmospheric flight testing designed to measure as wide a range of icing conditions as possible. The variables of interest were those of greatest significance within the icing process. They were liquid water content (LWC), temperature (T), droplet size and the horizontal extent of an icing encounter.

A multicylinder method allowed determination of droplet size information using cylinders of different diameter. These cylinders had different collection efficiencies and collected specific ranges of droplet size MED[1]. Droplets were captured by exposing the cylinders to the airflow for a known time and airspeed, thus their rotation allowed uniform accretion of ice. The mass of ice collected across the four cylinders allowed calculation of LWC, MED and drop size distribution. Kline (1949) reported results from one flight test cam-

[1]According to the FAA, 'the MED is the apparent mean volumetric diameter MVD that results from having to use an assumed drop size distribution when analyzing data from rotating multicylinder cloud sampling devices (old-style technology)'. (NTSB, 1998). MVD (the droplet size above and below which, 50% of the LWC exists) will be used to represent droplet size in the remainder of this document.

paign that provided several examples of icing encounters. Encounters varied in duration, flight-speed and altitude and the duration averaged values for T, LWC and MED were presented. Lewis and Begrun (1952) later explained that:

"since most of the rotating-cylinder observations represent averages over distances of about 3 miles in cumulus clouds and 10 miles in layer clouds, these distances are regarded for purposes of data reduction as standard values of horizontal extent, applicable to data from the principal two cloud types."

Kline and Walker (1951) explained that the exposure time was limited by the restrictions on how much ice could be allowed to accrete on the multi-cylinders and thus the accretion rate. The exposure time therefore varied from 2 to 6 minutes.

Following several years of flight testing a significant quantity of data had been gathered on the icing atmosphere. This led to a final recommendation published by NACA in 1949 (Jones and Lewis, 1949) that provided a set of meteorological conditions that should be considered during the design of the aircraft and associated ice-prevention and removal devices. Included within these recommendations were 'class II and class III' that described intermittent, high LWC cloud types and continuous low-moderate LWC cloud types respectively. These two categories of cloud were subsequently adopted as the two types of icing condition incorporated into what have become the Appendix C icing envelopes.

3.1.2 Established Methods of Cloud Characterisation

Since the early flight tests where data was captured and used to form the Appendix C envelopes, a number of alternative techniques have been developed for the characterisation of clouds in terms of LWC and droplet size. Some of these techniques, and their limitations, are described here in simple terms, in

order to depict the uncertainty associated with airborne cloud measurement techniques. Fully comprehensive descriptions are available in existing literature, published by cloud physics specialists, e.g Strapp et al. (2003) and Ide (1999).

Measurement of LWC, beyond using accretion-based techniques like the rotating cylinder or icing blade technique, is commonly undertaken using hot-wire instruments. These include:

- Johnson-Williams probe: this incorporates a 0.55mm sensing wire normal to the airstream, through which a constant voltage is applied. It measures LWC by evaporating impinging droplets, which cools the wire and alters its resistance. The wire is part of a bridge circuit, and the imbalance of the bridge circuit allows calculation of LWC.

- CSIRO-King probe: this incorporates a sensor of three wire coils (two slaves, one master), 1.9mm in diameter. This device also evaporates the impinging droplets, but does so at constant temperature. LWC is determined from the rate of heat transfer from the sensor coil, which is related to the power required to maintain a constant temperature.

- Nevzorov probe: this incorporates two sensing elements aligned into the airflow on a vane. One is mounted on the vane leading edge to capture liquid water. Another is mounted inside a cylindrical cone to capture liquid water and ice crystals. This probe is thus designed to measure both total water content and liquid water content, and can determine the contributions from droplets or ice crystals.

In general the accuracy that is realisable for hot-wire probes is 20% (Isaac et al., 2005), and this requires appropriate application and monitoring of the equipment in use, and maintenance in between flights. Beyond reduced probe condition, which can cause improper measurements, some of the limitations of these devices include:

1. Incomplete evaporation - where the device does not completely evaporate all water, leaving some to 'run off'. The excess liquid water is thus not accounted for in the reading.

2. Partial impingement - where only part of the droplet impinges the sensing wire.

3. Droplet splashing - where droplets do not fully adhere to the sensing wire, and a proportion of impinging water lost.

4. Ice particles - for devices that measure LWC only, ice particles can strike the sensor where they can be partially melted and evaporated, causing an artificially high reading.

5. Ice accretion - accretion on the device can cause additional problems, for example shedding of ice built up on supporting parts of the probe would cause fluctuations in LWC, ice accretion over time would eventually affect the LWC measurement (Ide, 1999).

Droplet sizing instruments can also be used to estimate LWC. The most commonly used device for droplet sizing in Appendix C conditions is the Forward Scattering Spectrometer Probe, or FSSP. This determines drop size by measuring the light as it is scattered when a droplet passes through a laser beam, and droplets are assigned to one of 15 size 'bins', which are 3μm wide. Such instruments can determine MVD with an accuracy of 15% at MVD $\leq 30\mu$m (Isaac et al., 2005), subject to their own limitations including partial droplet passage through the beam, multiple droplet passage through the beam, fogging of optical lenses and misinterpretation of ice crystals, as well as ice accretion effects. This type of probe introduces much greater uncertainty if used for determining LWC. This is associated with calculation of volume, and hence mass, using the cube of the droplet diameter.

3.2 Application of the Appendix C Icing Envelopes

Appendix C is commonly utilised within the aircraft design/certification process, and has served the icing community well for several decades. The information within these envelopes has allowed engineers to determine an ice shape as a matter of procedure, following certain rules, and this engineering ice shape is called the 'critical ice shape'. Identification of the critical ice shape using Appendix C is a standard technique within the aircraft icing field. A generally accepted practice for identifying candidates for the critical ice shape was described by Yeoman (1989). Yeoman described the interdependence between variables involved in the icing process, and explained how to employ properties of the aircraft and its operational profile with characteristic variables of the icing environment to identify suitable test conditions for simulation of the critical ice shape. He also sets out a procedure engineers can follow to identify the expected critical conditions for their aircraft. This procedure is reviewed and confirmed by Parkins (2007), who incorporates modern tools available to the icing engineer (such as the latest ice accretion codes) into the standard methodology. Parkins also comments on the steps identified recently for consideration of SLD (supercooled large droplet) icing. This type of icing involves water droplets that are considerably larger than the maximum drop size covered by Appendix C, and can result in severe ice accretions that would not be expected within that envelope. This is a result of the droplets' inertia and impingement physics that are not hugely influential with small droplets; including splash, bounce and freezing at regions otherwise expected to be clear of ice. However, considering SLD icing is not within the scope of this project.

The publication by Boer and Van Hengst (1991) provides an excellent example of Appendix C being used for aircraft certification. It describes the classification of icing conditions, ice protection system design using icing codes and the test programme incorporating laboratory tests, artificial flight tests and natural flight tests. Olsen (1998) comprehensively describes the ac-

tivities undertaken in certifying the Gulfstream GV aircraft. Olsen describes a similar procedure to Boer and Van Hengst (1991) and provides further details on the analysis work undertaken. This includes information on the functionality of the icing code, the conditions selected for simulation and the manoeuvres performed to assess performance and handling capability in artificial & flight testing. More specifically though, the publication discloses the icing conditions that were selected using Appendix C in conjunction with information on the aircraft's operational profile:

"Before shapes could be generated, Gulfstream had to put forth a critical condition at which the shapes would be built up on the unheated surfaces. Based on FAA continuous maximum (CMAX) icing and the GV flight envelope, the condition was a 45 minute CMAX encounter at 160 knots calibrated airspeed, at 14,000 feet and $23.5°F$ ambient temperature."(Olsen, 1998).

The above description from Olsen (1998) provides an excellent example of how Appendix C is conventionally used to define a critical condition, based on constant flight and atmospheric parameters over the encounter duration. Olsen (1998) published values for encounter duration, flight speed, altitude and temperature. Temperature will have been determined using the temperature versus altitude plot in Appendix C. Then using temperature and the minimum droplet size expected to strike the aircraft (calculated elsewhere) for MVD, another chart would have given LWC for the standard horizontal extent. This would then have been adjusted for an encounter duration of 120 nautical miles.

3.3 Scope for Improvements to Aircraft for Flight in Icing

The concept behind this research project emerged when considering the operations of aircraft and the different flight regimes that could be encountered.

Values of LWC, T and MVD that feature within Appendix C have their origins in the data collected by the Ames Aeronautical Laboratory in the 1940s and thus represent 'duration averaged values'. The variability inherent in the atmosphere at ground level; as well as the distributed placement of clouds evident from simple observation would suggest that cloud conditions do not remain constant in flight. The project therefore contemplates whether or not there is any benefit in considering icing conditions using a time-history approach rather than a time-averaged approach.

3.3.1 Potential Applications of Recent Technological Advances in Icing

The current drive for quiet aircraft with better fuel economy, less emissions and reduced noise has a huge impact upon aircraft design, manufacture and operation. Within icing the environmental agenda can essentially be considered in the efficiency and effectiveness of the ice protection system's design and operation, and the resultant fuel economy.

A great deal has been invested in furthering meteorological detection systems for aircraft icing. The AIRS II study (Isaac et al., 2005) was designed to "assist in providing the aircraft community better tools to avoid aircraft icing, and to improve the efficiency of airport operations." Whilst this technology is evidently of great use in avoiding icing conditions, it is less helpful in identifying real-time information on an encounter once the aircraft enters a cloud. Furthermore from a fuel economy perspective avoiding icing conditions might not be the ideal choice for the operator as it could involve a not insubstantial addition to the flight distance.

Existing patent information on the control of anti-icing systems (Rumford and Norris, 1988), (Norris et al., 1989) allows supposition suggests that smarter control of bleed air supplied to airframe aerodynamic surfaces for ice protection could be possible. An optimised ice protection system could

potentially provide sufficient heat to ensure the airframe remains clear of ice, whilst operating more efficiently than current devices. Such a system would require real-time information on the icing conditions. It seems apparent that such information could be provided via other spheres of modern icing technology. An appropriate example is that of Lilie et al. (2005) whose publication succinctly describes the design and resultant capability of a measurement device that if successful, would allow knowledge of icing conditions on-board the aircraft in real time. They list a number of potential applications for the instrument including "flight deck icing severity indicator for general and commercial aircraft." If such a device were capable of providing severity levels to the cockpit it would potentially be able to inform a smart ice protection system similarly. Further enhancement of such a system could take advantage of other technologies. Saeed and Paraschivoiu (2003) provide one such example where genetic algorithms can contribute to the optimisation of a hot-air anti-icing system to reduce the bleed air extracted from the engine compressor. Alternatively application of neural networks could prove useful. Ogretim et al. (2006) reported that:

"The neural network can be trained to make ice accretion predictions, given a set of data including the flight and atmospheric conditions, along with the Fourier coefficients and the extent of the resulting ice shape".

and:

"The preliminary results show that the proposed method has reasonable capabilities and has merit for further investment, because it can be coupled with other systems to create advanced computational ice accretion models and ice protection systems."

It is therefore feasible that knowing the impact of variable conditions, being able to measure variable conditions, and being able to subsequently tailor the design and operation of an ice protection system, could produce useful performance enhancements to the protection systems and their efficiency.

With anti-icing systems presently switched between one of the 'on' and 'off' settings by the pilot, and extracting enough heat for a worst-case condition when switched on, there is scope for a tangible reduction in IPS power required in icing encounters where more frequent icing conditions are of a comparably reduced severity.

3.3.2 Potential to Better Identify the Critical Ice Shape

Identification of Atmospheric Variability of Icing Conditions.

The data collected and analysed by the Ames Aeronautical Laboratory has been used ever since in the application of the Appendix C envelopes. Whilst their application has produced simulated encounters where conditions are constant over time, the parameters recorded over the test flights demonstrate that variability is in fact quite possible. Kline (1949) provides tabulated meteorological data from the 1947-1948 test flights that provides early evidence of an aircraft recording conditions that are noticeably variable, with measurements taken at short intervals like every 10 minutes (equivalent to around 30nm at 190 knots). Take for example icing condition 3 recorded on 03/03/1948 as shown in table 3.1.

Time	LWC (g/m^3)
1214	0.24
1221	0.40
1233	0.15
1240	0.08

Table 3.1: LWC measurements from Kline (1949), icing condition 3 on 03/03/1948.

A similar occurrence was recorded during icing condition 9 recorded on 01/04/1948. At 0904hrs and 5880ft altitude the reported LWC was $0.47 g/m^3$. Five minutes later at 5720ft the reported LWC was less than half, at $0.20 g/m^3$.

In Kline and Walker (1951) one encounter data recording is for a single traverse through icing conditions.

Flight 22 on 29/03/1950 travelled in a near arc from Columbus, Ohio to Elkins, West Virginia via Huntingdon and Charleston, West Virginia. The 200 mile distance was covered in just over one hour, travelling at airspeeds averaging 191 miles per hour. At constant altitude of 7000ft the following values were recorded for T, LWC and MVD.

Time	T ($°C$)	LWC (g/m^3)	MVD (μm)
1031	-12.2	0.30	11
1040	-11.1	0.50	8
1044	-12.2	0.31	14
1049	-12.2	0.14	10
1056	-11.7	0.32	14
1103	-11.7	0.33	10
1110	-11.1	0.53	10
1115	-10.6	0.35	11
1123	-10.6	0.43	11
1137	-10.0	0.38	11

Table 3.2: Data from Kline and Walker (1951) flight 22.

The data in table 3.2 demonstrates that variable icing conditions were recorded as far back as 1950. Moreover the variability is not small, with mean values and standard deviations of T, LWC and MVD of -11.3$°F$ & 0.78$°C$, 0.36g/m^3 & 0.11g/m^3 and 11μm & 1.83μm respectively.

LWC variability can be seen in more recent publications including Miller et al. (1998). The research looked into SLD icing conditions specifically, but found small droplet, large droplet and mixed phase icing in 29 flights. One such flight provides a clear example of LWC variation over time and is presented in figure 3.1:

The distribution of cloud liquid water in such a non-homogeneous manner is

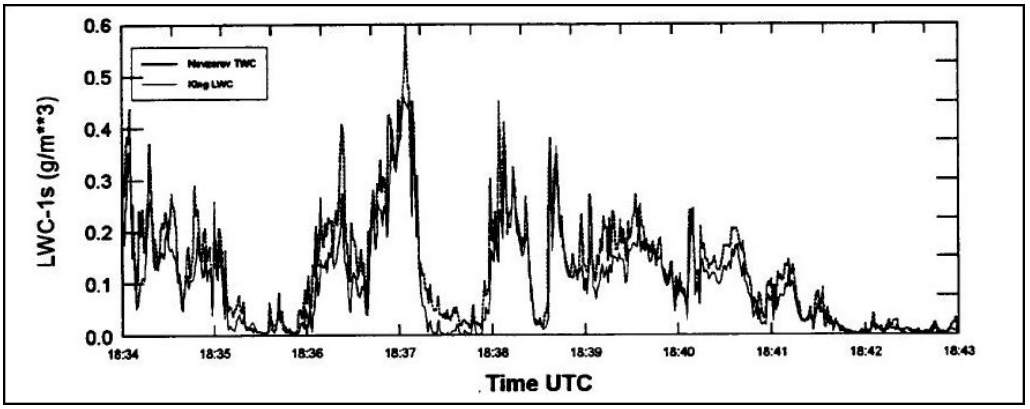

Figure 3.1: Example of LWC variability in flight, as published by Miller et al. (1998), measured with NEvzorov & King hot-wire probes.

explained by Kostinski and Jameson (1997). They state that "an initially homogeneous 'blob' of cloud droplets (assumed sufficiently light to be regarded as passive tracers) will be twisted and distorted by a succession of turbulent eddies as time progresses." The 'homogeneous blob' therefore becomes what is referred to as clumps and/or clusters of cloud (that includes stratiform cloud), and as a result it exhibits the 'patchiness' that results.

In a later publication Jameson and Kostinski (2000) relate their research into the clustering of LWC to aircraft icing, and they refer to the Schumann-Ludlam limit, (Schumann, 1938), (Ludlum, 1958). This term was introduced in section 1.1. It is believed by many that since clustering and patchiness inevitably leads to occurrences of LWC in excess of the limit's 'critical water content'[2], then clustering can potentially lead to more severe growth conditions and ice accretions.

Ryerson et al. (2001) performed flight-test analysis of icing conditions in the Great Lakes region of North America. They provide a number of examples demonstrating the presence of LWC clustering including that presented here in figure 3.2:
The coherence length relates to the spatial extent of the clustering, where the

[2]As well as occurrences of LWC beneath the critical water content.

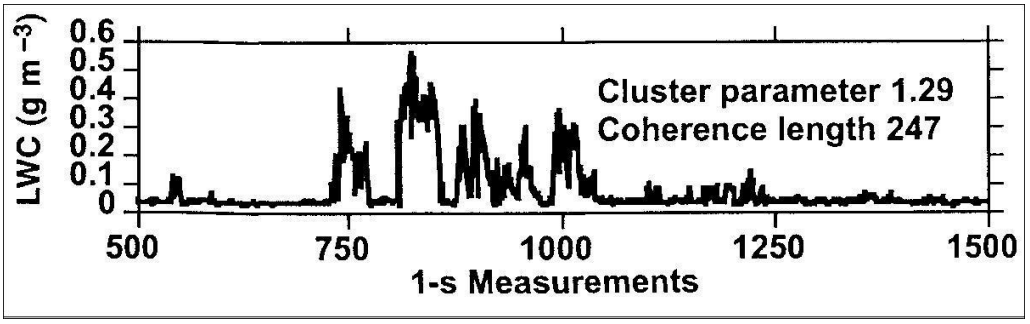

Figure 3.2: Example of LWC variability in flight, as published by Ryerson et al. (2001).

value of 247 is connected to a cluster encounter of approximately 15km. The large fluctuations in LWC are represented by the cluster 'intensity' parameter of 247, where the clustering intensity provides insight into the magnitude of the values associated with clustering, relative to the mean. Two data series can have the same mean, but the series that contains values that differ the most from the mean will have the greatest clustering intensity (Ryerson et al., 2001). This is further illustrated in figure 3.3, where these two figures contain LWC traces resulting in different coherence lengths and cluster parameters.

Hoffmann and Roth (1990) present data with examples of variable water content over the course of a 'horizontal sounding'[3]. In addition to this however, 'vertical soundings'[4] are also provided in graphical and tabular form. Numerous examples of vertical variability are presented in this paper, and in Hoffmann (1989). In these publications the authors report (a) steady increases in LWC with height above the cloud base; (b) fluctuating increases in LWC with height above the cloud base; (c) increase then decrease in LWC; and somewhat unexpectedly, (d) a decrease then an increase in LWC. Of the four descriptions above (a) and (b) are most prevalent within the two publications. Temperature variation is also reported for some of the cases,

[3]Horizontal soundings are data samples collected at a number of locations at constant altitude.

[4]Vertical soundings are data samples collected at a number of vertical locations at the same horizontal position.

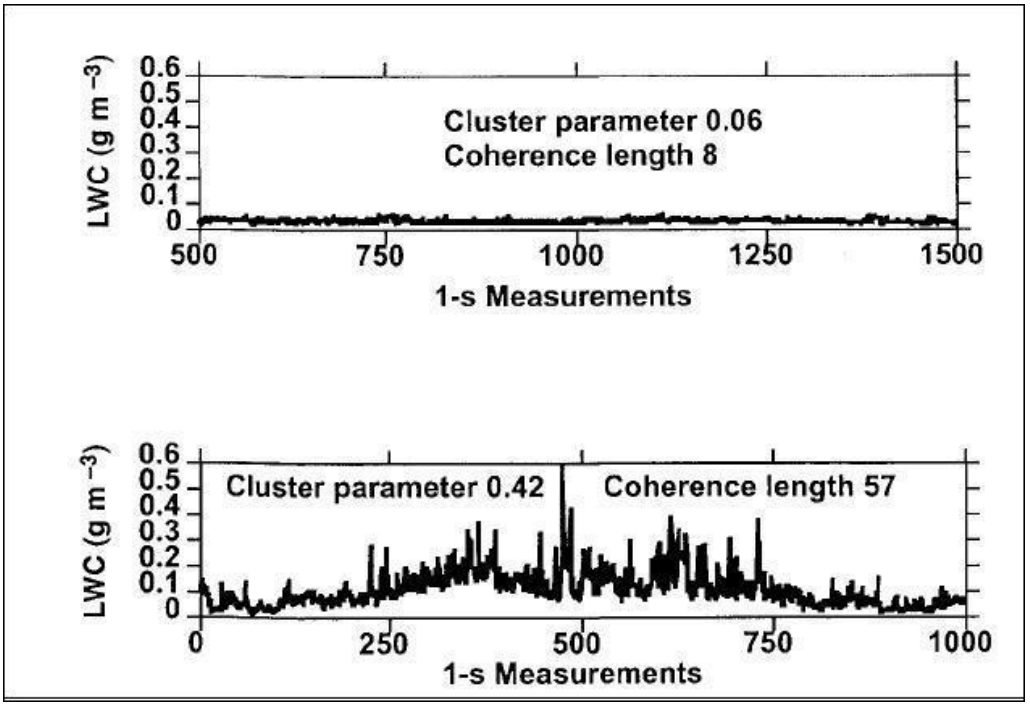

Figure 3.3: Two further examples of LWC variability in flight, as published by Ryerson et al. (2001).

and temperature generally reduces with height above the base of the cloud, but not always. A simple example of icing condition variability with height above the cloud base is shown in table 3.3.

Height above cloudbase (m)	TWC (g/m^3)	T ($°C$)	MVD (μm)
243	0.16	-2.4	15.0
426	0.35	-3.4	21.0
704	0.49	-4.5	23.0
775	0.01	-1.7	280.5

Table 3.3: Data on unglaciated icing conditions varying with height above the cloud base (at approximately 1500ft) from Hoffmann and Roth (1990).

This example represents the way icing parameters might often be considered to vary with height, with increasing LWC (until the top where clearly the water content disappears), and reducing temperature.

Potential Impact of Variable Icing Conditions on Ice Growth Behaviour.

The nature of ice growth is largely dependant upon a combination of the water impinging on the leading edge and the local thermal environment in which accretion could occur. This was described by Messinger (1953) in his publication that derived the freezing fraction, 'n', one of the most prevalent terms within the field of aircraft icing[5].

The freezing fraction can have any value from zero to unity. A freezing fraction of zero in a leading edge region indicates that none of the water that enters the region freezes. Conversely a freezing fraction of unity in a leading edge region indicates that all of the water that enters the region freezes. A value in between zero and unity indicates that a proportion of the water entering the region freezes. In general terms a freezing fraction of zero indicates no ice growth, a freezing fraction between zero and unity indicates wet or glaze ice growth and a freezing fraction of unity indicates dry or rime ice growth. Mixtures of rime and glaze ice are not unusual. Messinger illustrated the heat fluxes involved in the energy transfer as presented in figure 3.4.

The fluxes described by Messinger were:

1. Convective heat loss, i.e. the heat extracted from the leading edge region by the airflow,

2. Heat lost due to sublimation, i.e. heat lost as water vapour sublimed into ice,

3. Heat lost due to warming of supercooled, impinging fluid, to $0°C$ (equilibrium temperature of ice),

4. Heat gained (given off) when the liquid water changes to a solid state - the latent heat of fusion,

[5]Anderson and Tsao (2003) recently evaluated the Messinger freezing fraction, confirming its value within aircraft icing.

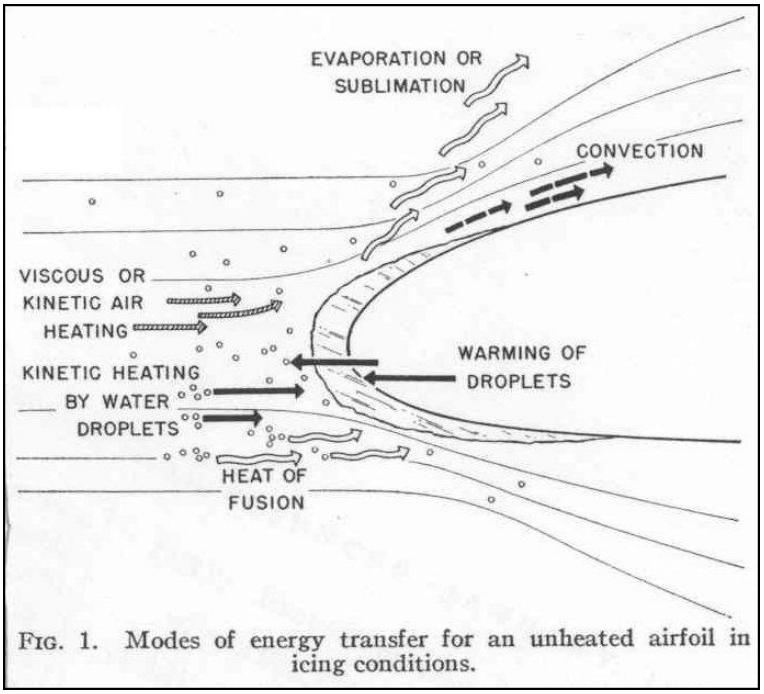

Figure 3.4: Illustration describing the energy transfer within the ice accretion process, as published by Messinger (1953).

5. Heat gained through aerodynamic, or frictional heating within the boundary layer,

6. Heat gained by kinetic energy - the energy of the particles impinging onto the leading edge.

The values of these fluxes can be directly influenced by the atmospheric parameters. Take for instance, the heat gained by the latent heat of fusion. This value is directly related to the unit rate of water catch, which depends upon both LWC and MVD. Convective heat loss is largely dependant upon the ambient temperature, T. These two heat fluxes are significant within the overall thermal environment and their dependence upon water content, droplet size and temperature highlights the impact the three parameters can have on ice growth (and hence freezing fraction). Several studies have taken place over recent years, investigating the sensitivity of ice shapes and aircraft performance to the three primary icing cloud parameters, (Miller et al.,

2005), (Miller et al., 2006), (Campbell et al., 2007).

By making small changes to nominal icing conditions, Miller et al. (2005) were able to demonstrate that the impact of changes to LWC, T and MVD upon the ice accretion could be significant. Horn thickness and horn angle (as defined by Miller et al. (2005)) were amongst the ice features that were shown to be susceptible to the icing parameter changes. The perturbations to the nominal conditions were $\pm 0.1 g/m^3$, $\pm 1.7°C$ and $\pm 50 \mu m$. The authors also concluded that perturbations smaller than those applied within their study might produce "discernible feature changes". Campbell et al. (2007) report that for the NACA 0012 aerofoil, a variation in LWC of $\pm 0.12 g/m^3$ creates an ambiguity in stall speed of $\pm 3 knots$.

The freezing fraction and Schumann-Ludlam limit concepts are similar in that they both relate to the type of growth regime that is expected to result from a specific icing encounter. The Schumann-Ludlam limit[6] is specified in terms of water content but the critical value, W_c, is dependent upon the flight and icing conditions - as is the freezing fraction. Therefore certain icing conditions can create an encounter where the amount of water is greater than W_c, and the freezing fraction is between zero and unity ($0 \leq$ n ≤ 1), indicating wet/glaze ice growth. Conversely icing conditions can create an encounter where the amount of water is less than W_c, and the freezing fraction has a value of unity, indicating dry/rime growth. Politovich (2000) utilised the relationship for critical water content (W_c) to identify conditions leading to rime, mixed and glaze ice growth behaviour for a number of aerofoils.

The concept of transition from dry to wet growth behaviour is particularly important in considering the impact of variable conditions. This is because it is conceivable that an aircraft might experience different ice growth regimes within flight through fluctuating conditions, i.e. in patchy/clustered cloud in level flight or in flight in the vertical plane. Furthermore aircraft could encounter differing degrees of the wet growth regime as well as the dry growth

[6] A derivation is provided by Makkonen (1981).

regime during flight through sufficiently variable conditions. Under such circumstances the eventual ice profile would be influenced by the changing conditions, the ice growth regimes/severity encountered under such conditions and the sequence in which those conditions were encountered.

Koenig et al. (2003) demonstrated the influence changeable conditions can have by undertaking an experimental investigation into the effect of cloud clustering. To do so they simulated nominal conditions to generate a nominal ice shape before applying variable LWC. The variable LWC utilised two values where one was applied for the first 50% of the simulation with the other applied for the second 50%. Varying water content in this simple manner provided profiles generated under nominal and variable conditions where the input values were selected to ensure the total (or average) LWC was the same for comparable cases.

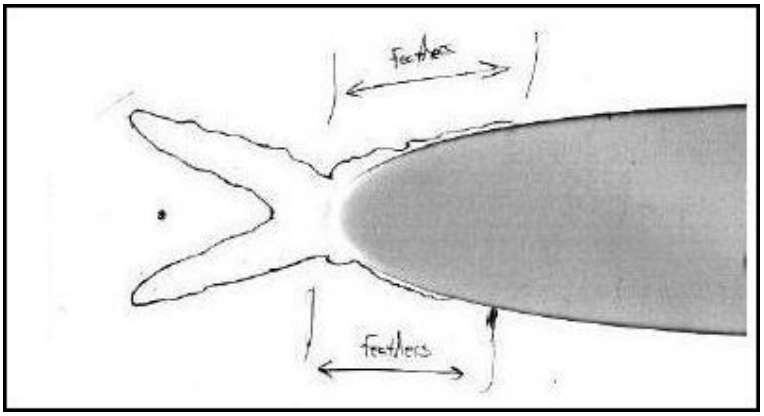

Figure 3.5: Ice trace from a run consisting of a single LWC distribution of $1.025 g/m^3$ with a duration of 900 seconds, as published by Koenig et al. (2003).

In comparison figures 3.5 and 3.6[7] are quite different from one another, thus variable conditions had a notable impact upon the ice profile. The study

[7]The tracing for figure 3.6 shows two tracings of the upper horn. This is not mentioned but presumably, there were different horn thicknesses within the region of interest that both warranted recording.

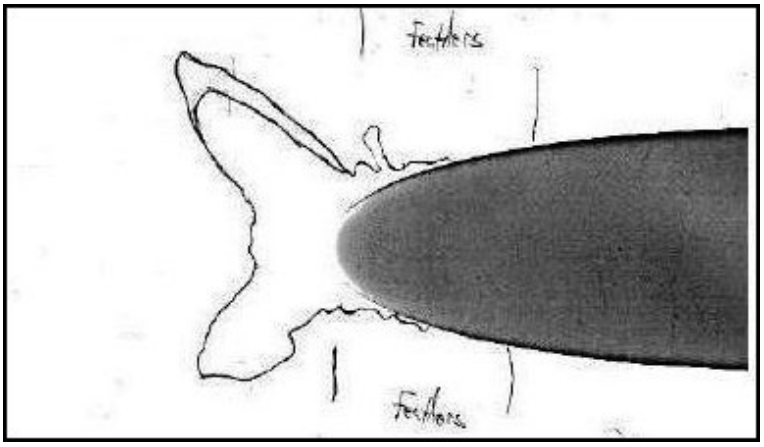

Figure 3.6: Ice trace from a run consisting of two clusters $0.35g/m^3$ and $1.7g/m^3$ each with a duration of 450 seconds, as published by Koenig et al. (2003).

conducted by Koenig et al. (2003) indicates that there may be considerable scope for variable conditions to influence the ice accretion process and the resultant ice shapes.

In summary, sections 3.1.1 and 3.2 have described the origins of the Appendix C envelopes and their application in constant parameter icing encounter modelling. Section 3.3 has confirmed via numerous literature sources, the existence of variable icing conditions and the potential for variability to impact ice growth behaviour and resultant shapes. It is therefore possible that the 'critical ice shape' as generated under constant conditions could be different to ice shapes generated under variable conditions, and could be either more or less aerodynamically detrimental. Thus it would be of interest to conduct an investigation to identify the impact of variable conditions on the severity of aircraft icing, with particular emphasis on the simulation of the critical ice shape.

Section 3.3 also presented numerous references to show the existence or emergence of technologies that could, with an understanding of ice accretion in variable conditions, be utilised for potential cost advantage.

Therefore chapter 3 identified that research into the impact of flight-path variability of icing conditions may be worthwhile in terms of flight safety and in terms of cost. It was on this basis that the project was undertaken and the full aims and objectives are presented in chapter 4.

Chapter 4

Aims & Objectives

The early sections of this document seek to to demonstrate the industrial relevance and reasoning behind the research work. In doing so they outline themes concerning aircraft safety, aircraft efficiency and potential opportunities & costs connected to the research themes and associated findings. Further to these sections it is appropriate to state the aim of the research project:

The research work aims to identify what benefits there might be in considering the impact of variability of flight path conditions on aircraft icing; concerning primarily definition of the critical ice shape for flight safety reasons, plus opportunities to reduce costs in aspects of aircraft design/development and operation related to aircraft icing.

The research work was undertaken as two different sets of activities; one performing primarily commercially oriented research, the other performing primarily technically oriented research. To complete the commercial aspects of the main aim it was necessary to deliver the following objectives:

1. Create and distribute a questionnaire designed to examine the likelihood of the icing community supporting any safety-oriented recommendations for encounter modelling to incorporate variability.
2. Conduct follow up discussions with targeted industry representatives

to consider further the positions of differing organisations within the industry.

3. Investigate (via literature and other methods) any areas where icing variability could be exploited for commercial opportunity.

To complete the technical aspects of the main aim it was necessary to be able to analyse the aerodynamic performance of an aerofoil that had been iced following simulation in constructed time-varying conditions. This required delivery of the following objectives:

1. Develop a simple conceptual aircraft model whose performance capabilities and constraints can be utilised to determine flight conditions, expected non-varying icing conditions and more realistic flight-path dependent icing conditions.

2. Utilise atmospheric data and publications to determine appropriate and applicable examples of variation in atmospheric conditions for testing purposes.

3. Develop or acquire a capability in numerical modelling (CFD) of the flow around iced aerofoils.

4. Assess the predictive capabilities of the numerical method, using experiment and appropriate sources from literature.

5. Utilise the Cranfield University Icing Tunnel (CIRT) to simulate constant and variable icing encounters, capturing the ice profiles and selected geometric parameters from the simulations.

6. Utilise the CFD methodology to identify if the flight-path dependent (time varying) simulation profiles are significantly more detrimental to aerodynamic performance in comparison with time-invariant results.

Steps taken in delivery of these objectives are described in chapters and 5.

Chapter 5

Research Methodology

5.1 Commercial Research Methodology

The objectives for the commercial research were presented in chapter 4.

The first of these objectives required design of a questionnaire that investigated respondents' propensity to support a recommendation for the impact of flight-path variability to be recognised in the design/certification process. The design of the questionnaire was in line with established principles (QuickMBA, 2008), involving definition of required information, question content, form of response (to encourage a suitable response appropriate for subsequent analysis), question order and method of distribution for credible responses.

The questions, 1 to 6, are presented below, whilst questionnaire responses are presented in Appendix B:

1(a) How would you classify the operations of the organisation you work for?

1(b) How did you become involved in icing related work?

1(c) How would you describe your familiarity with the field?

2 Which of the following would you say your role most closely resembled (engineer, project engineer, project manager, programme manager)?

3 Please try to weight you role and responsibilities by how much attention you give to technical matters, project resources, project cost, project scheduling, programme management.

4 What activities related to aircraft icing simulation does your organisation regularly engage in?

5(a) How long might a typical icing programme take to complete (weeks/months)?

5(b) Do you consider an icing programme to be resource intensive (engineer time, equipment, software)?

5(c) Is an icing programme significantly expensive as a proportion of total cost of a project that will incorporate icing work?

6(a) If a more comprehensive, more accurate simulation methodology for predicting 'critical' ice growth was suggested, would you support it considering potential time and cost implications for the design and certification process, and for your organisation?

6(b) If a suggested simulation methodology provided better information for design of Ice Protection Systems and associated power requirements, would this significantly affect your answer to (a)?

Question 1 was designed to identify the kind of organisation the respondent worked for plus their level of familiarity with, and experience in the field. Information on organisation type (question 1(a) in figure B.1) was useful as it would allow assumptions to be made about the impact of any recommendation on the organisation and the the organisation's potential position with regard to that recommendation. It was desired that the majority of respondents had a sufficient level of familiarity with and/or expertise in icing to form a valid opinion on the matter; questions 1(b) and 1(c) (in figure B.2 and B.3) were designed to draw this out.

Questions 2 and 3 (figures B.4 and B.5) were designed to ascertain the kind of position the respondent held as this would affect their responsibilities and potentially influence their answers to later questions.

Question 4 (figures B.6 and B.7) was designed to identify the icing activities different organisations engaged in. This was because recommendations could affect some activities, and hence organisations, more than others.

Question 5 (figures B.8, B.9 and B.10) was designed to gather information on the relative cost of an icing programme as this was previously difficult to ascertain.

Question 6 (figures B.11, B.12 and B.13) was designed to ask respondents if they would support a recommendation for the impact of flight-path variability to be recognised in the design/certification process; and to find out what factors might further influence their support/opposition.

In fulfilling the second objective discussions were held with leading specialists and icing engineers & regulators from Airbus UK, Qinetiq, BAE Systems and the Civil Aviation Authority. The discussion topic followed a similar theme to the survey, but was naturally less restricted. These involved a standardised, open-ended interview, where the same open-ended questions were asked to each interviewee (Valenzuela and Shrivastava, 2002). Interviewees were introduced to the topic, with some visual aids to ensure they understood what they were being asked to comment upon. All interviewees were asked the same general questions, with some slight differences as follow-up discussions were particular to interviewees and their responses.

The third objective was fulfilled via literature and internet investigations, informal discussions with icing colleagues and in attending the Aircraft and Engine Icing International Conference 2007; where a significant number of attendees were prominent members of the icing community.

5.2 Technical Research Methodology

The purpose of this section is to demonstrate how the differing technical activities undertaken within the research project ensured completion of the technical objectives. It also serves to provide sufficient information for subsequent efforts to implement, repeat or adapt any part of the research methodology.

5.2.1 Simulation and Measurement of Ice

One of the two primary technical objectives of this research project was to conduct simulations of icing encounters with variable conditions. This was to allow comparison of key geometric characteristics with one another and, more importantly, with the reference ice shape created under constant conditions. The duration averaged values for LWC and T were to be the same for variable scenarios and the constant reference scenario. Within this section the different tasks contributing to that objective are described.

Selection of the UAV as the Test Vehicle

Selection of a test vehicle was useful for the project because it allowed appropriate determination of icing conditions for a potentially realistic flight case that could act as a reference case. A reference case was necessary because comparison of results from variable encounters required results from a non-variable encounter generated using Appendix C defined conditions. A test-vehicle, its flight capabilities and a desired operation would allow determination of such an encounter. Now because of the significant scaling issues associated with aircraft icing (Anderson and Ruff, 1997) and the moderately sized working section ($0.76m$ x $0.76m$) it was decided that the test vehicle should be a small, full-scale UAV. To generate an icing encounter it was necessary to have a defined and accessible operational capability for the test vehicle, and this required both the aerodynamic performance capabilities and

propulsive capabilities of any candidate UAVs.

The X-Rae 1 UAV was a Royal Aircraft Establishment vehicle with which Cranfield was involved. Consequently it was possible to identify literature sources written at the time that contained relevant aerodynamic data for the aircraft, (Trebble, 1985), (Trebble, 1986), (Stollery and Dyer, 1988). This data was used to determine a performance capability for the UAV, based on the lift and drag profiles and powerplant options. Powerplant options came from the Quadra Aerrow range of motors/engines for model aircraft. The X-Rae 1 is presented in figure 5.1.

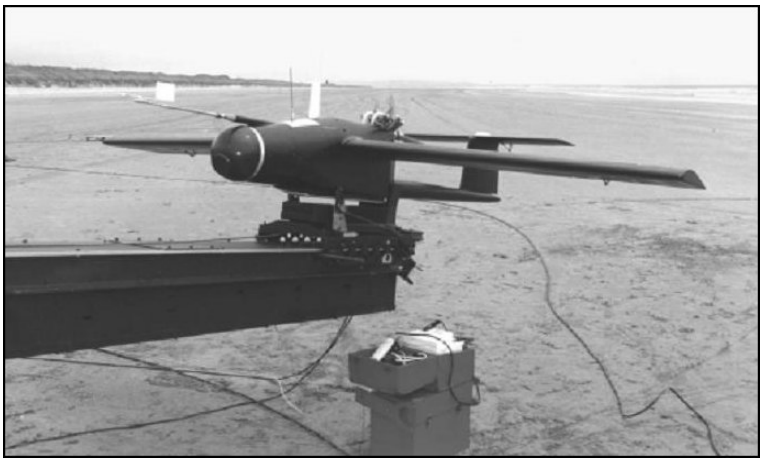

Figure 5.1: Royal Aircraft Establishment, XRae 1 aircraft.

Applicability of UAV Findings to Commercial Aircraft

In selecting a small UAV as the test vehicle for the experimental study, it was of interest that the results and their implications could be extended to commercial transport aircraft, on the basis of investigating operational & safety benefits of understanding variability effects.

The UAV test vehicle has, in comparison with commercial transport aircraft, lower Mach and Reynolds numbers. This is due to a markedly lower flight speed and smaller physical dimensions. However whilst the these parameters

may ordinarily prevent the application of small scale results to larger, faster aircraft, they are far less limiting for the present topic of study, which has considered 'critical' icing conditions, and the aerodynamic penalty of resultant accretions.

Studies have shown for glaze ice accretions, that the influence of Reynolds number is reduced in those areas where it is conventionally most prevalent. In their 2005 publication Lee et al. (2005) cite Papadakis et al. (2001), Addy et al. (2003) and Dunn et al. (1999) as having demonstrated that iced-airfoil aerodynamics is relatively insensitive to Reynolds number effects. Pan and Loth (2003) attribute this to the forced flow separation that occurs at the ice shape location, where this is independent of upstream boundary layer development, and hence Reynolds number. Lee et al. (2005) go on to conclude that for a 22.5-minute failure shape[1] 'nearly identical lift curves were maintained (with the geometrically scaled ice shape) as the full-scale model was reduced to 1/12-scale model and the Reynolds number was reduced from 4.1 million to 0.15 million'.

Chung and Addy (2000) assessed the impact of Reynolds number and Mach number numerically, comparing predictions with experiment. When assessing a large, dual-horned glaze ice shape, the numerical results suggested that increasing Mach number from 0.12 to 0.21 & 0.29 resulted in a reduction of $C_{L_{max}}$ of approximately 10% and 12% respectively. Experimental results suggest the magnitude of any Mach number difference is much less, showing only 0.5% difference in $C_{L_{max}}$ between Mach numbers of 0.12, 0.21 & 0.29.

A critical icing scenario would ordinarily give rise to large glaze ice horns, resulting from a combination of conditions that are very favourable for ice growth. Aircraft size, velocity and attitude combine with the atmospheric conditions to produce a particular water catch rate[2] and thermal environ-

[1]This shape was generated for a flight speed of 160 knots ($82ms^{-1}$), LWC = $0.6gm^{-3}$, MVD = 15μm and an outside air temperature of approximately -10°C.

[2]Water catch rate governs how fast ice can build up on an object; and is calculated by multiplying the collection efficiency, the LWC and the airspeed.

ment. Whilst the specific set of parameters required for a small-scale UAV is different to that for a commercial passenger aircraft, both sets result in a critical ice growth regime, in which this research topic is centred.

In order for critical icing conditions to exist at higher Mach & Reynolds numbers, where aerodynamic heating is a larger component within the energy balance, colder conditions are required. Whalen et al. (2005)[3] provide sample critical conditions for a typical business jet, including those for a 'warm hold' full-scale flight condition, giving the highest water catch rate based upon Appendix C conditions. With a flight speed of 205 knots ($105ms^{-1}$), the warm hold involved LWC = $0.5gm^{-3}$, MVD = 20μm and a total temperature of -1.0°C. These values for water content, droplet size and total temperature are very similar to the reference conditions applied in the present study and serve to highlight how research into critical ice accretions, at one flight speed, can be relevant for critical flight conditions at another. It is on this basis, and in assuming reduced influence of Reynolds and Mach numbers for glaze-ice aerodynamics, that plausible extension of UAV-scale findings to passenger transport aircraft has been presumed on a technical basis.

From an operational perspective, larger aircraft generally only suffer from aircraft icing (other than in circumstances too severe for the IPS) on unprotected areas of the aerodynamic surface, or when the IPS fails to operate. Residual icing and runback ice accretion, beyond the protected areas are also very pertinent for transport aircraft. In one sense, identifying the impact of variability upon the critical ice shape is of reduced relevance due to the greatly decreased likelihood of such a shape occurring across large parts of the wing & tail spans. In another sense, however, the impact of variability remains relevant, as the ice growth mechanism remains largely the same for runback ice. The difference for runback icing is that accretion is delayed until further aft, where similarly, or more dangerous horn shapes can grow. Influencing factors such as runback, ridge development, collection efficiency development, water catch rate and overall thermal environment that are iden-

[3]Research conducted by NASA Glenn in conjunction with Cessna Aircraft Company

tified within the present technical research as potentially important factors, with particular pertinence for variability, are also expected to be important within runback icing, and as such, for commercial transport aircraft. That said, as much as the impact of variability on the critical ice shape has not received substantial attention before now, its impact upon runback icing is presently yet to be assessed. Any extension of these results to commercial aircraft must therefore acknowledge this important caveat, accepting that broaching this topic represents a substantial quantity of research work for anyone willing to take it on.

Use of Aerodynamic Data to Identify the Test Vehicle's Operational Profile

Having identified the X-Rae 1 aircraft as a suitable vehicle for the research project it was necessary to use the available aerodynamic performance data to calculate an operational profile. Doing this would indicate the altitudes at which it could operate and hence the icing conditions it might expect to encounter.

A spreadsheet model was designed using standard aircraft performance relationships along with the international standard atmosphere and the published data describing the X-Rae's aerodynamic performance. The equations that were used were:

$$L = m.g \tag{5.1}$$

$$\rho = \frac{p}{R.T} \tag{5.2}$$

$$C_L = \frac{L}{\frac{1}{2}\rho.V^2.S} \tag{5.3}$$

$$\alpha = \frac{C_L - C_{L_0}}{a} \tag{5.4}$$

$$C_D = k.C_L^2 + C_{D_0} \tag{5.5}$$

$$D = \frac{1}{2}.\rho.V^2.S.C_D \tag{5.6}$$

$$T_R = D \tag{5.7}$$

$$P_R = T_R.V \tag{5.8}$$

Sea-level values for temperature, pressure and density were used along with the lapse rate and ideal gas constant to calculate equivalent values at a specified altitude. The input variables were aircraft mass and velocity. Mass yielded the required lift for steady-level flight, and values for velocity and wing area allowed calculation of C_L. The aerodynamic data for the X-Rae 1 allowed a relationship to be determined for C_L versus α (of the form presented in equation 5.4) and similarly for C_D versus C_L (as per equation 5.5). This allowed calculation of the drag force, required thrust and required power. In assuming the aircraft encounters icing conditions during its mission, the Appendix C envelopes were used to determine the LWC, T and MVD values for the duration of the encounter at an operational altitude of $12000ft$ and velocity of $50ms^{-1}$. The spreadsheet model is presented in figure 5.2.

The overall operation of the test vehicle incorporated climb, a mission at cruising altitude and descent. The operational altitude for the icing encounter was set to $12000ft$ because this would produce a severe icing encounter in what Appendix C refers to as 'continuous icing' in stratiform cloud. Flight in Appendix C's 'intermittent icing' conditions, through cumulus cloud would result in encounters where the water content would be significantly higher, but the duration would be significantly shorter. It was

RAE: XRAE- 1, Climbing Forces Based Upon Weight, Velocity and Altitude

Lapse Rate	0.0		T (H)	264.2256		h (ft)	12000		Engine	Q52B	Q75RSS
T_0	288.0		P (H)	64403.7		h (m)	3657.6		η	0.78	0.78
P_0	101300		ρ (H)	0.849286		H	3657.6		P	3357	7460
g	9.8								P_A(SL)	2618	5819
R	287.0								P_A(H)	1815	4032

Note: θ simply denotes the flight path angle which in non-accelerating flight represents the direction in which the aircraft is ascending

m	W	θ	L	V	C_L	α	C_D	D	T_R	T_{A-Q52B}	$T_{A-Q75RSS}$	ROC (m/s)	ROC (f/m)
40	392.3	5.835	390.2	50	0.39	2.18	0.02	24.26	64.14	36.29	80.65	5.08	1000.68

Figure 5.2: Spreadsheet containing the test vehicle flight performance model, with capability in cruise, non-accelerating climb and descent.

decided to dismiss intermittent conditions as candidate conditions for the critical ice shape after calculation of the total water exposure (the product of LWC and encounter duration) for flight through the most severe conditions the vehicle might encounter in each type, where continuous maximum conditions produced the highest value by some margin. Therefore the icing conditions described in this document comprise stratiform cloud only.

Atmospheric Variability - An Overview

Aircraft icing arises because of the existence of icing conditions within the atmosphere. To investigate the variable nature of these conditions it was necessary to ensure any modes of variation applied were appropriate given existing knowledge. Therefore in advance of any activities designed to generate variable icing scenarios, numerous sources were consulted to gain a reasonable idea of how the values of LWC and T could vary within flight.

Existing literature provided a large source of information upon variability. Publications already cited within section 3.3.2, such as Kline and Walker (1951) were useful in identifying the kinds of LWC and T values that might exist within an icing encounter, and allowed calculation of mean values and

standard deviations within a reported encounter.

In addition to literature sources, data from flight tests in icing conditions was used as a source of reliable information on the variability of icing conditions within flight. This data was provided by NASA and incorporated measurements taken by Miller et al. (1998). The data provided had been reduced to ensure it was suitable for considering the variation of Appendix C conditions (the flight tests were conducted as part of SLD icing flight research). The measurements were categorised by flight when provided by NASA, and these were broken down further into icing segments of interest with near constant altitude. Examination of these segments provided information on modes and magnitudes of icing parameter variability that can exist in flight and examples from several segments are presented in this section. They also provided examples of icing encounters where the icing parameters were far less variable along the flight path. Such conditions serve a useful purpose as a reminder that conditions that can be considered near-constant exist. One such example is presented in figure 5.3.

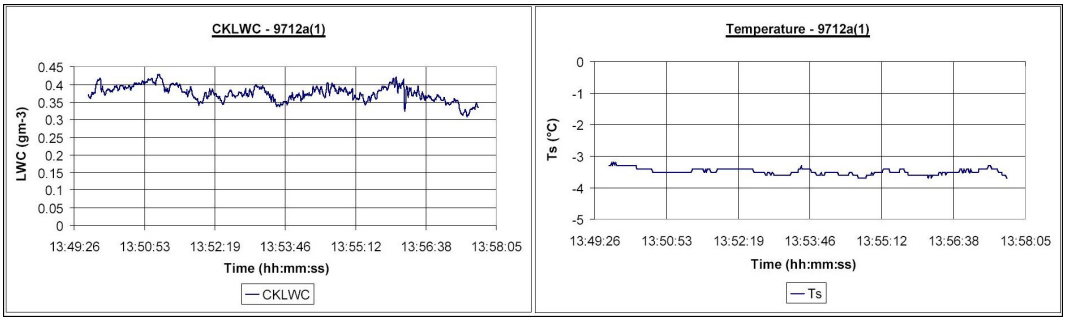

Figure 5.3: LWC and T plotted as a function of time for period 1 of flight 9712(a) of the 1997 SLD flight test-programme (as documented by Miller et al. (1998)).

The average LWC within flight 9712a part 1 was $0.37 g/m^3$ with a standard deviation of $0.02 g/m^3$, and the average T was -3.48°C with a standard deviation of 0.1°C. The traces representing LWC and T within figure 5.3 illustrate the generally invariant nature of these variables within the encounter. The

duration of the encounter was approximately 34 kilometres.

In comparison, the traces within figures 5.4 and 5.5 exhibit differing degrees of variability. The LWC tracing in figure 5.4 is highly variable with clusters of moderate LWC (up to at least $0.45g/m^3$) as well as regions of lower LWC and zero cloud contributing to the average water content value of $0.126g/m^3$ and a standard deviation of $0.134g/m^3$. The temperature was not hugely variable but the tracing in figure 5.4 does have minimum and maximum values that are different by $2°C$ (a not insubstantial quantity for icing in threshold conditions). The duration of the encounter was approximately 119 kilometres. The temperature variability in figure 5.5 shows a definite overall trend. Again the difference between maximum and minimum values was approximately $2°C$, this time with a steady yet fluctuating increase from around -6°C to around -4°C (average value of -4.8°C and a standard deviation of 0.65°C). The LWC for this flight segment was low, generally fluctuating between $0.04g/m^3$ and $0.1g/m^3$. values of LWC.

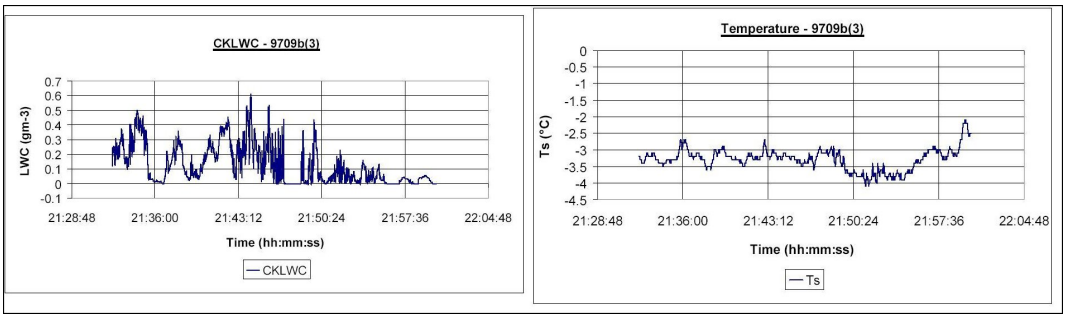

Figure 5.4: LWC and T plotted as a function of time for period 3 of flight 9709(b) of the 1997 SLD flight test-programme (as documented by Miller et al. (1998)).

These three examples of flight segment data are representative of the set that provided an insight into how cloud water content and temperature can vary along a flight path. Within the set there are cases that confirm that these parameters can vary within flight and also confirm that they can be near-constant. They also demonstrate the modes of variation like LWC clustering

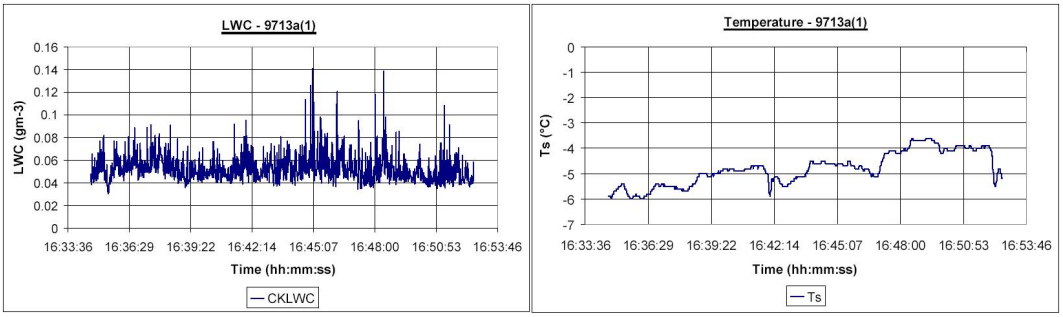

Figure 5.5: LWC and T plotted as a function of time for period 1 of flight 9713(a) of the 1997 SLD flight test-programme (as documented by Miller et al. (1998)).

and rise/fall variation[4], plus temperature variations with differing degrees of fluctuation.

In learning about possible modes of variation in the vertical plane several sources were again used. General information was available via the Appendix C envelopes (LWC and T values that can be expected at different heights) and temperature variation with height was available via the international standard atmosphere, (ESDU-77021, 1977). Some publications available on cloud profiles within the vertical plane provided data captured within specific studies looking at the variation of LWC, T and MVD within flight. Tables 5.1 and 5.2 present data from two 'vertical soundings' published by Hoffmann (1989) and Hoffmann and Roth (1990).

Within the research project, attempts to model the variability within icing conditions aimed to use a simple approach, and therefore the variability within the vertical plane described by the data in table 5.1, was selected. Consequently within an icing cloud it was assumed that water content increases with height (before decreasing towards the vertical limit) and temperature decreases with height, in a manner similar to the data in table 5.1.

[4]Rise/fall is characterised by the large-scale (in relative terms) increases and decreases in water content.

Altitude (m)	LWC (g/m^3)	T ($°C$)
0	0.02	-0.6
141	0.09	-1.7
241	0.16	-2.2
341	0.18	-2.8
419	0.35	-3.4
508	0.40	-3.8
617	0.47	-4.4
717	0.49	-4.4
791	0.01	-1.8

Table 5.1: Example of LWC and T variation vertically within a cloud, as documented by Hoffmann (1989).

Altitude (m)	LWC (g/m^3)	T ($°C$)	Altitude (m)	LWC (g/m^3)	T ($°C$)
136	0.02	0.9	885	0.19	-1.2
157	0.02	0.9	931	0.17	-1.7
228	0.13	1.7	975	0.33	-1.9
301	0.04	1.8	1034	0.28	-2.2
358	0.04	1.6	1075	0.18	-2.4
407	0.10	1.3	1118	0.17	-2.4
613	0.07	0.2	1154	0.21	-2.6
660	0.11	0.0	1184	0.27	-2.6
703	0.15	-0.2	1205	0.27	-2.9
727	0.11	-0.4	1273	0.29	-3.4
768	0.14	-0.7	1300	0.32	-3.4
807	0.31	-1.1	1322	0.39	-3.4
855	0.27	-1.2			

Table 5.2: Example of LWC and T variation vertically within a cloud, as documented by Hoffmann and Roth (1990).

These sources, describing variability of icing parameters in the horizontal and vertical planes, subsequently served to inform the design of variable icing encounters. This valuable insight informed the design of the magnitudes and modes of variation that could be attempted in simulation. The differing types of variability that were conceived for simulation in the CIRT are contained in a forthcoming section.

Modes of Variability for Application.

There were three phases of the experimental icing investigation:

1. Phase 1 studied the effect of LWC variability within the critical icing encounter.

2. Phase 2 studied the effect of temperature variability within the critical icing encounter.

3. Phase 3 studied the effect of coupled LWC-temperature variability within the critical icing encounter.

In phase 1 the modes and magnitudes of variation in liquid water content were designed to conform to a logical structure. This was because the variability exhibited within the flight data would be near impossible to replicate in detail and a logical structure would ensure an appropriate manner of simple variability that was easy to understand and straightforward to reproduce. The magnitudes of variation were determined by looking at a range of mean values and standard deviations (as a percentage of the mean), that were calculated from the encounters extracted from flight data. The modes attempted to incorporate different types of variability that, whilst remaining simple, exhibited variability that could exist within flight. The plot for 'LWC Measurements' in figure 5.6 demonstrates how much actual icing parameters can vary in addition to any general trend present. Such levels of variability could not realistically be modelled within the CIRT. The 'Time Averaged LWC (a)' shows how such variability could be modelled very well, given a small averaging duration, but this degree of fidelity is more comprehensive than can be achieved in the CIRT given the time constraints associated with an encounter simulation. Further averaging of the LWC measurements resulted in 'Time Averaged LWC (b)' as plotted in figure 5.6, which demonstrates how an icing encounter varying in LWC could be modelled to a basic but suitable degree of fidelity, whilst remaining feasible given the capabilities and limitations of the CIRT.

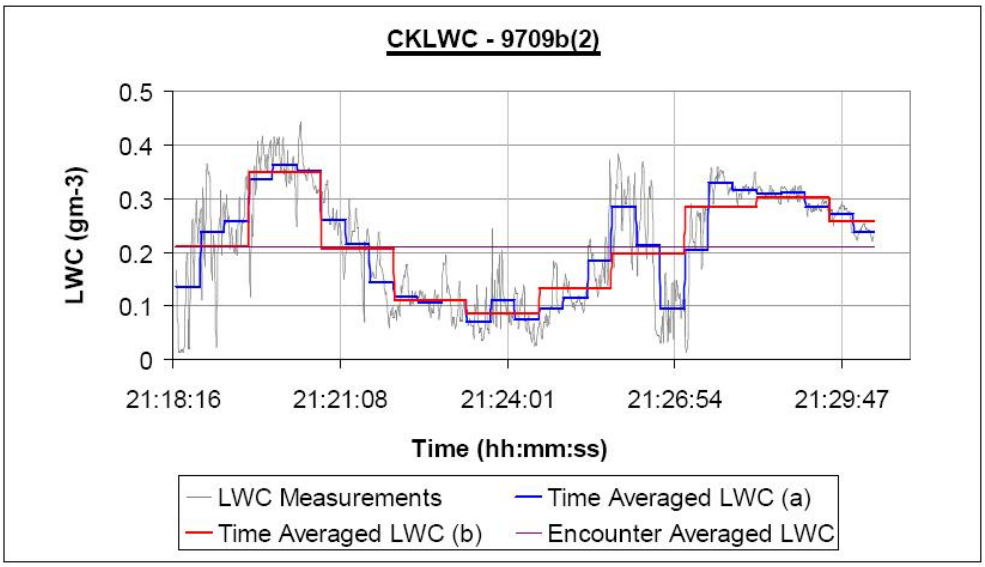

Figure 5.6: Plots of LWC during the second segment of flight 9709(b), recorded by Miller et al. (1998). Plots include the variability of raw data (LWC Measurements) with time plus values time averaged across three different intervals, including the entire duration of $52km$.

To ensure that all simulations incorporating variability in LWC conformed to a logical structure, a 'standard variability' case was constructed. This case was designed with variability in LWC about the reference case, all other factors remaining constant. It was decided to divide the the duration of the simulations into 10 segments of five minutes each. This standard case is presented in figure 5.7.

This 'standard variation' in LWC represented fluctuating values of cloud water on a relatively large scale. This variation was intended to provide a standard model of LWC variability within an icing encounter where the modes and magnitudes of variation resemble those exhibited in real encounters like figure 5.6. As the standard variation it was the basis for several other types of variability that deviated from the standard variation in a predetermined manner; these being:

1. Magnitude variation - this differs from the standard variation by having a different magnitude, i.e. $\pm 10\%$ LWC.

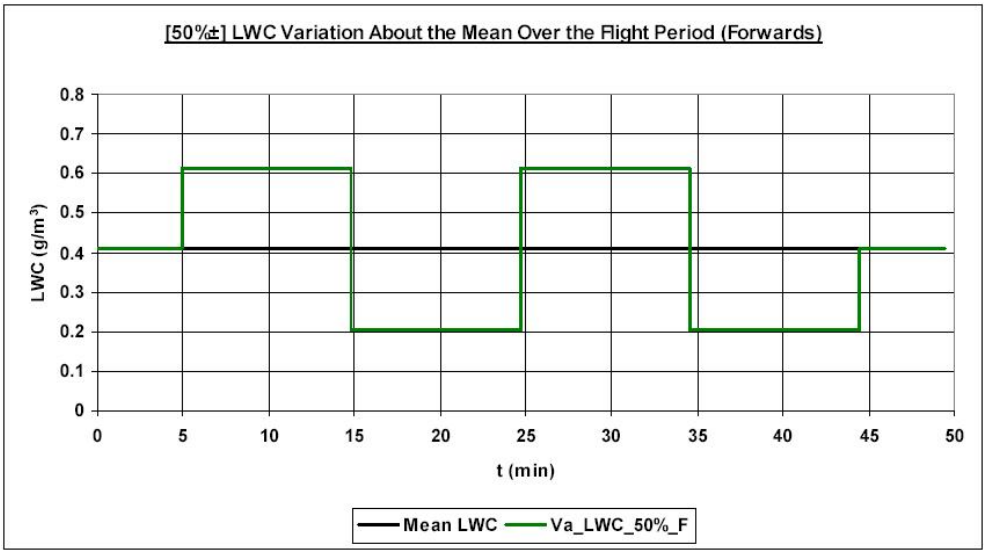

Figure 5.7: LWC variation about the mean value of $0.41gm^{-3}$, varying by $\pm 50\%$ at standard step change rate between segments 2 and 9 - the 'standard variation' in LWC.

2. Frequency variation - this differs from the standard variation by either halving or doubling the step change rate between segments 2 and 9.

3. Sequence variation - where reversing a sequence provided an alternate encounter.

These kinds of variation were designed to ensure that a suitable range of 'variable' conditions could be generated, with each having its origins in the standard variation type, and all being quantitatively differentiable from one another.

Two more kinds of variability were employed when varying LWC alone. The penultimate method was known as the rise/fall category. Here the LWC could either:

1. rise from x% below the mean value to x% above it,

2. fall from x% above the mean value to x% below it,

3. rise from x% below the mean value to x% above it before falling once more to x% below the mean,

4. fall from x% above the mean value to x% below it before rising once more to x% above the mean.

Figure 5.8 presents an example of a rise/fall encounter. In this case it is a decrease in LWC from 50% above the mean value to 50% below it, so falling from $0.6gm^{-3}$ in a stepwise manner to $0.2gm^{-3}$. This type of variation could be considered representative of LWC decrease during descent through a cloud.

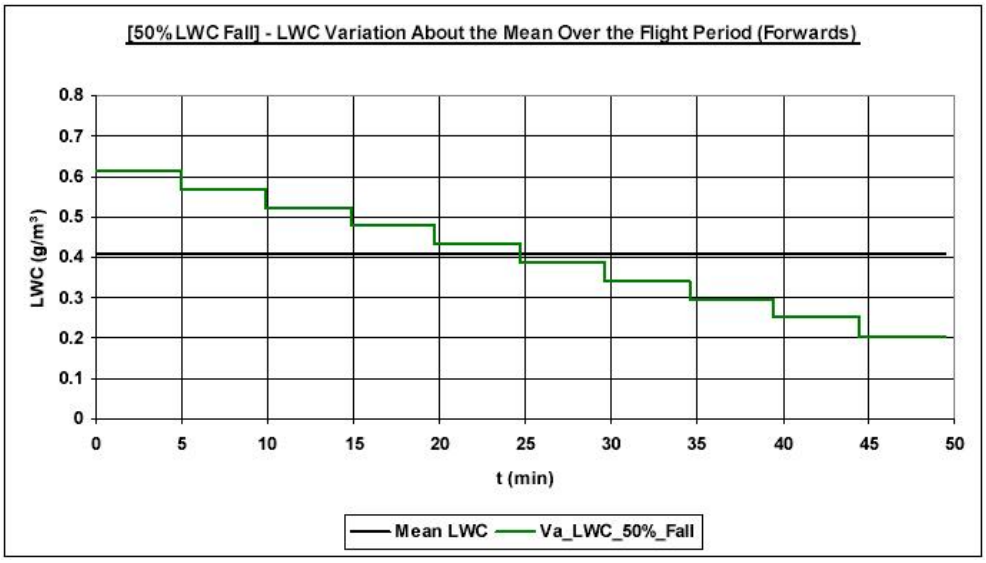

Figure 5.8: LWC variation about the mean value of $0.41gm^{-3}$, falling from 50% above the mean value to 50% below the mean value at a constant rate over ten step change segments.

The final method of LWC variation was termed the 'Cluster' variation. As the name suggests, this method attempted to simulate a simple cluster variation where the water content varied as it might were the test vehicle to fly in and out of clustered cloud (such as in figure 3.2). To have an equivalent duration-averaged LWC (bearing in mind that flying in and out of cloud would require some periods of zero water) clusters contained water content levels notably greater than the mean value. The LWC variation within the

cluster simulation is presented in figure 5.9.

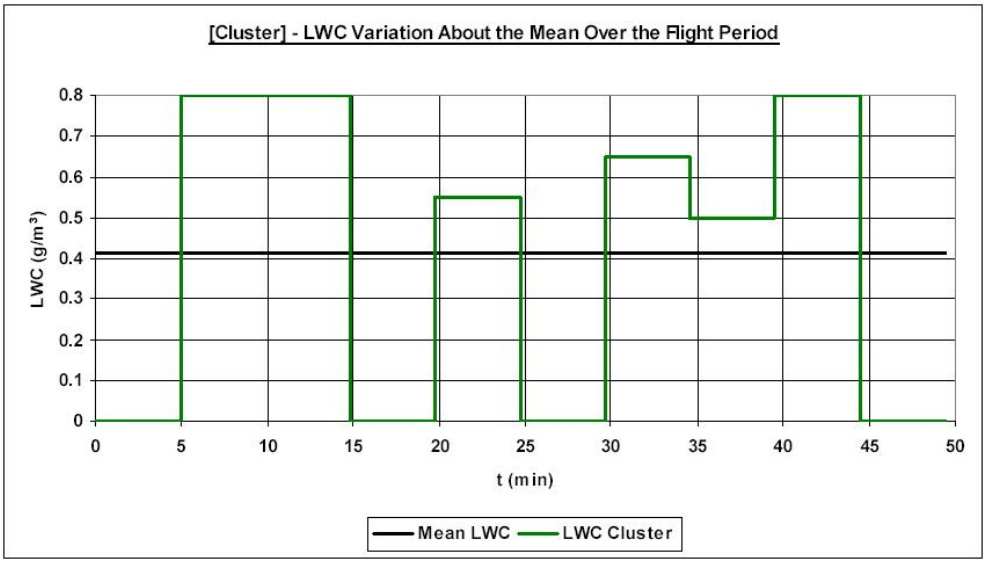

Figure 5.9: LWC variation according to the Cluster simulation.

As with phase 1, in phase 2 the modes and magnitudes of variation in temperature were designed to conform to a logical structure. Evidence of temperature variability in the flight data demonstrated that whether there was a significant overall trend or not, there would be some degree of small scale fluctuation in temperature. In addition the flight data highlighted the existence of definitive trends such as those present in figure 5.5 for constant and variable altitude flights respectively. The trace for static temperature in figure 5.10 shows temperature variability with rather less of a definitive trend. Yet the temperature does rise and fall over the course of the encounter and it would be possible to loosely describe the general trend in a sinusoidal manner. The 'Time Averaged Temperature' variability present within figure 5.10 shows how the actual temperature can be discretised appropriately to model the general trend in temperature to a suitable fidelity.

Initial variations in temperature, like those in LWC, were intended to represent basic but feasible variability within an icing encounter given the capabil-

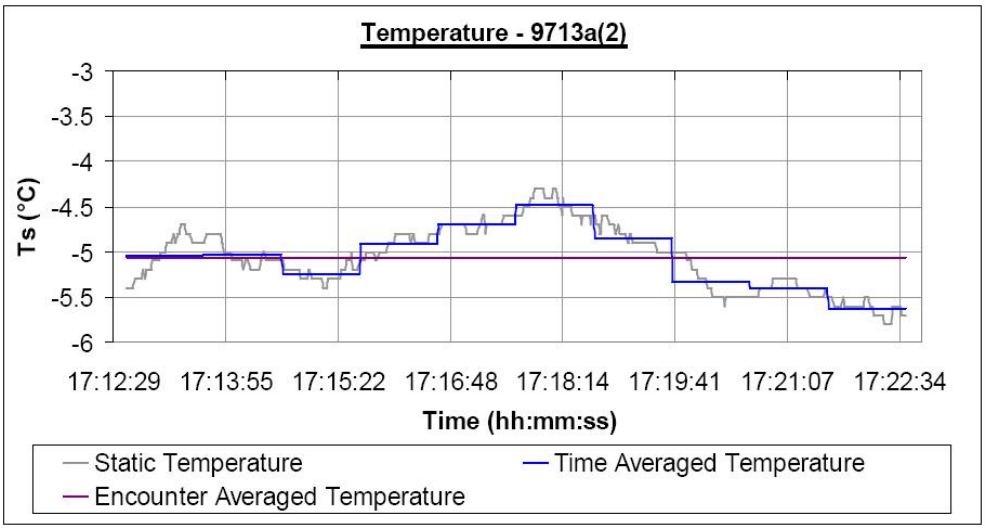

Figure 5.10: Plots of T during the second segment of flight 9713(a), recorded by Miller et al. (1998). Plots include the variability of raw data with time plus values time averaged across two different intervals, including the entire duration of $47km$.

ities and limitations of the CIRT. It was decided that initial efforts to model temperature variation would follow a sine wave mode of variation. This was because such a waveform would provide a logical structure and an appropriate pattern to represent constant altitude encounters. Sinusoidal variability was also suitable for incorporation into the CIRT[5]. Figure 5.11 shows how this was intended to be done, using stepwise changes in T to create nine segments of 5.6 minutes that allow basic modelling of a sinusoidal temperature variation. Phase change of $\pi/2$ radians generated a further three variants of temperature variability using this sinusoidal model.

Other examples of variability were evident from flight data. As a result, and because of interest in modelling encounters that did not conform to a predetermined structure, two further cases were generated. These cases provided the opportunity to model encounters with more drastic extremes in temperature, but like all others, had to have the same duration averaged conditions as

[5]The suitability is evident from figure 5.10 where temperature, time averaged over 10 segments, could be replicated within a facility like the CIRT

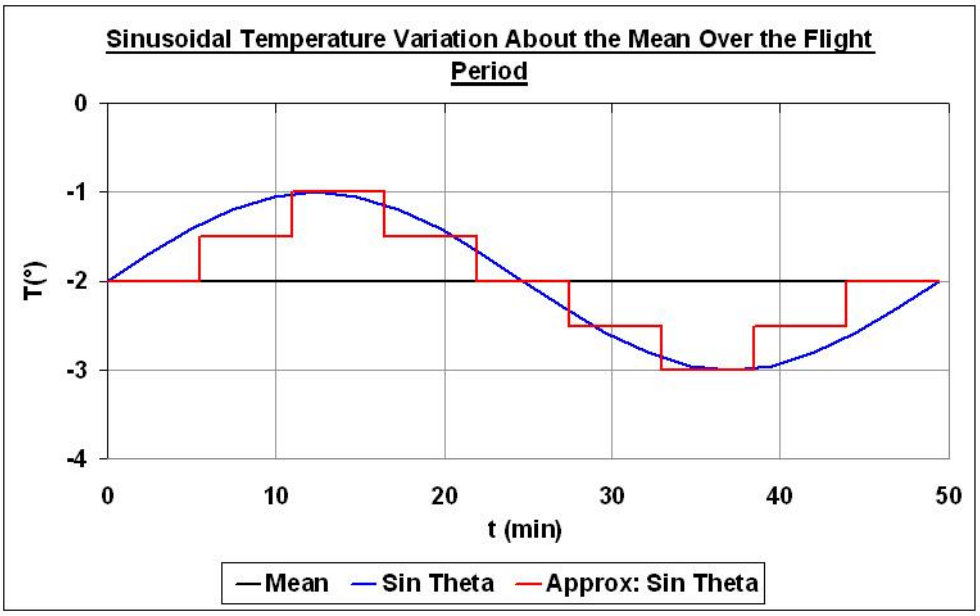

Figure 5.11: Temperature variation about the mean value of -2°C by ±1°C, varying in a stepwise manner that is aligned with the sine wave.

the reference conditions. Construct 1 and Construct 2, as they were named, were discretised into nine segments in the same way as the sinusoidal variability. The mode of variability for Construct 1 was based approximately on a 46km segment of flight 9712a (Miller et al., 1998), at near constant altitude, with -5.5°C ≤ T ≤ -2.0°C. The mode of variability for Construct 2 was based approximately on an 86km segment of flight 9713a (Miller et al., 1998), at near constant altitude, with -6.0°C ≤ T ≤ -3.5°C. Construct 1 is presented in figure 5.12 and again within figure E.39, Construct 2 is presented within figure E.41.

Phase 3 consisted of experimental simulations combining variability in liquid water content and temperature. Whilst being more difficult to achieve this was intended to provide a more comprehensive insight into the effects of variability, with consideration of the following:

1. The effect of combined LWC & temperature variability on the overall thermodynamic balance and ice growth rate;

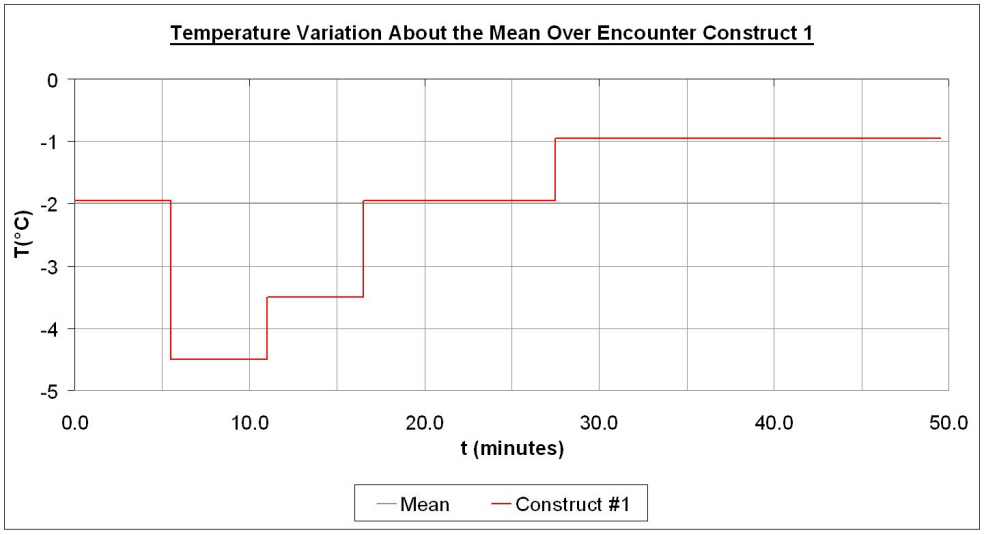

Figure 5.12: Constructed temperature variation about the mean value of -2°C, varying in a stepwise manner where temperature is predominantly colder early on, before warming for the latter majority.

2. The potential for encounters where combinations of LWC & temperature generate encounters and encounter segments with both enhanced and reduced icing severity, and associated growth behaviour;

3. The influence of aerofoil and profile collection efficiency, and collection efficiency development in variable conditions.

The complexity associated with generating icing conditions that were variable in LWC and temperature was significant, and had not been attempted before in the CIRT. Consequently it was anticipated that it might be problematic to generate more than a small number of coupled-variability encounters in the time available. Yet with appropriate design of simulations it was thought to be quite possible to gain a useful insight into coupled variability. Therefore five encounters were subsequently designed.

Four of these encounters were designed using different combinations of two LWC profiles and two temperature profiles. Two quite different LWC profiles were generated for coupled-variation. Two temperature variations were

selected from phase 2. The conditions applied in these four different simulations can be found in figure 5.13.

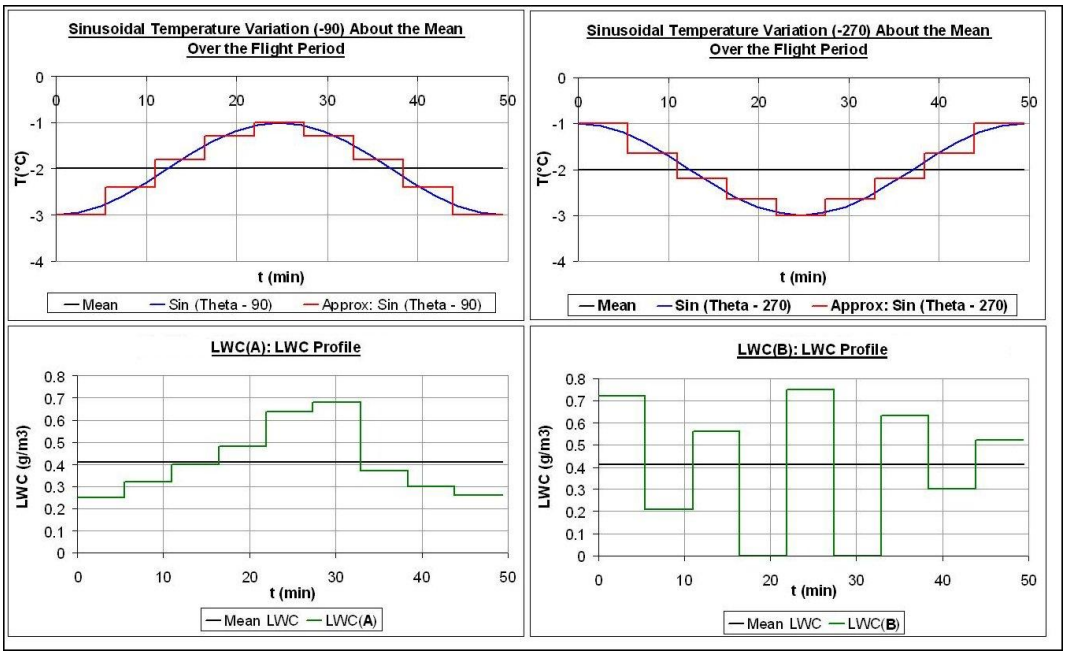

Figure 5.13: Temperature variations Sin(θ - 90°) and Sin(θ - 270°) and LWC variations P3-A and P3-B as applied in four of five phase 3 simulations.

These profiles were generated in an attempt to investigate more comprehensively, the impact of different combinations of conditions at different times within different simulations. They were designed to test the hypothesis that more severe icing conditions could result from combinations of wetter cloud conditions with colder temperature, and that the severity was dependent upon not just the nature of the conditions, but also the sequence in which they occur. By combining LWC profile P3-A with temperature profiles Sin(θ - 90°) and Sin(θ - 270°) the study looked at rising and falling LWC as the temperature, in one instance, increased then decreased, and in another, decreased then increased. The intent here was to see if temperature profile Sin(θ - 270°) would generate a larger ice accretion by virtue of its combination of higher LWC and lower temperature. Similarly in combining these profiles with LWC profile P3-B, the intent was to identify if the propor-

tionally higher LWC at the beginning and the end of the encounter would generate a more severe accretion with temperature profile Sin(θ - 90°); as opposed to with Sin(θ - 270°) whose conditions were warmer when large accretion rates were possible. The LWC profiles were deliberately different too, where P3-A sought to be representative of a cloud where water content was greatest in the centre and less towards the extremes. In contrast P3-B sought to be representative of a more clustered distribution of cloud water.

The fifth and final encounter generated in phase 3 (with case code 'LWC (30%) Rise and Temperature Drop') was designed deliberately to encourage a severe ice accretion. Over the course of phase 3 it had been observed that at times, combinations of conditions led to growth regimes that exhibited a large growth rate. It was thought that such a growth regime might be sustainable if the values of LWC and temperature were appropriate.

Knowledge gained via experience of icing encounters in phases 1 and 2, supported the view that higher horn growth rates were less likely with low LWC combined with warm temperatures; high LWC combined with warm temperatures; and low LWC combined with cold temperatures. Alternately then it could be conjectured that high LWC combined with cold temperatures would result in a rapid rate of ice growth. Designing the final encounter therefore required a combination of high LWC and cold temperatures. Achieving duration-averaged conditions equivalent to the reference case therefore required a period of warmer conditions and lower LWC. This was considered advantageous in attempting to generate a severe encounter for a number of reasons. Firstly with a lower LWC value, the loss of impinged water at warmer temperatures would be minimised, in advance of the appearance of surface roughnesses that would impede this process. Secondly, if designed to occur early in the encounter; this combination of conditions would tend to provide a level of initial ice growth at the leading edge that would form the basis of the final ice accretion. Thirdly, if icing severity were to increase with reducing temperature and increasing LWC, it would be further compounded with the increasing horn-tip collection efficiencies throughout the

encounter. Such a compounding effect would encourage accretion of a very severe ice shape. With this being the aim of the final simulation, the LWC and temperature profiles in figure 5.14 were generated for experiment. The initial temperature was very warm and was hence combined with a low LWC of $0.28g/m^3$. This was intended to initiate ice growth with minimal water loss before temperature reduction to cooler conditions. It was anticipated that initial ice growth would develop as a thin film before the appearance of small roughnesses. These roughnesses would encourage impingement of water drops, and impede the path of runback water, as the temperature cooled and the water content increased; thus promoting leading edge ice growth. This combination of increasing water collection (due to growing collection efficiency and increasing LWC) would then continue as the temperature fell over the remainder of the simulation. The final two stages of the simulation were designed to take the fullest advantage of the compounding effect of colder temperatures and high LWC, when the horn collection efficiency would be at its highest.

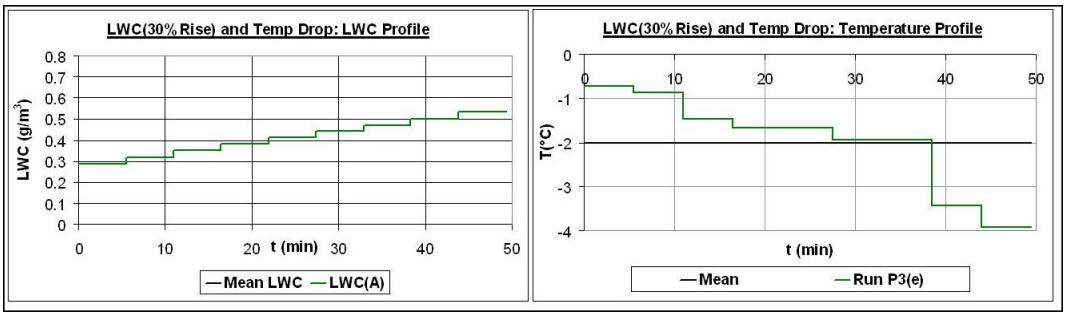

Figure 5.14: Temperature and LWC variation as applied in case 'LWC (30%) Rise and Temperature Drop'.

Description of the Cranfield Icing Research Tunnel

Before the first phase of the experimental icing programme it was necessary to assist in the commissioning of the CIRT and also to undertake several calibration activities specific to the experimental arrangement for the research

project.

A description of the icing tunnel is presented by Hammond et al. (2003). The facility generates icing conditions by driving the desired airflow from the diesel engine and fan; cooling the airflow using the refrigeration plant and producing the chosen cloud using the water spray system. In advance of phase 1 it was necessary to calibrate the airspeed, temperature, droplet size and liquid water content conditions within the working section to ensure the values simulated within the CIRT were correct. This was completed with a sequence of activities. These activities are described in forthcoming sections.

The Cranfield Icing Research Runnel is a closed-circuit tunnel. Air is driven around the icing tunnel circuit by a fan located at the end of the diffuser section. It is then ducted upwards towards the ceiling and into the roof-space where it traverses the upper section of the facility. Following the roof-space, turning vanes direct the airflow back towards ground-level via the heat exchanger, which cools the air as it passes. On route to the working section the spray system of six bars (each with 16 or 17 nozzle positions) injects cloud droplets into the airflow. The contraction causes the airflow carrying the droplets to accelerate towards the working section, during which time the droplets acclimatise to test conditions before the cloud arrives at the mid-section where the test article is commonly located. Figure 5.15 presents a schematic of the main tunnel facility.

Whilst the general design of the icing tunnel circuit is reminiscent of a conventional wind tunnel, key features like the presence of the heat exchanger, the spray system (bars, nozzles and flow control modifications) and when in operation, accreted ice, increase turbulence and reduce the aerodynamic quality of the airflow. It was therefore important to identify how uniform the freestream velocity was across the central plane of the working section. This was incorporated into the velocity calibration activity.

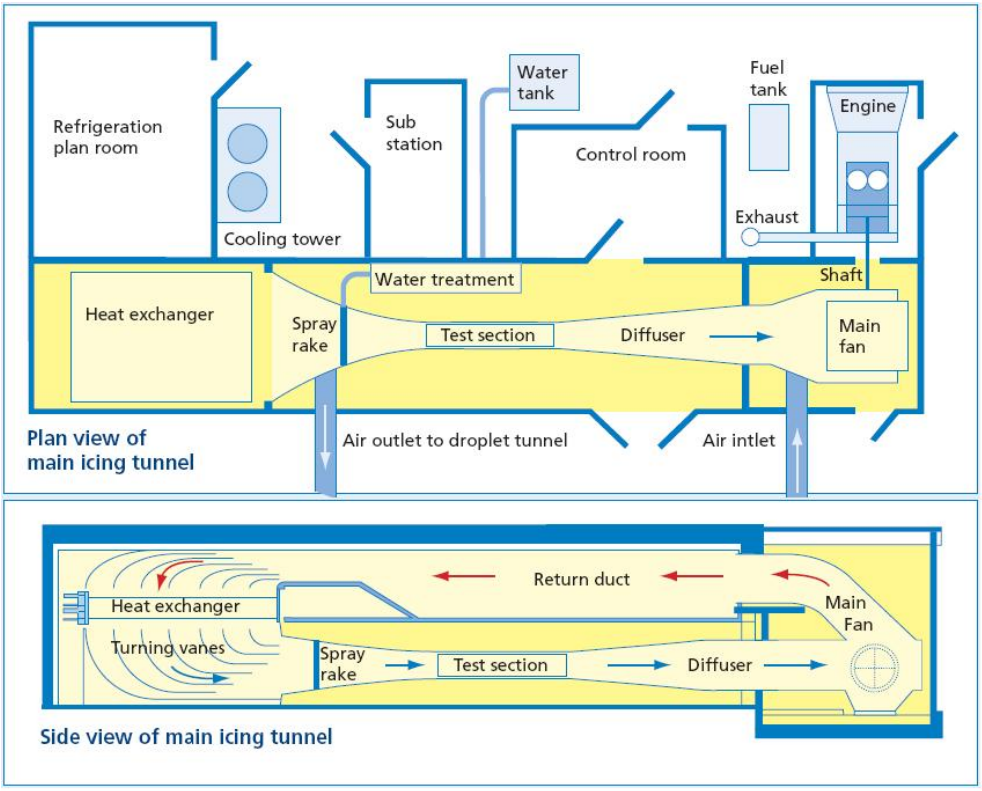

Figure 5.15: Schematic diagram including plan view and side view (elevation) of the Cranfield Icing Research Tunnel.

Calibration of Working Section Temperature

The refrigeration plant controller, through which tunnel temperature is controlled, reports temperature at a location upstream of the working section. Consequently there was an observable discrepancy between the values it reported and the working section temperature. It was therefore necessary to undertake a calibration that would provide a relationship for working section temperature, and this would allow calculation of the temperature for input via the refrigeration plant control (RPC)[6]. To do this calibration, a temperature probe was inserted into the centre of the working section and the icing

[6]The RPC displays tunnel temperature measured by a platinum resistance probe downstream of the turning vanes/upstream of the spray system, where the airspeed is much lower, approximately $10.0ms^{-1}$ at working section velocity of $50.0ms^{-1}$ (calculated on the basis of the area relative to the working section area).

tunnel was run at several temperatures input using the RPC. These values, combined with the values reported by the temperature probe allowed calculation of the calibration relationship. Working section temperature could subsequently be modified by setting T_{RPC} according to the calibration with T_{probe}.

Measurement of working section temperature was made intrusively using a Pt100 platinum resistance probe. The probe manufacturer states an accuracy of $\pm 0.1°C$. The probe was connected to the display meter using high quality copper wire to maintain accuracy. The probe was held stationary in the centre of the test section, with its longitudinal axis aligned with the tunnel's centreline wind axis. Since the probe was not moving with the airflow, nor was the air brought to rest (wholly) adiabatically at the sensor location; the temperature that was measured was neither static or total temperature, and was in fact somewhere in between. In noting this discrepancy, it is acknowledged that the temperature value specified as the reference temperature, T_{probe} = -2°C described neither the static or total temperature.

Within the region of interest[7] it was also noticed that there was a temperature variability of $\pm 0.2°C$. The measurement location was set according to the most uniform region of temperature and LWC (LWC uniformity is reported shortly) and was this was at the centre of the model.

Calibration of Velocity for the CIRT

A calibration of the working section velocity was obtained for two static pressure rings located at the entrance and exit of the tunnel contraction, calibrated against dynamic pressure in the working section measured using a pitot-static probe. For each static pressure ring, static pressure was taken at the centreline of each of the four walls, and these were connected together to provide an average static pressure. The differential static pressure between

[7]The region of interest on the aerofoil leading edge, is defined according to calibration limits to be ±25mm of the aerofoil centreline.

static rings was measured by a differential pressure transducer, and displayed on a digital indicator. Dynamic pressure from the pitot-static probe was measured using a hand-held differential pressure transducer incorporating a digital display.

In undertaking the calibration, velocity variation at the centre of of the working section was assessed by traversing the the pitot-static probe horizontally and vertically. The probe/housing arrangement used for this activity were analysed using CFD to ensure that the housing did not influence static or total pressure measurements. Velocity was measured at the middle of the working section's central plane, and at fourteen additional locations across the midsection where the wing model would be positioned. Measurement locations were as follows:

1. ±50% of the vertical distance from the centre to the top & bottom walls,

2. ±40% and ±90% of the horizontal distance from the centre to the near-side (control room) and far-side walls.

Figure 5.16 shows the pitot-static apparatus in the working section of the icing tunnel.

The relationships used to calibrate working section velocity were based upon those used by Edwards (2000), as presented below, where subscripts a and b refer to the upstream and downstream static ring locations respectively, whilst 'ws' represents the measurement plane in the working section. Applying the energy equation between the upstream and downstream locations, where K_1 is a coefficient accounting for pressure losses and other flow irregularities:

$$P_a + \frac{1}{2}\rho {V_a}^2 = P_b + \frac{1}{2}\rho {V_b}^2 + K_1 \frac{1}{2}\rho {V_b}^2 \tag{5.9}$$

and using the incompressible continuity, where A represents station cross-sectional area:

Figure 5.16: View of pitot static probe mounted in traversable probe housing within the icing tunnel working section.

$$A_a V_a = A_b V_b = A_{ws} V_{ws} \tag{5.10}$$

yield the following calibration equation, where K is the overall calibration factor.

$$\frac{1}{2}\rho_{ws} {V_{ws}}^2 = K(P_a - P_b) \tag{5.11}$$

As part of the calibration, in order to determine velocity from dynamic pressure (at a Mach number of approximately 0.15), the equation of state was used:

$$\rho_{ws} = \frac{P_{ws}}{RT_{ws}} \tag{5.12}$$

Working section temperature was calculated using the temperature calibration. When the calibration was performed, working section static pressure could not be measured, so an estimate of static pressure was used in conjunction with temperature to determine working section density. This assumption had an associated error term, where the estimation of static pressure

(101.3kPa) was expected to be approximately 1500Pa greater than the actual value for a target velocity of $50.0ms^{-1}$. The impact of this error upon the dynamic pressure and tunnel velocity at this target value is approximately +1.5% and +1.0% respectively. A +1.0% discrepancy for a target velocity of $50.0ms^{-1}$ is equivalent to $+0.5ms^{-1}$.

Other sources of error in the velocity calibration are:

1. The accuracy of the differential pressure transducer used to measure static pressure difference (Druck PDCR 4121), stated to be accurate to ±0.1% by the manufacturer. This is equivalent to an uncertainty of approximately $\pm 0.02ms^{-1}$ at a target airspeed setting of $50.0ms^{-1}$.

2. The accuracy of the display unit used to control airspeed via the calibration for the static pressure rings (Druck DPI 280), stated to be accurate to ±0.1% by the manufacturer. This is equivalent to an uncertainty of approximately $\pm 0.02ms^{-1}$ at the target airspeed.

3. The resolution of the display unit used to control airspeed via the calibration for the static pressure rings. The resolution was calculated to give an uncertainty in target airspeed setting of $\pm 0.45ms^{-1}$.

4. The accuracy of the transducer/display meter used to measure dynamic pressure from the pitot-static probe (Druck DPI 705), stated by the manufacturer to be ±0.1%. This is equivalent to an uncertainty of approximately $\pm 0.03ms^{-1}$ at a target airspeed setting of $50.0ms^{-1}$.

Turbulence measurements have not, at this stage, been undertaken within the CIRT. However the standard deviation in velocity was calculated using measurements at fifteen locations. The value of ±0.9% was considered to show reasonable uniformity across the working section despite a number of features present in the circuit that disturb the airflow (e.g. spray nozzles and heat exchanger).

Calibration of the Spray Cloud

The spray system generates the icing cloud conditions defined by droplet size and liquid water content. The nature of the cloud depends upon the input conditions applied to the spray nozzles, where atomised air mixes with the water jet and breaks it up to produce smaller droplets. The water pressure applied to the nozzles defines how much water is injected. To produce a specific droplet size MVD from the nozzles, a specific air pressure is required and this value increases as water pressure increases. The relationships between water pressure and air pressure for the CIRT were developed following the calibration that took place when commissioning the facility. The calibration used a Malvern Instruments Spraytec laser diffraction system (operating on similar principles to the Forward Scattering Spectrometer Probe introduced in section 3.1)and produced data describing the droplet size distribution for the icing cloud. Samples were captured across the range of water and air pressures of the spray system. The calibration relationship was calculated from the data presented in figure 5.17. There is generally a relatively large amount of scatter in the dataset used to generate the different drop-size calibration relationships presented in figure 5.17. This is much reduced, however, within the range of air and water pressures required for the present experimental programme at 17μm.

The error associated with setting the air and water pressures has been estimated to be $\pm$0.33 psi and $\pm$0.16 psi respectively. These values incorporate the following:

- The combined uncertainty in the accuracy of the pressure transducer ($\pm$0.3% $\equiv$ $\pm$0.1 psi) & display meter ($\pm$0.1% $\equiv$ $\pm$0.03 psi) for controlling air pressure[8].
- The uncertainty associated with manually setting the air pressure using a control valve, judged to be $\pm$0.2 psi.

[8]The air pressure transducer and display unit are a Druck PDCR 911 and a Druck DPI 272.

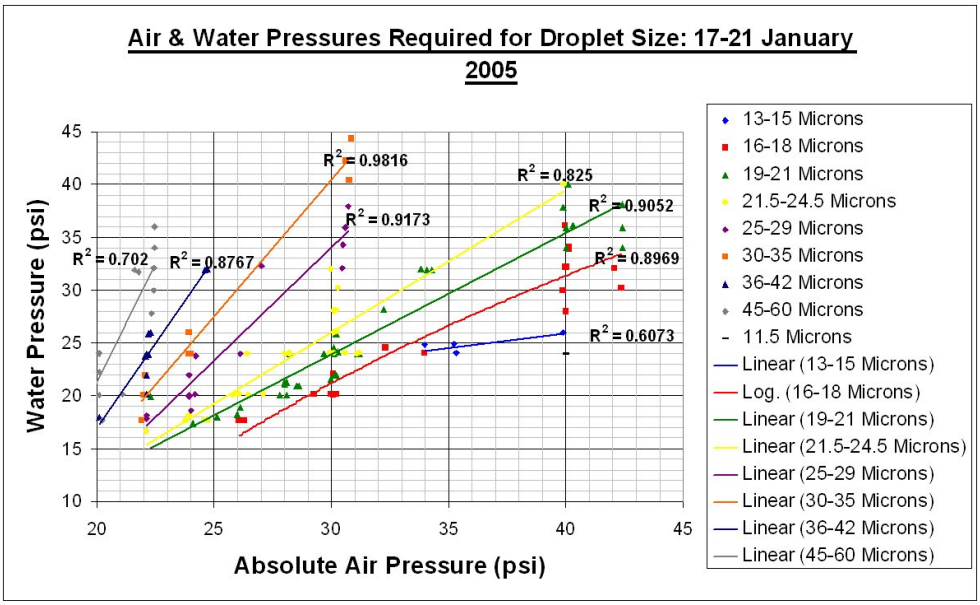

Figure 5.17: Data captured during the CIRT drop size calibration that allows determination of system air pressure according to system water pressure for different droplet size ranges.

- The combined uncertainty in the accuracy of the pressure transducer ($\pm 0.3\% \equiv \pm 0.08$ psi) & display meter ($\pm 0.1\% \equiv \pm 0.03$ psi) for controlling water pressure[9].

- The uncertainty associated with manually setting the water pressure using a control valve, judged to be ± 0.05 psi.

The impact of this error on MVD for the experimental icing programme (which had a target MVD of 17μm) is shown graphically in figure 5.18. Across the full range of air and water pressures figure 5.18 indicates that there are instances where there may be an error of up to +4μm (i.e. at an air pressure of approximately 30 psi). The range used for the experimental programme was approximately (25 psi $\leq p_a \leq 28$ psi) and (15 psi $\leq p_w \leq 18$ psi), where only data points from the 16μm-18μm category fall within the region of error. On the basis of the data set available and the above infor-

[9]The water pressure transducer and display unit are a Druck PDCR 922 and a Druck DPI 272.

mation, the contribution to expected error for the experimental programme was restricted to $\pm 1\mu$m.

The Malvern Spraytec system incorporates an instrument error of $\pm 2\%$ (Howard, 2008)[10] which, for MVD values of up to 60μm (the maximum MVD recorded during the CIRT calibration) results in a expected error of $\pm 1.2\mu$m. Combining this error with the $\pm 1\mu$m error reported above, the total uncertainty in specifying droplet size (MVD) for the experimental programme was $\pm 2.2\mu$m.

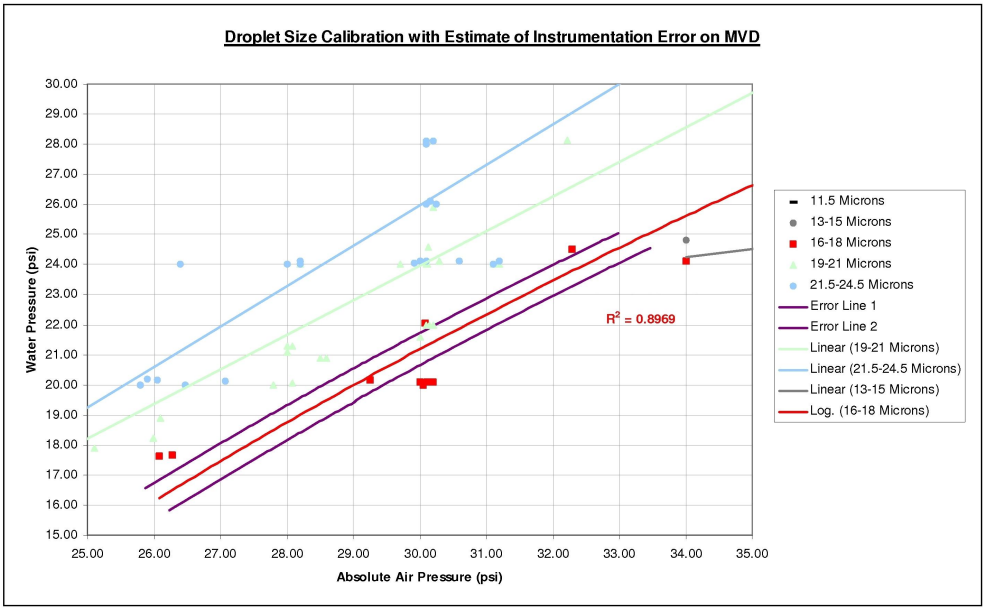

Figure 5.18: CIRT droplet size calibration curve for 17μm, presented showing the region of error expected in setting p_a and p_w.

The water content (units of gm^{-3}) of the cloud generated within the icing tunnel depends upon: (a) the rate of water injection into the icing tunnel, and (b) the rate of mass flow through the tunnel, i.e. the airflow velocity. So in preparation for the experimental programme it was necessary to calibrate the icing tunnel across a range of LWC values at the test velocity. However, before the LWC calibration could be undertaken it was necessary to assess

[10]Glen Howard is the manager of the GKN ATS Icing Wind Tunnel in Luton, UK, whose droplet sizing system was used for the droplet calibration.

and modify the spray bar configuration to be able to generate a cloud of suitable uniformity within the region of interest. To do this it was necessary to tailor the choice of spray bars and/or nozzles by choosing what combinations of spray bars to employ and which of the nozzles on the active spray bars to use. The spray bars and nozzles are presented in figure 5.19.

Figure 5.19: CIRT spray system viewed from inside the tunnel.

The first stage of the cloud development and calibration activity involved use of an icing grid to identify how uniform the icing cloud was over the whole working section and, in particular, in the region where the wing model would be mounted. An icing grid is a mesh made of thin metal with cylindrical elements approximately 5mm in diameter, used to capture cloud droplets across a large proportion of an icing tunnel. Figure 5.20 presents three examples of the icing grid installed within the CIRT.

At this stage relatively large modifications were able to be made to the spray system configuration because of the rapid nature of icing grid assessments. Also at this stage it was far more common to make changes via different combinations of spray bars in an attempt to assess how it might be possible

Figure 5.20: Photographs (a), (b) and (c) of the icing grid within the CIRT, having run a different spray configuration in each.

to achieve the most uniform cloud. There can be huge differences between the results derived from different combinations of spray bars, even when the nozzle configuration on each bar is similar. Photograph (a) from figure 5.20 shows that very little ice accreted on the icing grid. On this occasion spray bars near the top of the tunnel were employed and much of the cloud spray was carried above the grid. Photograph (b) shows better coverage of the grid as a whole; but the overall uniformity (assessed by visual inspection) was still inadequate because of the region of comparably light accretion running diagonally from top left to bottom right. Photograph (c) demonstrates that a good level of uniformity was achieved where the wing model would be installed, with little undulation in ice thickness observed. This area is contained within the red rectangle.

Once the basic cloud uniformity was considered adequate by use of the icing grid, a more detailed assessment of LWC uniformity was undertaken. This activity involved using the icing blade.

The icing blade technique has been used as a standard LWC measurement and calibration tool for many years (Stallabrass, 1978) and calculates the LWC values from the thickness of ice grown on the blade when inserted into the working section for a specific time. To do this reliably all droplets that strike the blade must freeze on impact, so the temperature required for

using an icing blade has to be cold enough to create rime ice. During the calibration, equation 5.13 was used to calculate LWC values.

$$LWC = \frac{t_{ice}\rho_{ice}}{60(EV_{ws}t)} \tag{5.13}$$

The icing blade had a small cross sectional height (facing the oncoming flow) of $6mm$. The collection efficiency (E) used in equation 5.13 was assumed to have a value of 1, assuming that all droplets in the upstream impingement zone would strike the forward surface of the blade. Therefore (assuming E=1) the ice accreted on the blade is the frozen mass of all water within the cloud that passed through the impingement zone upstream of the blade during the measurement period (t).

Having used the icing grid to identify a spray configuration that generated a relatively uniform icing cloud, the icing blade was employed to assess the uniformity more accurately to allow further refinement of the spray system.

In advance of phase 1 of the experimental programme, the CIRT and its systems were still at a fairly early stage in their development. Consequently for the cloud calibration activity, a spreadsheet tool was implemented to provide means of recording and visualising the results. A screenshot of the spreadsheet tool is presented as figure 5.21.

The spreadsheet tool allowed documentation of all information associated with the icing blade tests; including working section velocity, temperature and water & air pressures. The graphical representations show the number of active & inactive spray bars and the number of nozzles used on each active spray bar.

In advance of each icing blade test the bar/nozzle configuration was decided and recorded on the spreadsheet. The icing tunnel was started up and the conditions (velocity, temperature and water & air pressures) were set. Once the tunnel had been started and the desired velocity and temperature had

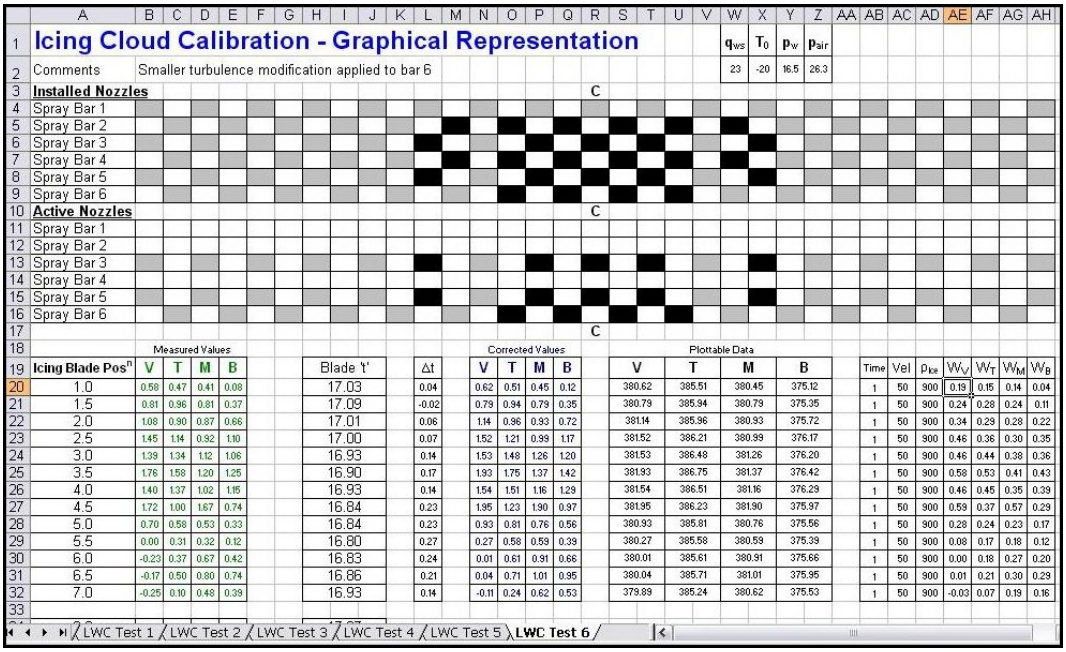

Icing Cloud Calibration - Graphical Representation

q_{ws}	T_0	p_w	p_{air}
23	-20	16.5	26.3

Comments: Smaller turbulence modification applied to bar 6

Installed Nozzles

	C
Spray Bar 1	
Spray Bar 2	■
Spray Bar 3	■
Spray Bar 4	■
Spray Bar 5	■
Spray Bar 6	■

Active Nozzles

	C
Spray Bar 1	
Spray Bar 2	
Spray Bar 3	■
Spray Bar 4	
Spray Bar 5	■
Spray Bar 6	■

	Measured Values						Corrected Values					Plottable Data												
Icing Blade Pos^n	V	T	M	B	Blade 't'	Δt	V	T	M	B		V	T	M	B		Time	Vel	ρ_{ice}	W_V	W_T	W_M	W_B
1.0	0.58	0.47	0.41	0.08	17.03	0.04	0.62	0.51	0.45	0.12		380.62	385.51	380.45	375.12		1	50	900	0.19	0.15	0.14	0.04
1.5	0.81	0.96	0.81	0.37	17.09	-0.02	0.79	0.94	0.79	0.35		380.79	385.94	380.79	375.35		1	50	900	0.24	0.28	0.24	0.11
2.0	1.08	0.90	0.87	0.66	17.01	0.06	1.14	0.96	0.93	0.72		381.14	385.96	380.93	375.72		1	50	900	0.34	0.29	0.28	0.22
2.5	1.45	1.14	0.92	1.10	17.00	0.07	1.52	1.21	0.99	1.17		381.52	386.21	380.99	376.17		1	50	900	0.46	0.36	0.30	0.35
3.0	1.39	1.34	1.12	1.06	16.93	0.14	1.53	1.48	1.26	1.20		381.53	386.48	381.26	376.20		1	50	900	0.46	0.44	0.38	0.36
3.5	1.76	1.58	1.20	1.25	16.90	0.17	1.93	1.75	1.37	1.42		381.93	386.75	381.37	376.42		1	50	900	0.58	0.53	0.41	0.43
4.0	1.40	1.37	1.02	1.15	16.93	0.14	1.54	1.51	1.16	1.29		381.54	386.51	381.16	376.29		1	50	900	0.46	0.45	0.35	0.39
4.5	1.72	1.00	1.67	0.74	16.84	0.23	1.95	1.23	1.90	0.97		381.95	386.23	381.90	375.97		1	50	900	0.59	0.37	0.57	0.29
5.0	0.70	0.58	0.53	0.33	16.84	0.23	0.93	0.81	0.76	0.56		380.93	385.81	380.76	375.56		1	50	900	0.28	0.24	0.23	0.17
5.5	0.00	0.31	0.32	0.12	16.80	0.27	0.27	0.58	0.59	0.39		380.27	385.58	380.59	375.39		1	50	900	0.08	0.17	0.18	0.12
6.0	-0.23	0.37	0.67	0.42	16.83	0.24	0.01	0.61	0.91	0.66		380.01	385.61	380.91	375.66		1	50	900	0.00	0.18	0.27	0.20
6.5	-0.17	0.50	0.80	0.74	16.86	0.21	0.04	0.71	1.01	0.95		380.04	385.71	381.01	375.95		1	50	900	0.01	0.21	0.30	0.29
7.0	-0.25	0.10	0.48	0.39	16.93	0.14	-0.11	0.24	0.62	0.53		379.89	385.24	380.62	375.53		1	50	900	-0.03	0.07	0.19	0.16

LWC Test 1 | LWC Test 2 | LWC Test 3 | LWC Test 4 | LWC Test 5 | **LWC Test 6**

Figure 5.21: Screenshot of the spreadsheet tool used to assist the assessment of cloud uniformity, refinement of spray system and calibration of LWC.

been achieved in the working section, the icing blade was inserted. It was inserted in one of four locations (three horizontal, one vertical) before the spray cloud was activated. Ice was accreted on the icing blade for 1-2 minutes before the blade was removed and placed in the freezer. Within the freezer a cold vernier caliper was used to measure the ice thickness at thirteen locations spaced equally across the blade. The relationship described by equation 5.13 had been incorporated into the spreadsheet to provide values for LWC distribution across the blade; and the thickness results were plotted automatically onto two charts. Figure 5.22 is one such plot, where the curves represent the ice thickness horizontal distribution across the working section in three vertical locations.

Examination of these plots allowed scrutiny of the results and analysis of the spray bar/nozzle arrangements that lead to those results. Modifications were then made, if necessary, to alter the LWC uniformity of the results. Modifications would include changing the location of active nozzles, adding

Figure 5.22: Horizontal ice thickness uniformity distribution across the working section at the middle location and ±5cm vertically.

spray bar attachments to encourage cloud mixing in specific regions and, if necessary, changing which spray bars were active. Over a period of days the cloud uniformity would reach an acceptable level. The experimental programme focused on ice growth within the centre of the aerofoil model, therefore adequate uniformity was required in this region. To achieve this the cloud was designed to be heaviest across the mid-section of the aerofoil span, reducing in water content towards the tips of the model and the walls of the working section. Figure 5.22 demonstrates the level of uniformity that could be achieved. The calibration region for LWC across the icing blade is from locations 3.5 to 4.5; across the three vertical locations. The level of uniformity within this region is adequate. The maximum level of discrepancy falls within ±10% of the mean value and the standard deviation describing uniformity within the region is only 5% of the mean value. This degree of uniformity within the region of interest compares favourably with the uniformity achieved by others (Ragni et al., 2005).

Once uniformity had been achieved and confirmed by the icing blade tech-

nique the LWC calibration could begin in earnest. This required measurements of LWC at constant velocity across a range of water pressures and corresponding air pressures. The MVD of $15\mu m$ that was selected for the reference conditions was only available at a very limited range of water pressures, according to the droplet size calibration (see figure 5.17). It was therefore decided to use a target droplet size of $17\mu m$ instead, since the water pressure range (and hence LWC range) would be much more suitable. As a result the 16-18μm relationship was employed for the icing blade assessment as well as the simulations thereafter.

By completing a sweep of water pressures, with corresponding air pressures; and using the spreadsheet tool (shown in figure 5.21) to identify the corresponding LWC, a curve was generated for LWC versus gauge water pressure. During the calibration, and in subsequent simulations, water and air pressures were handled as gauge pressures to remove the influence of atmospheric pressure, which had been observed to exist and to change over the course of the day. Following this calibration sweep and calculation of the LWC/gauge pressure curve it was possible to create a 'Required Pressure Calculator', a screenshot of which is presented in figure 5.23.

As mentioned the Required Pressure Calculator contains data taken during the LWC icing blade calibration that allows calculation of the required gauge pressures from the value of desired LWC. Using Microsoft Excel's trendline function, a cubic equation was generated giving LWC as a function of gauge water pressure. The calculator is essentially a spreadsheet implementation of the Newton-Raphson root finding method, that modifies and solves the cubic equation for water pressure for different entries of desired LWC. Additionally the temperature calibration described earlier was also incorporated into this spreadsheet, though not included in its title.

Therefore by using the spreadsheet tools and calibrations developed for temperature, velocity, droplet size and LWC, it was possible to identify the facility set-up requirements for any condition within a constant or variable icing

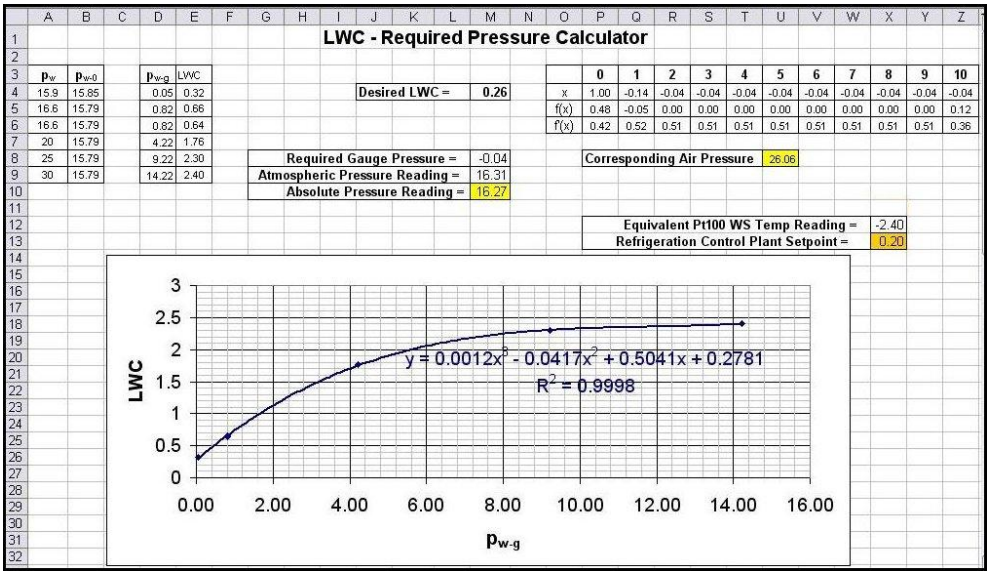

Figure 5.23: Water pressure, air pressure and refrigeration plant control temperature calculator utilised during the experimental icing programme.

case.

Tunnel Operation for Generation of the Reference Ice Shape

Having undertaken the calibration of the facility for the experimental programme it was necessary to generate the ice accretion at reference conditions. Having already defined the test vehicle's operation and flight capabilities the reference icing conditions had been identified from within the Appendix C icing envelopes.

The reference conditions were as follows:

V=50ms^{-1}, α=2°, LWC=0.41gm^{-3}, T=-2°C, MVD=17μm, t=50min.

These conditions resulted in a freestream Reynolds number of approximately 1.6E+06.

The aerofoil model, a $760mm$ span NACA 23015 profile was mounted at 2° incidence to the working section vertical centreline, fixed by two bolts at either side of the leading and trailing edges. The tips were flush against the perspex windows of the icing tunnel (the working section is $760mm$ in width and height). The model was mounted horizontally within the working section.

Tunnel start-up tasks comprised the following:

1. Start the air compressor and air drier to provide air to the spray bars;
2. Bleed the water system to remove any air and switch on;
3. Start the diesel engine to power the fan;
4. Start the refrigeration plant;
5. Switch on the air heater to supply air to the spray system.

These start-up tasks set the icing tunnel running, ready to be set to test conditions. Temperature was controlled via the refrigeration plant remote (setting T_{RPC}), giving a working section temperature of -2°C. The water pressure required for the reference LWC was set according to the icing blade calibration which also output the air pressure required to achieve the correct droplet size distribution of $17\mu m$. The velocity was controlled using the engine throttle, and monitored using the differential pressure readings, in accordance with the velocity calibration. The refrigeration plant was allowed to settle to its set-point value before the spray bars required for the pre-calibrated cloud were switched on for the duration of the test, which was approximately 50 minutes. The cloud took up to ten seconds to settle and this time was allowed (added on) each time the spray was started.

Application of Variability within Phases 1-3 of the Experimental Programme.

Each of the variable cases was initiated in the same manner as the reference case, differing only when the LWC and/or temperature values for the

first segment of the case differed from the reference conditions. The significant difference in terms of tunnel operation arose in applying the variability. When changing the cloud water content the spray bars were switched off to allow the water and corresponding air pressures to be changed accordingly. This took 1-3 minutes. When changing temperature the spray bars were switched off before setting the refrigeration plant controller appropriately so that working section temperature would change to its new setting. In reaching test temperature for each segment the refrigeration plant generally cooled or warmed towards and past the setpoint before the control system altered the cooling power to cause the temperature trend to reverse. In this manner the temperature oscillated 1-2 periods before settling at the desired value. Once the desired temperature was reached the spray system was switched back on to continue the simulation. The temperature change took from 3-15 minutes each time. Sometimes the temperature trend was such that it took relatively little user input to change from one temperature to the other. So once operators became experienced in doing this it was possible to anticipate the temperature system's behaviour, and exploit knowledge of the temperature trend to reduce the time in between spray segments.

Having described the method of incorporating variable conditions into the facility, it is important to note the dry periods. Between sprays the ice will have had a chance to acclimatise to the dry conditions, where the water film and other trapped water would have had a chance to either run off, freeze or evaporate, leaving a drier ice surface. This might have influenced any ice growth once the spray re-started, but there is no evidence to confirm or deny this. It would be suitable for subsequent research efforts to investigate this. An appropriate method would be to replicate the reference case, only switching off the spray cloud after each segment for three minutes, before switching on again for the following segment. A comparison of repeatability with the other constant condition profiles would indicate the magnitude of any associated effects.

Profile Capture

Once an icing simulation was completed the tunnel was shut down before one of the windows was removed to allow access. A hot metal plate was used to remove a slice of the profile at the measurement location, for which the LWC and temperature was calibrated and the cloud ensured uniform. A cardboard template that slid over the aerofoil was used, with graph paper attached to allow tracing of the ice profile by hand using a pencil. One such profile tracing is included in figure 5.24.

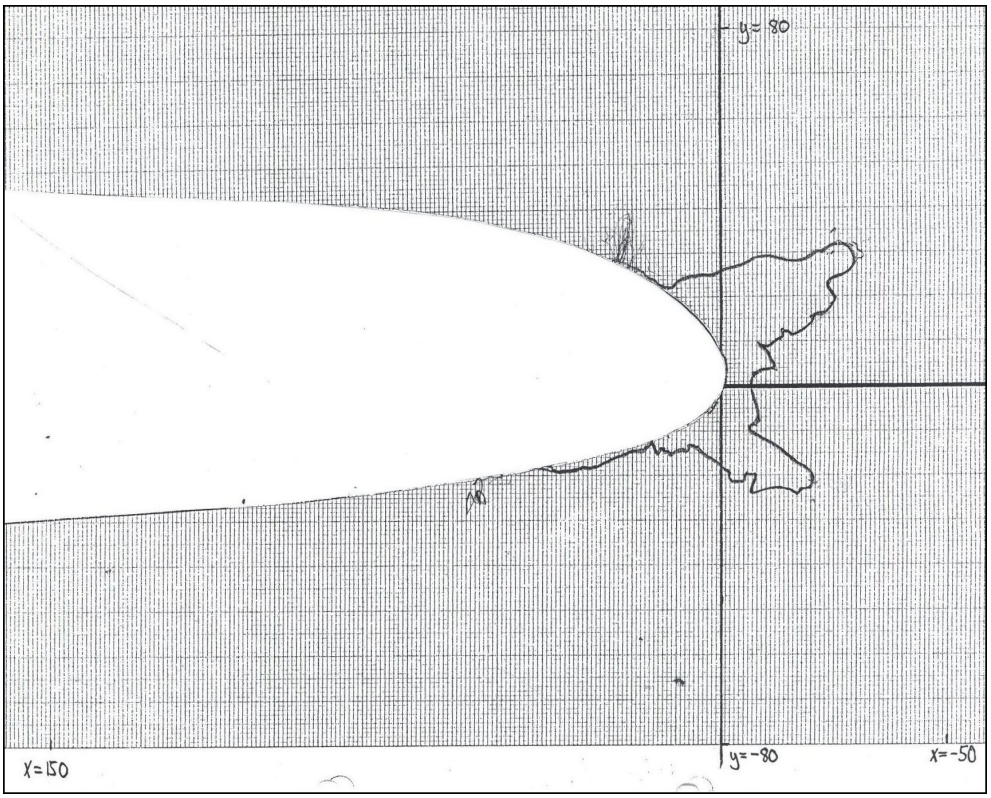

Figure 5.24: The tracing taken for one of the profiles created under reference conditions.

Whilst this method is basic it is used and accepted commonly within the aircraft icing field. The uncertainties that can arise when capturing the profile manually are caused by the difficulty in positioning the pencil against the ice, and the graphite point being larger than some of the gaps between roughness

elements. The error associated with the first uncertainty is $+1.5mm$, measured by drawing round an artificial ice accretion with an accurate pencil position and with an inhibited pencil position. The error associated with the second uncertainty is incorporated within this value, as the size of the roughness gaps not captured by the pencil were less than the thickness of the tip, which is approximately $1mm$. Despite this uncertainty, the primary features and the majority of the accretion's intricacies are captured well by this simple method. The subsequent geometry for CFD assessment is an adequate representation of the ice accretion, where the primary features of horn thickness and orientation are appropriately described.

Scanning the tracing, including the axis locations marked on the graph paper, allows a digitising package (DigitizeIt) to extract enough coordinates to represent the geometry of the ice accretion well. These coordinates can then be used in any number of software packages.

Measurement of Profiles' Primary Geometric Features

Capturing the ice profile as described above provided an excellent illustration of each result; in terms of the overall shape and primary features like horn size, as well as more intricate details. Such details were useful for in-depth examination of the profile shape and especially for comparison of profiles. Where the bulk features like horn thickness and orientation were similar between profiles; closer examination allowed identification of more subtle differences like the distribution of ice between the horns, how slender the horn might be, the sharpness of the tip, the gradient of the horn surface aft of the tips and the surface smoothness. These differences, important for geometric comparison, also assisted with interpretation of aerodynamic results. To generate these results, the detail captured was replicated in the CFD modelling, thanks to the resolution available in converting the profile tracing to cartesian coordinates.

Often ice accretions and their aerodynamic properties are discernable from

one another as a result of certain primary features, and it is very convenient to be able to describe these features using defined parameters. The use of such parameters extends to providing quantitative measures to the various differences between profiles, and also in identifying which of these measures is most aerodynamically significant. The geometric and aerodynamic analysis undertaken within this project benefitted from both the full profile tracing and subsequent quantitative measures of primary geometric features.

Miller et al. (2006) utilised the feature known as THICK in the NASA program SmaggIce to determine geometrical characteristics of ice accretions. The geometrical analysis utilised for this project produced very similar results to the THICK program, where seven of the values measured were defined identically to seven of the eight values calculated by THICK (accretion area is not calculated). It differed however, in that it the sign convention employed for angles is different to that reported by Miller et al. (2006). Also, in addition to horn angles (θ_{upper} and θ_{lower}), other measurements were made for the orientation of the horns on the upper and lower surfaces. These have been named horn growth vector angles (ϕ_{upper} and ϕ_{lower}). These angles measure the apparent growth direction of the horns from the root (from where h_{upper} and h_{lower} are measured) to the tip of the horn. It was considered appropriate to supplement the description/metric for horn orientation with the horn growth vector angles because of the horn angles' significant dependence upon horn thickness. During this project the geometric parameters were measured by hand from the profile tracings, in contrast to the THICK program which calculates the parameters for a given set of input coordinates for the clean aerofoil and the ice profile. Those parameters already introduced are presented diagrammatically in figure 5.25.

The diagram presents the horn thicknesses (h_{upper} and h_{lower}), the horn angles (θ_{upper} and θ_{lower}) and horn growth vector angles (ϕ_{upper} and ϕ_{lower}). In addition to that, THICK calculates the upper and lower freezing limit distances and the centreline thickness. The upper and lower freezing limits are the distances along the (+ve) x-axis, from x = 0 to where ice growth

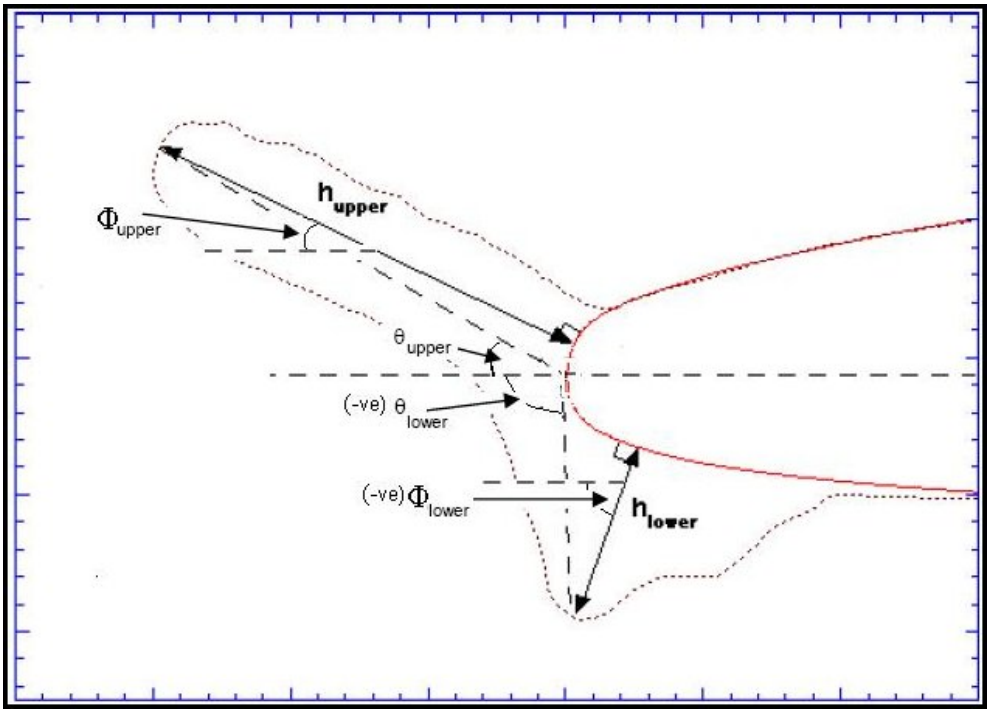

Figure 5.25: Diagram defining some of the parameters measured to describe the main features of the ice accretions, adapted from the parameters & associated conventions described by Miller et al. (2006).

ceases on the upper and lower surfaces respectively. The centreline thickness is the thickness of the ice along the (-ve) x-axis at y = 0. The centreline, i.e. the x-axis in figure 5.24, defines the direction against which all angles were measured. This line was first used in manufacturing the model and was considered a suitable reference. It is oriented at -0.4°C to the chordline at the trailing edge.

Careful measurement of horn thicknesses, leading edge thickness and freezing limit by hand, using a steel-rule with 0.5mm resolution allowed accuracy to approximately $\pm 0.5mm$. Similarly using a protractor for horn and horn growth vector angles allowed measurements, again by hand, to be accurate to within $\pm 1.0°$. Another aspect of these measurement techniques likely to introduce an uncertainty was identification of the surface location at which the perpendicular distance to the furthest extremity of the horn was maximised.

Errors in such locations will have influenced all angular measurements and those for horn thickness, by the order of 1.5° and 1.0mm respectively[11].

5.2.2 Aerodynamic Performance Analysis of Simulated Ice Accretion Profiles

The second of the two primary technical objectives of this research project was to develop and utilise a CFD technique (described fully in forthcoming sections) for the prediction of the airflow behaviour around heavily iced aerofoils; and for subsequent determination of the performance degradation for lift and drag. The purpose of this was to identify the relative performance degradation of accretions generated by variable-condition encounters as opposed to the constant-condition reference encounter. Within this section the different tasks contributing to that objective are described.

Airflow Prediction Around Iced Aerofoils - The State of the Art

CFD prediction of the airflow around iced aerofoils has been studied by numerous experts over recent years with differing degrees of success. Within the programme of research detailed in this document it was necessary to attempt adequate solution of the aerodynamic performance of iced aerofoils. It was therefore appropriate to review studies published within recent years.

Badcock et al. (2000) identify a number of important requirements for CFD simulation of an aerodynamic scenario. Included within their list are (a) suitable grid generation, (b) adequate airflow modelling (including turbulence modelling) and (c) negligible numerical error. These requirements are especially important for CFD solution of iced aerofoils. This is because the airflow around an iced aerofoil is highly complicated and difficult to model,

[11]This estimation was determined by measuring the discrepancy in the horn thickness and orientation parameters following accurate identification, and deliberately inaccurate identification of the horn root.

it involves highly complex and variable geometry, and turbulent & unsteady behaviour involved with flow separation and any subsequent reattachment.

Dafa' Alla (2002) generated a fully unstructured grid to model the airflow around a smoothed, numerically generated, two-dimensional iced aerofoil. This would undoubtedly have been quick to generate but such an advantage would likely have been counterbalanced by the huge number of grid points required in the vicinity of the profile. The results gave good agreement with experiment, but the heavily smoothed and simplified geometry was not particularly representative of a real ice accretion. The success was therefore restricted to the simple shape, and the grid generation technique was not proven to be applicable to realistic profiles.

Thompson and Soni (2002) demonstrated that automated grid generation of structured grids is possible and did so, impressively, for an experimentally generated ice accretion, with a notable degree of surface roughness and a large number of concave sections. Furthermore their grid-marching technique for reducing the grid size in less critical areas and reducing unnecessary bunching of grid points seemed very useful.

More recently the NASA tool SmaggIce has become capable of automatic grid generation, creating high-quality structured grids for experimentally generated ice accretions, (Vickerman et al., 2005) and (Kreeger et al., 2007). In development of this tool, the following capabilities have been found to be particularly useful:

- Surface smoothing functions that address tangles/twisted cells created by concave sections;
- The ability to create discrete near- and far-field grids that ensure the flow features near the profile are able to be predicted sufficiently with a highly refined near-field grid; whilst the clustered nature of the near-field grid is not propagated into the far field;

- Further decomposition of the flowfield domain into multiblocks that adequately discretise the domain and provide flexibility and control of the grid;
- Analysis that uses appropriate cell quality measures to indicate areas that require further effort to meet a minimum standard.

Chi has published extensively in this area: Chi et al. (2002), Zhu et al. (2002), Zhu et al. (2003), Chi et al. (2004), Chi et al. (2005), Chi et al. (2006) and Hindman et al. (2006). Chi et al. (2002) note that with aircraft icing, the presence of both horns and surface roughness complicates gridding and can at times make it necessary to incorporate surface preparation as one of the key steps. They discuss the relative merits of single block grids (based on the work of Tai (2000)) and multi-block grids. Single block grids do not suffer from reduced convergence speed due to data transfer at block boundaries, though they require strict specification to allow creation of a high quality grid despite surface roughness, concave and convex wall sections and large horn features. Multiblock methods deal with these features more easily since the blocking topology, controlled by the user, can be shaped to fit the physical domain. They also allow definition of what the authors of the publication refer to as the wrap-around layer and the transition layer. These two grid features prevent clustered grid points and the surface shape that exist in the near-wall region having an influence in the far-field. Their chief drawback however is that the block boundaries can impede convergence. Zhu et al. (2002) discovered that the blocking topology of a multiblock grid can have an impact on convergence rate, but that this can be avoided by minimising the occurrence of block boundaries being parallel to the flow direction. Where block boundaries are perpendicular to the flow direction the convergence rate was found to be almost as good as it was for a single-block grid.

Grid independence is also very important for any CFD modelling, and for ice shapes this is evident in the publication by Chung et al. (2000), where grid spacing adjacent to the wall (in the boundary layer), and in the normal direction outside the boundary layer were found to have significant influence

on the solution. The influence of streamwise grid spacing was not found to be significantly influential for the spacings tested during this research. It is important therefore to ascertain what level of grid refinement is required for grid independence and what can be afforded both in computational terms and project (timescale) terms.

Turbulence modelling (for use of the Reynolds Averaged Navier Stokes equations) has received a notable amount of attention for CFD prediction of iced aerofoils. Several turbulence models have been tested including Spalart-Allmaras (S-A) , RNG k-ϵ, v^2-f, a differential Reynolds Stress model (RSM) and the Sheer Stress Transport (SST) model. Chi et al. (2004) found the S-A model to work most effectively for a rime ice accretion and also for the glaze ice (although the accuracy of the prediction was much less successful for glaze ice). This was confirmed by a later publication (Chi et al., 2005) that also documented improved prediction performance from a Lattice-Boltzmann model which is explained by Li et al. (2005). Chung and Addy (2000) also reported the greatest success with the S-A model, which was again used by Dunn et al. (1999) with noteworthy success.

Other icing-CFD work exists. Several studies look to the extension of CFD work into three dimensions, using full CFD solution of a 3D model or alternate methods, like that of Chi et al. (2006) and Hindman et al. (2006). More advanced solver-based studies also exist - Pan and Loth (2004) undertook a Detached Eddy Simulation of an iced NACA 23012 (ice modeled with a quarter-round shape placed on the upper surface), where LES is utilised to resolve turbulent separated flow (solves N-S equations directly where the turbulence scale is greater than the fine resolution of the grid, RANS where the turbulence scale is smaller than the resolution of the grid) whilst RANS is used for attached flow at the solid surface. This method proved relatively promising but was only assessed for a limited set of incidences.

Identification of the Required CFD Capability

Having investigated the literature to confirm the main issues and requirements involved in CFD prediction of the aerodynamic performance of iced aerofoils; it was important to specify what information would be sufficient to distinguish between ice accretions by aerodynamic performance degradation.

Having generated an ice accretion from the constant-condition reference case and numerous others from variable-condition encounter simulations it was necessary to be able to ascertain whether one profile was aerodynamically more detrimental than another or not. Ideally CFD predictions would have accurately predicted the fluid-flow behaviour and associated force coefficients at a range of angles of attack; but in reality this was unlikely given the complex geometries and fluid behaviour as well as the limited prior success of others. Instead it would be acceptable if the predictions from the CFD technique could correctly ascertain trends between ice accretions, e.g. the overall drag polar from ice shape A has noticeably greater values than the overall drag polar from ice shape B, which has similar values to shape C. Additionally, in researching literature sources that discuss correlation of CFD results with test data, this requirement was ranked highest of nine categories describing the relative importance of validation information[12].

In order to achieve this requirement, the predictive capability needed adequate resolution of near wall flows and the boundary layer; an ability to predict separation and an ability to model turbulent shear layers and wakes with possible reattachment. This was required for two-dimensional profiles.

The technique required a method of high quality grid generation. The review of recent literature showed the most important factors to be the ability to smooth the geometry; multi-block topology discretisation (with block bound-

[12]Bussoletti (1994) surveyed CFD users within the Boeing Aerodynamic engineering community, assessing the relative importance of categories including 'Accuracy of agreement with respect to absolute levels of experimental data' and 'Knowledge of accuracy with respect to grid density'.

aries preferably perpendicular to the airflow); assessment and improvement of cell quality and appropriate grid spacing. The experimental icing programme produced over twenty-five ice accretions, with each profile requiring digitising & importing into a CAD-type package for geometry creation before gridding, flow solution and postprocessing could take place. With such a large amount of work involved it was imperative that the technique was not overly demanding on the time available. The technique was restricted to 2D analysis, as 3D computations would require computational capacity far beyond what was available.

The predictive capabilities required from the solver and the associated time constraints indicated that a Reynolds Averaged Navier-Stokes (RANS) solver would be most appropriate.

Development of the CFD Technique

Efforts during the first year of the project to model an aerofoil with a real ice accretion at the leading edge using Fluent proved very difficult. Fluent's preprocessor, Gambit, allows mesh generation in 2-D using multiblock build-up via specification of coordinates, creating edges between coordinates and faces from edges. This proved to be very difficult because of the large number of blocks required for an experimental ice accretion, and the resultant time required for inputting huge numbers of multiblock coordinates for which spatial location needed to be defined. This is illustrated in figure 5.26 for a particularly challenging ice accretion (regardless of the grid generation method) which took a minimum of 5 days to develop as a test-case. Unstructured grid generation was considered at the time, but structured, quadrilateral cells would have been required for the boundary layer, and the block discretisation required was such that once done, unstructured meshing would have provided little advantage in the near-field. Had this activity proved more successful, it may have been worthwhile exploring options for unstructured mesh in the far-field.

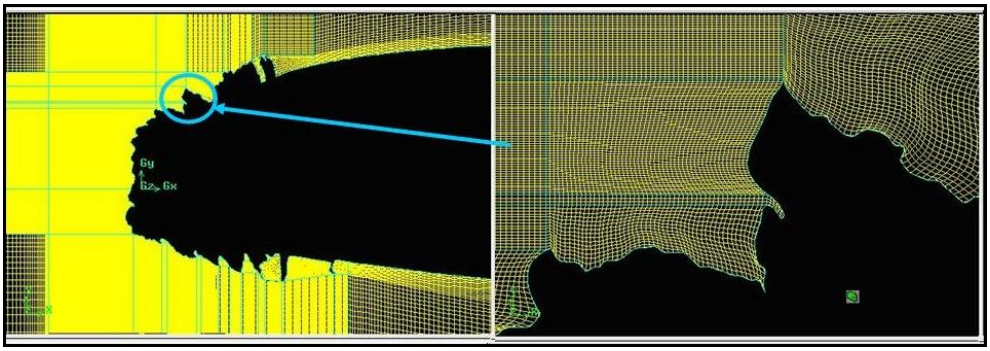

Figure 5.26: Screenshots taken from early grid generation efforts for an iced aerofoil.

In presenting initial CFD efforts at a meeting of the project's industrial steering committee, it was advised that colleagues at the University of Glasgow had some experience in CFD techniques for aircraft icing. During discussions with the University of Glasgow's Aerospace Engineering department it emerged that some success had been achieved for multi-block modelling of ice accretions similar to those modelled by Dunn et al. (1999) and Pan and Loth (2004) using quarter rounds, but airflow prediction of notably more complicated or experimentally generated ice accretions had not yet been attempted. It was therefore considered within the interests of both parties to work together to take this next step. Colleagues at the University of Glasgow subsequently joined the Department of Engineering at the University of Liverpool[13]. Grid generation techniques for computationally generated ice accretions were developed by the author with support from colleagues from Liverpool and Glasgow. The solver utilised was that developed by Professor Badcock and colleagues (Woodgate et al., 2000). The postprocessing tools employed were Tecplot 10.0 and Microsoft Excel. The wind tunnel data for comparison with CFD results was generated during a week's test in the Cranfield University low-speed aeronautical/automotive wind-tunnel, undertaken

[13]The lead collaborator at the University of Glasgow, and subsequently, the University of Liverpool was Professor Ken Badcock. Also involved at the beginning of the project was Stuart Gates, who worked on CFD of iced aerofoils as part of his research project whilst studying towards an MEng in Aeronautical Engineering at the University of Glasgow.

by the author and members of technical support staff. A member of academic staff was also involved, though did not take part in the testing.

Five ice accretions were selected for the development of the CFD technique. They were selected because of the differences and similarities between the profiles in the hope that those profiles deemed similar would be predicted to have similar aerodynamic performance whilst those notably different would be predicted to have equally different aerodynamic performance. The five profiles are presented in figure 5.27.

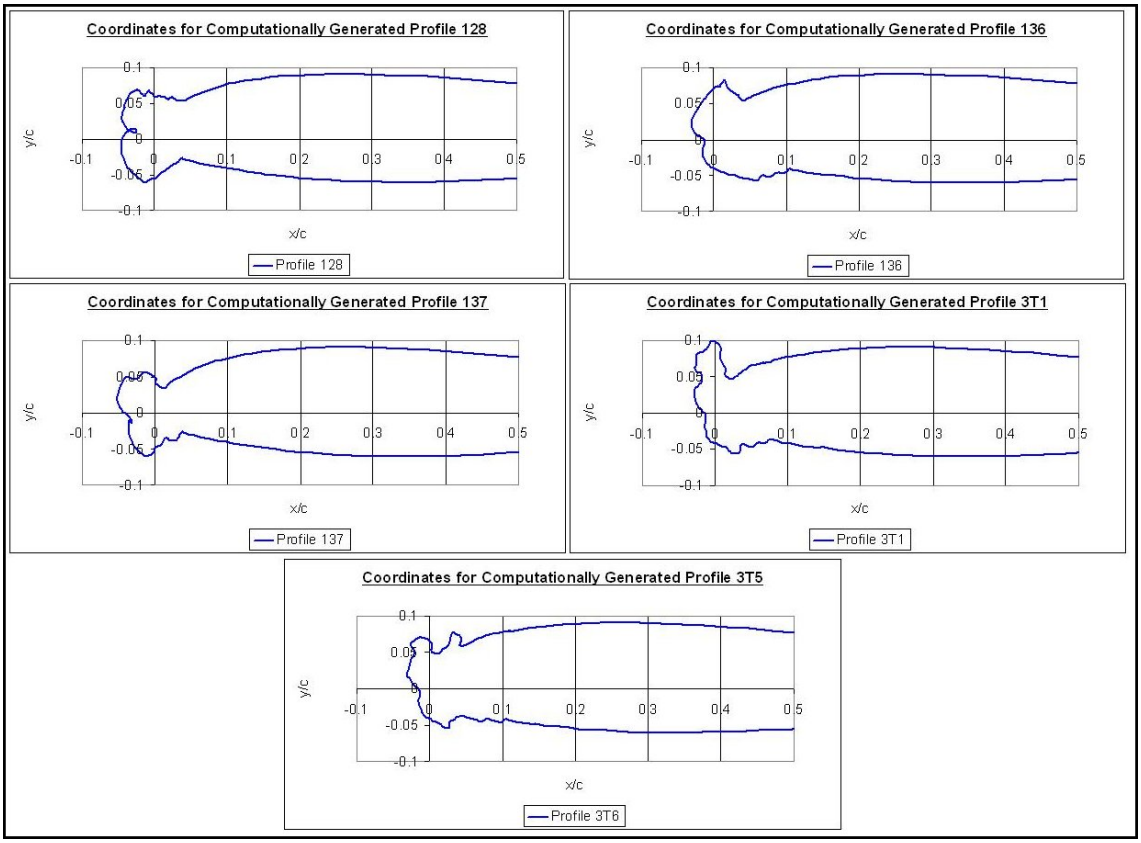

Figure 5.27: The five computationally generated ice accretions utilised during the CFD technique development - codenamed 128, 136, 137, 3T1 and 3T5.

Grid generation was a challenging activity, first for computationally generated ice profiles, then more so for experimentally generated ice profiles. The

procedure described here for computationally generated profiles is applicable to the more difficult grids. In addition, however, the major steps involved in gridding experimental ice profiles will be provided later.

Grid generation was undertaken using ICEMCFD by ANSYS. ICEMCFD is a grid generation tool that can be employed for any number of challenging mesh generation problems. The main benefit of ICEMCFD for this application was the ethos behind block topology preparation. Unlike Gambit and other packages that adopt a 'block building' approach to grid generation, ICEMCFD uses a block splitting method to 'carve' a topological domain that fits the physical domain, quickly and reliably.

Once the physical model and domain are created from points, curves and surfaces in two-dimensions; the process of block generation can begin. The process starts with a single two-dimensional block that encompasses the entire physical domain. The user is then able to introduce splits into the block to create further blocks where edges form part of either the solid surface of the iced profile, the far field boundary or the internal flowfield. An important step is the use of edge splitting to create the profile block. This is done by making two horizontal splits and two vertical splits to the original rectangle. This creates a central block that will represent the aerofoil. This block is deleted because the interior of the domain represents the fluid whilst the aerofoil is solid. The remaining edges (once part of the aerofoil block) can be considered solid and the vertices (corners of a block) can be re-located to exist on the aerofoil curves[14]. The two vertices furthest in the downstream direction are co-located at the appropriate trailing edge points.

Before undertaking much more in the way of splitting it is very much worth undertaking an activity known as 'association'. This activity informs the programme which vertices are associated with (assigned to be the topolog-

[14]Note: points represents corners in the physical domain, vertices represent corners in the topological domain; curves join points in the physical domain, edges join vertices in the topological domain; surfaces are made from curves in the physical domain, faces are made from edges in the topological domain.

ical equivalent of) specific points or surfaces. Similarly this is done with edges/curves and faces/surfaces. With edges/curves this is performed on edges at either the solid surface or the far-field boundary. This task informs ICEMCFD which edge should be mapped/projected to which curve or portion of curve and this is necessary for the curve geometry to be faithfully reproduced by the grid. With faces/surfaces this task is performed on surfaces at the exterior of the domain or at the solid surface. This allows ICEMCFD to project/map a collection of faces to a corresponding collection of surfaces and hence boundaries, so provides topological entities through which the boundaries and boundary conditions can be specified.

Block splitting then continues with the aim of shaping the block topology around the solid surface so that the profile geometry is well represented and the quality required within the blocks is assured. The blocking topology developed for one of the simplest cases is presented in figure 5.28.

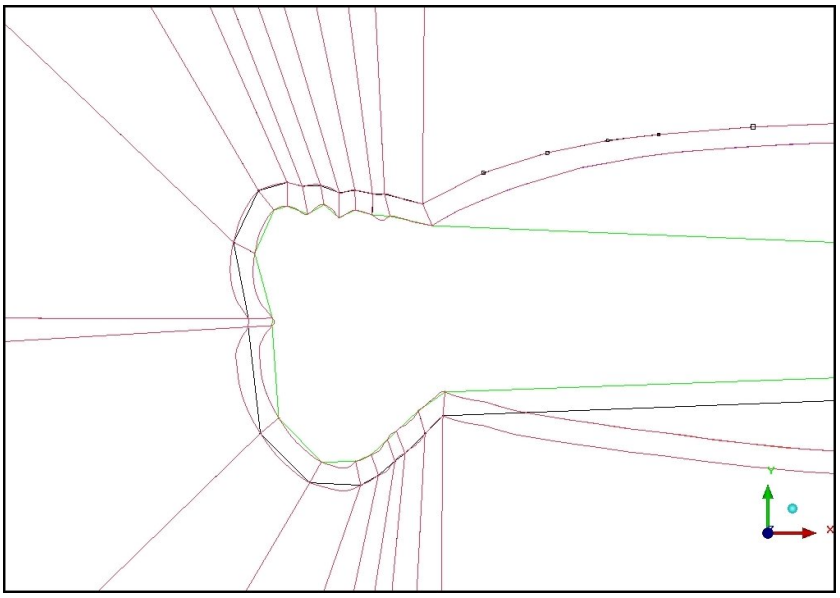

Figure 5.28: Profile curves (green) and blocking topology (with red edges) for profile 128.

The majority of block splitting involves splitting of the edge associated with

the aerofoil surface. This is to ensure sufficient discretisation of the topology to allow accurate representation of the profile geometry, without poor quality cells being influenced by highly variable curvature. A good rule of thumb is to ensure that any one block representing a region of fluid adjacent to the solid surface covers an area with continuous curvature. Block boundaries at points of inflection of solid surface curvature are effective tools for dealing with highly variable geometry. If there exists a gentle undulation in surface curvature, it is normally possible to have one block cover that region without encountering grid quality problems. The block discretisation examples presented in figures 5.29 and 5.30 give examples of good practise working effectively.

Once an appropriate number of splits has been made in the chordwise direction an appropriate number of splits should be made away from the wall. The first of these will allow appropriate grid spacing in the region next to the profile surface for boundary layer resolution. Any further splits can be introduced to create blocks whose vertices can be moved in order to ensure maximum grid orthogonality, especially regions of highly changeable curvature.

Once the blocking topology is complete and all vertices, edges and faces are associated to the relevant points, curves and surfaces; the next step is to set the grid-node distribution. In doing this it is initially wise to use the 'copy to all parallel edges' option to reduce user time involved in setting spacings on edges requiring a common grid distribution. The boundary layer spacing should be such that the y^+ value is equal to unity and grows at a rate of 1.1 away from the wall. Constant spacing around the aerofoil would be a suitable choice and an appropriate selection of spacing should be made, something of the order of 0.1 to 0.5 millimetres would likely be acceptable around the ice profile. Being smaller than the 1mm resolution of surface roughness achieved in tracing the ice accretion, these spacings would ensure that the surface of the captured profile is adequately represented. Mesh spacing in the normal direction should be selected to allow grid resolution to be coarsened when

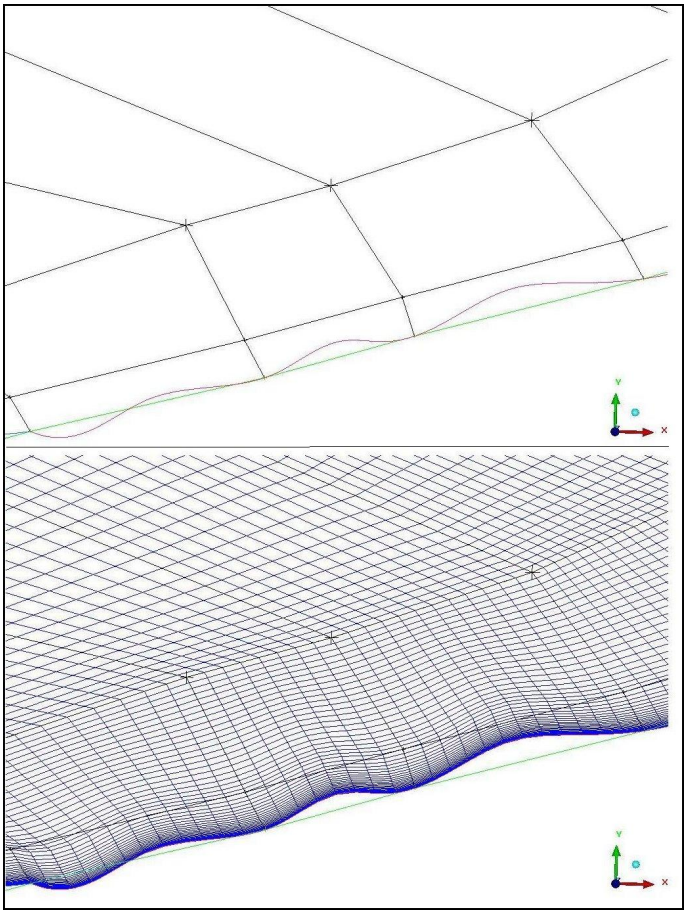

Figure 5.29: Example of multiple blocks being used to successfully negotiate undulating geometry.

moving away from the wall and into the far-field.

Once the nodal distribution has been set the 'pre-mesh option' under blocking should be selected to view the mesh as it is. This should allow visual inspection of the grid and its quality and allow correction of any obvious problems. It is also necessary to use the ICEMCFD tools to ascertain the quality of the cells within the grid. There are many parameters that can be used to ascertain quality and these are often related, so it is not necessary to select too many. Two very useful parameters are angle and volume. If the minimum skew angle is greater than 20° then this is considered acceptable,

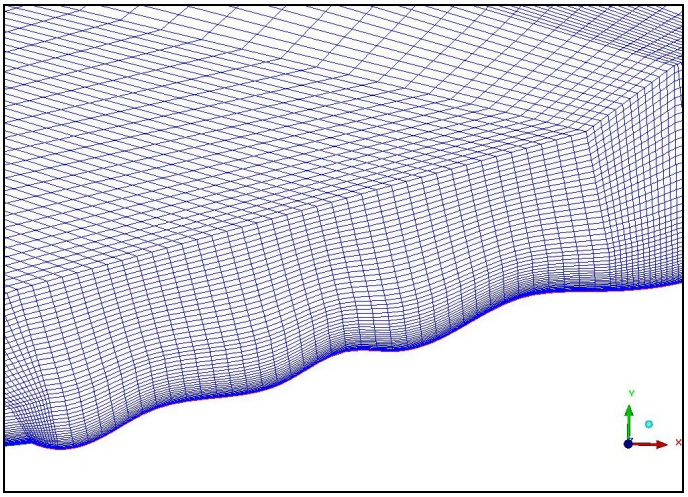

Figure 5.30: Example of a single block being used to successfully negotiate undulating geometry.

(Guo et al., 2005)[15]. By highlighting regions of cells with poor angles it is possible to modify the blocking topology to ensure adequate quality. All volumes must be positive and must have a local coordinate system that abides by the right-hand rule. Negative volumes in 2D suggests grid-line interference and will require definite attention.

Finally nodal distributions at topological boundaries must be matched to ensure grid smoothness. This is done by adapting the nodal distributions on edges where unacceptable changes in cell size exist. It is important to deselect 'copy to all parallel edges' for this activity since modifications do not need to be made to parallel edges (including the profile edges). The area where this activity is most intense is at the far-field. Upon completion of a 2D grid this can take 1-2 hours.

Once the 2-D grid is complete it is time to complete the pseudo-3D grid by taking the following steps:

[15]This angle was quoted in reference to CFX-TASCflow. It is also applicable to other CFD applications including grid generation with ICEMCFD. TASCflow and ICEMCFD are both ANSYS products.

1. Copy the 2D points, curves and surfaces to a location in the z-direction equal to the aerofoil chord (clean).

2. Create 3D surfaces for the profile and for the far-field.

3. Extrude the 2D blocking topology to create a 3D mesh that fills the 3D geometry. Vertices, edges and faces already associated will be automatically associated to the corresponding points, curves and edges in three dimensions.

4. Associate the faces comprising the profile with the corresponding surfaces. Similarly associate the faces comprising the far-field with corresponding surfaces.

5. Check the cell quality again using both angles and volumes. Attend to any areas where further treatment is required.

Once this is complete the grid should be converted into a Multiblock mesh using meshing options and exported in .grd format using the Multiblock-info output option for writing grid files. Figure 5.31 shows the result of this procedure for the simple case whose blocking topology was presented earlier. In attempting this procedure, or a variation thereof, the ANSYS ICEMCFD user manual is of significant assistance.

The solver used was the University of Liverpool PMB3D CFD code (formerly University of Glasgow PMB3D CFD code) (Woodgate et al., 1999) which is a three-dimensional fully implicit unsteady multiblock code for solution of the Reynolds Averaged Navier Stokes equations. The solver was implemented in steady mode, i.e. it marched towards a steady state solution, using an upwind discretisation scheme with second order accuracy. Early iterations were performed explicitly to solve the differential equations using time marching. This provided a preliminary prediction to serve as a start-point for implicit solution of the system of equations at all grid points.

Literature sources generally report limited success in matching CFD data for heavily iced (glaze) profiles with established experimental data. Many

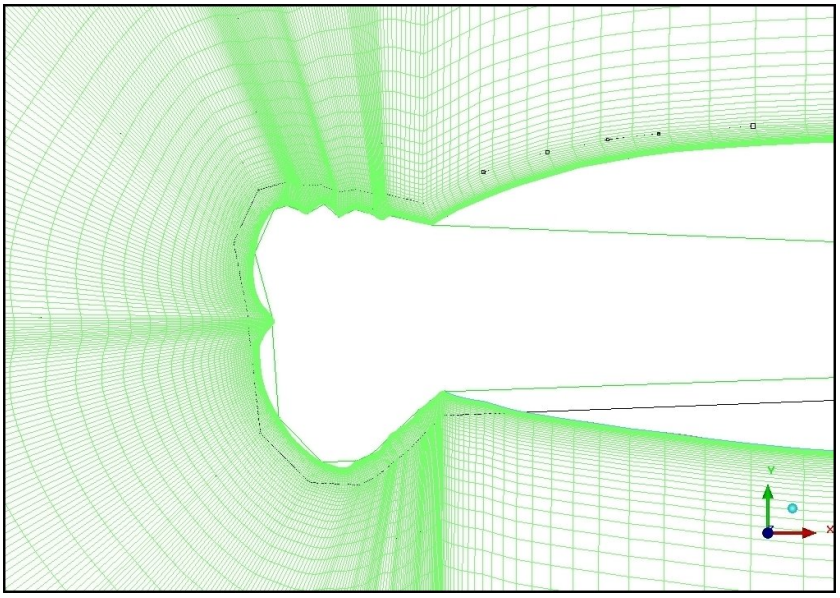

Figure 5.31: High quality mesh generated for profile 128.

such sources report the closest predictions in matching C_L and C_D[16] data with experiment using the Spalart-Allmaras turbulence model. This model is a one-equation turbulence model that solves for turbulent viscosity, whose original applications primarily included attached flows for aerospace applications. With flows for ice accretions involving large flow separation, and subsequent reattachment, the reason for this model's superiority over others was not clear. In contrast the k-ω model, a two-equation algebraic model solving for turbulence kinetic energy (k) and the specific dissipation rate (ω), is applicable to both attached and separated flows (Inc., 2006). On this basis the k-ω model, the turbulence model most established in the use of the PMB code, was selected for the CFD analysis.

This code was employed for CFD prediction of the airflow behaviour around each of the profiles in figure 5.27 and also for the uniced aerofoil at predetermined angles of attack. In each simulation 200 iterations were performed

[16]Within literature sources considering aerodynamic penalty of ice accretions, lift and drag are by far the most common measures used for comparison. Therefore this was adopted in the current study.

explicitly, after which an implicit approach was used. The total number of iterations performed for each computationally generated profile was 20,000. This number of iterations was performed to ensure the solution reached a steady state. PMB reports iterative convergence in terms of the k and ω residuals, where the convergence criteria is typically set to be $1E^{-5}$. In running the solver for the five ice profiles, it was observed that convergence in terms of k and ω residuals did not guarantee a steady solution in terms of C_L and C_D. Therefore in order to ensure solution convergence to a steady state, additional criteria were used. Convergence parameters were determined in terms of C_L and C_D as follows:

$$R_{C_L}(\%) = 100(\frac{C_{L_n} - C_{L_{n-100}}}{C_{L_{n-100}}}) \tag{5.14}$$

$$R_{C_D}(\%) = 100(\frac{C_{D_n} - C_{D_{n-100}}}{C_{D_{n-100}}}) \tag{5.15}$$

where values were reported every 100 iterations, i.e. at 100, 200, 300, ... , n-100 and n iterations.

In general, solutions were considered to have converged if the magnitudes of R_{C_L} and R_{C_D} were less than 0.2%. Where either C_L and C_D were small enough that very small changes led to unrepresentative values of R_{C_L} and R_{C_D}[17], the iterative history of C_L and C_D were examined to determined the adequacy of solution steadiness.

Once the solution had converged the data was post-processed using both Excel and TecPlot. Excel was used to calculate C_L and C_D whilst TecPlot allowed generation of velocity and pressure contours, as well as plotting of the pressure coefficient distribution around the profile. C_P distribution proved useful on occasion for more detailed inspection of results but this was difficult and time consuming because of the complexity of the geometry involved. An

[17]E.g. if $C_{L_{n-100}} = 0.050$ and $C_{L_n} = 0.05015$, $R_{C_L} = 0.3\%$

example of the solution for one of the computationally generated profiles is presented in figure 5.32.

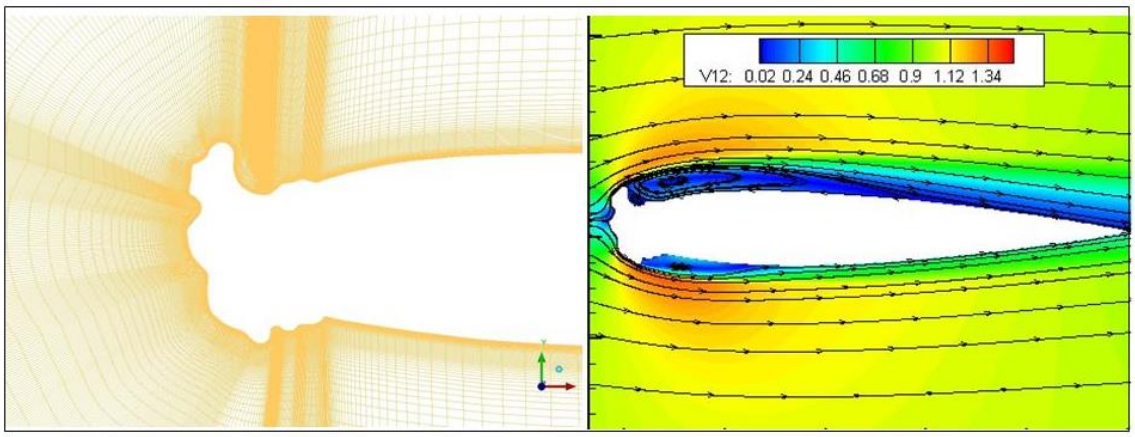

Figure 5.32: Mesh and flow solution (in the form of velocity contours with streamlines) for profile 3T1. Local velocity magnitude is presented as a ratio of freestream velocity, by the parameter 'V12'.

The capability of the CFD technique was assessed by comparing results for each profile with values generated by experiment and with data from sources in open literature. Description of the experimental approach and subsequent assessment of the CFD follow.

Experimental Prediction of the Aerodynamic Properties of Iced Aerofoils

To provide experimental data against which CFD results might be compared, the Cranfield University low-speed wind tunnel was used to undertake an experimental assessment of lift and drag for each of the iced profiles and the clean model.

This firstly required the NACA 23015 aerofoil wing model and 'ice shapes' to represent the computationally generated profiles. The wing model had been made in advance of this wind-tunnel programme and the ice shapes were

manufactured from a high density foam. The profile coordinates were used to make metallic templates that were used to guide the wire that carved the ice shapes from the foam. One of the foam profiles is presented in figure 5.33.

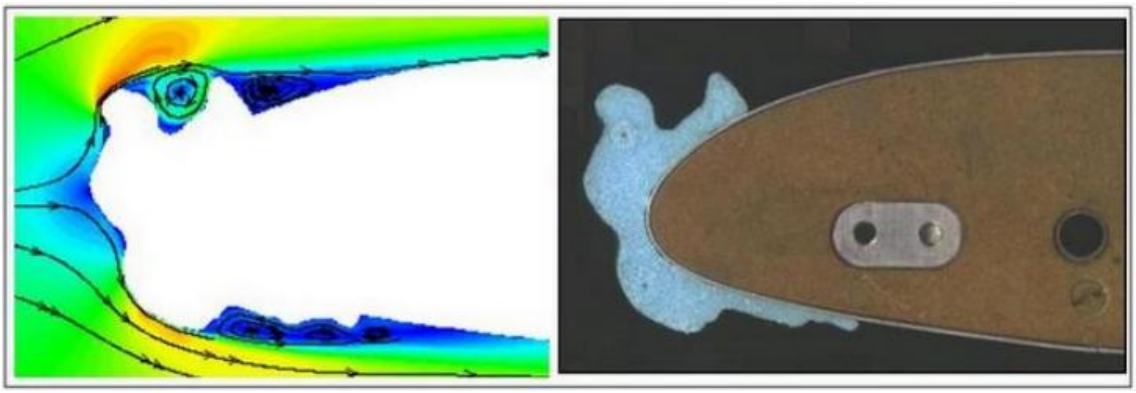

Figure 5.33: Comparison between CFD profile (in velocity contour plot) and profile created for experiment, both representing shape 3T5.

Limitations in this technique were observed when small features required shaping of the foam beyond what was feasible. This appears to have affected one aspect of the experimental measurements used in assessing the CFD methodology. This is discussed further in this section.

Figure 5.34 shows the experimental arrangement in the aerodynamic wind-tunnel. The model was mounted between two end-plates and connected to the six degree-of-freedom mechanical balance above the working section for measurement of forces and moments.

Lift and drag assessments were undertaken for three different values of test-section velocity for the clean wing section and for profile 137 (airspeed was monitored using a readout that displayed dynamic pressure). These were $25.0ms^{-1}$, $37.5ms^{-1}$ and $50.0ms^{-1}$, giving Reynolds numbers of approximately 0.8E+6, 1.2E+6 and 1.6E+6 respectively. Thereafter the test-section velocity was restricted to $25.0ms^{-1}$, as there seemed to be minimal Reynolds number effects for iced profiles, and because it was felt that at higher veloci-

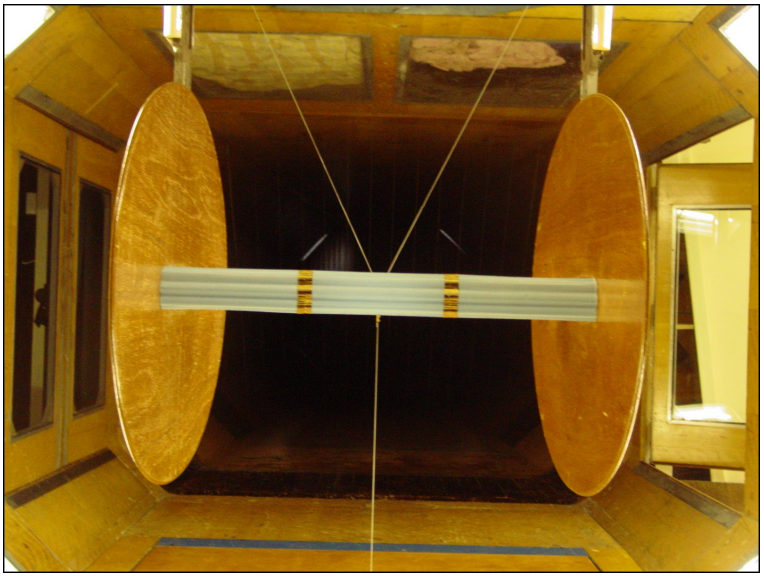

Figure 5.34: Photograph showing the experimental set-up in the aerodynamic wind tunnel.

ties the foam shapes might detach from the model. The mounting mechanism incorporated tensile wire tethers (pictured in figure 5.34) that were used to control the angle of attack of the aerofoil. Thus for each of the five profiles, values were recorded for normal, streamwise and sideforces and also moments. Using a spreadsheet model these values were used to calculate preliminary estimates for C_L and C_D for each angle of attack during the tests. To attempt to identify the lift curve slope and stall angle for each profile, the angle of attack was increased incrementally from a starting value (e.g. -4°) by 4° until a reduction in lift curve slope was detected or until a maximum of $20°C$ was reached. In the regions where pertinent trends in results were identified a number of additional measurements were taken at intermediate angles of incidence.

Before the loading results could be used the data had to be corrected to remove the additional loading caused by the presence of the model supports and end-plates; and to remove the influence of the wind tunnel walls upon the test section airflow and subsequent angles and aerodynamic coefficients.

Once the tare loading had been calculated for velocity and incidence and the values were subtracted from the original balance measurements for lift force, drag force and sideforce; the data was corrected according to techniques provided by Rae and Pope (1984). Corrections considered included buoyancy, solid blockage, wake blockage and streamline curvature corrections. These terms can be explained as follows:

- Buoyancy - development of the boundary layer (thickening) along a working section of fixed dimensions results in a reduction in effective area for the freestream to pass through. Therefore according to continuity a pressure drop will exist exerting additional force on the model which would not exist were the walls not present. This force is known as buoyancy.

- Solid Blockage - the model, mounting supports and end-plates all contribute to a reduction in cross-sectional area available for the same mass flow to negotiate the working section. The subsequent addition to the aerodynamic loading is attributed to the solid blockage.

- Wake Blockage - When the flow around the model is fully attached the detachment of the boundary layer at the trailing edge creates a very small wake. This wake is larger for flows where the boundary layer is thicker or separated. The air in the wake has a decreased velocity relative to the freestream so again there is an incremental increase in airspeed outside the wake to maintain continuity. The additional loading associated with this phenomenon is known as the wake blockage. The effects of this blockage are therefore dependant upon body shape and angle of attack.

- Streamline Curvature - The presence of the walls restricts the curvature of the streamlines in the upwash and downwash regions. This creates artificially high angles of attack and lift coefficient, and is dependant upon the dimensions of the working section and the size of the model.

Following consultation with colleagues in Cranfield's Aerodynamics, Performance and Control group, it was decided that a correction for buoyancy was

not necessary. This was because of the low-speed wind tunnel's negligible working section pressure gradient due to buoyancy, with the C_p change measured at $0.00004m^{-1}$.

When positioned in the wind tunnel, the model did not fully span the working section and was supported by internal apparatus. Consequently the three dimensional blockage correction technique was applied. Likewise the three-dimensional wake blockage correction was applied, and was proportional to uncorrected drag coefficient. These two terms were summed to calculate the total blockage correction which therefore reflected the contributions to solid and wake blockage for fully attached, separating and fully separated flow. The variance of total blockage with uncorrected drag coefficient was advantageous because this accounted for differing degrees of separated flow that could occur at lower-than-normal angles of attack with ice accretions. Details of the methods applied for each of these calculations are provided by Rae and Pope (1984).

The use of end-plates to attain a two-dimensional flow over the model led to the use of the two-dimensional correction for streamline curvature. The tunnel height was significantly greater than the model thickness and the effect of streamline curvature proved minimal.

After completion of the wind tunnel test, a further source of error was identified. Examination of photographs (see figure 5.35) showed that several screw heads had been left exposed, and once this was identified it was not possible to re-test. Furthermore, the quality of surface finish, with small scratches evident in the spanwise direction, was a potential source of error in the values determined for drag coefficient. These sources of error could not be reliably quantified following the test programme and so the data could not be corrected accordingly.

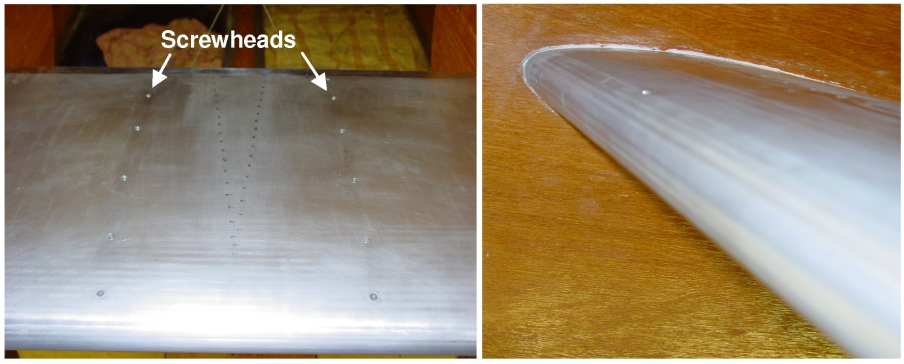

Figure 5.35: Photograph showing the clean wing section with exposed screw heads.

Assessment of CFD Capability for Prediction of Clean Aerofoil Performance

Section 5.2.2 identified the requirement for the CFD technique to ascertain trends between ice accretions. To assess the CFD capability, the first stage was to evaluate the results generated for the clean aerofoil. Figure C.1 (in Appendix C) presents the variation of C_L and C_D with α for experiment and CFD. The error bars represent the standard deviation of the discrepancy present in repeated experimental measurements.

As is evident from figure C.1, the agreement between experiment and CFD for lift coefficient is poor. Good agreement exists only at α = -3.6°, where the two values differ by approximately 0.02 units. Thereafter the different slopes of the two lift-curves lead to increasing discrepancies between experiment and CFD. The difference is greatest at α = 14.4°, with a value of approximately 0.3 units. The prediction of maximum C_L also differs in incidence, with experiment predicting the peak value of lift 2° later than CFD, at α = 18.4°. The discrepancy between the experimental and CFD data is notably greater than that explainable by experimental repeatability.

With this unexplained discrepancy in C_L data present, the CFD data has been further compared against accepted data for the NACA 23015 aerofoil,

as published by Abbott and Von Doenhoff (1959). The data presented from Abbott and Von Doenhoff is for a Reynolds number of approximately 2.6E+6. In addition to presenting data in curve form for C_L and C_D in figure C.2, Abbott and Von Doenhoff also present additional information for the NACA 23015 (in the section 'Experimental Characteristics of Wing Sections'), including:

1. Slope of the straight-line section of the lift curve slope ≈ 0.103 units/°, compared with ≈ 0.097 units/° as predicted by PMB.

2. Maximum C_L (at Re = 2.6E+6) ≈ 1.50 units, compared with ≈ 1.47 units as predicted by PMB.

For the purposes of data comparison, the lowest available Reynolds number for the NACA 23015 in Abbott and Von Doenhoff was 2.6E+6. This is greater than the 0.8E+6 applied to the CFD simulations and some degree of discrepancy between CFD and Abbott and Von Doenhoff data would be expected. It would not however, be expected to alter the slope of the straight-line section of the lift curve, which agrees well with CFD. Also, given the generally similar Reynolds number regimes (with both greater than the critical Reynolds number), the difference in C_L and α at maximum lift between Abbott and Von Doenhoff and CFD might be expected to be relatively small. Accepting that CFD would not be expected to precisely agree with the established Abbott and Von Doenhoff data approaching stall, and that some degree of uncertainty will be present in both sets of data, good agreement for C_L between both sources suggests the CFD method is generally satisfactory in determining clean aerofoil lifting behaviour.

Examination of C_L curves for the three different data sets suggests that there is an unidentified source of error in the experimental data generated in the low-speed wind tunnel at Cranfield. Its effect on the lift curve is to reduce the overall slope, move the C_L-axis intercept very close to zero (which might be expected for a low-camber aerofoil), and delay/reduce the value of C_L at the point of maximum lift. Further examination of Abbott and Von Doenhoff

(1959)[18] was unable to identify any aerofoil sections from the NACA 4-digit, 5-digit, 63-, 64-, 65- or 66-series with a similar lift-curve slope.

At present it is only possible to speculate as to the source of this error. Following the test the wing profile geometry was confirmed to match NACA 23015 geometry, and this is not believed to have caused the discrepancy. Furthermore the error introduced by the exposed screw heads would be expected to predominantly affect drag. It seems this discrepancy must have resulted from some other aspect of the experimental arrangement as yet unidentified.

Examining figure C.1 to assess the agreement for C_D between CFD and experiment, would suggest that whilst the agreement away from low angles of attack is poor, the two modelling techniques predict a C_D range that is similar. Using figure C.2 for additional comparison, suggests that the predicted values for drag are too high for both CFD and experiment.

The experimentally over-predicted values for C_D imply that one or more sources of error has led to artificially high readings being taken for C_D. It seems plausible that the source of the unknown error in the lift readings could contribute to the drag readings. It also seems plausible that the exposed screw heads and scratched surface finish, mentioned in section 5.2.2, could contribute to the discrepancy in drag readings in comparison with Abbott and Von Doenhoff's established data. The magnitude of this contribution to wing drag could be determined, but would require further assessment.

Drag over-prediction seems to be relatively common within CFD modelling, (Levy et al., 2002), (Rumsey et al., 2004), (Cosentino, 2007). According to Cosentino:

'Drag calculation is another general area of CFD weakness. Since the drag is usually, for most aircraft configurations, small when compared to the lift

[18]Figure 57. Variation of lift-curve slope with airfoil thickness ratio and camber for a number of NACA airfoil sections in both smooth and rough conditions.

and moment forces, inaccuracies play a larger role in the values obtained. Also, since drag onset due to separation is largely a viscous-dominated flow characteristic, the extent of separation is difficult for CFD to compute well. This weakness will manifest itself when comparing drag polars of the configuration to the wind tunnel data. It should be mentioned here that even for the benign flow conditions and lower angles of attack, the absolute drag computed by the CFD method may be "off" by an almost constant increment over the entire range of the data, diverging finally at the more severe conditions. This increment may come about from the difference between the calculated skin friction drag and the wind tunnel data.' Cosentino (2007).

With PMB as the solver, the overprediction in drag can be characterised to a certain degree, by Cosentino's observation above. At low angles of attack (-4.4° $\leq \alpha \leq$ 4.4°), the drag curve describes C_D values up to 0.0085 units greater than the equivalent curve describing Abbott and Von Doenhoff's drag data, however, 'divergence' occurs earlier, from around 4.4°.

Divergence, as it is termed above, is evident at lower angles of attack. By α = 8.4°, the discrepancy between CFD and Abbott and Von Doenhoff's drag data has increased to approximately 0.011 units, and to 0.023 units at α = 14.4°.

In contrast to the clean aerofoil, the drag for iced profiles is dominated by boundary layer separation at relatively fixed locations and the associated turbulent wakes. It is therefore plausible that the cause of the discrepancy evident for the clean aerofoil, will be less influential for iced aerofoil profiles.

Assessment of CFD Capability for Prediction of Iced Aerofoil Performance Degradation

Comparisons with experiment were performed for each of the five ice profiles. The experimental and CFD results for C_L versus α and C_D versus α

are presented for each profile in figures C.3 to C.7. Figures C.3 to C.7 each contain plotted data generated via experiment, from CFD using a standard (or coarse) grid, and from CFD using a denser, more refined (or fine) grid. Once again, the error bars represent the standard deviation of the discrepancy present in repeated experimental measurements.

Figure C.3 presents results for ice profile 128. Agreement between experiment and CFD for C_L is generally poor. At negative incidence, C_L predicted by CFD is notably greater than that predicted by experiment. This discrepancy reduces with increasing α (due to differing curve gradients), before the curves intersect and diverge ahead of maximum $C_{L_{Exp}}$. One of the main differences between the curves produced by experiment and CFD, is the lack of a pronounced 'drop' in $C_{L_{CFD}}$, in contrast to $C_{L_{Exp}}$, at the expected stall incidence (identified using velocity contours) of $\sim$6.4°. Agreement between experiment and CFD for C_D is generally better, especially with respect to the overall shape of the curves, but there remains a discrepancy between $C_{D_{Exp}}$ and $C_{D_{CFD}}$. This discrepancy is most notable for $0.4° \leq \alpha \leq 10.4°$.

Figure C.4 presents results for ice profile 136. Agreement for C_L is good for $\alpha \leq 0.4°$, though this worsens where there is a general reduction in slope at greater positive incidence for the CFD prediction. Again a pronounced drop in $C_{L_{CFD}}$ is not present, and the lack of this feature, in comparison with experiment, contributes to poor agreement from $\alpha > 0.4°$. Instead of a pronounced drop, the CFD curve exhibits more of an inflection at the expected stall incidence (identified using velocity contours) of $\sim$4.4°. Agreement between for C_D is generally fair, though more notable differences exist for $0.4° \leq \alpha \leq 6.4°$.

Figure C.5 presents results for ice profile 137. Agreement for C_L is generally poor, except where the curves from experiment and CFD converge due to differing slopes, and at $\alpha \geq 14.4°$. A slightly more pronounced inflection in the CFD curves exists around the expected stall incidence (identified using velocity contours) of $\sim$8.4°. Agreement for C_D is generally at least fair, ex-

cept for $4.4° < \alpha < 12.4°$, where there is a more pronounced discrepancy.

Figure C.6 presents results for ice profile 3T1. Agreement for C_L is generally poor, except where the curves from experiment and CFD converge due to differing slopes, and at $\alpha \geq 8.4°$. A relatively pronounced inflection in the CFD curves exists at the expected stall incidence (identified using velocity contours), approaching $\sim$4.4°. Agreement for C_D is generally good, except at $\alpha = 0.4°$ and $\alpha = 4.4°$, where there is a more pronounced discrepancy.

Figure C.7 presents results for ice profile 3T5. Agreement for C_L is generally fair at $\alpha \leq 0.4°$. The C_L curves for profile 3T5 exhibit an observable drop in C_L, and at similar values of α as experiment. However, these maximum values for $C_{L_{CFD}}$ are notably less than $C_{L_{Exp}}$, and agreement is generally poor approaching, and after, maximum C_L. Agreement for C_D is generally at least fair for a large range of angles of attack, though less so for $\alpha < 0.4°$ and $\alpha \geq 7.4°$, where there is a more pronounced discrepancy.

Comparisons between experiment and CFD for each ice profile above, have identified that the CFD generally differs from experiment, in terms of lift curve, with a lower slope at low values of α and an inflection in the curve where experiment defines a pronounced drop at stall. This is confirmed in figure C.8. Plotting the C_L curves for all five profiles, for the the experimental data, also highlights that for low positive, and negative angles of attack (-4.4° $\leq \alpha \leq$ 4.4°) there is little difference between the experimental predictions of lift. In contrast the plots of CFD predictions suggest notable differences between profiles across the range of incidences, and these are greatest for angles up to approximately 10.4°. In comparing trends for C_L the overall agreement is at least fair. Away from the angles where very similar values were determined, experiment predicted the most detrimental profile to be 3T1, followed by 3T5, 136, 128 and 137, whilst for $\alpha > 0.4°$ CFD predicts the most detrimental profile to be 3T1, followed by 136[19], 3T5, 128 and 137.

[19]Upon examination of the foam shape used to represent profile 136 for the experiment, and comparing with the shape used for CFD, the upper surface horn feature is flatter

Comparison between experiment and CFD for each profile, for drag, identified that agreement between the two was generally fair, with examples of better agreement across the five profiles. There were also several discrepancies between experiment and CFD, where the agreement was relatively poor. The effect of these discrepancies is evident in figure C.9, where identification of areas of good agreement between experiment and CFD is less straightforward. As a result, the spreadsheet presented in figure C.10 was used to present rankings of drag coefficient for the five profiles at selected angles of attack. Referring to figure C.10, the trends between experiment and CFD generally agree within $4.4^\circ \leq \alpha \leq 6.4^\circ$, except where there is a reversal of the trend between 136 and 3T5 in comparison between experimental and CFD data. Outside this range, agreement worsens.

On the basis of the comparison between trends in C_L and C_D for experiment and CFD, for the profiles 128, 136, 137, 3T1 & 3T5, the CFD would be most likely to correctly ascertain trends between ice accretions within a relatively limited angle of attack range, $4.4^\circ \leq \alpha \leq 6.4^\circ$, where the range for C_L alone would be slightly greater, as specified above. Where there was a notable degree in ambiguity in the ranking of ice accretions undertaken above, this is considered to be partly attributable to experimental fidelity and partly attributable to the overall limitation in capability of the CFD technique. Given the limited confidence in the experimental results (arising mainly from the issues associated with the assessment of the uniced aerofoil), it is not possible to quantify the degree of uncertainty associated with the CFD results.

Nevertheless, in order to be able to rank the ice profiles generated within the CIRT, it was decided to proceed using CFD, accepting that the application of CFD in order to rank experimentally generated ice accretions is limited,

and less sharp. This discrepancy is due to the accuracy of the manufacturing method and would be expected to produce a less detrimental effect upon lift and drag. This may, at least partially, account for the differing positions of profile 136 in the trends identified by experiment and CFD.

and that the results should be treated with care.

Grid Dependence Study

The grid dependence study generated two curves for each profile. Both grids had a y^+ value of 1 at the profile surface. In the block adjacent to the wall the coarse grid had 31 nodes in comparison with the fine grid's 44. In the next block away from the wall the coarse grid had 12 nodes in comparison with the fine grid's 24. Hence in the normal direction the coarse grid is slightly less densely spaced in the block adjacent to the wall, and further coarsened in the subsequent block. In the chordwise direction, the coarse grid had spacing of 0.3mm per cell in comparison with 0.1mm for the fine grid.

The CFD data for both shows that there are some differences between the results. Again considering each profile individually:

128 (figure C.3) The C_L and C_D data produced for this profile differed little suggesting grid independence.

136 (figure C.4) Discrepancies exist for this profile with $C_{L_{coarse}}$ being greater than $C_{L_{fine}}$ at $\alpha = 4.4°$ and above by around 0.06 to 0.08 units. Drag agreement, however, was good.

137 (figure C.5) Some discrepancies existed for this profile between coarse grid and fine grid data, but it was discovered that this was primarily because the coarse solution would have achieved better convergence with further iterations.

3T1 (figure C.6) Agreement between coarse grid data and fine grid data was fair for C_L beneath $\alpha = 10.4°$ and was very good for drag at similar incidences. Agreement in C_D was good at higher incidences also.

3T5 (figure C.7) Agreement for this profile between coarse grid data and fine grid data is excellent until stall, where the coarse grid solution predicts stall up to two degrees later than the fine grid data (the coarse

grid agrees with experiment for the stall incidence). Drag agreement is good.

As mentioned earlier, the assessment of iced profiles' aerodynamic performance was restricted very much by tight timescales. Solving on the fine grid could take over five days on the university's computing cluster, solving for eleven angles of attack simultaneously on eleven processors. The solution time for the coarse grid was approximately three days, which meant that twice as many cases could be completed per week. Some grid dependence in the solution was identified, though this was not extensive enough to justify the longer runtimes, if coarser grids could be used effectively. Subsequently the coarse grid density was employed for the CFD assessment of experimentally generated ice profiles.

Application of Linear Regression Modelling to Support CFD Assessment of Ice Accretions

The FAA (2000) provides a summarised a large number of references within existing literature that contain data, determined by experiment, that describes the performance penalty imposed by a particular ice accretion, or an artificially simulated ice accretion attached to the upper surface of the wing to simulate an upper surface glaze horn. The data, for the majority of cases, includes drag rise (ΔC_D) for specific values of α, in reference to an untapered clean wing section. Plus for a small number of cases it provides the lift loss at maximum C_L, as a result of the ice accretion.

Using this data this reference demonstrates that the loss of aerodynamic performance for an untapered, iced wing, is directly proportional to upper horn size and location. A key figure that features within this reference plots drag rise (ΔC_D) against the term[20] $(b/c)sin(\gamma+\alpha)$. This term gives the non-dimensional height of the ice or protruberance normal to an undisturbed

[20]The notation for horn size and horn orientation in FAA (2000) have been exchanged with (b) and (γ) in this document.

streamline.

Figure C.11 presents sample results from linear regression modelling performed as part of this study, in order to provide an alternate means of estimating aerodynamic performance loss due to a glaze ice accretion. For selected cases from FAA (2000), regression analysis allowed determination of models describing both lift loss at maximum C_L and drag rise (ΔC_D) with $(b/c)sin(\gamma+\alpha)$. To provide a contrasting approach to CFD prediction, these linear regression models were applied to the ice profiles generated during the CIRT experimental programme to allow an alternate method of ranking. The results of this are introduced as part of chapter 7.

Grid Generation of Experimentally Generated Ice Profiles

With development of the CFD assessment technique complete, it was necessary to undertake CFD analysis for a large set of experimentally generated ice accretions. Whilst the procedure for grid generation was essentially the same as that described earlier, it was considerably more challenging because of the enhanced roughness associated with real ice growth and intrusive upper and lower surface horns. Consequently grid generation took longer and required a greater level of skill on the part of the user.

That said, ICEMCFD proved to be very powerful as a grid generator for experimentally iced profiles and it was considered that any future users would benefit from having access to an example showing how the major steps led to the development of a high quality grid. Such an example is presented in Appendix D which describes the devlopment of the grid for the profile from case Va_LWC_30%_Fall.

5.2.3 Investigation of the Impact of Water Content, Overall Thermal Environment and Collection Efficiency on Ice Growth Potential

Over the course of the experimental investigation a large number of conditions were simulated and these involved combinations of LWC (either reference LWC of $0.41g/m^3$ or a perturbation about the reference LWC) or temperature (either reference temperature of -2°C or a perturbation about the reference temperature). Over the course of these simulations, different combinations of conditions had been observed at different stages over the duration and had coincided with varying sizes of ice accretion. Consequently it became increasingly intriguing to understand what differences exist between differing combinations of collection efficiency, cloud water content and working section temperature. The outcome was an additional technical activity designed to make a preliminary assessment of such input conditions on ice growth behaviour with a view to informing any discussion of ice accretion results.

The engineering tool employed within the activity was Trajice2, a 2D ice accretion prediction code. The theory behind this icing code is similar to certain others and detailed information can be found in the publication by Gent (1990); briefly however, the code operates as follows:

1. A panel method is used to predict the airflow over the wing section, assuming incompressible, potential flow.

2. The impingement limits for the aerofoil are calculated along with the collection efficiency distribution in between these limits around the leading edge. The collection efficiency calculation, combined with the input value for LWC, allows determination of the amount of water entering the 2D control volumes at the solid surface[21].

[21] "For the ice accretion calculation the aerofoil surface is divided into a number of equi-spaced elements..." (Gent, 1990)

3. Surface temperature and freezing fraction are evaluated according to the Messinger model (Messinger, 1953) before "the local ice growth rate is calculated from freezing fraction and an ice profile is obtained by extrapolating the growth rates to the given time in icing." (Gent, 1990)

Further explanation of the theory implemented in icing codes of the Trajice2 generation can be found in Potapczuk et al. (1997).

Over the course of the investigation Trajice2 was run using nine sets of conditions for three pre-specified ice profiles, making twenty seven cases in total. The three profiles that were used for the investigation are presented in figure 5.36 with conditions as described by cases (a) to (i) in table 5.1.

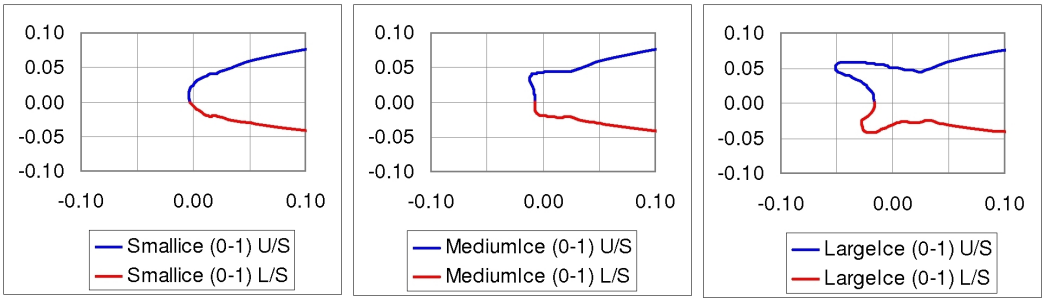

Figure 5.36: Small-ice, medium-ice and large-ice; the three profiles created for the Trajice2 investigation.

LWC/Temp	$0.1g/m^3$	$0.4g/m^3$	$0.7g/m^3$
$-0.5°C$	Case (a)	Case (b)	Case (c)
$-2.0°C$	Case (d)	Case (e)	Case (f)
$-3.5°C$	Case (g)	Case (h)	Case (i)

Table 5.3: The nine combinations of conditions simulated in the Trajice2 investigation into the combined impact of collection efficiency, LWC and temperature.

Each case was run at the same velocity, angle of attack and droplet distribution as the reference conditions for a five minute period. In using Trajice2

this exercise proved quite useful because of the data generated by the code for each case. The results files for each case included: collection efficiency distribution, freezing fraction distribution and growth rate distribution around the leading edge. Subsequently the growth rate distribution (defined by Gent (1990) as the local surface ice growth rate in millimetres per minute, mm/min) was used as the indicator of ice growth potential for each of the cases simulated. This was considered to be a good measure of icing severity for this investigation.

This page has been left intentionally blank.

Chapter 6

Commercial Results

Results from the commercial research include questionnaire responses from twenty members of the icing community, minutes from discussions with members of the aerospace industry and more. The results of the commercial research programme is presented in this chapter and associated appendices.

The commercial objectives were satisfied by means of undertaking a survey of twenty members of the icing community; by listening to the thoughts of industrialists, regulators and academics during formal and informal meetings and presentations; and by conducting desk-based research of conference & journal publications and more publicly available information such as press releases, company websites and internet-based articles. Theses results are presented in the following sections, grouped into to the topics they relate to as opposed to the research method.

6.1 The State of the Art in Ice Protection

To appreciate what benefits an understanding of variability can bring to in-flight icing applications, it is necessary to know what relevant technologies & processes exist and how these are changing due to advances in science, engineering and operations. This section provides a brief description of the

former, focusing on existing technologies and processes for in-flight icing that are relevant to the research.

Candidate sets of conditions with the potential to generate the critical ice shape[1] are identified using the Appendix C icing envelopes as described by Yeoman (1989) and Parkins (2007), as mentioned in section 3.2. In doing so engineers need to consider "geometric design of the aircraft, the atmospheric environment, the design envelope of the aircraft and the operational envelope of the aircraft" (Parkins, 2007). The earlier candidate shapes can be identified the better, as they can impact a number of design considerations including "selection of ice protection systems and power budgets for ice protection"(Parkins, 2007). The Appendix C icing envelopes are utilised to specify sets of candidate conditions and these do not incorporate atmospheric flight-path variability.

A wide range of aircraft exist that are certified for flight into known icing conditions and the majority of these have some degree of ice protection. Such a range, that includes very large aircraft such as wide-body (e.g. Boeing 747) and narrow-body jets (e.g. Boeing 757) as well as moderately sized regional airliners (e.g. ATR 72) and small commuter aircraft (e.g. Cessna Caravan), employs a correspondingly wide range of ice protection systems suited to the different protection requirements and to limitations such as space, weight and power availability.

The main types of ice protection system include bleed-air anti-icing systems and pneumatic de-icing systems. Such systems have been installed and certified for flight on a large number of aircraft for many years. Other more recent types of system include electro-thermal anti-icing systems and fluid-based ice protection systems. Bleed-air anti-icing systems use the hot air to heat aerodynamic surfaces so that they remain free of ice. Electro-thermal systems

[1]Parkins (2007) recommends consideration of shapes associated with: 45 minute hold - unprotected surfaces; failed deicer while in a hold; delayed deicer activation; intercycle ice; ice contaminated tailplane stall; runback ice shapes; large droplet icing, and icing during take off.

do the same, but employ electrical methods for heat generation. Pneumatic de-icing systems inflate periodically to alter the geometry of the protected surface and break off any ice present. Fluid-based systems release a solution from a permeated surface so that the solution coats the wing (or other part) and prevents the freezing of impinging water.

The future of such systems is very much dependent upon the requirements of current in-service aircraft, of aircraft being developed presently, and of future aircraft. In 2006 at the 2nd International Conference on Icing Technology, Wells (2006) spoke of ice protection implications of future engines; stating a belief that bleed-air ice protections systems would remain as a highly utilised option for the medium-term. Certainly companies prominent within the ice protection business continue to recognise that this system has a place within their portfolios, including Goodrich with its RohrSwirl system for engine inlets (Goodrich-Anti-Ice, 2007) and Hamilton Sundstrand who offer wing bleed-air anti-ice as one of its products. Indeed the continuance of bleed air would seem to be confirmed by its use on the all of the Airbus fleet (Barley, 2007), presumably including the A380. However the publication by Barley (2007) actually reports research efforts by Airbus that investigate the possible incorporation of electro-thermal and electro-mechanical ice protection systems into their aircraft. This is reportedly due to efficiency considerations.

Pneumatic systems are commonly found on smaller aircraft with altogether different requirements and limitations to larger aircraft, and whose power generation capabilities are insufficient to allow implementation of bleed-air systems. Aircraft that might consider a pneumatic system include small commuter aircraft and regional airliners. This category is therefore of significant size, making provision of products suitable for these aircraft a lucrative business opportunity. Companies offering such products include Goodrich (Goodrich-De-Ice, 2007) with its FASTboot pneumatic de-icer and Cox & Co (Cox&Co, 2007) with its EMEDS product.

Other systems that are becoming, or have become prevalent in the IPS mar-

ket are fluid-based systems that inhibit the freezing process by introducing a freezing point suppressant (such as the TKS Ice Protection System by Flight-Ice, Inc., (Flight-Ice, 2007)). It seems though, that much of the current direction is towards electro-thermal anti-icing technologies. One of the most widely publicised adoptions of this technology was that of the Boeing 787, described as a 'super-efficient' airliner. Part of the drive for efficiency requires a significant reduction of bleed-air extracted from the engines, reducing the feasibility of conventional anti-ice systems.

6.2 Propensity to Support Incorporation of Flight Path Variability into In-Flight Icing Simulation

In considering the potential impact of the technical research, it was recognised that any recommendations for amendment or addition to identification of critical ice shapes might received a mixed response from the icing community. A questionnaire was designed to survey the opinion of twenty members of the icing community to see whether or not such recommendations would receive support or opposition. Full responses from this questionnaire are presented in Appendix B.

The responses to question 1(a) (figure B.1) demonstrate that a wide range of icing-involved organisations were represented by the respondents, including academic research (Cranfield University); government research (NASA, ONERA & CIRA); IPS manufacturers (GKN Aerospace and CAV Aerospace) and fixed wing aircraft, helicopter and engine manufacturers (Airbus & BAE Systems, Bell Helicopter and Rolls Royce respectively).

Answers to questions 1(b) and 1(c) demonstrate the calibre of respondents with regard to their knowledge and experience of aircraft icing which is in the majority of cases, very impressive. Moreover these respondents are cred-

ibly representative of the larger icing community whose views are taken into account during regulatory bodies' rulemaking and advisory activities.

Answers to question 2 show the type of roles respondents occupy[2], where 4 of 20 state engineer, 5 of 20 state project engineer, 5 of 20 state project manager and 6 of 20 state programme manager as the role they occupy that has maximum responsibility level. This indicates that at least half of the respondents hold positions of moderate responsibility for icing related activities within their organisation. Those selecting programme management include representatives of Airbus, GKN Aerospace, Ultra Electronics and CAV Aerospace, demonstrating the seniority of some respondents within aircraft and ice protection system manufacturing.

Answers to question 3 confirm the good technical awareness of the respondents whose activities are 60% technically oriented. Degrees to which respondents are involved in cost, scheduling, resources and overall programme management is dependent upon their role and organisation, as well as what a programme meant to each respondent. Certain respondents have significant responsibility for such matters; with respondents from Airbus, GKN Aerospace and CAV Aerospace quoting 60%, 50% and 60% of their time for such activities respectively.

Overall the responses to questions 1, 2 and 3 indicate that the respondents made a very credible group and represented a wide range of organisational types; making it likely that their responses to the remaining questions are informative, credible and reliable.

The responses to question 4 show that the organisations represented engage

[2]Where for the purposes of the survey: an engineer completes technical work including icing tasks; a project engineer has responsibility for completion of a number of technical tasks and takes a lead role in their completion; a project manager is responsible for a number of different projects at one time, that could involve aircraft icing; and a programme manager is responsible for an entire programme, e.g. the design and manufacture of an IPS for a customer.

in a large proportion of the icing tasks identified in the questionnaire and significantly; 70% have experience of using Appendix C to define critical conditions, 60% have experience of numerical icing simulation and 70% have experience of experimental icing simulation. This can only serve to enhance the credibility of answers to question 6, which relates to icing simulation using Appendix C conditions.

Answers to question 5(a) show that the length of an icing programme depends upon the aircraft and the organisation, but can vary from months to years. Responses from particular organisations' respondents are telling; with Airbus respondents estimating 5 years, the BAE Systems respondent estimating 3 - 4.5 years, the GKN Aerospace respondent estimating 1 - 3 years and the CAV Aerospace estimating 0.5 - 1 year. These differences in response seem to be related to aircraft size, where a small general aviation aircraft (according to CAV Aerospace respondent) takes up to a year whilst a large jetliner takes approximately five years. The majority of responses (70%) to question 5(b) confirm that icing activities are resource intensive. The Airbus comments highlight this, mentioning activities like ice prediction modelling, wind tunnel testing, ground test rigs, icing tunnel tests, CFD and flight testing. Answers to question 5(c) might suggest that icing activities are very costly, but perhaps less so in comparison with the overall programme. The respondent from Bell Helicopter added a pertinent comment however, explaining that "the entire aircraft certification has to be revisited to account for effects of icing." In other words unforeseen problems caused by icing need to be solved during the programme, and this requires additional attention and resources that can contribute to overall cost.

Answers to question 6(a) show that if incorporation of flight-path variability in icing conditions was shown to be important enough to be incorporated into icing simulation; and a recommendation was made to that effect, then it would receive a positive level of support. Most importantly none of the respondents said they would not support such a recommendation - with 65% answering 'Yes', 5% answering 'Likely', 10% answering 'Maybe', 15% an-

swering 'Don't know' and 5% not answering. Question 6(b) was designed to see if there were any benefits associated with considering variability that would result in a 'No' answer to 6(a) being changed to a 'Yes' answer to 6(a). The positive outcome from (a) resulted in answers to (b) being less relevant, but several comments are still indicative of what benefits respondents might welcome. These would include a reduction to the amount of physical testing (natural icing flights, icing tunnel tests), reduction of ice protection system power requirements. Other pertinent comments came from the CIRA respondent (whose organisation operates one of the world's most advanced icing facilities), who considered that icing tunnels could be upgraded to fit new requirements; a NASA respondent whose recommendation depended upon what the more accurate simulation methodology is and its potential improvement in the state of the art relative to what it is now; and an Airbus respondent who wrote: "the way we choose the critical case today, whilst not completely rigorous, is okay and it is accepted by the airworthiness authorities, so any improvement would not give any cost benefit."

Following on from the survey several meetings allowed further conversations with icing experts on the topics raised within and outwith the survey. These meetings were conducted in late 2006 and early 2007 and involved colleagues who (at the time) worked as part of Airbus UK, Qinetiq, BAE Systems and the Civil Aviation Authority (CAA).

During these meetings a number of points were made, the most pertinent of which are summarised below.

- The Airbus UK colleague commented that regulators would be interested in ascertaining how conservative estimates for the critical ice shape are.
- The CAA colleague commented that significant differences in critical ice shape would be likely to result in recommendations being taken on board. Differences not considered significant would be far more difficult to take forward.

- The CAA colleague elaborated that less significant differences would be unlikely to result in a change to regulations because of the likelihood of introducing a further degree of complexity into the requirements to generate ice shapes that are little different, or are different but have similar aerodynamic penalties.

- The BAE Systems colleague suggested that large aircraft manufacturers might accept recommendations for incorporation of variability quite readily. This was because any requirement that might emerge would have accompanying advice and instructions for incorporation into simulation activities, and additional tasks could be added to a test plan for numerical or experimental simulation.

- The BAE Systems colleague contended that if recommendations were to have associated fuel savings (e.g. through reduced bleed-air anti-icing requirements) then large manufacturers would be more likely to look upon any recommendations favourably.

- The CAA colleague suspected that were there scope for commercial benefits to arise from considerations of variability it might be eminently plausible for manufacturers to support associated recommendations. One such example of this would be the reduction of flight testing in natural icing conditions.

- The Airbus UK colleague stated that information on variability effects would be valuable to scrutinise the validation of icing codes, where real flight tests are simulated using averaged conditions to assess codes' capabilities.

- The Qinetiq colleague felt that icing codes could certainly be modified to account for variability, though some kinds of variability would be much less straightforward than others.

- The CAA colleague questioned whether flight-path variability of icing conditions was something solely to be considered in relation to safety and efficiency of aircraft of the current generation; or whether it should

be addressed as part of our continual technological development and advancement of knowledge. Should we debate the need to consider variability now or assume that an understanding will prove beneficial in the future? In speculating about future aircraft, possibly with slender wings, will ice protection capacity be traded off for stability and efficiency? In anticipation of such an event, is refining the process of simulation ultimately a good and important thing to do?

6.3 The Cost of Icing

In considering the benefits of addressing flight-path variability it is necessary to have some idea of what the costs associated with icing are. This section reports information gathered on costs over the course of the commercial research.

Questionnaire responses suggest that preventative costs[3] vary, with $30M for icing related activities identified by an Airbus aircraft icing programme manager. A different value was quoted to Thompson (2007) for a UK based helicopter manufacturer (by a relevant employee), that value being $5m; a programme duration of five years was also quoted. Furthermore the impact of icing upon the overall aircraft delivery was stressed (concurring with the statement from the Bell Helicopter questionnaire respondent); where delays to the icing programme impact the overall programme to the extent that revenues from sales of the product are not received when they otherwise would be. In such a circumstance this would inflate the costs attributable to icing significantly from $5m. Such figures are entirely believable when considering costs including (a) personnel required for (icing) encounter definition and simulation; (b) numerical simulation of ice accretions (plus purchase or development costs of the code); (c) experimental simulation (icing tunnel costs can be expected to range from $10000/day to $50000/day); (d) artificial flight tests and (e) natural flight testing. The costs for the aforementioned activ-

[3]Preventative costs include what it costs to the manufacturer and operator in aiming to ensure safe flight in icing conditions.

ities do not consider design and development of the ice protection system itself which would also amount to a significant sum.

Once entered into operation the cost of icing is incurred mainly by employing ice protection, and is incurred by the operator. One of the main drivers behind the movement towards electro-thermal ice protection systems is cost. Bleed-air systems that exist on many large-jet airliners have a direct impact on fuel consumption because pressurised hot air is extracted from the engines' compressors before being routed to heat parts of the aerodynamic surfaces, (Yeoman, 1994). According to Lear (2007) commercial airliners seating 150-300 passengers will lose up to 6% direct efficiency upon operating the ice protection system, and this reduction in mass flow has further undesirable effects over later stages in the engine. So in operating the ice protection system the aircraft becomes less fuel efficient and more expensive to operate.

The importance of icing related costs is evident upon inspection of Ryanair's annual accounts (Ryanair, 2007), where 'de-icing' costs are mentioned for the years ending 31st March 2006 and 2007 to be \$8.9m and \$6.8m respectively[4]. In comparison with the company's profit after tax for those years (\$448m and \$636m) then de-icing costs were between 1-2% of PAT for each of these two years. In comparison with Ryanair's operating expenses (\$2.7bn and \$3.7bn) this equates to approximately 0.26% per annum. Such costs are moderate in the overall scope of Ryanair's financial model but they are not insignificant and are certainly large enough to be important. Furthermore Ryanair's operational cost of icing helps estimate the cost of icing to other airlines. Many air carriers operate smaller aircraft that are more susceptible to icing (and require more extensive protection), in an environment that is more conducive to icing. So it is conceivable that for these aircraft, if operating a bleed air system, the proportion of operating cost that is due to ice protection could be nearer 1-2% as opposed to the 0.26% reported by Ryanair. This could be greater still since the drag of unprotected surfaces will increase in icing

[4]These values relate to in-flight ice protection, as they feature as part of an explanation of risk associated with rising fuel costs.

conditions, again directly impacting fuel consumption.

Another cost associated with icing is the cost of an accident. Such an event involving injury and loss of life is momentously tragic and so the financial penalties for organisations involved are huge. After the Roselawn accident of 1994 (NTSB, 1996), which was attributed to icing, 28 of 68 families accepted a settlement of $110m (Clifford-Law, 2007). Assuming a similar value was awarded to the remainder of these families the total damages are likely to have been of the order of $250m, which works out to be approximately $2.5m per fatality. When asked how much ATR and AMR Corp. (the manufacturer and airline owner respectively) paid in damages, the lawyer for ATR estimated that the two parties would have contributed approximately even amounts (Clifford-Law, 2007), though both parties would have been insured. Other costs to consider would include the loss of confidence in the ATR-72 and a resultant fall in sales for the manufacturer, a fall in passenger revenue for the American Eagle carrier and also the loss of one of the American Eagle fleet.

6.4 Potential Benefits of Understanding Flight-Path Variability

6.4.1 Ice Shape Prediction

Incorporating variability into icing simulation, were it considered necessary, poses challenges for both experimentalists and software engineers. However some involved in the development of next-generation icing software seem to be confident that accurate numerical prediction of ice accretions and their impact upon aircraft performance is eminently possible.

In a recent publication Habashi (2006) claimed that advances in the application of modern CFD methods to icing "signal an inexorable march towards

a virtual certification methodology for all types of aircraft, and simultaneously reduce the likelihood of ice-induced hazardous events in operation." If this is the case; and with codes becoming capable of accurate simulations for highly complex scenarios for helicopters and tilt-rotors, for droplet bounce and splash and for water-film modelling, the incorporation of variability should be comparatively straightforward.

Similarly incorporating variability into icing tunnels was performed, albeit in a fairly unsophisticated manner, for the experimental programme described in this thesis. An experimental capability cannot therefore, be beyond our capabilities.

Therefore, if considered necessary, the simulation of flight-path variability should be possible, and could form an integral part of any future effort towards 'virtual certification'.

6.4.2 Technological Applications

To exploit any understanding of flight-path variability effects will likely either require adaption to current technologies and/or their uses. Several of these have already been identified to be of potential use and have been mentioned in section 3.3.1. These technologies include the anti-icing valve and anti-icing management system, (Norris et al., 1989), (Rumford and Norris, 1988); and a probe capable of water content and droplet size measurements (Lilie et al., 2005). A number of alternate options for water content measurement also exist including a total water content probe developed by Tan et al. (2004). This probe is intended, ultimately, to be able to accurately measure LWC in known icing conditions. Another product that is already available is the Penny+Giles Ice & Snow Detection System, (Penny+Giles, 2007). This device provides "reliable prediction of unacceptable icing", by detecting LWC with "a rapid response time of less than 2 seconds for $1.0g/m^3$", and seems to be targeted specifically for rotorcraft.

Chapter 7

Technical Results

The experimental icing programme generated profiles, photographs and ice shape metrics for over thirty ice accretion profiles; and the aerodynamic analysis of the iced profiles generated a similar amount of information including aerodynamic performance curves and contour plots. The results of the technical research programme is presented in this chapter and associated appendices.

7.1 Results from the Experimental Icing Programme

Section 5.2 described how the different icing scenarios were designed for phases 1, 2 and 3 of the experimental icing programme. In designing and simulating the range of encounters in this programme one of the primary aims was to ensure that the duration averaged conditions for each encounter were equivalent to the reference conditions. Doing this ensured that all ice accretions generated in the experimental programme were comparable with one another in profile, geometric parameters and in reduction to aerodynamic performance capability.

In advance of phases 1, and then phases 2 & 3 that were simulated during

the same test campaign; it was necessary to undertake the calibration activities described in section 5.2.1. The instruments and display devices utilised include those for airspeed, temperature regulation and spray system air & water pressures. Following the calibration repeatability was assessed for the reference conditions.

The reference conditions were simulated on four occasions over the experimental programme. One of these was considered invalid because the average temperature recorded was insufficiently close to the -2°C target [with T_{ave} = -1.71°C[1] and $SD_{T_{ave}} = 0.14°C$]. The other three cases that were considered valid were:

1. Phase 1 Run 10Rep, with T_{ave} = -1.93°C and $SD_{T_{ave}} = 0.18°C$,
2. Phase 1 Run 10Rep2, with T_{ave} = -1.97°C and $SD_{T_{ave}} = 0.09°C$,
3. Phase 2 Run 3, with T_{ave} = -2.04°C and $SD_{T_{ave}} = 0.03°C$.

The air and water pressures for these cases were set appropriately for LWC of $0.41g/m^3$ and MVD of $17\mu m$. The three profiles are presented in figure 7.1 and the geometric parameters in table 7.1.

RunNo	h_{upper}	θ_{upper}	ϕ_{upper}	L_{upper}	h_{lower}	θ_{lower}	ϕ_{lower}	L_{lower}	t_{c-l}
P1-10Rep	34.50	44.00	25.50	27.50	28.50	-58.50	-45.00	65.50	5.50
P1-10Rep2	36.50	48.75	32.50	23.00	28.50	-48.50	-41.00	38.00	7.00
P2-3	37.00	47.00	33.75	22.00	27.50	-52.00	-43.50	57.50	9.50
RefIS	36.00	46.58	30.58	24.17	28.17	-53.00	-43.17	53.67	7.33
StDev	1.32	2.40	4.45	2.93	0.58	5.07	2.02	14.15	2.02

Table 7.1: Geometric parameters for the three profiles generated under reference conditions (Co_LWC&T) with resultant average values and standard deviations.

[1] T_{ave} is the average working section temperature as calculated using the calibration between T_{probe} and T_{RPC}. It is essentially equivalent to what the average temperature of T_{probe} would be if the probe were installed to measure temperature.

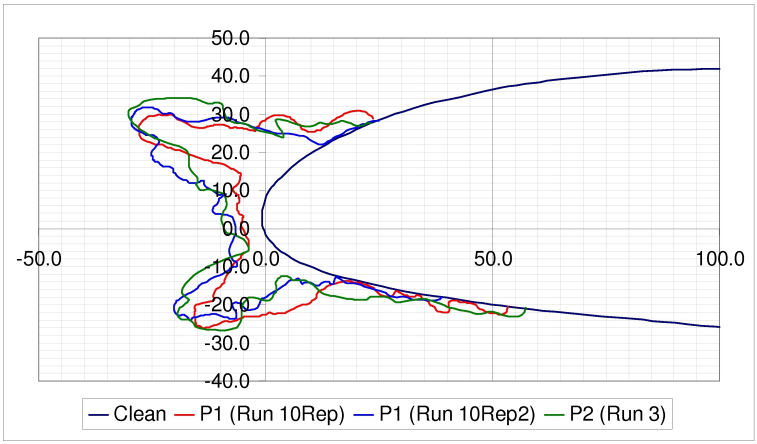

Figure 7.1: The three profiles created under reference conditions.

Some differences exist between these profiles but the location of the major features, the upper and lower surface horns, agree well with one another when examining their coordinate location and in considering their deviation from the mean value denoted by *RefIS*. A slightly larger deviation in upper horn orientation exists when examining θ_{upper} and ϕ_{upper} for profile P1-10Rep in comparison with the other two runs, however this is largely due to the impact of the different locations identified as the root of the horn, and so is reflected to a significantly lesser degree in the profile plot. The difference between the smallest and largest horn growth vector angles for the lower horn is evident in the plot.

The greatest discrepancy arose in the measure for L_{lower}. The fidelity associated with the freezing limits is reduced because of the scope for ice in these regions to melt or sublime once spraying ceases; because of the likely reduction of ice in the freezing limit region when a groove is cut for tracing using a hot metal plate; and because of the reduced fidelity associated with tracing thin parts of the ice accretion.

These profiles have been judged to exhibit acceptable repeatability on the basis of their parametric values that describe the main features in conjunction with overall similarity (observed by eye) that can explain larger differences

apparent in the aforementioned parameters. In addition a final, and very pertinent measure taken into account, is the distance between the locations deemed to be the horn tips. These are again subjective and are related using the similarity in profile plots. The largest distance between upper horn tips was calculated to be approximately 3mm. The largest distance between lower horn tips was calculated to be approximately 9mm. This is slightly larger than would be desired; distances less than 5mm would be desirable. However one of the horn tips is not smooth, and this impacts its location, reducing the largest distance. Of course, some variability is inevitable given the nature of icing tunnels and the ice growth process. Therefore, accounting equally for each of: visible similarity, recorded geometric features and horn-tip locations, the repeatability was deemed acceptable.

Note 1: Over the remainder of this document the averaged values given by *RefIS* are used for comparison of variable parameters with those generated under reference conditions. Of the three profiles, the profile from run P1-10Rep2 was selected for visual comparison.

Note 2: Also, in describing ice accretions in this document, standard uniformity is assumed for each case unless stated to be otherwise. Standard uniformity refers to a generally prismatic shape, with some small non-prismatic features, either side of the measurement location (approximately ±5cm). Outside this region the size of the accretion began to reduce to nothing at the wing tips, where there was no cloud coverage.

7.1.1 Phase 1 Results - LWC Variability

Within phase 1 each simulation case was assigned a case-code that describes its variation. In table 7.1 run numbers P1-10Rep, P1-10Rep2 and P2-3 were used to describe each of the three profiles generated under reference conditions Co_LWC&T (constant liquid water content and temperature). This was done to distinguish between the three instances where one case code was applicable. Hereafter the term 'RefIS' (reference ice shape) will refer to the

profile from constant conditions run P1-10Rep2 or to the geometric parameters calculated by averaging the values from P1-10Rep, P1-10Rep2 and P2-3.

In presenting the variability results from phase 1 the case code is used. The meanings of the case codes are provided in table 7.2.

Case Code	Description of the Nature of the Variability
Va_LWC_10%_F	±10% variation in LWC about the mean (reference) value at the standard variation.
Va_LWC_50%_F	±50% variation in LWC about the mean (reference) value at the standard variation.
Va_LWC_10%_Half-Freq_F	±10% variation in LWC about the mean (reference) value *at half* the standard variation.
Va_LWC_50%_Half-Freq_F	±50% variation in LWC about the mean (reference) value *at half* the standard variation.
Va_LWC_50%_B	±50% variation in LWC about the mean (reference) value at the standard variation *in the opposite sequence*.
Va_LWC_50%_Half-Freq_B	±50% variation in LWC about the mean (reference) value *at half* the standard variation *in the opposite sequence*.
Va_LWC_50%_Double-Freq_F	±50% variation in LWC about the mean (reference) value *at double* the standard variation.
Va_LWC_10%_Rise	Rise from 10% below the mean (reference) value to 10% above it.
Va_LWC_30%_Rise	Rise from 30% below the mean (reference) value to 30% above it.
Va_LWC_50%_Rise	Rise from 50% below the mean (reference) value to 50% above it.
Va_LWC_30%_Fall	Fall from 30% above the mean (reference) value to 30% below it.
Va_LWC_50%_Fall	Fall from 30% above the mean (reference) value to 30% below it.
Va_LWC_30%_Fall-Rise	Fall from 30% above the mean (reference) value to 30% below it before a rise back to 30% above the mean value.

Cluster	LWC variation that follows a unique clustered cloud profile.

Table 7.2: Phase 1 simulation codes (case codes) and their meanings.

The input conditions and resultant accretions (profile plot, photograph and geometric parameters) for RefIS and the cases in phase 1 are presented in figures E.1, E.3, E.5 etc. until figure E.29. A brief comment on each case is provided in the following section.

Individual Phase 1 Icing Cases

Case Va_LWC_10%_F: Figure E.3 shows the conditions and the ice accretion generated for case Va_LWC_10%_F. The variation represented in the LWC plot is small but the resultant profile suggests that it has had a noteworthy effect. Whilst the overall shape of the accretion is similar to that from the constant conditions the upper and lower horns are longer. This is reflected in the parametric values for horn thickness with a difference from RefIS of approximately $13mm$ and $9mm$ respectively. The orientation of the horns is slightly different too, with ϕ_{upper} increased slightly and ϕ_{lower} becoming notably less negative. The photograph of the ice accretion shows the uniform nature of the accretion; so it is appropriate to conclude that the profile is quite suitably representative of the ice accretion within the region of interest.

In summary the ice accretion generated under case Va_LWC_10%_F conditions was of similar shape to RefIS but had longer horns with a slightly greater growth vector angle on the upper surface and a slightly reduced growth angle on the lower surface.

Note: The results for this first case are useful to demonstrate the need to interpret the profile and parameter information together. Here values for ϕ_{upper} and ϕ_{lower} suggest a very small difference in

upper horn orientation and a larger difference in lower horn orientation. The differences in orientation observable in inspecting the profile plot are greater than suggested by parameters for the upper horn and less suggested by the parameters for the lower horn. This is due to the parameter definition and must be taken into account when assessing geometric values.

Case Va_LWC_50%_F: Figure E.5 shows the conditions and the ice shape generated for case Va_LWC_50%_F. The profile suggests that the significant difference in conditions from Co_LWC&T resulted in a notably different ice accretion that protruded far more significantly into the freestream. Examination of the photograph of the accretion however, reveals a non-uniform peak in the region of interest that indicates this might have been less representative of the overall accretion. Inspection of other photographs suggest that at this location the horn height (y-axis measurement) might have had a y-value approximately $15mm$ greater than at other locations. Nevertheless if the upper horn were reduced in thickness (by y-axis height) accordingly it would still be composed of significantly more mass than the equivalent for RefIS, and would also be slightly more intrusive with a horn tip located around x = -$32mm$, y = 33mm. Examination of original tracings suggest horn thickness might be around $5mm$ greater than that for RefIS. What is worth noting is the greater quantity of ice between the horns; and enhanced growth aft of the main horn shapes shown in the profile plots. The horn orientation presented by the profile plots and parameters was notably greater for the upper surface in comparison with RefIS, though the difference would be significantly lessened were the the non-uniform peak not present. The orientation of the lower horn is similar to RefIS.

In summary the profile plot generated under case Va_LWC_50%_F describes a small spanwise section with an unrepresentative upper horn thickness. Discounting this enhanced section the amount of ice accreted is notably greater, with a greater quantity of ice between the upper and lower horns and an enhanced amount of freezing aft of the main horns. It is likely that the upper

horn was slightly thicker away from the tracing location.

Va_LWC_10%_Half-Freq_F: The LWC plot in figure E.7 describes the conditions applied in this case, i.e. slightly wetter than the mean for the first half of the simulation and slightly less wet than the mean in the second half (or a slightly increased freezing fraction for the first half of the simulation, and a slightly reduced freezing fraction for the second half). The photograph confirms good spanwise uniformity despite the occasional individual feature; one of which is responsible for the pronged nature of the lower horn shown in the profile plot. Overall the shape deviates from RefIS primarily due to horn thickness, prolonged aft freezing on the lower surface and a slightly reduced upper horn growth vector; confirmed by measured h_{upper} and h_{lower}, L_{lower} and ϕ_{upper}. The difference in measured ϕ_{lower} is not reflected in the profile plot; and is due to a difference in horn root location.

In summary the accretion generated under case Va_LWC_10%_Half-Freq_F has elongated horns in comparison with RefIS, as well as enhanced freezing behind the main accretion. Against RefIS, the upper horn is also oriented marginally toward the x-axis.

Va_LWC_50%_Half-Freq_F: The LWC plot in figure E.9 describes the conditions applied in this case, i.e. significantly wetter than the mean for the first half of the simulation and significantly less wet than the mean in the second half (or a greatly increased freezing fraction for the first half of the simulation, and a greatly reduced freezing fraction for the second half). A feature that is significantly different from RefIS is the greatly enhanced chordwise extent of freezing; up to 10% chord on the upper surface and 20% chord on the lower surface (c = $480mm$). This is reflected in values for L_{upper} and L_{lower}. Horn thicknesses are similar but the reduced value of ϕ_{upper} combined with the gently sloping upper horn top surface ensures the profile is notably different in appearance. There is also a greater quantity of ice between the horns. The photograph shows predominantly good uniformity with one noteworthy spanwise deviation outside the region of interest. More interestingly it shows

that areas of the upper and lower horns had regions of rime ice at the end of the simulation where the LWC returned to the mean value of $0.41g/m^3$ for one segment after four segments with a value of $0.205g/m^3$.

It is worthwhile noting the occurrence of the non-uniformity at a spanwise location outside the region of interest; and to show its origin. This is because there are other instances of this phenomenon. In a very wet ice growth regime, like that observed early in Va_LWC_50%_Half-Freq_F, what can only be described as 'spikes' have been observed to appear on both upper and lower surfaces. These spikes are initially very small glaze ice features that remain attached because the aerodynamic forces are insufficient to cause them to break. The spike present in case Va_LWC_50%_Half-Freq_F is presented early in figure 7.2 picture 1. Pictures 2, 3 and 4 illustrate how the spike, initially with a very high collection efficiency grew to dominate the segment of the wing span that it occupied such that the shape of the accretion at that location deviated significantly from an otherwise uniform profile. This behaviour introduces what might be considered a potential volatility in ice accretion growth behaviour and uniformity under such conditions.

In summary the accretion generated under Va_LWC_50%_Half-Freq_F conditions was notably different to RefIS by virtue of more extensive chordwise freezing, more ice mass between the horns and a notably less intrusive upper horn with a comparably flat upper horn top surface.

Va_LWC_50%_B: Figure E.11 shows the conditions and the ice accretion generated for case Va_LWC_50%_B. The photograph shows that a spanwise non-uniformity exists but this is outside of the region of interest; within the region of interest (and measurement) the accretion is sufficiently uniform. The profile is therefore considered representative of the ice accretion generated under these conditions. The profile itself is quite similar to RefIS, especially over the lower part of the leading edge where there is little difference between the lower horns. This is confirmed by parameter values for lower horn thickness and orientation. The most notable difference is in the

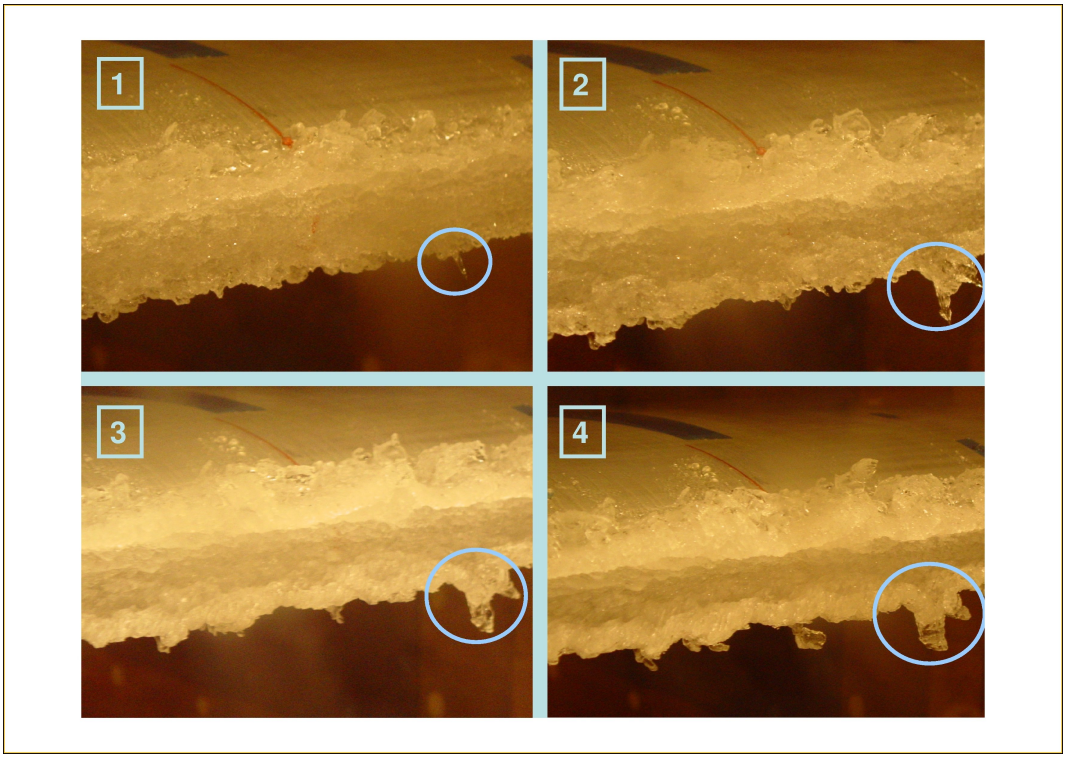

Figure 7.2: Appearance and development of a spike into an isolated spanwise feature.

upper horn which is slightly longer but is less intrusive into the airflow, with ϕ_{upper} approximately 5° less than the corresponding RefIS value and θ_{upper} smaller by approximately 13° (with θ_{upper} perhaps better reflecting the difference on this occasion). The upper horn also has a less steep top surface than RefIS. The chordwise freezing extent is also significantly greater on both upper and lower surfaces, with Ł$_{upper}$ nearly double, and Ł$_{lower}$ just over double the RefIS value.

In summary the ice accretion generated under Va_LWC_50%_B conditions differs to the RefIS profile & geometric parameters by virtue of notably more extensive chordwise freezing and a moderately less intrusive upper horn with a less steeply sloped top surface. The upper horn thickness is also slightly greater. The lower horn thickness and orientation are very similar.

Va_LWC_50%_Half-Freq_B: Figure E.13 shows the conditions and the ice accretion generated for case Va_LWC_50%_B. While no photographs were not taken during this simulation there were no comments during the run log to suggest non-uniformity. The LWC plot shows that the variation for this case is much drier over the first half of the simulation and much wetter over the second half. In one sense the profile plot looks remarkably similar to RefIS; were the red Va_LWC_50%_Half-Freq_B shifted aft by approximately five millimetres it would match the RefIS profile well. In reality though there are differences; the upper and lower horns protrude further into the airflow (reflected in larger h_{upper} and h_{lower} values) whilst the lower horn is oriented less intrusively (there is a reduction in θ_{lower} and ϕ_{lower} of approximately 17° and 13° respectively in comparison with corresponding RefIS values). The value of L_{lower} describes the greater region of runback on the lower surface evident from the profile plot. This enhanced runback is not observed on the upper surface.

In summary the ice accretion generated under Va_LWC_50%_Half-Freq_B differs from the RefIS profile because of slightly greater upper and lower horn thicknesses, a less intrusive lower horn orientation and more frozen runback on the lower surface.

Va_LWC_50%_Double-Freq_F: The increased rate of variability of LWC about the mean value is shown in figure E.15's LWC plot. Two ice profiles were traced following simulation of these conditions; this because of significant features that deviate from the uniform profile at the centreline, and an otherwise uniform accretion elsewhere. The profile measured at the non-uniform spanwise features shows the double horns on the upper and lower surfaces of the aerofoil. These were created after the appearance of spikes early in the simulation, and provide another example of the volatility exhibited under high LWC scenarios. The significant difference for the non-uniform segment is obvious in examining the profile plots and geometric parameters associated with Va_LWC_50%_Double-Freq_F, run number P1-25CL; and needs little further comment. Interestingly the profile and param-

eters at the uniform location is not hugely different from the RefIS accretion. The horn thicknesses are similar, with the upper horn slightly thicker than the upper horn of RefIS; whilst the lower thicknesses are very similar. In comparison with the RefIS values the values of ϕ_{upper} and θ_{upper} do not convey the reduction in the upper horn's intrusiveness to the same degree as the profile plot. This orientation combined with the comparably gently sloped top surface of the upper horn creates a shape whose difference to RefIS (with a comparatively steep upper horn top surface/leeward side) is notable. The other difference worth noting is the significantly extended freezing limit on the lower surface in comparison with RefIS.

In summary the profile representing the uniform majority of the accretion was quite similar to the RefIS profile in terms of horn thickness and orientation. The slightly lower upper horn orientation led to reduced intrusion into the airflow; and this combined with the relatively flat nature of the upper horn top surface gave rise to a difference that was interesting for aerodynamic reasons. A further aft freezing limit was also present on the lower surface.

Va_LWC_10%_Rise: The LWC variation chart in figure E.17 shows the steady increase in water content applied over the simulation from 10% below the mean value to 10% above it. Interestingly the profile for this case looks quite simply to be the RefIS profile with elongated horns; h_{upper} and h_{lower} for Va_LWC_10%_Rise were measured as $16mm$ and $11mm$ longer than the corresponding values for *RefIS* respectively. The similarity in upper horn orientation is recognised by ϕ_{upper} but ϕ_{lower} registers an approximate difference of 6°; this is due primarily to the differences in the location of the roots of the two lower horns. The distribution of ice mass in the horns between Va_LWC_10%_Rise and RefIS is very alike; accounting of course for the fact that the horn thicknesses are greater for Va_LWC_10%_Rise. The lower surface freezing limit is also approximately $15mm$ further aft in comparison with RefIS.

In summary the ice accretion generated by Va_LWC_10%_Rise differs from

RefIS almost solely by virtue of notably thicker upper surface horns which, with similar orientation to RefIS, protruded notably more intrusively into the airflow. The freezing limit is also extended aft by approximately 30% in comparison to RefIS.

Va_LWC_30%_Rise: Figure E.19 shows the LWC increase applied in case Va_LWC_30%_Rise. The photograph shows that the accretion was uniform across the span within the region of interest. In comparison with the RefIS profile there is a notable similarity in the concave region connecting the two horns, where the profiles match very well. This does not, however, lead to the accretions being similar overall. The upper horn has a slightly greater thickness and whilst the value of ϕ_{upper} is similar to that of RefIS; this is based on the defined root and tip locations only, and does not consider the slope of the upper horn top surface. Hence it does not reflect the comparatively steeper leeward side of the Va_LWC_30%_Rise upper horn that might be expected to be important aerodynamically. The lower surface horn is simply larger than the RefIS equivalent; with a more intrusive horn tip reflected in values of h_{lower} and ϕ_{lower} that are $7mm$ and 14° larger than corresponding RefIS values. Va_LWC_30%_Rise also has slightly more extensive freezing on the lower surface.

In summary the ice accretion generated by Va_LWC_30%_Rise is similar to the RefIS profile in the windward concave section between the horns but differs by virtue of greater horn thicknesses, a steeper upper horn top surface/leeward side, a notably more intrusive lower horn and a slightly further aft freezing limit.

Va_LWC_50%_Rise: The greater extremes in LWC applied during case Va_LWC_50%_Rise are presented in the LWC plot in figure E.21. Comparing the two profiles, that generated during case Va_LWC_50%_Rise has notably further forward freezing limits. On the upper surface the entire ice accretion is further forward; and a combination of increased horn thickness and reduced horn vector angle (approximately $5mm$ greater and 10° less respec-

tively) describe a different horn tip location that could be considered more or less aerodynamically intrusive, depending on the angle of attack. The lower horn thickness is also significantly greater (approximately $10mm$) with a similar orientation, making it more intrusive than the corresponding RefIS lower horn. The photograph confirms that there is adequate spanwise uniformity.

In summary the profile from Va_LWC_50%_Rise has accreted further forward than the RefIS profile, with a slightly thicker horn with reduced horn growth vector angle on the upper surface; and a notably greater horn thickness and similar horn growth vector angle on the lower surface.

Va_LWC_30%_Fall: Figure E.23 shows the variation in LWC as applied in case Va_LWC_30%_Fall and the accretion results. The profile generated during this case has notable similarities to the RefIS profile. In fact it would be believable that the Va_LWC_30%_Fall (without more extensive lower surface runback) profile could be the RefIS profile if it were to encounter icing conditions for a further period of icing. The predominant difference is in the horn thickness, where the $7mm$ and $9mm$ difference in h_{upper} and h_{lower} describe the increase in horn root to tip thicknesses well, but perhaps reflect the visibly greater extension of the tips into the airflow less accurately. Whilst the horn growth vector angles being smaller than RefIS might suggest a less intrusive ice accretion, this is not the case because of the more extensive horns. In additions whilst the upper horn is more intrusive there exists a noteworthy feature in the reduced slope of the top surface in comparison with the RefIS profile. The secondary protrusion on the upper surface is a non-uniform feature captured in the ice tracing. This would likely impact any aerodynamic assessment of the profile. Whilst the freezing limit on the upper surface is similar the limit on the lower surface is significantly more extensive, as reflected by the values for L_{lower} for Va_LWC_30%_Fall and RefIS. The photograph shows that the ice accretion exhibited a good degree of uniformity.

In summary the profile for Va_LWC_30%_Fall is similar to that for RefIS; but has notably greater horn thicknesses, slightly reduced horn growth vector angles and a more gently sloping upper horn, as well as more extensive chordwise freezing.

Va_LWC_50%_Fall: Figure E.25 shows the conditions applied in, and ice profile resultant from, case Va_LWC_50%_Fall. The photographs illustrates that the level of uniformity in the ice accretion was good, and the more opaque ice shown to have accreted at the end of the run suggests a drier icing regime. This profile is similar in many ways to the RefIS profile upon visual inspection and this is confirmed by the corresponding geometric parameters. Upper and lower horn thicknesses are very similar to the corresponding values for RefIS, as is the upper surface horn orientation and upper surface freezing limit. These similarities are confirmed by inspection of h_{upper}, h_{lower}, ϕ_{upper}, θ_{upper} and Ł$_{upper}$. The differences in lower horn orientation (ϕ_{lower} and θ_{lower}) are due to a slightly different lower horn tip location. There is also a moderate ($15mm$) difference in the freezing limit, with freezing occurring further aft for the Va_LWC_50%_Fall profile.

In summary the profile is similar to the RefIS profile in upper and lower horn thickness, upper horn orientation and upper surface freezing limit. Differences exist primarily in lower horn orientation (and hence horn tip location) and lower surface freezing limit.

Va_LWC_30%_Fall-Rise: Figure E.27 shows the conditions and resultant profile results from Va_LWC_30%_Fall-Rise. This accretion differs from RefIS predominantly because of horn thickness, with h_{upper} and h_{lower} differing from the RefIS values by approximately $7mm$ and $12mm$ respectively. These differences, in conjunction with very similar horn growth vector angles, describe a moderately more intrusive ice accretion. The freezing limit on the upper surface is reported to be very similar to that of the RefIS profile and parameters whilst on the lower surface the freezing limit is some $15mm$ further aft than for RefIS. The photograph shows that some non-uniformity exists for

this profile; and that different profiles might exist at other spanwise locations.

In summary the profile for Va_LWC_30%_Fall-Rise is similar but slightly more intrusive than the RefIS profile predominantly by virtue of horn thickness. h_{upper} and h_{lower} describe the primary differences, with L_{lower} describing the greater aft extent of freezing.

Cluster: The LWC variability applied in the cluster scenario is presented in figure E.29 along with profile plots, geometric parameters and a photograph. The photograph shows the significant degree of spanwise non-uniformity in the accretion generated under these conditions. This non-uniformity was evident both within and outwith the region of interest. The non-uniformity was captured by three profiles; one made at the centre-line (CL), one 3cm towards the 'control room' side of the working section (CR) and another 3cm towards the 'freezer side' of the working section (FS). An upper surface deviation was dominant at the CL location and a lower surface deviation was dominant at the FS location. Both of these grew from spikes at early stages of the simulation in very high LWC. This is well illustrated by the photograph displayed in figure 7.3.

Interestingly where the deviations were not present the difference between the Cluster profiles and the RefIS profile was much less. Specifically the upper horns at the CR and FS locations and the lower horn at the CR location were similar to the upper and lower horns for RefIS. In addition the horns at these locations were less intrusive than the RefIS profile. Notably more intrusive features existed for the upper surface horn at the CL location and the lower surface horn at the FS location, where the increased intrusiveness was reflected in measures for h_{upper} and ϕ_{upper} at the CL location and h_{lower} and ϕ_{lower} at the FS location. Of further note was the significant quantity of freezing immediately aft of the main horn at all locations with runback freezing extending to around $40mm$ on the upper surface and up to and beyond $100mm$ on the lower surface.

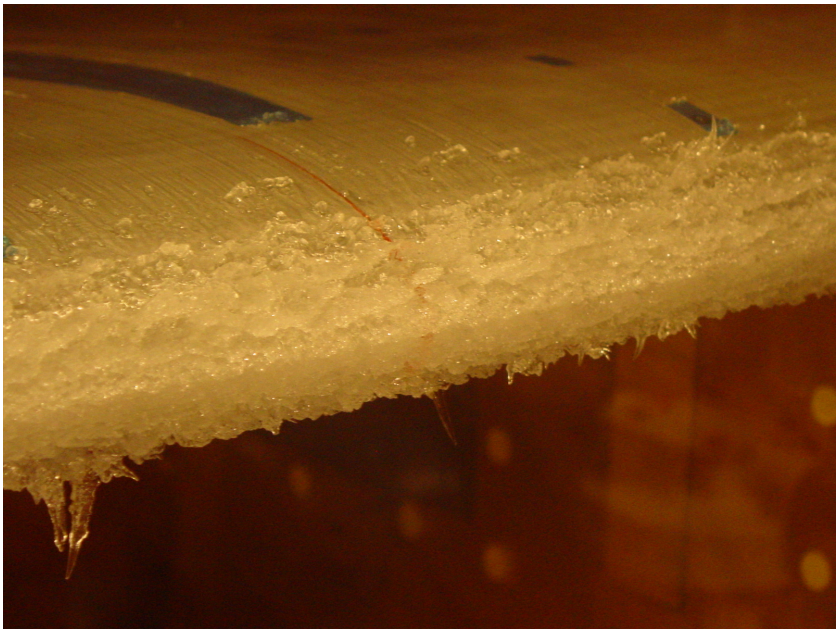

Figure 7.3: Photograph showing the appearance of spikes in the ice accretion along the span of the aerofoil during the Cluster simulation of phase 1.

In summary the Cluster conditions introduced significant three-dimensionality to the accretion within the region of interest, characterised by very intrusive horn features on the upper surface at the CL location and on the lower surface at the FS location. Greater similarity with RefIS was found where such deviations were less prominent and in such locations the intrusiveness was generally less than that for RefIS. The freezing aft of the horns and beyond was significantly more extensive.

7.1.2 Phase 2 Results - Temperature Variability

Over the course of phase 2 six icing encounters were modelled in the CIRT. Within this section these encounters will be referred to by their case code as described in table 7.3.

The input conditions and resultant accretions for RefIS and the cases in phase 2 are presented in figures E.31, E.33 etc. until figure E.41.

Case Code	Description of the Nature of the Variability
Sin(θ - 90°)	Sinusoidal variation in temperature about the mean by $\pm 1°C$, rising initially from -3°C.
Sin(θ - 270°)	Sinusoidal variation in temperature about the mean by $\pm 1°C$, falling initially from -1°C.
Sin(θ - 180°)	Sinusoidal variation in temperature about the mean by $\pm 1°C$, falling initially from -2°C.
Sin(θ)	Sinusoidal variation in temperature about the mean by $\pm 1°C$, rising initially from -2°C.
Construct #1	Temperature variation as described by the temperature plot in figure E.39.
Construct #2	Temperature variation as described by the temperature plot in figure E.41.

Table 7.3: Phase 2 simulation codes (case codes) and their meanings.

Individual Phase 2 Icing Cases

Sin(θ - 90°): Figure E.31 contains plots for temperature and LWC over the course of the encounter simulation with resultant profile plots, geometric parameters and photograph. The temperature plots show very good agreement between the target temperature and the achieved temperature and the duration averaged temperature was calculated to be -2.01°C. The photograph shows the existence of a local peak in upper horn thickness near the centreline that is not representative of the remainder of the accretion which is notably more uniform. This peak was the result of a spike that appeared on the upper surface in segment 5 of the simulation, where the target temperature was -1°C. Since this peak affected the profile measured at the centreline (as shown by the green profile in the profile plots) another location was se-

lected for profile measurement 2-3cm right of the centreline; and it is this profile (the red profile plot) that is considered to be representative of the ice accretion for this case. This profile is not dissimilar to the RefIS plot with the lower horn and centreline region between the horns very like that of the RefIS profile; this confirmed by small differences between Sin(θ - 90° and RefIS for h_{lower}, ϕ_{lower} and θ_{lower}. The upper horn has a similar thickness to the RefIS profile but is notably different in that it has a value of ϕ_{upper} that is approximately 10° lower than the corresponding value for *RefIS*. The freezing limit is similar to RefIS on the upper surface and approximately 10mm further aft on the lower surface.

In summary the profile representing the uniform Sin(θ - 90°) ice accretion is very similar on the lower surface, differing only slightly in freezing extent. The main difference exists in the less intrusive orientation of the upper horn (upper horn thickness is very similar). The upper surface freezing limit difference is minimal.

Sin(θ - 270°): The temperature plot in figure E.33 shows good agreement between achieved temperature and target temperature. The average temperature was calculated to be -1.94°C. The photograph and the green profile in the profile plots show a non-uniform feature. On this occasion no spike could be identified from other photographs to be where this feature originated from. Under warmer initial conditions the growth of roughness protrusions seems less continuous and more likely to create non-uniformity. This is shown by other photographs like those in figure 7.4(a). Photos (a) and (b) in this figure also identify glaze protrusions occurring further aft on the upper surface at two spanwise locations; both of which developed into significant features, but only one of which remained attached until the end of the simulation. This was the feature described by the green profile. These features were a result of the growth conditions in the early part of the simulation.

The red profile was representative of the remainder of the ice accretion within the region of interest. On the upper surface this profile was very similar to

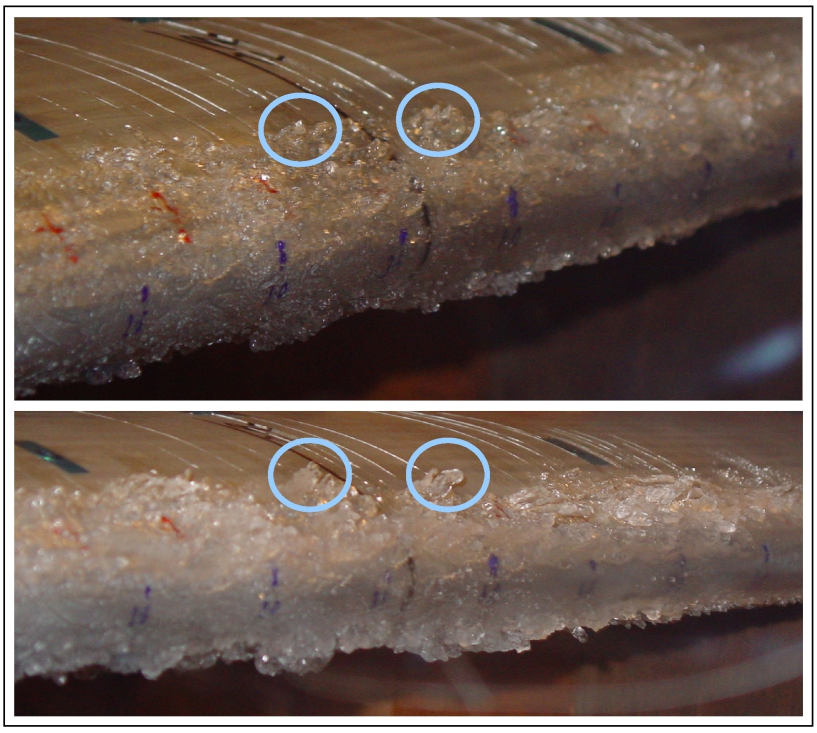

Figure 7.4: Photographs (a) and (b) showing the appearance and growth of glaze protrusions further aft at two different spanwise locations in case Sin(θ - 270°).

the RefIS profile with very similar values for h_{upper}, ϕ_{upper} and θ_{upper} and a freezing limit $11mm$ further forward. The horn thickness on the lower surface is similar but the more intrusive horn orientation (giving values for ϕ_{lower} and θ_{lower} greater in magnitude than the RefIS values by 8° and 8° respectively) was a notable difference. The freezing limit was also further aft on the lower surface.

In summary the profile representing the uniform accretion for this case was very similar on the upper surface and was differentiable from the RefIS profile predominantly because of a more intrusive lower horn described by a similar horn thickness and greater horn growth vector angle.

Sin(θ - 180°): The achieved temperature plot, ice profile and geometric pa-

rameters for this case are presented in figure E.35; the average temperature was calculated to be -1.97°C. The photograph does not show any significant features that would create a profile significantly different to that captured. The profile created is notably different to the RefIS profile; with upper and lower horn thicknesses increased, a reduced horn growth vector angle on the upper surface and an increased horn growth vector angle on the lower surface. The freezing limits differ little on either surface, by around $4mm$ on the lower surface and $3mm$ on the lower surface.

In summary the profile for Sin(θ - 180°) is different from RefIS predominantly by virtue of greater horn thicknesses, a reduced horn growth vector angle on the upper surface and an increased horn growth vector on the lower surface.

Sin(θ): The achieved temperature plot (with a calculated average value of -1.99°C) is presented in figure E.37 along with the profile plot, photograph and geometric parameters. The photograph shows there might be reduced uniformity on the upper surface. However other photographs from the simulation (see figure 7.5) show that the areas that grow into large features grow from glaze protrusions further aft of the main ice accretion (photograph (b)) and from spikes (photograph (c)). These features seemed to develop in stages 3 and 4. The pattern of ice growth shown after stage 1 in photograph (a) shows ice growth similar to others from cases with the same initial conditions. Photograph (d) shows that the significant horn shapes, whose growth resulted from the appearance of small features in early stages, are relatively dominant and do seem to provide a moderate degree of uniformity across the centre third of the aerofoil. Therefore the profile presented in figure E.37 is considered to be adequately representative of the ice accretion. The profile itself is significantly more intrusive than the RefIS profile, with $10mm$ and $7mm$ increases in h_{upper} and h_{lower} at a value of ϕ_{upper} greater by 8° and a similar ϕ_{lower} value. The increased intrusiveness of the upper horn is by far the most significant feature of the ice profile and the most notable difference from the RefIS profile. The differences in freezing limit are small, but are

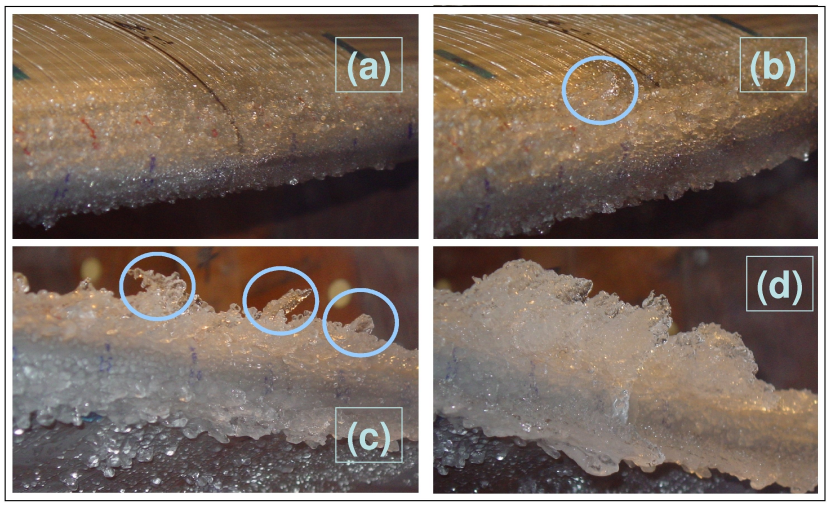

Figure 7.5: Photographs (a) to (d) showing the growth of the ice accretion in case Sin (θ).

interestingly further forward in comparison with the RefIS profile.

In summary the profile generated under Sin(θ) conditions was significantly more intrusive, primarily because of a greater upper horn thickness at a more intrusive orientation; also because of a slightly thicker lower horn shape. In comparison with RefIS, the freezing limits were slightly further forward.

Construct #1: Figure E.39 shows the altogether different temperature profile applied in this case, along with the resultant profile, geometric parameters and a photograph. The average of the achieved temperature measurements was -1.99°C. The photographs shows that some non-uniformity seemed to exist but the main horn features seemed relatively uniform. The profile was different from RefIS in a number of ways, with reduced upper and lower horn thicknesses (both smaller by approximately 6mm) and a less intrusive upper horn vector angle. The upper horn also has a very flat top surface. The lower horn has something of a double-tip and the second tip creates the larger value of ϕ_{lower}. The freezing limits are also further aft, more notably so on the lower surface.

In summary the ice profile for Construct #1 is notably less intrusive than the RefIS profile by virtue of a less thick upper horn, oriented at a reduced horn vector angle with a very flat top surface; combined with a reduced lower horn thickness albeit at a more intrusive horn vector angle.

Construct #2: The conditions modelled; resultant profile, geometric parameters and photograph taken for this case are presented in figure E.41. The calculated average temperature was -2.00°C. In comparison with the RefIS profile the Construct #2 profile is significantly different. The upper horn is shorter and oriented at a less intrusive angle (h_{upper} and ϕ_{upper} reduced by 11.5mm and 10° respectively); as is the lower horn (h_{lower} and ϕ_{lower} reduced by 9mm and 15° respectively). The freezing limits for this case are similar to the RefIS profile. The photograph indicates that some spanwise variation exists to a sufficient degree that the profile taken at the centerline might under-represent the lower horn thickness and/or orientation. The impact of the colder temperatures at the end of the simulation are evident in the rime nature of the ice growth photographed after segment nine.

The profile generated by Construct #2 differs significantly from the RefIS profile, having significantly less intrusive horns by virtue of smaller horn thicknesses and horn growth vector angles. The freezing limits are relatively similar to the averaged RefIS values.

7.1.3 Phase 3 Results - Combined LWC and Temperature Variability

Over the course of phase 3 five icing encounters were modelled in the CIRT varying both LWC and temperature simultaneously. In describing the results of these encounters they will be referred to by their case code as described in table 7.4.

Case Code	Description of the Nature of the Variability
LWC(A)/Sin(θ - 90°)	LWC and Temperature variation as described by plots P3-A and Sin(θ - 90°) in figure 5.13.
LWC(A)/Sin(θ - 270°)	LWC and Temperature variation as described by plots P3-A and Sin(θ - 270°) in figure 5.13.
LWC(B)/Sin(θ - 90°)	LWC and Temperature variation as described by plots P3-B and Sin(θ - 90°) in figure 5.13.
LWC(B)/Sin(θ - 270°)	LWC and Temperature variation as described by plots P3-B and Sin(θ - 90°) in figure 5.13.
LWC (30%) Rise & Temp Drop	LWC and Temperature variation as described by plots in figure 5.14.

Table 7.4: Phase 3 simulation codes (case codes) and their meanings.

The input conditions and resultant accretions for RefIS and the cases in phase 3 are presented in figures E.43, E.45, E.47,E.49 and E.51.

Individual Phase 3 Icing Cases

LWC(A)/Sin(θ - 90°): Figure E.43 contains all necessary information on LWC and temperature variation applied during this case; plus the profile plot, geometric parameters and photograph. The calculated average temperature was -2.00°C. The photograph shows little spanwise non-uniformity and the profile presented is considered to be sufficiently representative of the ice accretion. Overall the profile is quite similar to the RefIS profile with similar horn thicknesses and freezing limits. The horn orientation is also similar, with the only noteworthy difference between the profiles described

by a value of ϕ_{upper} that is 10° smaller than the RefIS equivalent. This value suggests a difference in upper horn orientation that is greater than is evident upon visual inspection of the profile, but this is again because horn thickness values are dependent upon the defined location of root and tip.

In summary the RefIS and LWC(A)/Sin(θ - 90°) profiles are notably similar; differing slightly, solely because of the reduced upper horn orientation described by the lower horn growth vector angle.

LWC(A)/Sin(θ - 270°): Figure E.45 contains plots describing LWC and temperature variation for case LWC(A)/Sin(θ - 270°) along with profile, parameter and photo based results. The calculated average temperature was -2.01°C. The uniformity is demonstrated to be adequate by the photograph. The horn thicknesses for the upper and lower surfaces are larger than for RefIS (by 8mm and 10mm respectively). The upper surface horn has a growth vector angle that is less than the RefIS equivalent by approximately 11° whilst the profile plots show the orientation of the lower horns are somewhat more similar than a 5° difference in ϕ_{lower} would suggest. The freezing limits for this ice profile described by L_{upper} and L_{lower} are notably further forward than those described by the RefIS values.

In summary the profile for LWC(A)/Sin(θ - 270°) differs from the RefIS profile with greater upper and lower horn thicknesses, further forward freezing limits, a smaller upper horn vector angle and a slightly greater lower horn vector angle.

LWC(B)/Sin(θ - 90°): The clustered LWC variation, accompanying temperature variation and resultant profile plot, parameter geometry and photograph for this case are presented in figure E.47. The calculated average temperature was -2.00°C. The resultant profile for this case is similar to the RefIS profile and has only subtle differences. The difference is due to slightly larger horn thicknesses. The horn thicknesses are greater by small amounts, by approximately 5mm for the upper horn and 4mm for the lower horn. The

upper horn also has a sharper tip in comparison with RefIS; and this might prove to be an important difference. Other than that the parameters are remarkably similar with small differences between freezing limit values and almost identical horn orientation values. The main difference in parametric terms is the centreline thickness. Subtle differences exist between the plots with slightly different distributions of ice across the horns and different total ice masses.

In summary the LWC(B)/Sin(θ - 90°) profile differs little from the RefIS profile with very similar horn orientation and freezing limits. The main difference is due to slightly thicker horns. The sharper upper horn is also worth noting.

LWC(B)/Sin(θ - 270°): The variability, and accretion results for this case are presented in figure E.49. The calculated average temperature was -1.95°C. This ice accretion is quite different to the RefIS profile with much shorter horns and a different distribution of mass where there is effectively no concave region between the horn tips. In fact the measurement location for centreline thickness is not significantly closer to the y-axis than either horn tip. The profile captured at this location is not due to any non-uniformity; the photograph confirms excellent uniformity for this simulation. The upper and lower horn thicknesses are smaller in comparison with the RefIS equivalent by approximately 8mm and 6mm respectively; however any subsequent reduction in intrusiveness is more than counterbalanced by the difference in horn orientation, with upper and lower horn growth vector angles being greater in magnitude by approximately 14° and 10° respectively. The top surface (leeward side) of the upper horn has also got a greater slope in comparison with the RefIS profile.

In summary the profile resulting from LWC(B)/Sin(θ - 270°) is notably different to the RefIS profile; primarily because of upper and lower horns that are reduced in thickness and oriented at larger horn growth vector angles and a flat (non-concave) windward face.

LWC (30%) Rise & Temp Drop: The conditions and accretion results for this case are presented in figure E.51. The calculated average temperature was -1.96°C. The photograph shows that the ice accretion is sufficiently uniform and confirms the large size of the accretion described by the profile plot. The profile is significantly different to the RefIS profile in a number of senses, not least in the difference in the mass of ice accreted. The horns are significantly more intrusive on both the upper and lower surfaces by virtue of upper and lower horn thicknesses and upper and lower horn growth vector angles notably larger than the equivalent measurements for the RefIS profile. h_{upper} is larger by approximately $10mm$, h_{lower} is larger by approximately $7mm$, ϕ_{upper} is larger by approximately 5°, ϕ_{lower} is larger by approximately 7°; and these values seem small in comparison with the difference observable in the profile plots. Regardless the LWC (30%) Rise & Temp Drop profile is significantly more intrusive than the RefIS profile with more accreted ice (also notable by the difference in centreline thickness). Interestingly little difference was recorded in upper and lower freezing limits.

In summary the profile from case LWC (30%) Rise & Temp Drop is notably different from the RefIS profile; being significantly more intrusive by virtue of larger horn thicknesses oriented at more intrusive angles. Significantly more ice was accreted during this simulation.

7.2 Aerodynamic Assessment of Experimentally Iced Aerofoils

Following the experimental icing programme, the CFD technique described in section 5.2.2 was used to predict the aerodynamic performance of each iced profile over a range of angles of attack. Full condensed CFD prediction results are presented in Appendix E; where the grid used for each iced pro-

file, velocity contour plots[2] at $\alpha = 2.4°$ and lift & drag coefficient predictions versus angle of attack graphs are presented for nearly all ice profiles recorded during the experimental programme. The lift and drag predictions are plotted against the corresponding predictions for the reference ice shape/profile, RefIS.

As described in section 5.2.2, solutions were considered to have converged to a steady state if the magnitudes of R_{C_L} and R_{C_D} were less than 0.2%, and if the k and ω residuals reached $1E^{-5}$. In all cases for experimental ice shapes, the k and ω residuals converged to values less than $1E^{-5}$, generally approaching $1E^{-6}$ and beyond. On the basis of this criteria the solutions could be deemed to have converged. This was generally not the case, however, as convergence to a steady solution (in terms of C_L and C_D) required further iterations. Once the criteria for solution steadiness had been reached (R_{C_L}, $R_{C_D} \leq 0.2\%$), the case was considered to be fully converged with negligible unsteadiness. The majority of data points plotted in the C_L & C_D results represent CFD predictions with negligible unsteadiness in the solution.

There are some results plotted, where the values of R_{C_L} & R_{C_D} indicate that unsteadiness in C_L & C_D remains. In the majority of these cases the values of R_{C_L} & R_{C_D} after 30,000 iterations are less than 0.4% and the resultant data points (those with 'remaining unsteadiness' are plotted as green triangles) do not visibly deviate from the trend predicted by data points representing solutions with negligible unsteadiness[3]. In certain cases, namely Va_LWC_50%_Half-Freq_F and LWC(A)/Sin(θ - 270°) (see figures E.10 and E.46), values of R_{C_L} & R_{C_D} (predominantly R_{C_L}) have notably greater values, e.g. 1%, 9%. Such unsteadiness is evident in the plots of C_L and C_D where the resultant data points do visibly deviate from the trend produced

[2]Within the contour plots, local velocity magnitude is presented as a ratio of freestream velocity, by the notation 'V12', a term that used during postprocessing with Tecplot.

[3]A good example of this is the prediction for the Va_LWC_30%_Fall-Rise profile (see figure E.28). Here, for $\alpha = 6.4°$, R_{C_L} is approximately 0.3%, yet the fit with the overall trend is as it might be expected for a steady solution.

by points representing solutions with negligible unsteadiness. This data has been presented in order to demonstrate instances where the CFD solution is not reliable, in contrast to the majority of cases where convergence to a steady solution has been achieved.

There is a notable array of results with some ice profile predictions providing similar results to RefIS, some providing visibly less detrimental results and others providing visibly more detrimental results. Whilst similarities and differences in graphed data are evident for both C_L and C_D, there is a more striking difference in the shape of the C_L trends predicted for around half of the ice profiles.

The CFD results are presented in figures E.2; E.4; E.6 etc.; until figure E.52. Ideally the current section would present velocity & pressure contours and C_P distributions for each profile at a number of incidences to portray the specific details of each C_L prediction; and allow determination of the impact the predicted flow features have on the lifting capability of the aerofoil. Such a level of detail is, however, not possible since the number of contour plots and C_P distributions required are too many for this document. Instead this section presents a detailed description of the CFD results produced for four iced aerofoils that suitably represent the different C_L trends that exist in the full set. The results selected were those for the profiles generated under the following conditions:

1. RefIS (Co_LWC&T);
2. Sin(θ - 90°);
3. Sin(θ);
4. LWC(B)/Sin(θ - 90°).

Full results (C_L vs α; C_D vs α; velocity contour plots and C_P distribution) are described in the coming sections.

In explaining the C_P results certain terms are useful to describe what is reported. Pressure coefficient distributions are very descriptive and are implemented in presenting results for the four profiles listed above. Figure 7.6 (based on the C_P distribution for RefIS at $\alpha = 2.4°$) shows the kind of C_P distribution that can be expected from iced aerofoils.

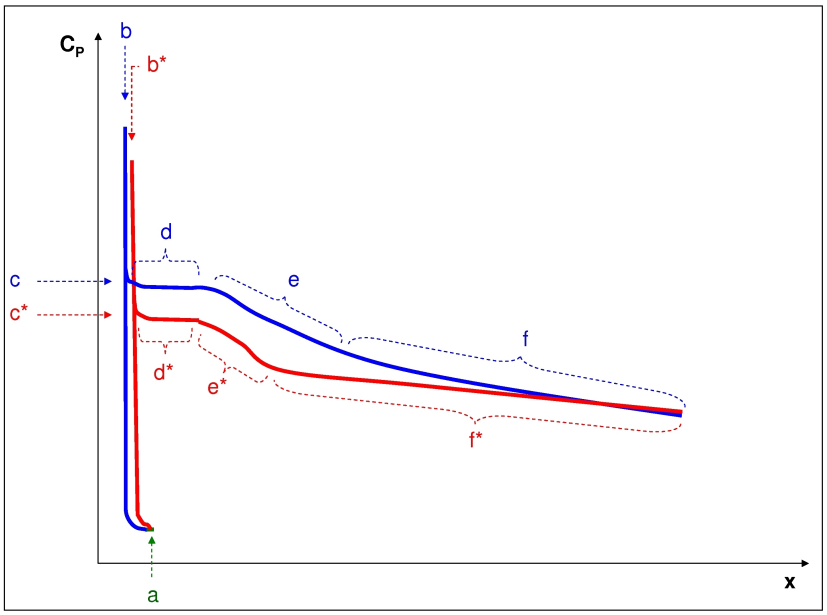

Figure 7.6: Diagram showing a possible C_P distribution for an iced aerofoil, labeled and colour coded for upper (blue) and lower (red) surfaces.

In figure 7.6 the stagnation point is labeled (a). Air accelerates around the upper horn creating the suction peak at (b) before encountering an adverse horn-tip pressure gradient that initiates boundary layer separation at (c). The separation C_P is labeled (d); this is a straight line in figure 7.6, but in actual CFD results the values fluctuate because of the surface geometry of the aft section of the ice horn. The section labeled (e) represents the C_P change during reattachment, with the slope of the line dependant upon how soon reattachment occurs, or the reattachment length. Section (f) represents the C_P distribution once the flow is reattached and has to negotiate an adverse pressure gradient, or pressure recovery.

Over the lower surface the lower horn tip suction peak is labeled (b*) ahead of separation at (c*); (d*) represents the separated C_P again without the fluctuations observed in a real icing CFD C_P solution. The shorter reattachment length creates the C_P section labeled (e*). The shorter the reattachment length, the steeper the slope connecting the separated C_P to an attached value. The longer pressure recovery is labeled (f*).

Note that in figure 7.6 reattachment occurs outside any significant favourable pressure gradient. Were this not the case an increase in suction (-ve) C_P would be expected before the onset of pressure recovery further aft.

CFD Results for the Reference Ice Shape (RefIS)

CFD generated plots of lift and drag coefficient variance for the RefIS profile are presented in figure 7.7; velocity contours for incidences of -1.6° to 7.4° are presented in figure 7.8 and pressure coefficient distributions for incidences of -1.6° to 6.4° are presented in figure 7.9.

Figure 7.7 shows that the maximum predicted C_L (before a post-stall lift recovery) occurs at α = 2.4° following increases in lift from α = -1.6°. Lift decreases after α = 2.4° before the lift recovery that occurs at α = 5.4°.

Velocity contour plots (in figure 7.8) show that the largest separated region on the lower surface occurs at α = -1.6°, and this decreases in size with increasing incidence. The opposite occurs for the upper surface with reattachment last observed at α = 3.4°. The C_D plot associated with such behaviour is as expected, falling initially as α increases to 0.4° from -1.6° before increasing thereafter.

At α = -1.6°, in figure 7.9, similar suction pressures upon separation at the upper and lower horn tips make distinction between C_{Pupper} and C_{Plower} dif-

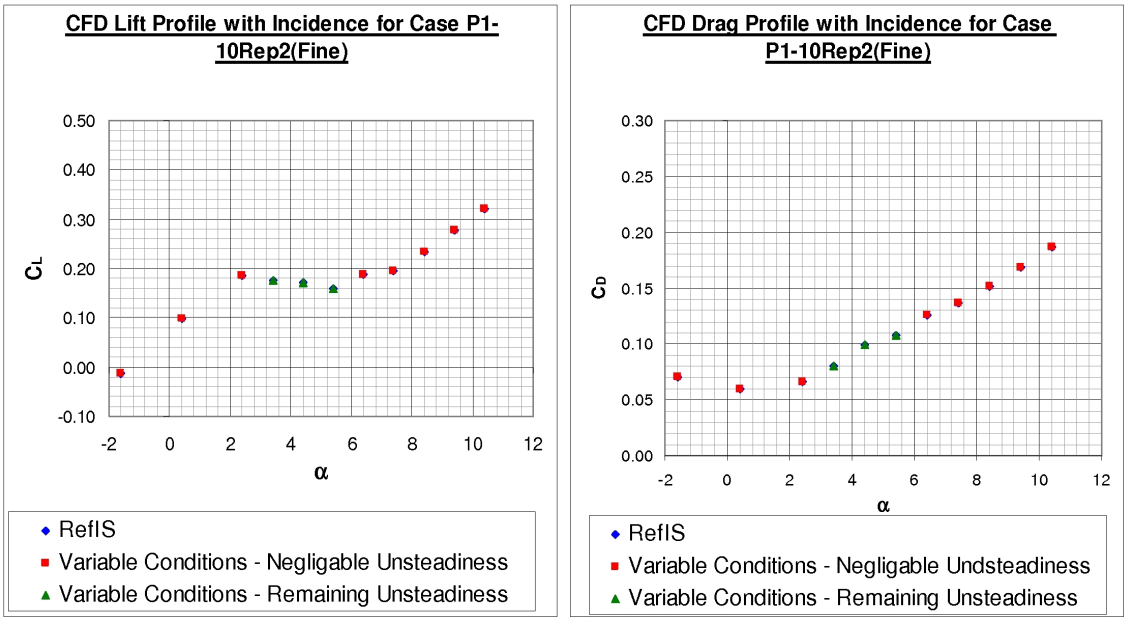

Figure 7.7: Lift and drag coefficient versus angle of attack from CFD predictions for the RefIS profile.

ficult. A shorter reattachment length; with flow reattaching near the end of the favourable pressure gradient, leads to reduced suction C_P earlier on the upper surface in comparison with the lower surface where full reattachment isn't achieved until further aft. The resultant difference in upper and lower C_P distributions over the forward section of the aerofoil (behind the ice accretion) leads to a slightly negative predicted C_L at this incidence.

At α = 0.4° the upper surface suction is enhanced and the lower surface suction is reduced before separation occurs (in comparison with α = -1.6°), contributing more notably to lift. Later upper surface and earlier lower surface reattachment results in very similar upper and lower surface C_P values from x = 0.1. This diminishes any effective downforce over the majority of the clean section of the aerofoil and therefore contributes to the slightly positive C_L reported.

At α = 2.4° a further enhancement to upper surface suction and a further

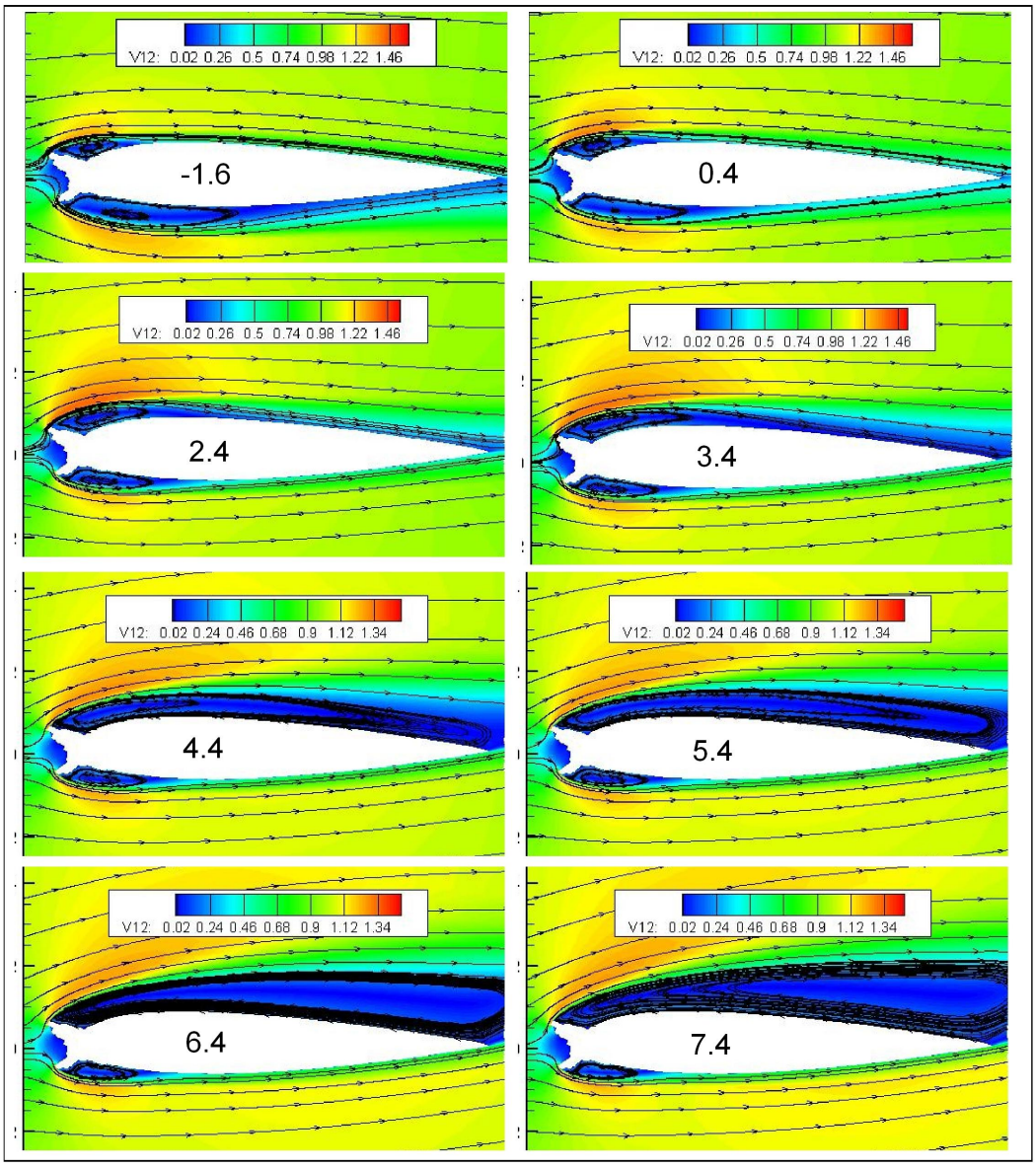

Figure 7.8: Velocity contour plots from CFD predictions for the RefIS profile for α = (-1.6°, 0.4°, 2.4°, 3.4°, 4.4°, 5.4°, 6.4° and 7.4°).

reduction to lower surface suction occurs before separation creating the difference shown on the C_P distribution ahead of reattachment and pressure recovery. A greater suction C_P exists on the upper surface until around x = 0.6, producing an increase in predicted C_L as incidence is increased from α

= 0.4° to $\alpha = 2.4°$.

At $\alpha = 4.4°$ the C_P distribution shows that with full upper surface stall the suction generated in advance of separation is reduced, leading to a loss of upper surface lift. The effect of the shorter lower surface separation bubble is minimal in comparison, hence the overall C_L reported has decreased in comparison with $\alpha = 2.4°$ and the aerofoil is deemed to have stalled (note stall actually occurred before $\alpha = 4.4°$, with reduced lift reported at $\alpha = 3.4°$).

At $\alpha = 6.4°$ the upper surface C_P distribution is much the same as at $\alpha = 4.4°$, yet the decrease in lower surface separation bubble length in comparison with $\alpha = 4.4°$ reduces overall lower surface suction, hence contributing to lift. Correspondingly the aerofoil C_L is reported to exhibit a small recovery at $\alpha = 6.4°$.

CFD Results for the Sin(θ - 90°) Conditions Profile

CFD generated plots of lift and drag coefficient variance for the RefIS profile are presented in figure 7.10; velocity contours for incidences of -1.6° to 7.4° are presented in figure 7.11 and pressure coefficient distributions for incidences of -1.6° to 6.4° are presented in figure 7.12.

Relative to the the RefIS profile the Sin(θ - 90°) profile is less intrusive primarily by virtue of the reduced horn growth vector angle. It also has a flatter upper horn top surface.

As shown in figure 7.10, maximum predicted C_L (before a post-stall lift recovery) occurs some 2-3° after it does for the RefIS profile with higher lift at each incidence by between 0.06 and 0.2.

Contour plots in figure 7.11 show small separation bubbles on the upper sur-

face at low angles of attack (α = -1.6° to 2.4°). Lower surface separation bubbles are larger at α = -1.6°; and these decrease in size with increasing incidence and have correspondingly earlier reattachment. On the upper surface the separation bubble continues to grow aft from the leading edge extending almost the full length of the chord at α = 6.4° where stall occurs.

The C_P distribution for α = -1.6° in figure 7.12 shows that greater suction is maintained on the lower surface up to x = 0.25 after separation from the upper and lower horns. Following reattachment the camber of the upper surface restores sufficient suction pressure (in advance of the pressure recovery) to ensure there is some lift production over the aft section of the aerofoil. The lift produced over the aft section (plus that due to the suction peak of the upper horn tip) must be almost equal to, but slightly greater than the downforce produced over the forward section; leading to the very small value for predicted C_L reported at this incidence.

At α = 0.4° there is much less distinction in C_P for the upper and lower surfaces at separation and in the subsequent separated region. The upper surface flow reattaches before the lower surface flow. The early upper surface reattachment occurs before the onset of the adverse pressure gradient, leading to greater suction on the upper surface relative to the lower surface from x = 0.2 to the trailing edge. This enhanced aft lift production was likely significant in the increased value of C_L predicted at this incidence.

At α = 2.4° and α = 4.4° the increase in lift continues because of reduced suction on the lower surface and increased suction on the upper surface before separation. This ceases however, at α = 6.4°, with the reduced suction associated with full upper surface stall leading to a decrease in predicted C_L.

CFD Results for the Sin(θ) Conditions Profile

CFD generated plots of lift and drag coefficient variance for the Sin(θ) profile are presented in figure 7.13; velocity contours for incidences of -1.6° to 7.4° are presented in figure 7.14 and pressure coefficient distributions for incidences of -1.6° to 6.4° are presented in figure 7.15.

Relative to the RefIS profile the Sin(θ) profile is far more intrusive primarily by virtue of the significantly increased upper horn thickness and a larger upper horn growth vector angle, as well as an increased lower horn thickness.

The lifting performance predicted by CFD for this aerofoil (see figure 7.13) does not follow convention because of the presence of such an ice accretion. The C_L is positive at α = -1.6° and decreases with increasing incidence with a first reported negative C_L at α = 2.4°. After α = 2.4° the reported lift values increase with incidence, with the last negative value occurring at α = 6.4°. The full C_L variation occurs across a range of only 0.3 units.

Contour plots (7.14) show the largest separated region on the lower surface, which is fully separated, at α = -1.6°, decreasing in size with increasing incidence. The opposite occurs for the upper surface with full separation observed at α = 2.4°. Increasing the incidence thereafter results in a larger separated wake in the region above the upper surface.

At α = -1.6° the contour plot reports full separation on the lower surface and reattachment by 40-50% chord length on the upper surface. Correspondingly the C_P distribution reports greater suction as the flow negotiates the upper horn before separation, reattachment and pressure recovery; relative to the suction as it negotiates the lower surface before total separation. The result is the positive C_L predicted at α = -1.6°.

At α = 0.4° the contour plots report similarly sized separation bubbles on both surfaces. This is confirmed by the C_P distribution where greater upper

surface separation is reflected in the reduced level of suction created as the flow negotiates the upper horn tip; and reduced lower surface separation is reflected in the slightly enhanced level of suction created as the flow negotiates the lower horn tip. Similar reattachment and pressure recovery on both surfaces give a slight downforce loading over the aft 80% of the aerofoil which, combined with the slight resultant lift over the forward 20%, contributes to a near zero reported resultant lift.

At $\alpha = 2.4°$ the suction associated with upper surface horn-tip separation is less with the onset of full upper surface stall. The earlier reattachment on the lower surface (shorter reattachment zone) combined with enhanced forward lower surface suction, increases the slope of the line representing lower surface C_P from around x = 0.1 to x = 0.4. This line now sits above the line representing upper surface C_P and the gap between the two lines describes the difference in upper and lower surface loading that leads to a negative value for C_L.

At incidences above $\alpha = 2.4°$ there is little change in upper surface C_P distribution; whilst on the lower surface the reducing size of the separation bubble via reattachment means that the lower surface C_P becomes less negative more quickly, crossing beneath the upper surface line near the start of pressure recovery. For $\alpha = 4.4°$ this results in a slight increase in C_L which occurs again at $\alpha = 6.4°$.

CFD Results for the LWC(B)/Sin(θ - 90°) Conditions Profile

CFD generated plots of lift and drag coefficient variance for the LWC(B)/Sin(θ - 90°) profile are presented in figure 7.16; velocity contours for incidences of -1.6° to 7.4° are presented in figure 7.17 and pressure coefficient distributions for incidences of -1.6° to 6.4° are presented in figure 7.18.

Relative to the RefIS profile the LWC(B)/Sin(θ - 90°) profile is a little more

intrusive, predominantly by virtue of slightly thicker upper and lower horns. There is also an additional growth on the lower surface aft of the main horn.

The lifting performance predicted by CFD, and presented in figure 7.16, is not conventional; with a decrease in C_L from α = -1.6° to 2.4° before an increase thereafter.

The contour plots presented in figure 7.17 provide an initial insight into the predicted solution. The lower surface separation bubble is largest at α = -1.6° and decreases with incidence. The separation bubble on the upper surface is slightly different in nature to that observed with RefIS (which is quite similar in shape); being less extensive along the chord and more extensive vertically. It also seems more resilient to increasing angle of attack, extending far less aft than the equivalent RefIS feature; so much so in fact that the onset of upper surface stall is caused by separation starting at the trailing edge (α = 4.4°) and moving forwards until the two separated regions merge into one.

At α = -1.6° the C_P distribution (figure 7.18) shows slightly greater suction predicted for the upper surface than the lower surface in advance of reattachment and pressure recovery. There is also a period of favourable pressure gradient before pressure recovery from approximately x = 0.1 to 0.4 on the upper surface. A reducing lower surface suction C_P during reattachment and also in the adverse pressure gradient contribute, along with the C_P distribution over the upper surface, to the positive C_L reported.

Over incidences of $\alpha = 0.4°$ and $\alpha = 2.4°$ there is little change in the predicted upper surface pressure distribution. Combined with the apparent resilience of the upper surface separation bubble to increased angles of attack shown in velocity contours, these upper surface distributions suggest the entrainment of less retarded fluid is predicted to re-energise the boundary layer in this case; to the extent that stall occurs via trailing edge separation.

Increasing incidence has the effect of shortening the lower surface separation bubble, i.e. creating smaller reattachment zones. The main effect of this initially, is to reduce the difference in C_P between upper and lower surfaces from x = 0.2 to x = 1.0, and hence to reduce lift (α = -1.6° to 2.4°). However as incidence increases further there is a predicted decrease in suction C_P magnitude from x = 0 to x = 0.2 (approximately) on the lower surface. This is a result of reducing suction at the lower surface horn tip before separation (that then influences the separated C_P) with increasing incidence, plus more rapid reattachment with increasing incidence. This effect leads to the recovery in lift predicted after α = 2.4°.

The difference in predicted lifting performance between this profile and the RefIS profile is somewhat greater than expected given their geometrical similarities. Inspection of the C_P distributions available for both profiles shows that the differences in predicted C_L seem to be attributable mainly to the nature of the separation. The C_P distribution for the upper surface of the LWC(B)/Sin(θ - 90°) profile would seem to contribute less to increasing lift than the upper surface for the RefIS profile; this line moves notably less over the course of increasing incidence in advance of stall. Two features are thought to contribute to this and are: (a) the sharp discontinuity at the upper horn tip and (b) the shorter but more vertically extensive separation bubble. Any slight change in separation location at differing incidences will be diminished with such a discontinuity and consequently, the change to C_P will reduce also. The slope of the C_P line associated with reattachment is also less changeable at lower angles of attack with the presence of the more vertically extensive separation bubble whose horizontal extent is less affected by increasing angle of attack.

The difference in lift trend therefore seems to be due to the difference between the upper surface loading and the subsequent interaction with lower surface loading. As already described the upper surface C_P distribution for the LWC(B)/Sin(θ - 90°) profile changes less with incidence, especially over lower values of α. The LWC(B)/Sin(θ - 90°) profile's earlier lower surface

reattachment serves to reduce the loading difference between upper and lower surfaces aft of x = 0.2 which, at the early angles of attack, reduces lift. Similar behaviour is evident on the lower surface of RefIS but this is less influential because of the initial increase in lifting performance with incidence.

7.2.1 Further Considerations of CFD Results

The results presented in section 7.2 highlight what is already evident in observing the C_L plots throughout Appendix E, which is that two different general trends exist in the lift coefficient plots; one of which would conventionally be expected, the other would not. Around half of the C_L plots in Appendix E exhibit a conventional trend, with the smallest value of C_L corresponding to the lowest angle of attack and increasing lift with increasing angle of attack before stall. However the other half of the results do not exhibit this behaviour; beginning with a higher C_L at the lowest angle of attack and having initially reducing C_L as incidence increases before a lift recovery. Observation of such a trend prompted further consideration of these results' fidelity.

The simplest interpretation of this trend is that for the majority of incidences, the lift coefficient is lower than it is for the RefIS profile and for others exhibiting the more conventional lifting behaviour; i.e. its aerodynamic lifting performance is worse. Certainly the performance associated with drag for aerofoils whose lift performance conforms to this trend is predicted to be worse in comparison with those aerofoils exhibiting the conventional trend.

The pressure distribution analyses for the Sin(θ - 90°) and Sin(θ) profiles have described in some detail why the predicted flow behaviour gives such lift loading. The 'LWC (30%) Rise & Temp Drop' profile is presented as a final example, selected because its predicted C_L and C_D results make it the ice profile with the most detrimental impact upon aerodynamic performance. The 'profile colour key' for this profile is presented in figure 7.19.

The velocity contours for this profile at $\alpha = 2.4°$ are plotted with the associated C_P distribution in figure 7.20. The contours show that at this incidence the upper surface is fully stalled while lower surface reattachment occurs at around 70% of the clean chord. The suction C_P associated with the lower surface before separation is greater in magnitude than the equivalent associated with the upper surface, remaining so until the trailing edge. This therefore results in the negative C_L value at this angle of attack.

The velocity contours for this profile at $\alpha = 8.4°$ are plotted with the associated C_P distribution in figure 7.21. At this incidence the contours show that the upper surface is still fully stalled but lower surface reattachment occurs at around 30% chord. This reattachment restores the lower surface C_P to a value more expected for attached flow. This C_P is smaller in magnitude than the upper surface C_P. Consequently at this angle of attack the upper surface suction proves slightly more dominant, giving a slightly positive C_L value.

Whilst the fluid behaviour associated with this trend seems plausible, the trend is present because the solver either predicts the fluid flow and associated C_P values correctly, or it does so incorrectly. Yet the most salient issue associated with this trend, is perhaps that it arises for certain profiles first and foremost because of the significantly detrimental influence of the upper horn on the airflow. Were this feature less intrusive and the upper surface more capable of producing a greater level of suction, then the small levels of downforce predicted to occur would be far less influential on the overall loading. Therefore despite the uncertainty associated with this trend, it is expected that iced profiles exhibiting such a characteristic are less capable of producing aerodynamic lift.

Plots of drag coefficient versus angle of attack report a more conventional variation in C_D. Smallest values generally occurred at the lowest incidences (α = -1.6° to $\alpha = 2.4°$) before increasing correspondingly with higher angles

of attack. The difference in C_D magnitude between those profiles at opposite ends of the drag spectrum is significant; at $\alpha = 2.4°$ the 'LWC (30%) Rise & Temp Drop' profile has a predicted C_D of 0.136, approximately 4.5 times the corresponding value for the 'Construct #2' profile with $C_D = 0.029$.

Given the significant number of ice profiles generated and analysed during the research programme, each profile was placed within one of four categories that reflected their impact upon the aerodynamic performance of the aerofoil relative to the RefIS profile. The profiles were categorised according to similarity of the lift curve to the RefIS lift curve. The category containing those profiles predicted to be least detrimental to aerodynamic performance was the Sub-Critical category, followed by the Near-Critical category (which contained the RefIS profile), then the Super-Critical category and finally the Super-Critical$^+$ category which contained those profiles predicted to be most detrimental to aerodynamic performance.

The C_L versus α and C_D versus α plots for the profiles in each category are presented within figures 7.22, 7.24, 7.26 and 7.28. These are presented at the end of this section along with figures 7.23, 7.25, 7.27 and 7.29; which show the profiles that exist in each category.

In figure 7.22 the aerodynamic detriment presented by the C_L and C_D curves for the Sub-Critical category is observably less than that for the RefIS profile, and the trend in lift is conventional, with C_L increasing with α until stall.

In figure 7.24 the aerodynamic detriment presented by the C_L and C_D curves for the Sub-Critical category is generally more similar to that for the RefIS profile than for the Sub-Critical category, though the trend in several of the lift curves cannot be clearly identified as conventional.

In figure 7.26 the aerodynamic detriment presented by the C_L and C_D curves for the Super-Critical category is generally more severe than that for the reference profile, and the trend in the lift curves is not conventional, with C_L

reducing as α increases, until a minima is reached where the trend reverses.

In figure 7.28 the aerodynamic detriment presented by by the C_L and C_D curves for the Super-Critical$^+$ category is notably more severe than that for the RefIS profile, and the unconventional trend present in the lift curve is more pronounced than for the Super-Critical category.

The impact of some of the ice shapes generated has been predicted to be so severe that they would only be expected to be able to maintain any lifting capability (if at all) at low angles of attack. So for this reason, and because it is very similar to the UAV flight model angle of attack in cruise, $\alpha = 2.4°$ has been selected as the incidence used to rank the severity of the ice profiles by C_D. This ranking is presented in table 7.5.

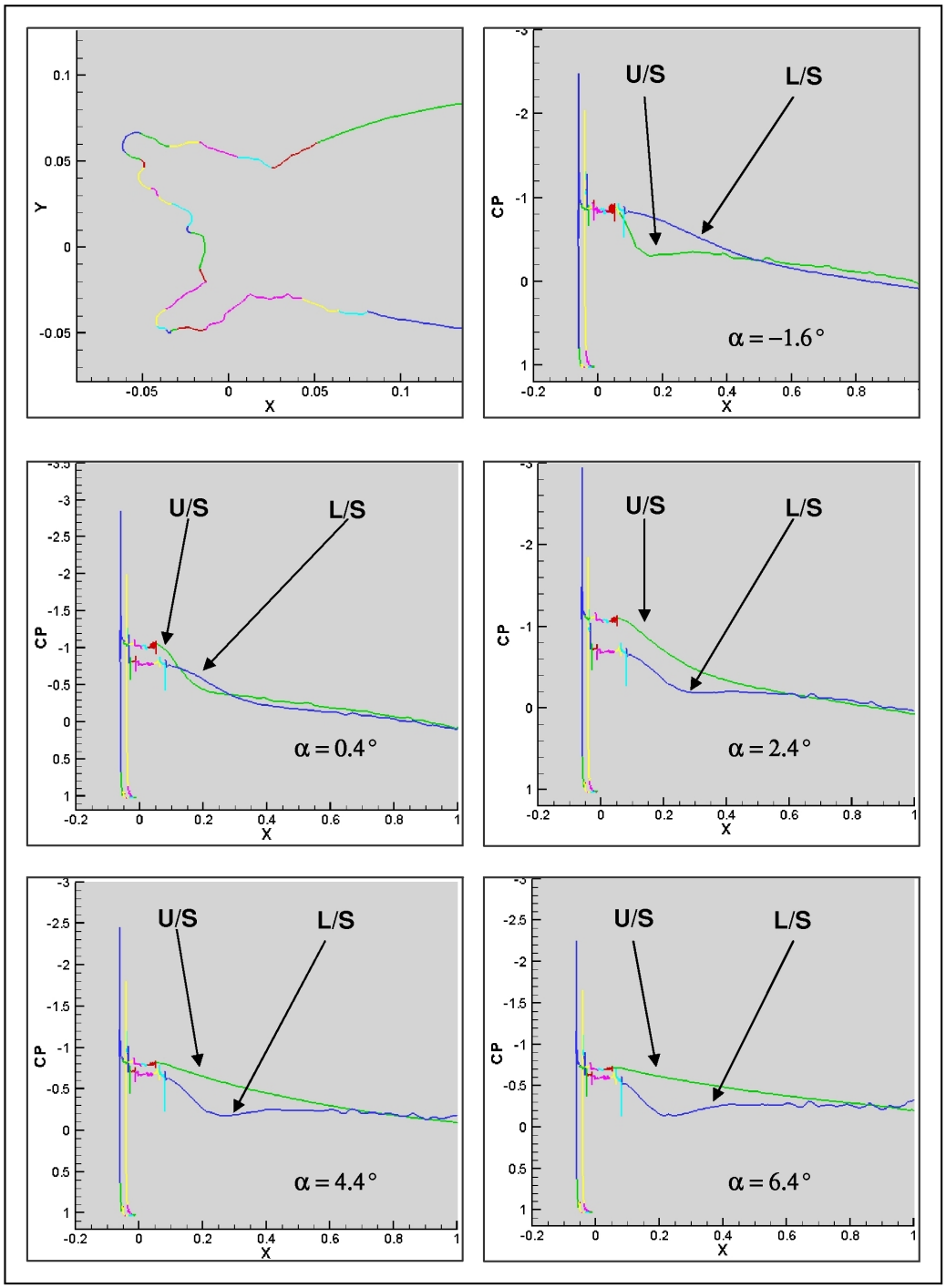

Figure 7.9: Pressure coefficient distributions from CFD predictions for the RefIS profile for α = (-1.6°, 0.4°, 2.4°, 4.4° and 6.4°), with profile colour key.

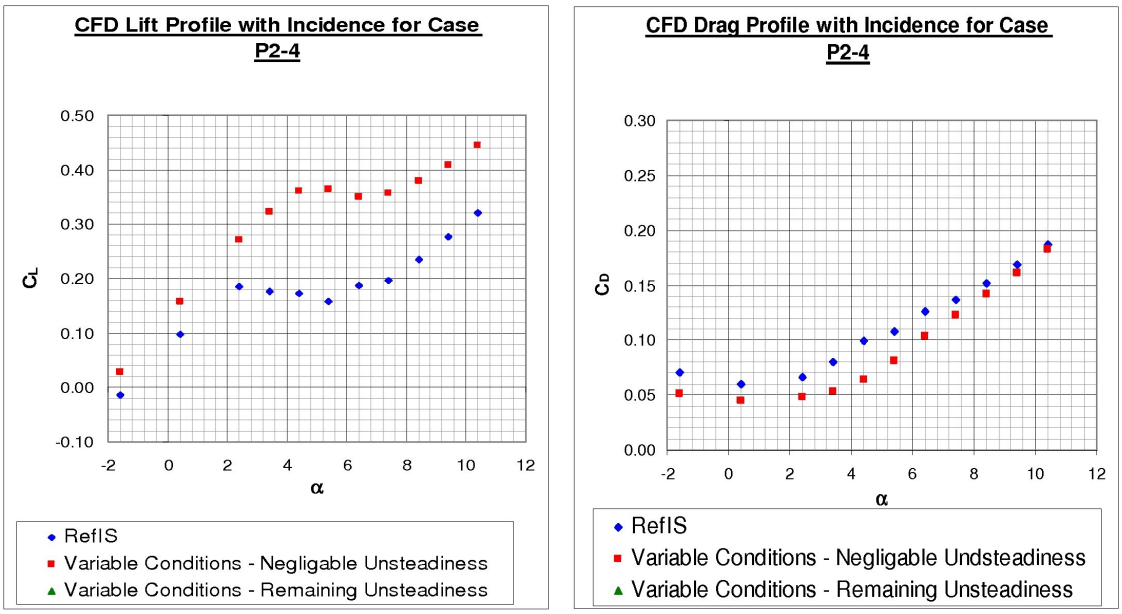

Figure 7.10: Lift and drag coefficient versus angle of attack from CFD predictions for the Sin(θ - 90°) profile.

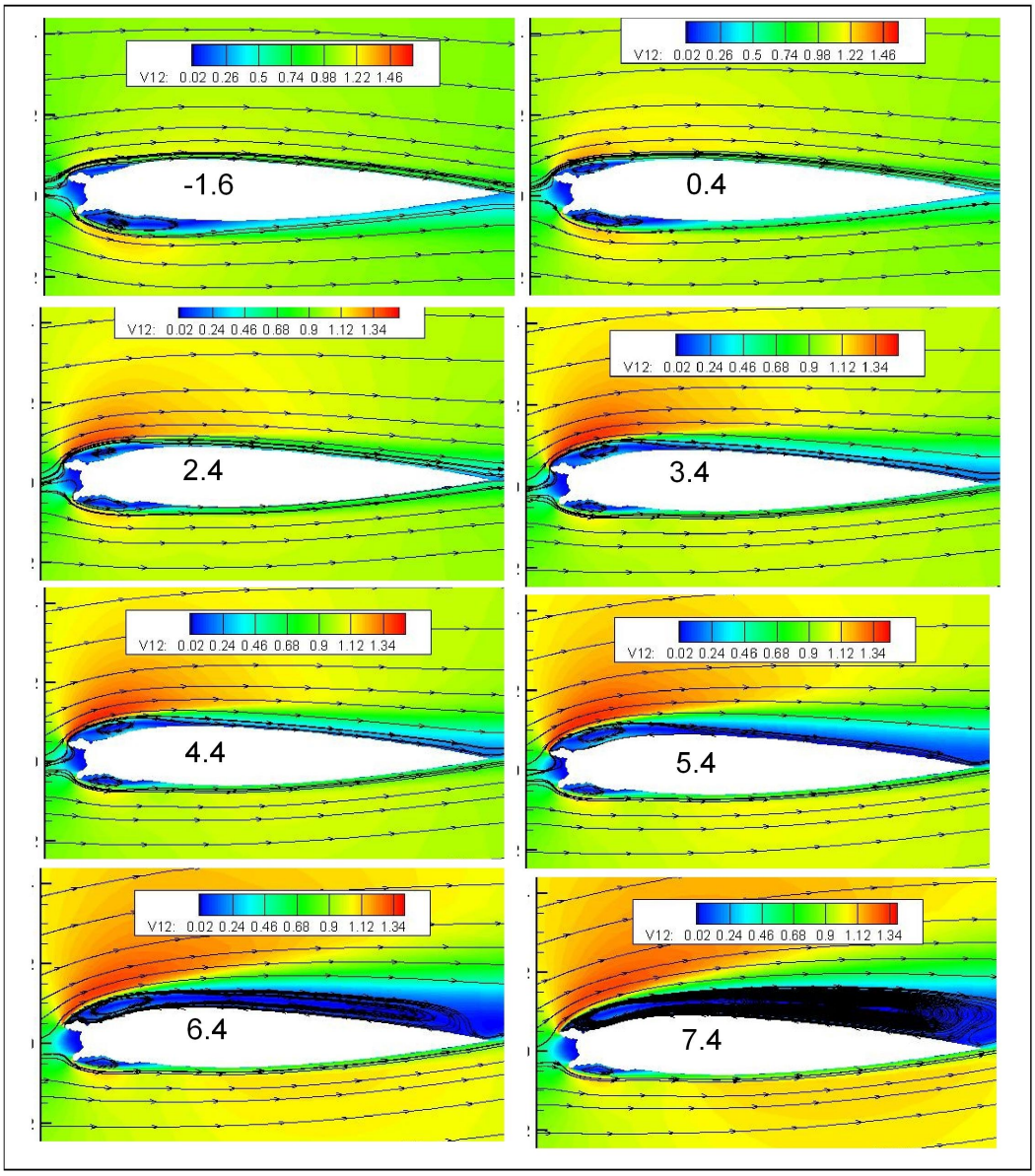

Figure 7.11: Velocity contour plots from CFD predictions for the Sin(θ - 90°) profile for α = (-1.6°, 0.4°C, 2.4°, 3.4°, 4.4°, 5.4°, 6.4° and 7.4°).

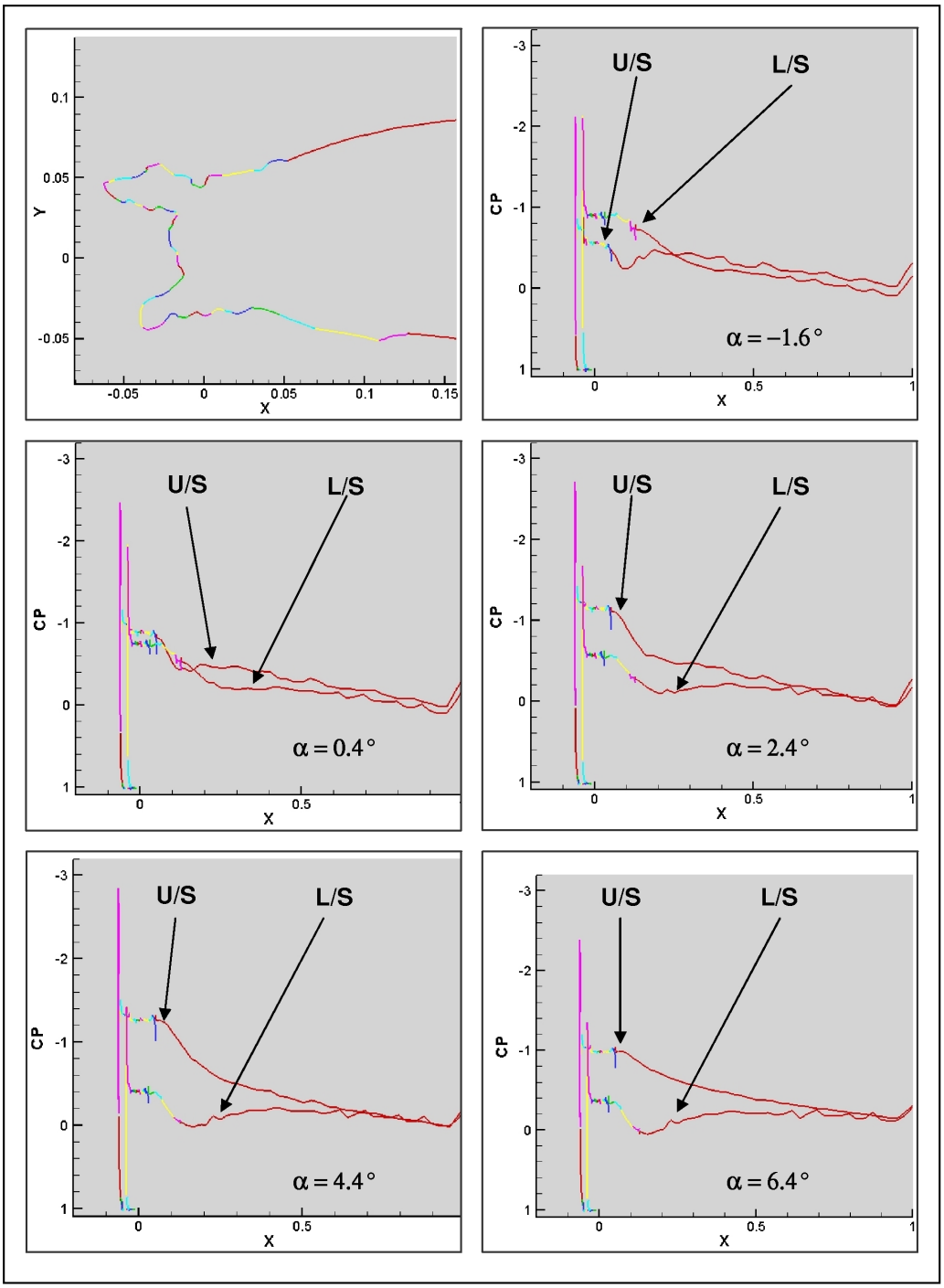

Figure 7.12: Pressure coefficient distributions from CFD predictions for the Sin(θ - 90°) profile for α = (-1.6°, 0.4°, 2.4°, 4.4° and 6.4°), with profile colour key.

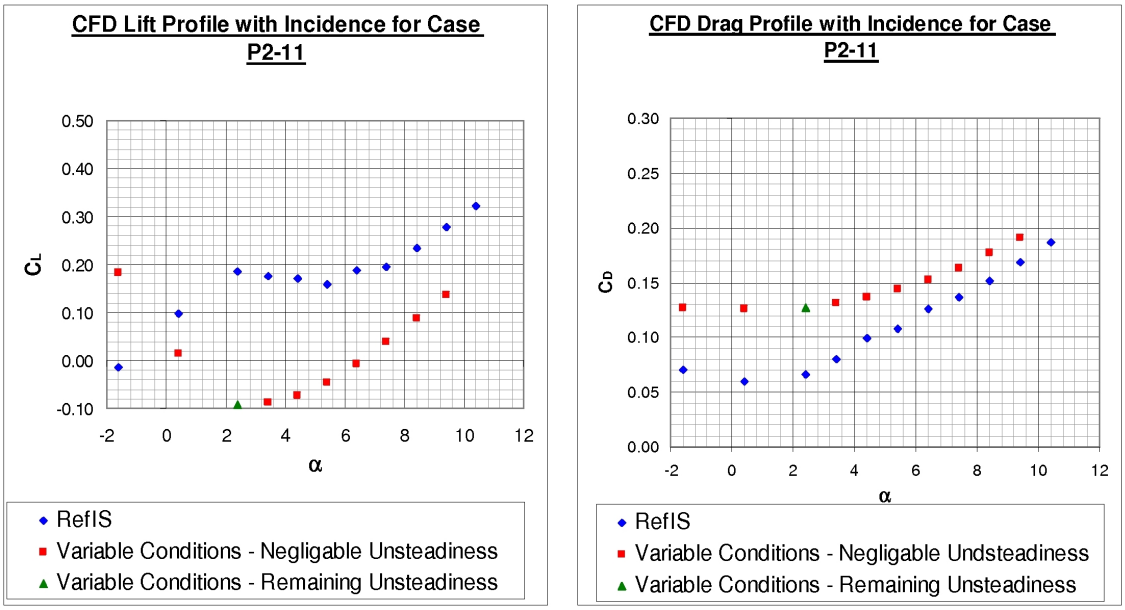

Figure 7.13: Lift and drag coefficient versus angle of attack from CFD predictions for the Sin(θ) profile.

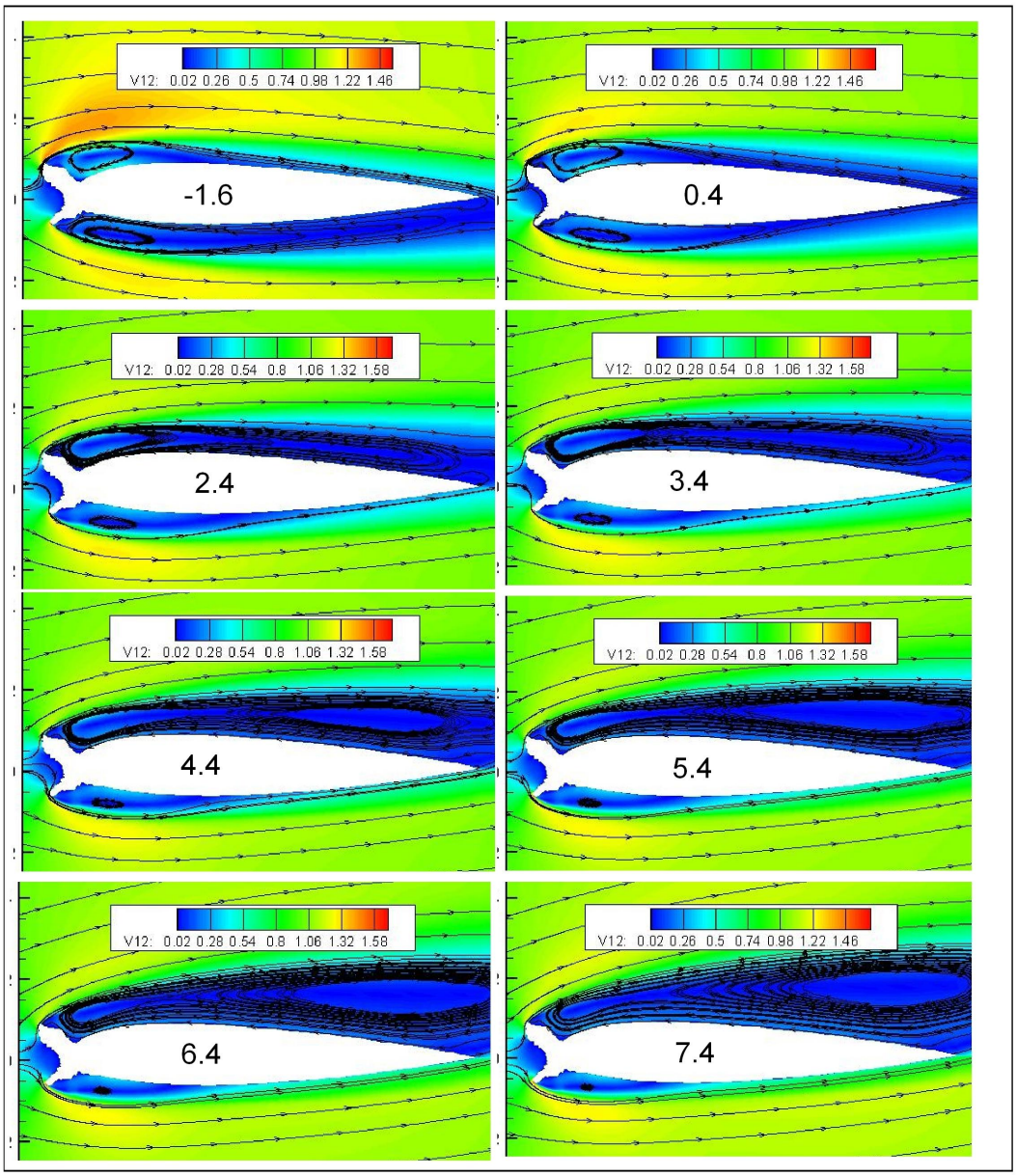

Figure 7.14: Velocity contour plots from CFD predictions for the Sin(θ) profile for α = (-1.6°, 0.4°, 2.4°, 3.4°, 4.4°, 5.4°, 6.4° and 7.4°).

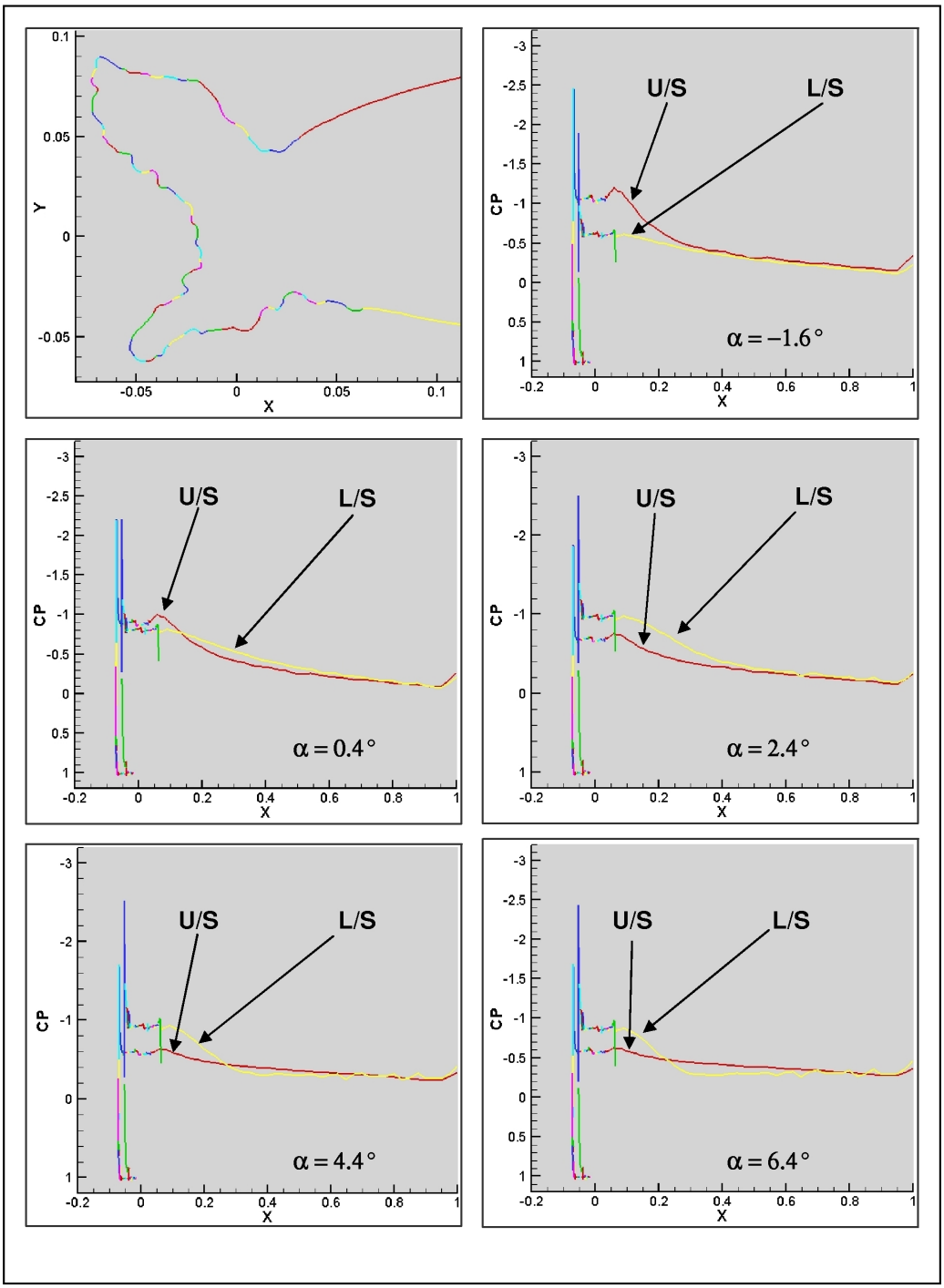

Figure 7.15: Pressure coefficient distributions from CFD predictions for the Sin(θ) profile for α = (-1.6°, 0.4°, 2.4°, 4.4° and 6.4°), with profile colour key.

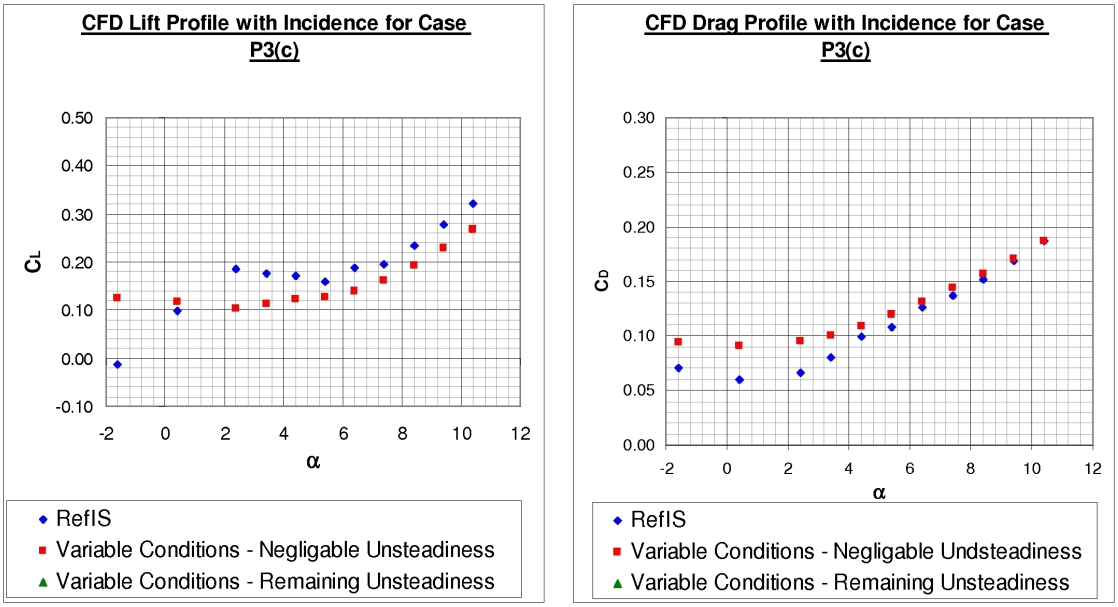

Figure 7.16: Lift and drag coefficient versus angle of attack from CFD predictions for the LWC(B)/Sin(θ - 90°) profile.

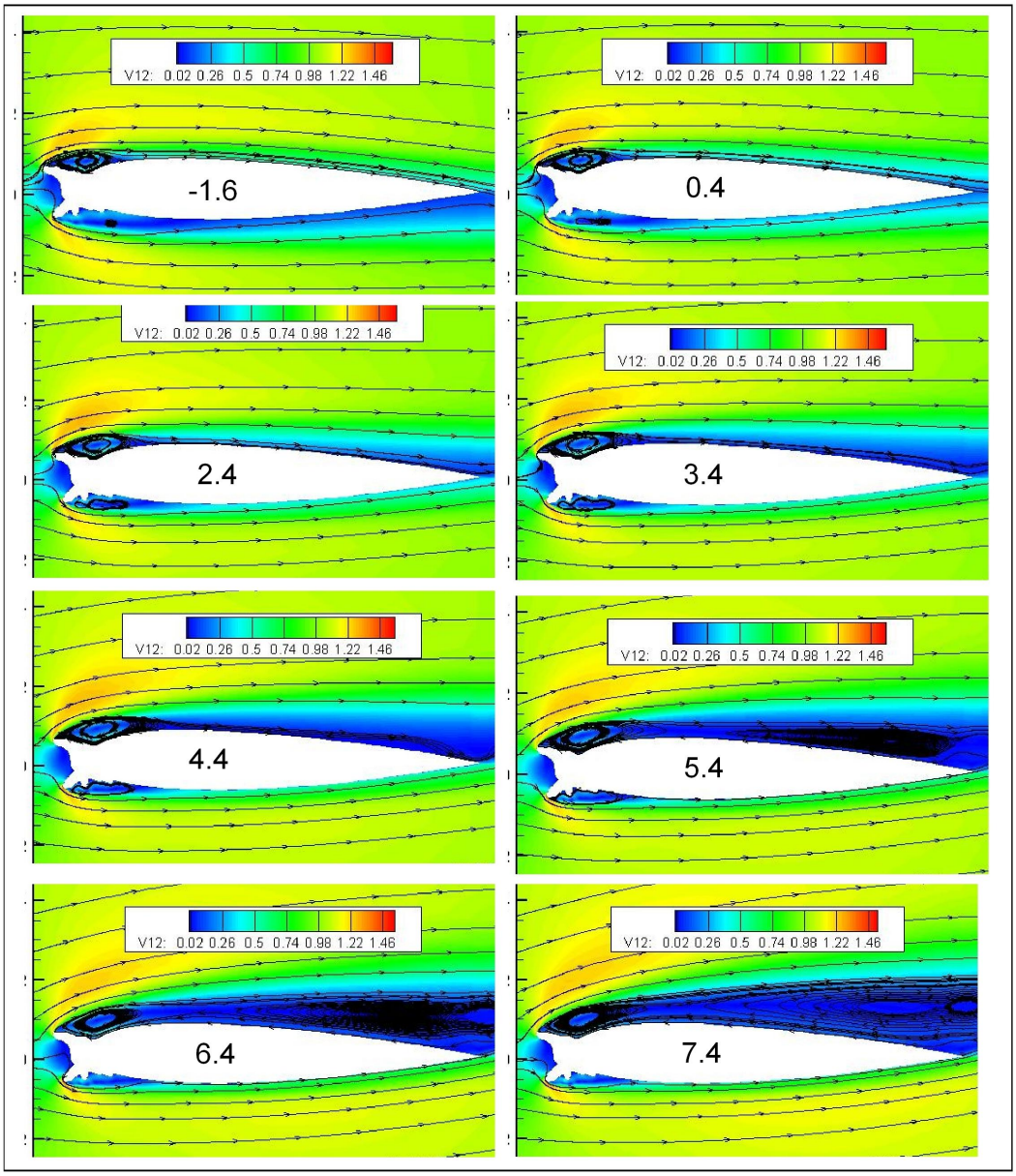

Figure 7.17: Velocity contour plots from CFD predictions for the LWC(B)/Sin(θ - 90°) profile for α = (-1.6°, 0.4°, 2.4°, 3.4°, 4.4°, 5.4°, 6.4° and 7.4°).

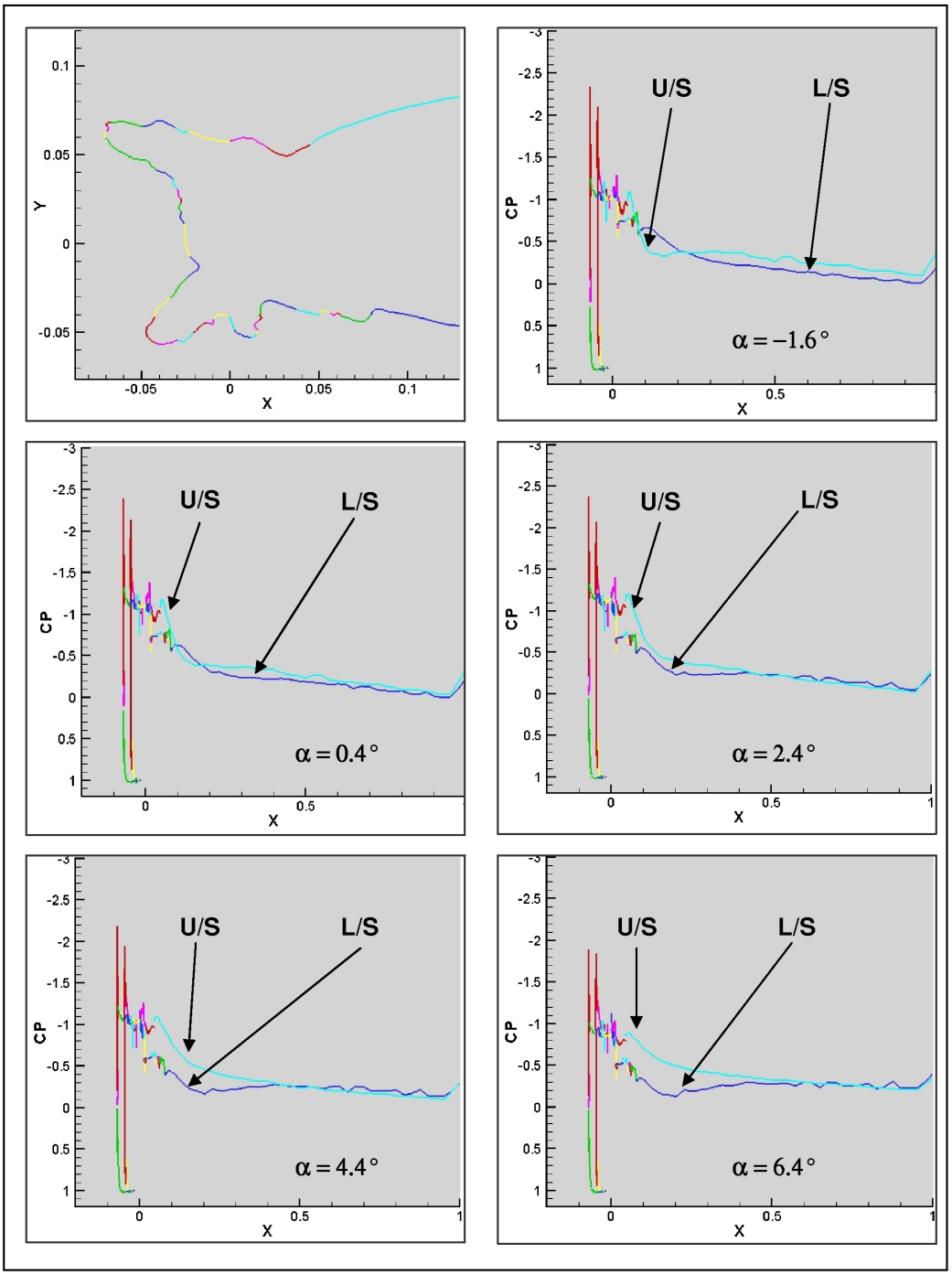

Figure 7.18: Pressure coefficient distributions from CFD predictions for the LWC(B)/Sin(θ - 90°) profile for α = (-1.6°, 0.4°, 2.4°, 4.4° and 6.4°), with profile colour key.

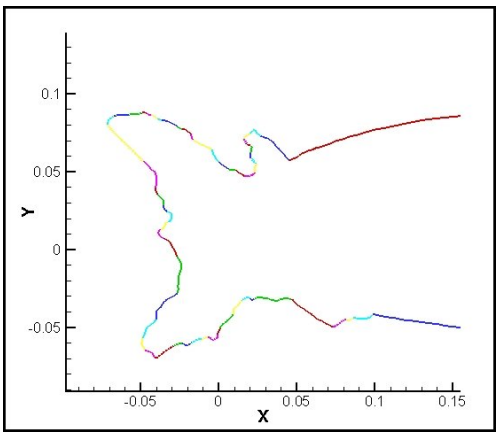

Figure 7.19: Profile colour key for C_P distribution analysis of the LWC (30%) Rise & Temp Drop profile's aerodynamic performance.

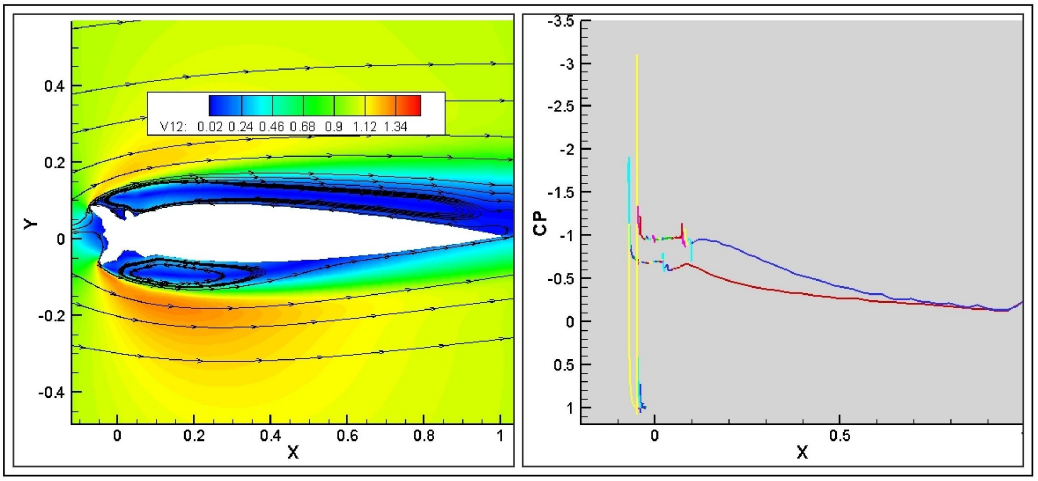

Figure 7.20: Velocity contour plot and C_P distribution from CFD predictions for the LWC (30%) Rise & Temp Drop profile at $\alpha = 2.4°$.

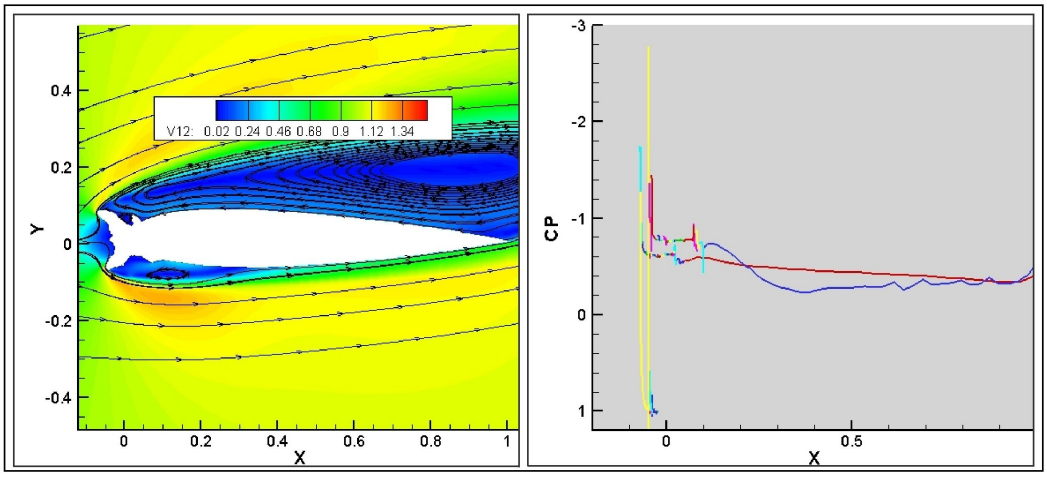

Figure 7.21: Velocity contour plot and C_P distribution from CFD predictions for the LWC (30%) Rise & Temp Drop profile at $\alpha = 8.4°$.

This page has been left intentionally blank.

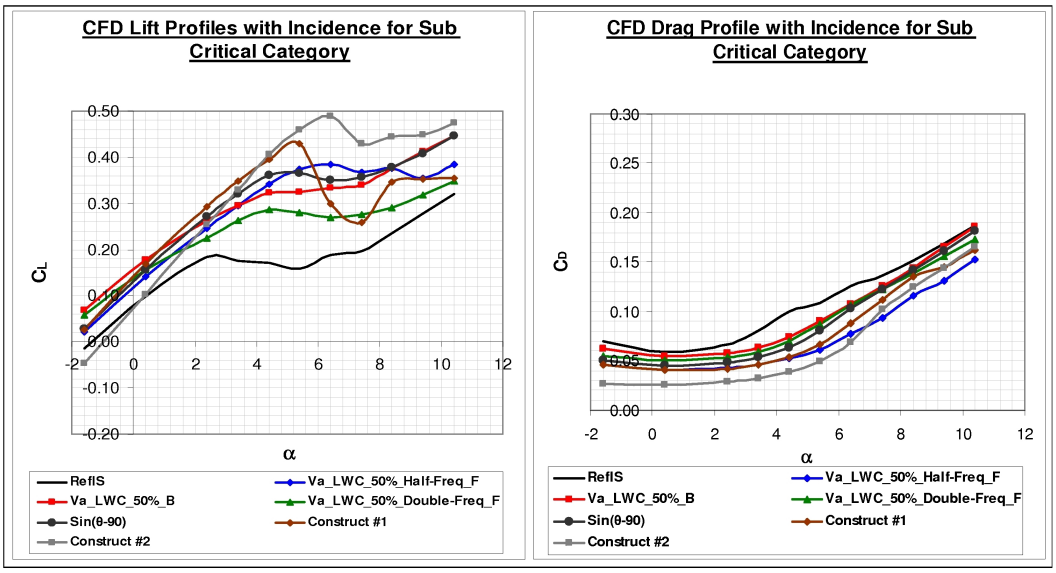

Figure 7.22: Lift and drag coefficient plots, varying with angle of attack; for the profiles in the Sub-Critical category.

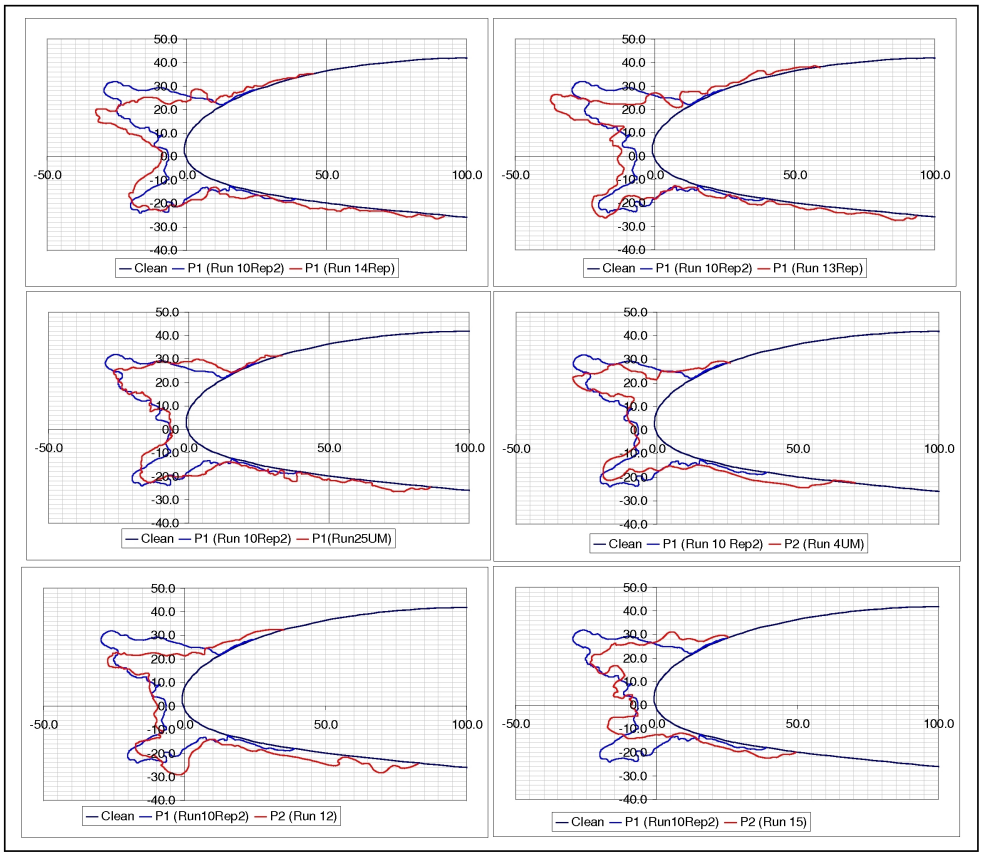

Figure 7.23: The ice accretion profiles whose predicted C_L and C_D results place them in the sub-critical category.

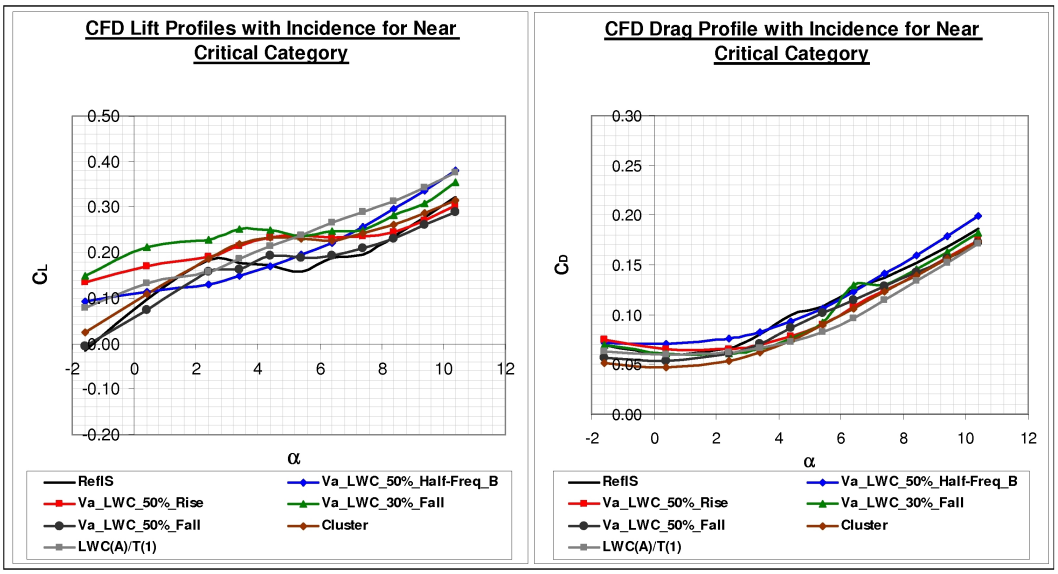

Figure 7.24: Lift and drag coefficient plots, varying with angle of attack; for the profiles in the Near-Critical category.

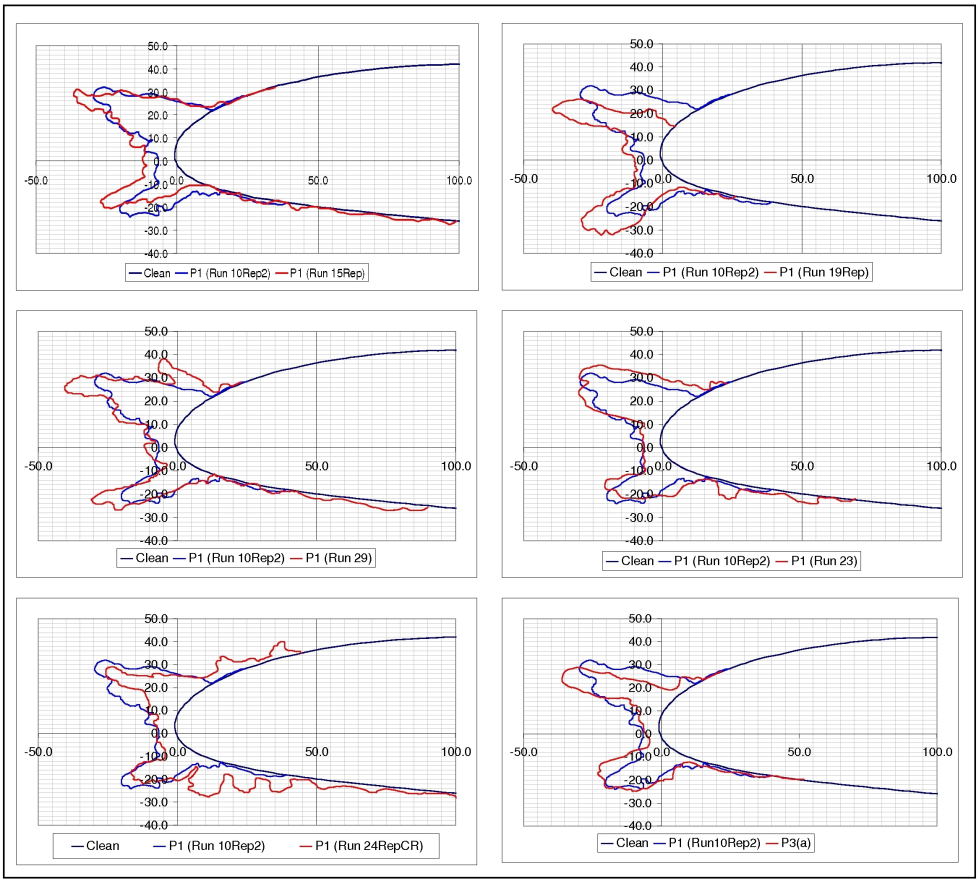

Figure 7.25: The ice accretion profiles whose predicted C_L and C_D results place them in the near-critical category.

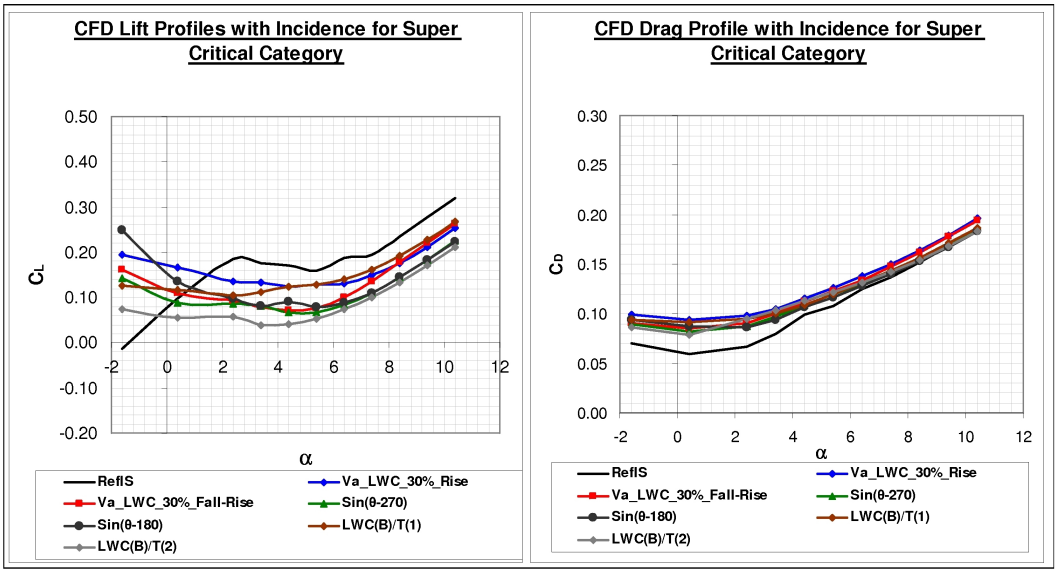

Figure 7.26: Lift and drag coefficient plots, varying with angle of attack; for the profiles in the Super-Critical category.

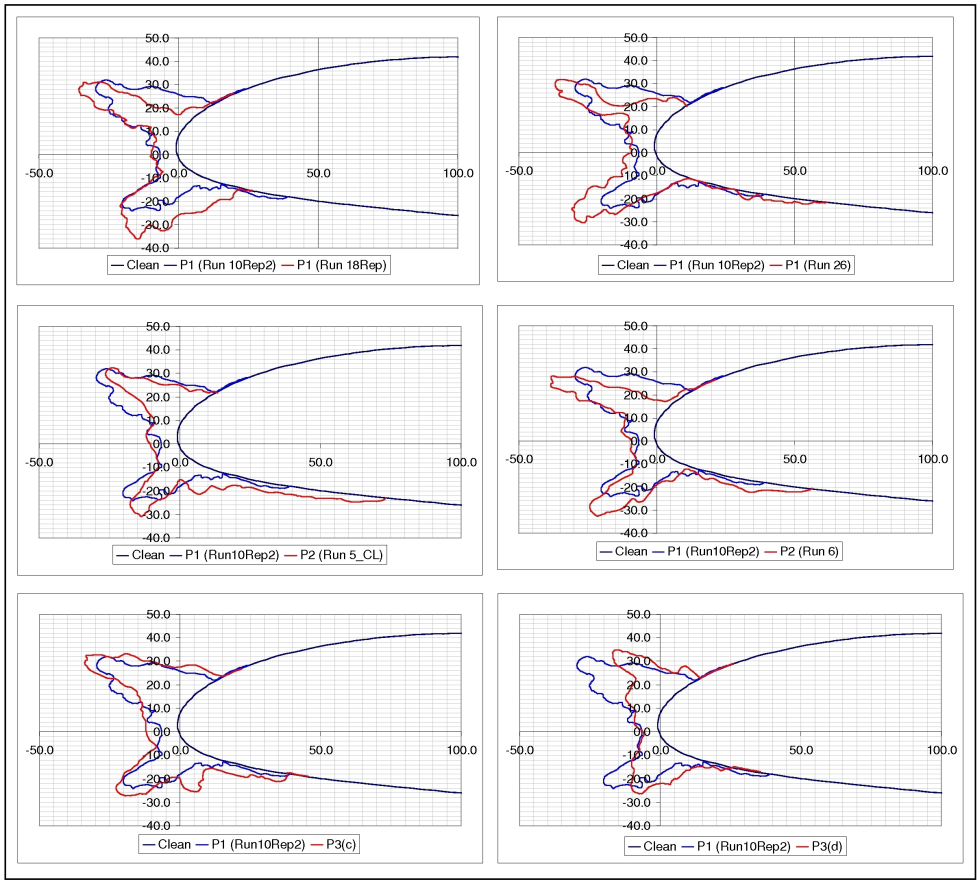

Figure 7.27: The ice accretion profiles whose predicted C_L and C_D results place them in the super-critical category.

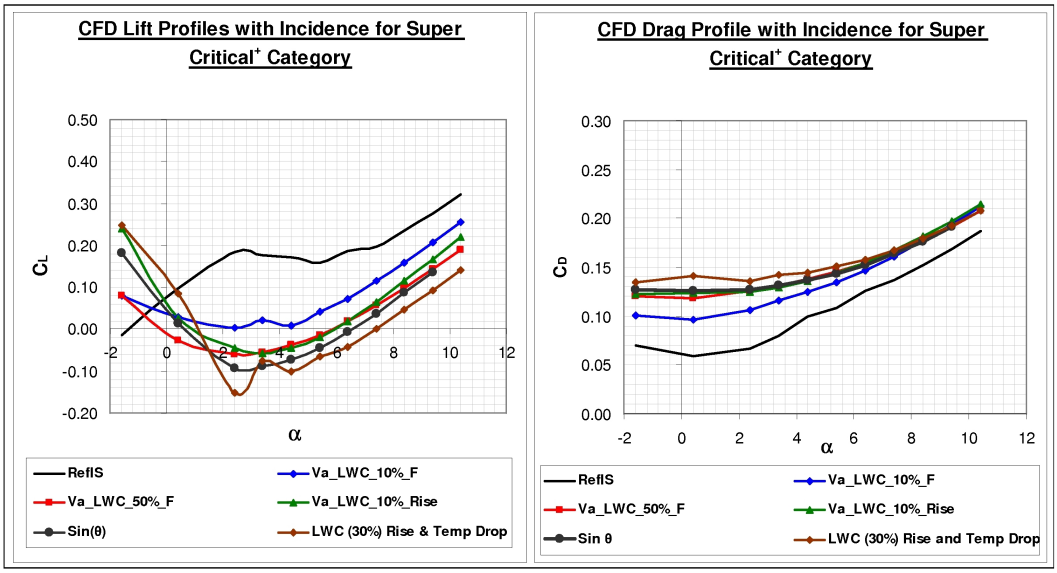

Figure 7.28: Lift and drag coefficient plots, varying with angle of attack; for the profiles in the Super-Critical^{+} category.

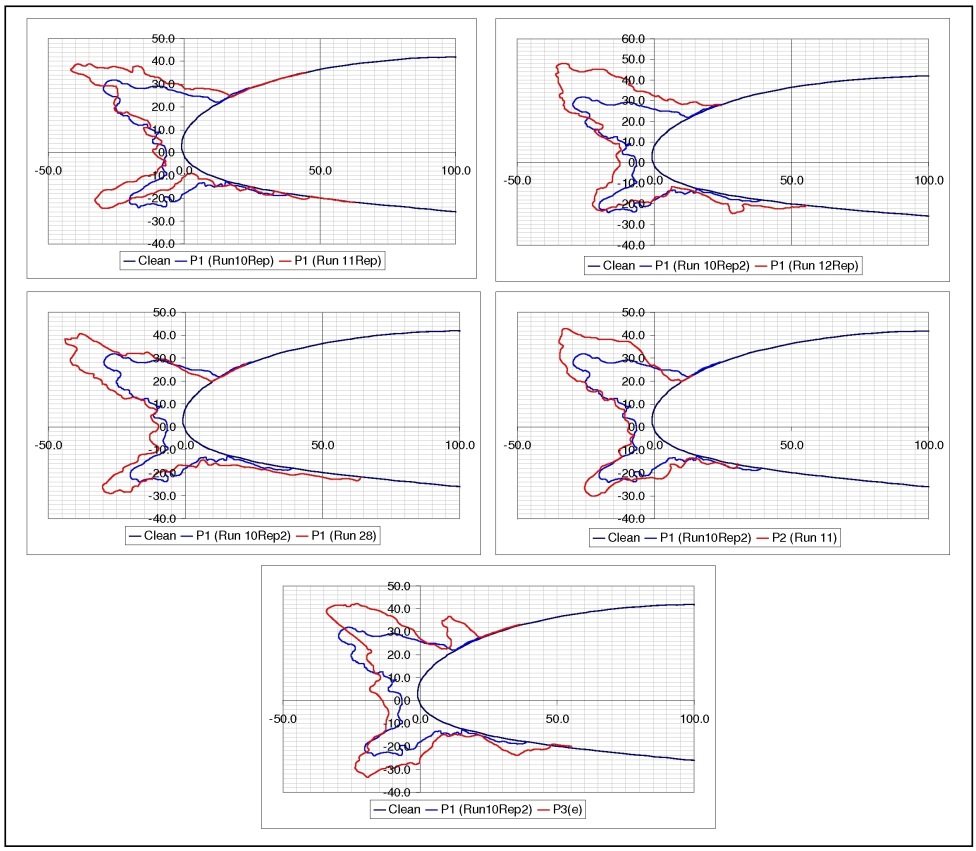

Figure 7.29: The ice accretion profiles whose predicted C_L and C_D results place them in the super$^+$-critical category.

Ranking	Case Code	C_L	C_D	Category
1	LWC (30%) Rise & Temp Drop	-0.152	0.136	Super-Critical$^+$
2	Sin(θ)	-0.094	0.128	Super-Critical$^+$
3	Va_LWC_50%_F	-0.059	0.126	Super-Critical$^+$
4	Va_LWC_10%_Rise	-0.039	0.125	Super-Critical$^+$
5	Va_LWC_10%_F	0.003	0.106	Super-Critical$^+$
6	Va_LWC_30%_Rise	0.137	0.098	Super-Critical
7	LWC(B)/Sin(θ - 270°)	0.064	0.096	Super-Critical
8	LWC(B)/Sin(θ - 90°)	0.104	0.095	Super-Critical
9	Va_LWC_30%_Fall-Rise	0.093	0.091	Super-Critical
10	Sin(θ - 270°)	0.086	0.087	Super-Critical
11	Sin(θ - 180°)	0.099	0.086	Super-Critical
12	Va_LWC_50%_Half-Freq_B	0.130	0.076	Near-Critical
13	RefIS	0.185	0.067	Near-Critical
14	Va_LWC_50%_Rise	0.192	0.066	Near-Critical
15	LWC(A)/Sin(θ - 90°)	0.159	0.062	Near-Critical
16	Va_LWC_30%_Fall	0.228	0.061	Near-Critical
17	Va_LWC_50%_Fall	0.159	0.061	Near-Critical
18	Va_LWC_50%_B	0.263	0.058	Sub-Critical
19	Cluster	0.186	0.054	Near-Critical
20	Va_LWC_50%_Double-Freq_F	0.225	0.054	Sub-Critical
21	Sin(θ - 90°)	0.271	0.048	Sub-Critical
22	Va_LWC_50%_Half-Freq_F	0.246	0.042	Sub-Critical
23	Construct #1	0.293	0.042	Sub-Critical
24	Construct #2	0.254	0.029	Sub-Critical

Table 7.5: Iced aerofoil profiles' aerodynamic severity, ranked by drag coefficient.

7.2.2 Aerodynamic Assessment Using Linear Regression Models

Section 5.2.2 describes the use of established aerodynamic and geometric data for protuberances and experimentally & computationally generated ice accretions, to develop linear regression models designed to predict drag rise and lift loss (at maximum C_L) on the basis of upper horn geometry. In order to provide a contrasting method of ranking the ice profiles in terms of aerodynamic severity, suitable linear regression models were applied for $\alpha = 2.4°$, for each of the ice accretions generated during the experimental icing programme.

Figure 7.30 presents the ranking of ice shapes (by C_D) as determined by applying the linear regression model, and a colour-coded comparison with the CFD-ranking presented in table 7.5. There is some difference between the exact position of accretions within the two rankings, and this is expected, on the basis of the scatter in aerodynamic performance data that is not accounted for by the linear regression model. Overall, figure 7.30 shows that the categorisation of accretions by CFD generally agrees well with the ranking determined from the regression model, particularly with the Sub-Critical and Super-Critical$^+$ categories.

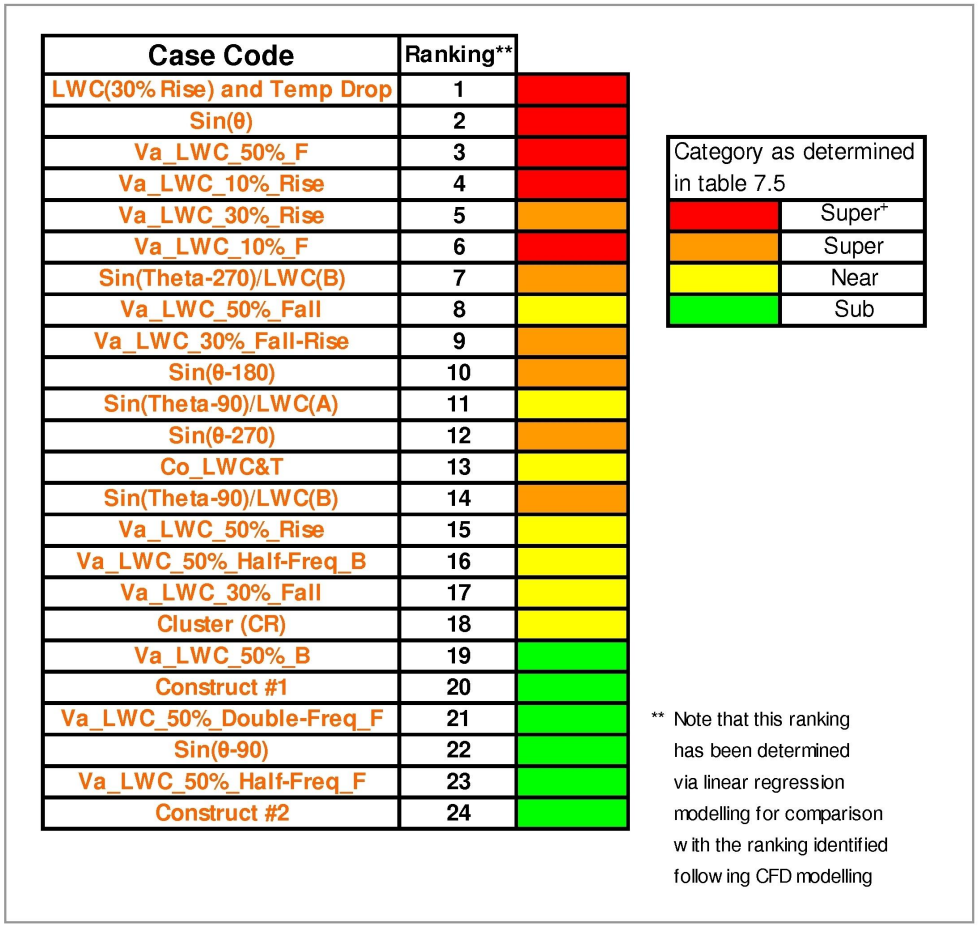

Figure 7.30: Tabular comparison of the ice profiles' severity ranking between CFD and linear regression modelling.

7.3 Results from the Trajice2 Investigation

Section 5.2.3 described the reasoning behind this activity, which was to investigate how different combinations of LWC, temperature and collection efficiency (via profile shape) could influence the potential for icing severity. The growth rate parameter (GR) reported by Trajice2 was selected as an appropriate measure of icing severity. This was because it would reflect the influence of temperature and LWC on the local thermal environment, the influence of collection efficiency on the proportion of water encountered that would strike the aerofoil and the influence of LWC on the amount of water available to strike the aerofoil.

An important objective of the investigation was to undertake a sufficient number of simulations to assess the impact of several sets of LWC and temperature conditions, and of three collection efficiencies via three different profiles. Doing so generated 27 different plots of growth rate distribution for comparison with one another. These plots are presented in figures 7.31, 7.33 and 7.35 for the Small-Ice, Medium-Ice and Large-Ice profiles respectively.

To simplify the growth rate distribution comparison for reporting purposes, each of these figures is presented alongside another, which serves to briefly describe the differences in growth rate distribution that arise when either: increasing LWC by $0.3g/m^3$, or by increasing T by $1.5°C$. So using the terminology present in table 5.1, each of figures 7.31, 7.33 and 7.35 describe the differences in growth rate distribution between case (a), and cases (b) and (d); where these cases differ from (a) in either LWC (by $0.3g/m^3$) or T (by $1.5°C$). This kind of comparison is helpful because describing these cases, whose conditions are perturbations of one another; shows how such perturbations can influence ice growth potential, and this at different stages in an ice accretion's development. Learning about such behaviour is of great relevance to this project.

In addition to considering the effects of LWC and temperature the influence

of collection efficiency associated with ice profiles of different sizes was of interest. It was therefore possible to compare collection efficiencies for each profile, and to undertake a comparison of the growth rate distributions for each case for two different profiles. These comparisons are presented in figures 7.37 and 7.38 respectively.

In describing the growth rate distributions several terms are used, namely GR, GR_{max}, FL, u/s and l/s. These represent growth rate, maximum growth rate, freezing limit, upper surface and lower surface respectively.

This page has been left intentionally blank.

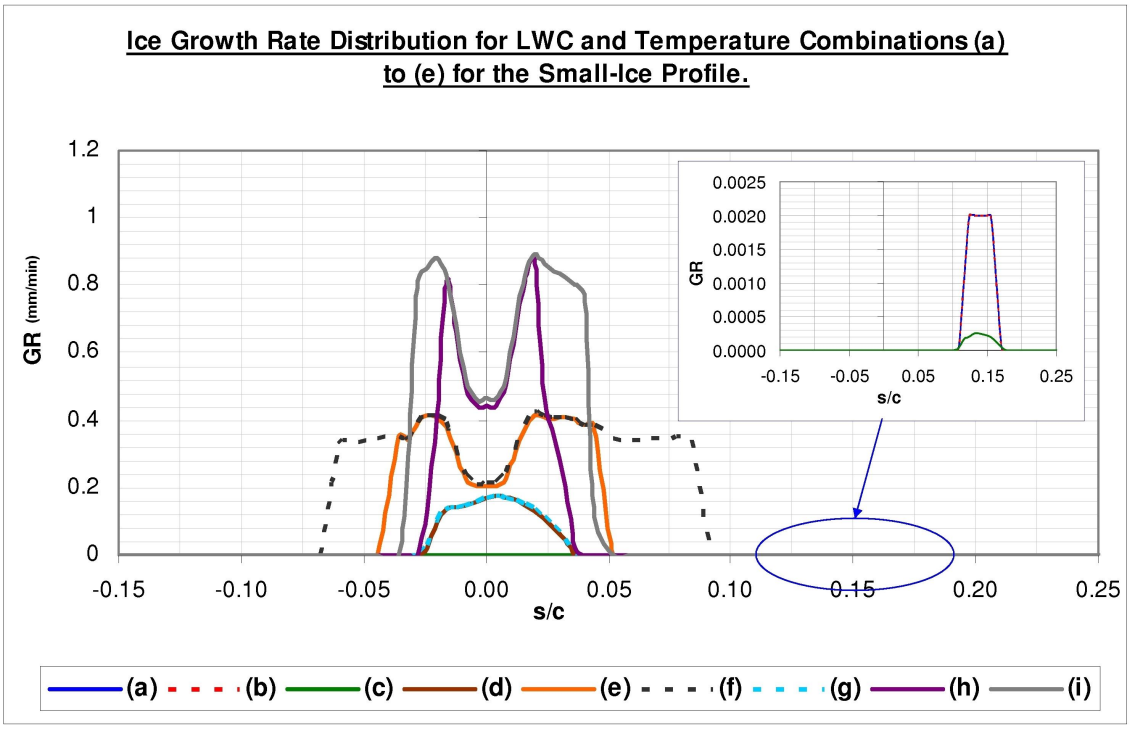

Figure 7.31: Growth rate distributions calculated for conditions (a) to (i) for the Small-Ice profile.

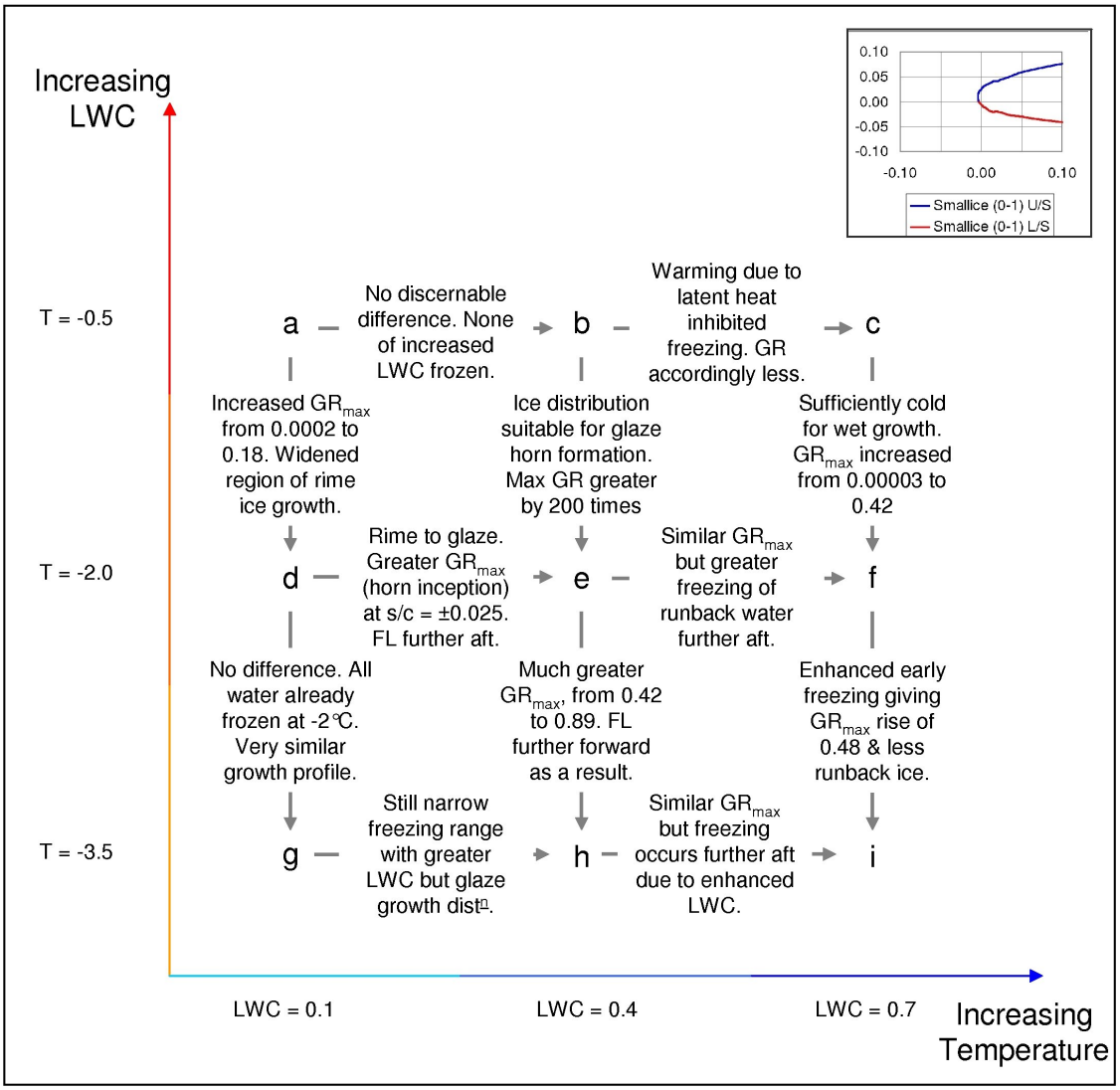

Figure 7.32: Descriptions of the change in calculated Growth Rate distribution following a change in either LWC or temperature, for the Small-Ice profile.

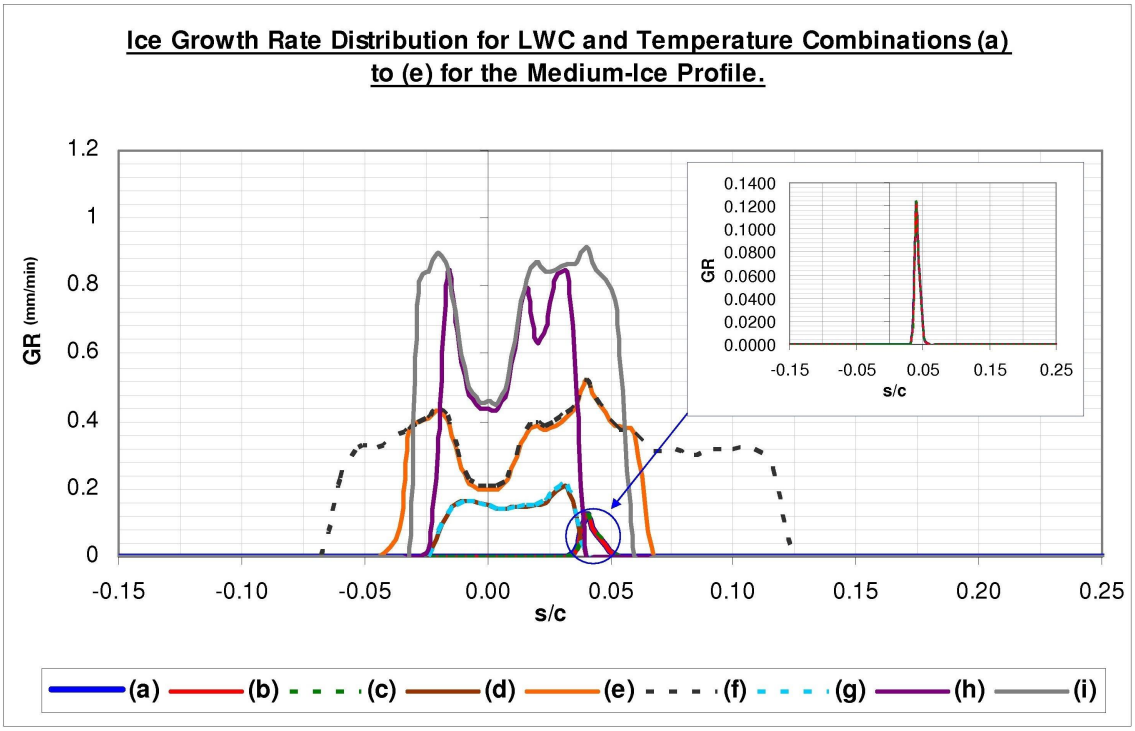

Figure 7.33: Growth rate distributions calculated for conditions (a) to (i) for the Medium-Ice profile.

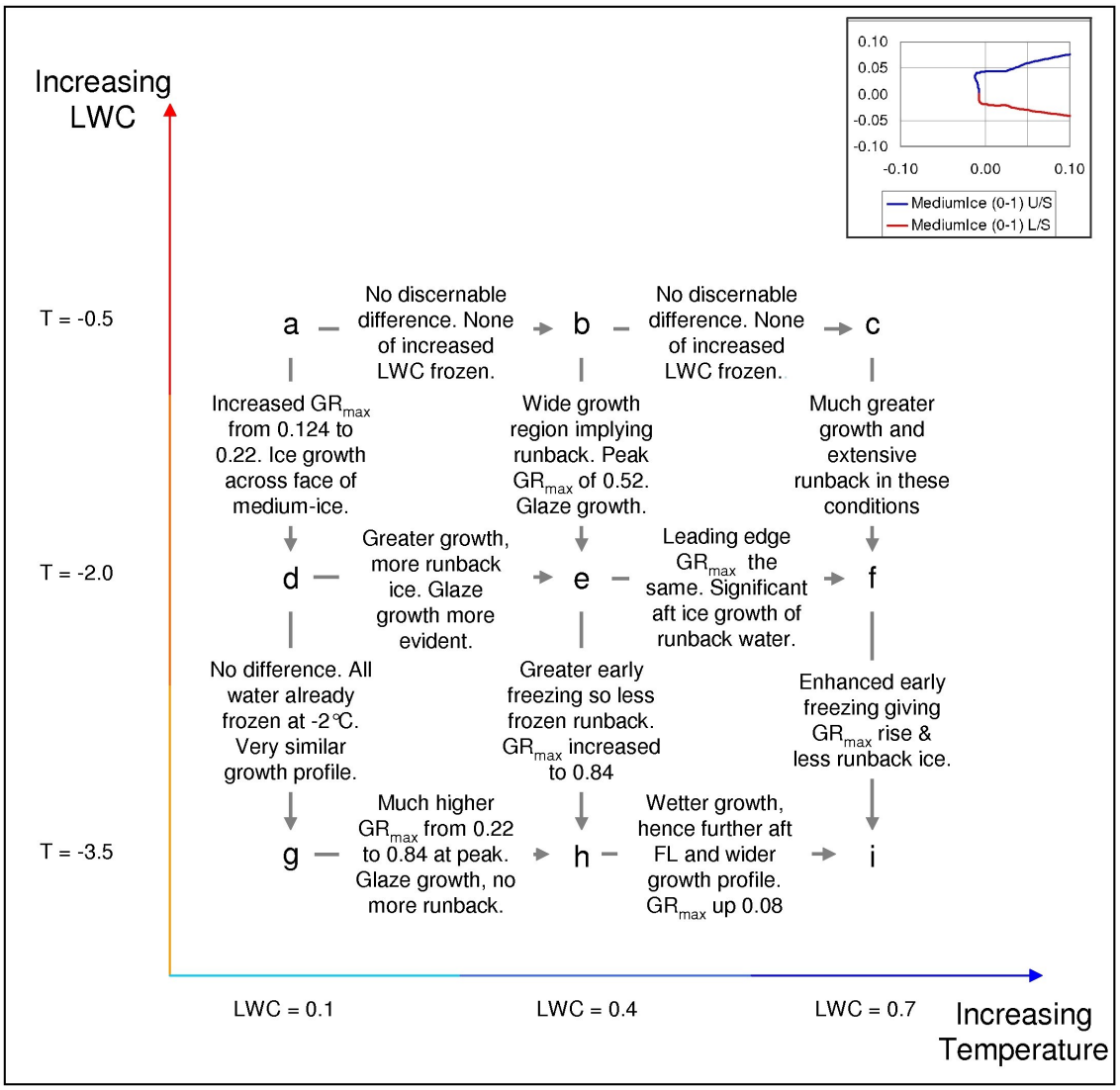

Figure 7.34: Descriptions of the change in calculated Growth Rate distribution following a change in either LWC or temperature, for the Medium-Ice profile.

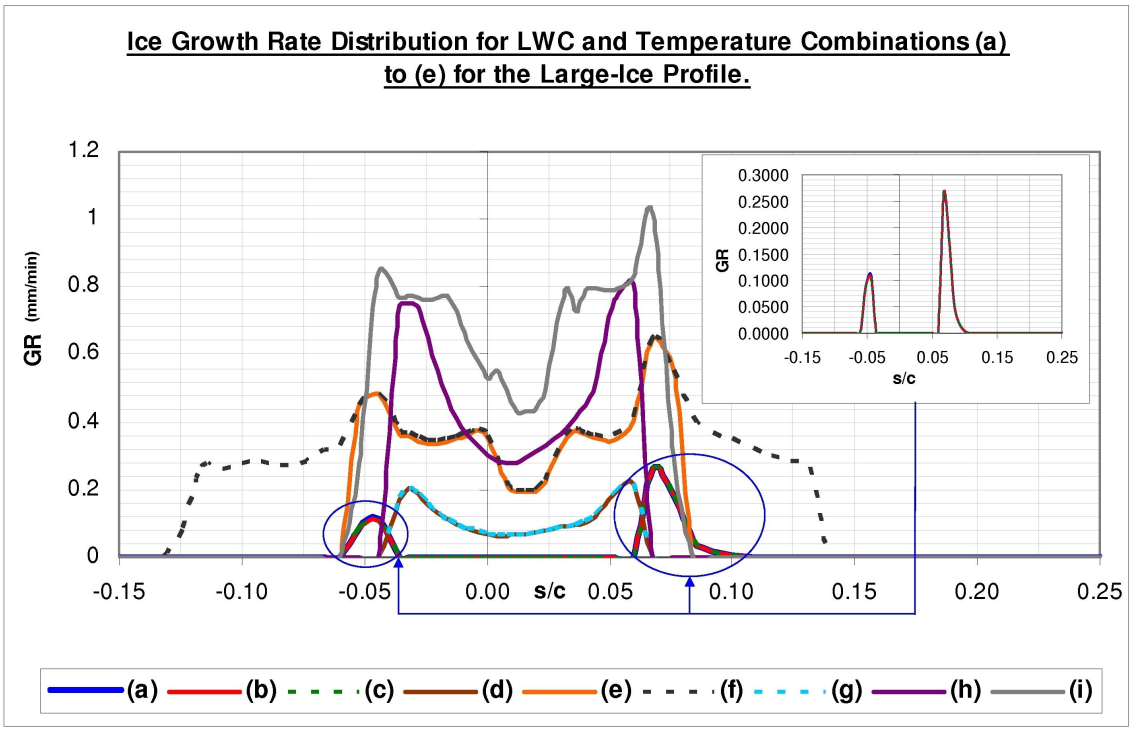

Figure 7.35: Growth rate distributions calculated for conditions (a) to (i) for the Large-Ice profile.

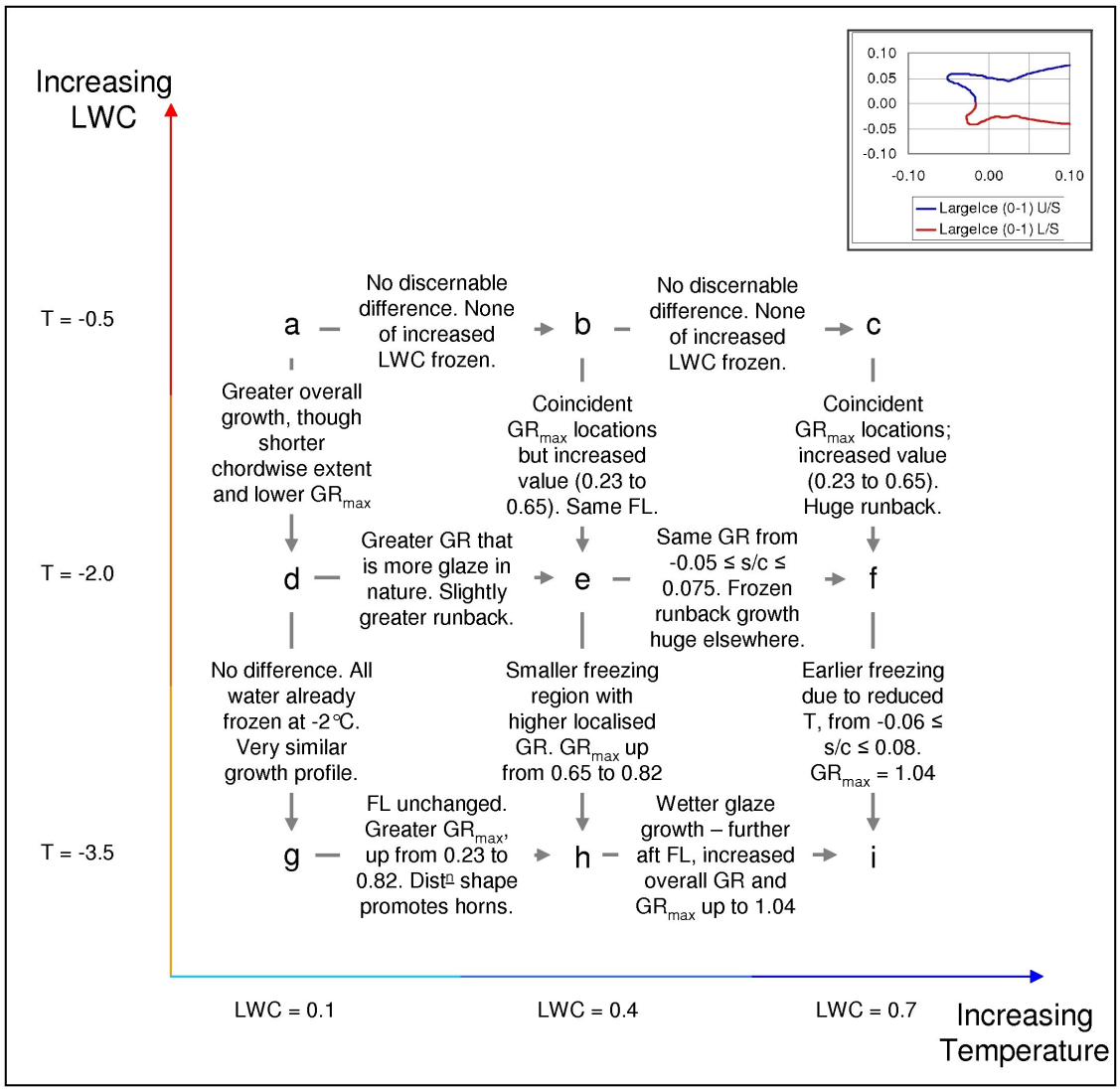

Figure 7.36: Descriptions of the change in calculated Growth Rate distribution following a change in either LWC or temperature, for the Large-Ice profile.

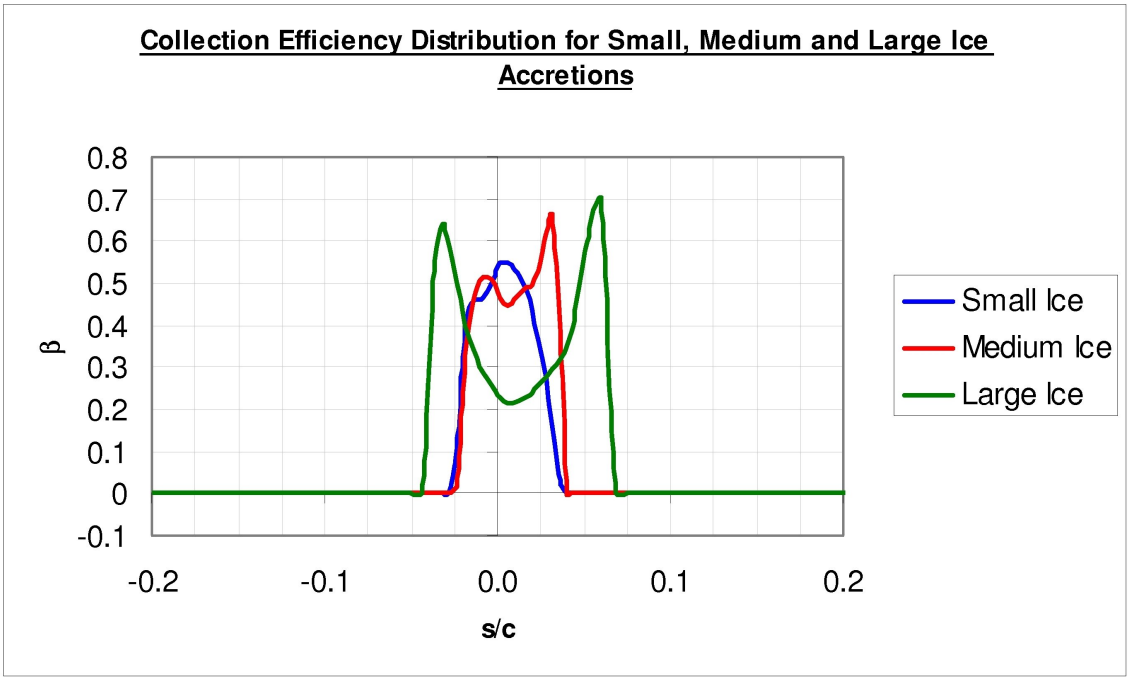

Figure 7.37: Calculated collection efficiency distribution for the Small-Ice, Medium-Ice and Large-Ice profiles.

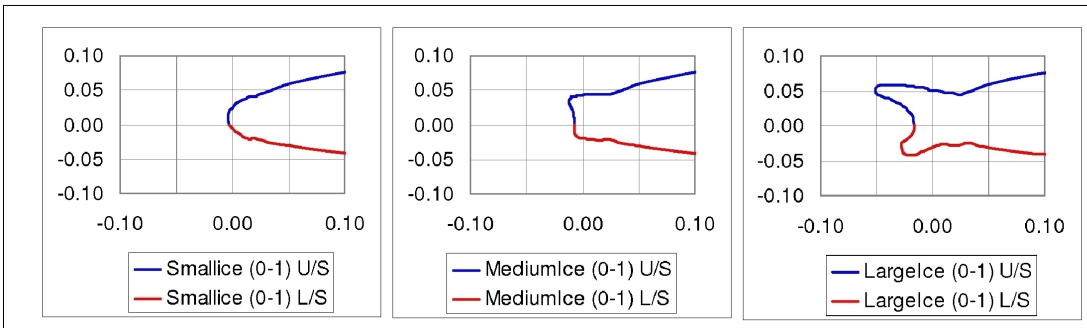

	Small to Medium	Medium to Large
(a)	Still very small, but much larger GR (by 60 times) around the upper ridge 'tip'.	Larger ice growth is calculated to occur on both upper and lower surfaces, in the horn-tip regions.
(b)	Still very small, but much larger GR (by 60 times) around the upper ridge 'tip'.	Larger ice growth is calculated to occur on both upper and lower surfaces, in the horn-tip regions.
(c)	Still very small, but much larger GR (by 500 times) around the upper ridge 'tip'.	Larger ice growth is calculated to occur on both upper and lower surfaces, in the horn-tip regions.
(d)	Similar stag^n GR (slightly lower than small-ice), and higher GR values at tips of u/s & l/s ridges.	Growth occurs over a wider range $-0.04 \leq s/c \leq 0.07$; with GR lower at stag^n & higher at horn tips.
(e)	Greater overall GR and peak GR (GR_{max} up from 0.42 to 0.52). Slightly further aft FL.	Growth occurs over a wider range $-0.06 \leq s/c \leq 0.085$; with greater peak (0.64) and overall GR.
(f)	More extensive freezing and FL on the u/s. Greater overall GR and peak GR ($GR_{max} = 0.52$).	Greatly wider freezing zone $-0.13 \leq s/c \leq 0.14$; with greater peak (0.64) and overall GR values.
(g)	Similar stag^n GR (slightly lower than small-ice), and higher GR values at tips of u/s & l/s ridges.	Growth occurs over a wider range $-0.04 \leq s/c \leq 0.07$; with GR lower at stag^n & higher at horn tips.
(h)	Little change. Undulation in u/s GR for medium-ice. Same freezing limits.	Peak GR locations are significantly further apart with similar values. Freezing limits are further aft.
(i)	Slightly greater peak GR. Slightly further aft FL on u/s. More sustained u/s growth (wider peak).	Enhanced u/s GR_{max} by 0.13, reduced l/s GR_{max} by 0.04. Further aft FLs. Greater overall freezing.

Figure 7.38: Descriptions of the difference in calculated Growth Rate between profile types, for the conditions (a) to (e).

This page has been left intentionally blank.

Chapter 8

Discussion of Results

8.1 Technical Research - Impact of Variability on the Critical Ice Shape

8.1.1 Results of the CFD Assessment of Aerodynamic Performance

The results of the CFD assessment of the aerodynamic penalties imposed by the differing iced accretions in comparison with the reference ice accretion, RefIS, showed substantial differences. Figures 7.22, 7.24, 7.26 and 7.28 show the four sets of CFD results categorised by similarity of C_L. In each of these plots the solid black lines are the C_L and C_D curves for the RefIS profile, whilst other curves with symbols represent C_L and C_D for other profiles.

In the sub-critical category, each of the C_L curves sits above the RefIS equivalent, predicting a better overall lifting performance. Similarly each of the C_D curves sits below the RefIS equivalent, predicting a better drag performance. The profiles that gave rise to these results are presented in figure 7.23. A description of each of these profiles was provided in section 7.1 with a summary statement. The common descriptors used for the profiles in figure 7.22 are (a) less intrusive orientation of the upper horn, (b) flatter (or less steep) upper horn top surface. Certainly this seems to be the case where

each profile has a less intrusive upper surface horn, and this is more often by virtue of a reduced horn growth vector angle than smaller horn thickness. Only the profile for case Construct #2 has an observably smaller upper horn thickness, and this is the reason why it is the least aerodynamically poorly performing profile.

In the near-critical category the C_L and C_D curves are far closer to the equivalent curves for the RefIS profile, and so exhibit similar aerodynamic performance penalties that place them in this category. The profiles that gave rise to these results are presented in figure 7.25. Common descriptors used for these profiles in the summaries of section 7.1 are (a) greater upper horn thickness, (b) reduced upper horn orientation; except for Va_LWC_50%_Fall which is very similar to RefIS (both in shape and in aerodynamic performance) and the cluster profile with a similar orientation but smaller horn thickness.

In the super-critical and super-critical$^+$ categories the lift and drag performance is predicted to be worse than RefIS, as shown in the plots in figures 7.26 and 7.28. Depending upon their severity (and hence category) these profiles are more intrusive either because of an increased upper horn thickness or an increased upper horn orientation. The profiles that fall into these two categories are presented in figures 7.27 and 7.29. The five worst profiles all fall into the super-critical$^+$ category and each of these exhibits a hugely more intrusive upper horn that destroys any useful lifting capability of the upper surface, even at low incidence.

The dominant influence of upper horn thickness and upper horn orientation is shown in figure 8.1. Figure 8.1 presents additional linear regression models produced separately from, and in advance of, those produced using FAA (2000). Linear regression modelling here, was performed using geometric parameters specific to this study, as introduced in figure 5.25. The equations of these lines and the associated R^2 values show how the influence of these two parameters can be used to describe the aerodynamic perfor-

mance degradation of different profiles. Lift decreases in a manner that can be approximated linearly (to a 79% goodness of fit) with an increase in the value of $h_{upper}sin\phi_{upper}$. Drag increases in a manner that can be approximated linearly (to an 85% goodness of fit) with an increase in the value of $h_{upper}sin\phi_{upper}$. The wider scatter of data points around the line modelling lift variation with $h_{upper}sin\phi_{upper}$ indicates that there are other factors that impact lift beyond upper horn intrusion, which is the primary factor. These additional factors are believed to be the thickness & orientation of the lower horn and the chordwise location of upper and lower surface separation. This last factor is believed important because it influences the opportunity for reattachment; e.g. if two horns cause separation at the same vertical position (y/c), but one is very close to the leading edge (x/c = -0.02) and another is visibly further upstream (x/c = -0.07). Were the above example to describe the separation of two upper horn separation locations then the reattachment location would be expected to be further forward for x/c = -0.07, resulting in understandably different lift and drag values.

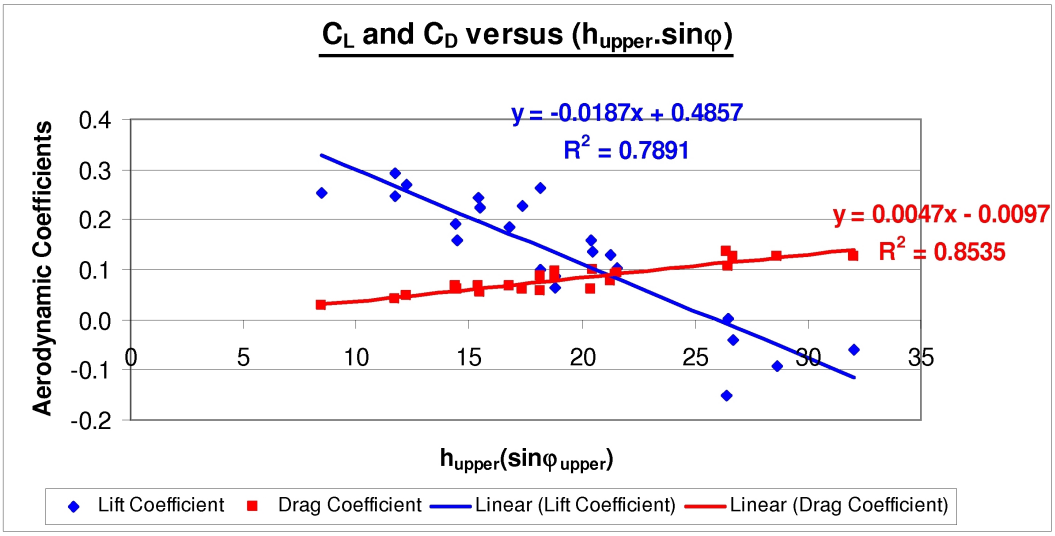

Figure 8.1: Lines of best-fit attempting to model the relationships between aerodynamic performance and horn thickness & horn growth vector angle.

The magnitude of the differences in aerodynamic performance penalty is evi-

dent from the C_L and C_D plots, and this is supported by the ranking in table 6.5. In this table, C_L and C_D values assessed at 2.4° incidence are listed for each profile. The profiles are ranked by decreasing drag coefficient, where the profile that has the highest value of C_D is ranked #1, and the profile with the lowest value of C_D is ranked #24. The reference profile, RefIS, falls in the middle of the table showing that there are profiles whose aerodynamic performance is both significantly better and significantly worse. The value of C_D for the #1 ranked profile in the table is 2.03 times greater than the equivalent RefIS value and 4.69 times greater than that for the #24 ranked profile. Similarly for the #1 ranked profile the value of C_L is 0.337 less than the equivalent RefIS profile value and 0.407 less than that for the #24 ranked profile.

These results show firstly, that profiles generated by variable conditions can have a significantly worse aerodynamic performance penalty when compared to the profile generated by constant reference conditions. Plus they show secondly, that variability effects can lead to profiles with a reduced aerodynamic performance penalty when compared to the profile generated by constant reference conditions.

It is therefore of significant interest to attempt to understand why certain combinations of conditions generate ice accretion profiles that can be either significantly more damaging or significantly less damaging to the aerodynamic performance of the aerofoil than the RefIS profile created under constant reference 'critical' conditions.

8.1.2 Flight-Path Variability: How Might the Conditions Create the Accretions?

This project's experimental programme has demonstrated that its incorporation of variability into icing tunnel simulations can lead to significantly different ice shapes. In considering the development of these shapes it is

necessary to acknowledge the importance of sequencing effects of icing encounters. Each ice accretion generated was entirely dependant upon not only the conditions encountered, but upon the order in which those conditions were encountered. In each case the conditions in segment 1 created the ice growth behaviour and resultant accretion in segment 1; the conditions in segment 2 and the accretion from segment 1 created the the ice growth behaviour and resultant accretion in segment 2, etc. So to understand how such variability led to the ice accretions that were recorded it is necessary to consider the overall local icing environment[1] and its changeability with LWC, with temperature and with ice profile development.

The Trajice2 investigation demonstrates the effects that different combinations of LWC and temperature can have upon the overall local icing environment by predicting a growth rate distribution that varies with profile shape and the different input conditions of LWC and temperature.

Figure 7.31 and the description that accompanies it in figure 7.32 provide a number of interesting insights into the potential or otherwise, for one icing condition to provide a greater growth rate than another. Examination of the growth rates predicted for cases (a), (b) and (c) allows observation that it is possible to increase LWC and find very little change or even a reduction in the predicted growth rate. Here in increasing the LWC from $0.1g/m^3$ to $0.4g/m^3$ there is no increase in the already very small growth rate because the temperature is too warm. Increasing the LWC further to $0.7g/m^3$ increases the total energy contribution of impinging droplets such that the overall thermal environment is predicted to inhibit freezing to such a degree that the growth rate decreases. Hence these three cases suggest that at -0.5$^\circ C$ no increase to ice growth rate would occur with increased water content. A similar examination at -2.0$^\circ C$ shows a small ice growth rate for (d) with the lowest LWC that would be expected to create rime ice. At the intermediate LWC value of (e) the increase to LWC has altered the overall

[1]Local icing environment refers to that in the immediate vicinity of the aerofoil leading edge.

thermal environment to such a degree that it is no longer able to maintain a dry growth regime. As a result the majority of freezing potential described by the growth rate, occurs either side of the aerofoil centreline and no further aft than s/c = ± 0.05. Though there is a growth regime change from dry to wet ice growth, the temperature is cold enough to sustain freezing without runback beyond s/c = ± 0.05. Freezing of this nature, combined with LWC = $0.4g/m^3$, resulted in the enhanced growth rate prediction that would result in development of glaze horns. Conditions at (f) involve a further increase in LWC to $0.7g/m^3$. At these conditions, the increase in LWC has not resulted in a significant increase in the predicted growth rate. Instead the outside air temperature is insufficient for all water to be frozen within -0.05 $\leq$ s/c $\leq$ 0.05 and there is greater predicted runback and freezing of runback water further aft. The predicted growth rates suggest that at this temperature the highest value for LWC does not necessarily create the conditions most conducive to a severe ice accretion. Examination of cases (g), (h) and (i) suggest that there is a similar pattern but the impact of increased LWC on the thermal environment is diminished (relatively speaking) at a temperature of -3.5$^\circ C$.

Similar patterns exist between the same combinations of conditions for the Medium-ice and the Large-ice profiles, as well as the Small-ice profile, though the differences from condition (a) for one profile shape to condition (a) for another is not purely due to the difference in shape. Figure 7.37 illustrates one reason for differences in growth rate patterns for different shapes and that is the collection efficiency. Relatively unsoiled surfaces like the Small-Ice profile capture the greatest number of droplets near the stagnation region. As the distance from this location around the aerofoil increases there is a greater likelihood of droplets failing to impinge on the surface. Once this happens the collection efficiency becomes zero. Hence for the Small-Ice profile the collection efficiency is maximised near s/c = 0 and this reduces as the magnitude of s/c increases. This is not the case for other profile shapes like Medium-Ice and Large-Ice. In these cases the collection efficiency is greatest at the upper and lower ridge/horn protrusions, with some sort of minima in between and a steady decrease aft on both surfaces. In addition convective

heat transfer is notably greater as the airflow negotiates the convex ridge and horn type features in advance of separation. Therefore the emergence of such ridge and horn formations serves to encourage a greater degree of water collection and a greater degree of heat loss in those areas; meaning that horn growth promotes further horn growth.

Interpretation of these predictions and the differences in results show how different combinations of LWC and temperature can lead to correspondingly different degrees of severity. In addressing the degrees of icing severity that result from different input conditions it is useful to introduce the concept of 'optimum severity'. Were an icing encounter to have optimal severity then the sequence of input parameters would lead to the single most damaging ice shape that could be accreted given the duration averaged conditions. This concept essentially accepts that the common definition of critical conditions is an effective start-point, about which optimum conditions can be sought. This is not an established concept in the field of aircraft icing, but such a term is necessary in attempting to understand how variable conditions could result in the significantly more damaging ice profiles recorded as part of this research project.

Examples of sub-optimal severity from the Trajice2 investigation include case (f) [$0.7g/m^3$, -2.0°C], whose growth rate distribution would not have resulted in an accretion that was any more severe than the case (e) [$0.4g/m^3$, -2.0°C] for each of the input profiles. In comparison with case (e), case (f) lost approximately all of the additional LWC to runback. Similarly with (d) [$0.1g/m^3$, -2.0°C] and (g) [$0.1g/m^3$, -3.5°C] the same growth rate was predicted for the two cases, but with one case having T = -2.0°C and another having T = -3.5°C. In considering these cases the conditions specified for (d) are more optimal, achieving the same maximum ice growth rate at a warmer temperature.

This way of thinking allows appreciation of how an encounter may arise where there is a compounding of icing severity, segment after segment, that creates

an ice accretion that is substantially more severe than that selected using conventional methods with constant conditions. The input conditions and accretion profile for case 'LWC (30%) Rise and Temperature Drop' gives an excellent illustration of this 'compounding' concept. An argument on how these input conditions led to such a severe accretion will be provided later in this section.

Whilst the ice growth process is caused by the progressive combination of different set of conditions and their effect, there are several aspects of the icing process considered particularly relevant for variable condition scenarios, more so than for constant conditions. These are:

Runoff Water The amount of runoff water is wholly dependent upon the input conditions, and arises when the icing environment is unable to cause the freezing of all impinging water before the trailing edge. The temperature and LWC influence the local thermal environment and the LWC and collection efficiency influence the amount of impinging water. Clearly water lost due to runoff cannot contribute to the overall ice accretion so it is fair to state that conditions that minimise the quantity of runoff will enhance the growth rate of the ice. At the beginning of experimental simulations an initial period was observed where a proportion of the impinging water remained liquid until the trailing edge and was lost as runoff water. The degree to which this happened differed according to the input conditions. Runoff for example, was not observed to any real extent for case Va_LWC_50%_Rise whose initial [LWC,T] conditions were [$0.205g/m^3$, -2.0°C]. In stark contrast, the case whose sequence had the opposite sense and initial conditions of [$0.615g/m^3$, -2.0°C] was observed to lose a large quantity of water in segment 1 and experience notably slower ice growth in the early stages of the encounter simulation.

Runback Water Runback water arises for the same reasons as runoff water, but it freezes before reaching the trailing edge of the aerofoil. The effect of variable conditions upon runback is of notable importance because

in the glaze growth regime the location of eventual solidification defines the overall shape of the ice accretion. Therefore the thermal conditions and water collection are heavily influential in runback because they define both the amount of water available for freezing and the freezing capacity. LWC and temperature largely define the thermal conditions and water collection properties, and are therefore primary factors in runback behaviour and the associated freezing.

Roughness Growth/Location The appearance of roughness around the leading edge occurs upon freezing of droplets or water collected on the aerofoil surface. The degree of roughness, its chordwise extent and the height of roughness elements all have an impact upon the ice accretion behaviour by affecting heat transfer, collection efficiency, impingement limits and the flow-path available to runback water. Rapid development of surface roughness would, in comparison with the clean aerofoil, increase local collection efficiency and fix impingement limits, directly impacting the regions where water collection and freezing will be most prevalent. Furthermore the impact of roughness on heat transfer and on the flow-paths available for runback water will also impact accretion.

Ridge Formation Following the formation of surface roughness, further impingement and freezing cause the enlargement of small roughness elements into larger roughness elements. The mechanism for this is the collection of water in the gaps between small roughness elements, plus the impingement of water onto the roughness elements themselves. Freezing of water between small roughness elements forms the foundation of the ice accretion. Freezing of water collected by the roughness elements themselves causes growth in both breadth and height of the roughnesses. This process will generally define an initial shape for glaze ice accretions, which is dependent upon the distribution of ice between the warmer stagnation region and the freezing limits.

Local Thermal Environment The term 'local thermal environment' refers

to the thermodynamic balance in the region of the ice accretion. It is dependent upon a huge number of different factors that contribute to the main heat fluxes associated with convective heat transfer, sublimation/evaporation, warming of impinging droplets, kinetic heating by airflow, kinetic heating by droplet impingement and the latent heat of fusion. The state of the local thermal environment is of paramount importance for the icing process and is especially important with variable conditions. This is because with constant conditions the thermal environment changes only with the emergence of the ice accretion. With variable conditions the thermal environment changes because of the emergence of the ice accretion, changes to the LWC, changes to temperature and consequently, the differing development of the ice accretion that results.

Collection Efficiency Development Collection efficiency development is of great importance. This is essentially because changeable values of LWC and temperature have the potential to create a series of severe icing segments with high growth rates. If these combinations of values occur where there is a high collection efficiency at the horn tips, then there is scope for very rapid ice accretion. Such a situation might be considered to be an optimum opportunity for ice accretion. If such combinations occur where the collection efficiency is sub-optimal then the opportunity for enhancement of icing severity is foregone.

Water Catch Rate The concept of water catch rate is very pertinent for consideration of variability. It is described by Jeck (1994), who states that this term governs how fast ice can build up on an object; and is calculated by multiplying the collection efficiency, the LWC and the airspeed. It is of particular relevance when considering variable conditions precisely because it acknowledges that knowing the LWC is of limited benefit without being able to grasp how much of it strikes the body of interest. Most importantly it allows appreciation of the difference in the potential for ice growth in various scenarios, accounting for the main influencing factors (when considered along with temperature)

of (a) how much water?; (b) where does the water strike?; and, (c) is slow/moderate/rapid freezing anticipated?

Spike Appearance The emergence of one or more 'spikes', as introduced in section 7.1, can have a dominant impact upon the eventual form an ice accretion takes. These spikes generally appear in conditions that lead to, in relative terms, a warm and wet encounter. These could also be termed 'threshold conditions' where here the threshold is between zero ice formation or wet ice growth. Upon their appearance, these spikes have a very high collection efficiency and would expectedly experience a high rate of convective heat transfer. Consequently their growth is rapid, to the extent where they dominate the ice accretion as singular features that deviate greatly from the overall shape of the ice.

Residual/Intercycle Ice Though the experimental model did not incorporate any ice protection, this will be employed on the majority of aircraft. Use of de-icing systems does involve inter-cycle ice and sometimes residual icing[2], so some aerodynamic penalty is present. If such ice is present, it may respond differently to sequencing effects.

The remainder of this section contains an examination of the input variables for specific cases and groups of cases, in an attempt to offer some initial thoughts on how specific sequences of conditions could have led to the profiles that resulted:

Va_LWC_10%_F; Va_LWC_10%_Half-Freq_F and Va_LWC_10%_Rise:

Both cases Va_LWC_10%_F and Va_LWC_10%_Rise (see figures E.3 and E.17) are in the super-critical$^+$ category. Interestingly, whilst these two cases differ from the RefIS case by their input conditions, the magnitude of the deviation from the reference conditions is relatively small. In relating those conditions

[2]Inter-cycle ice builds up in between operation of deicing boots. Residual ice describes any ice that is not completely removed by the system, or cannot be removed as it is accreted aft of the system limits.

to the concept of optimum severity as introduced above, it is possible to speculate as to how such relatively small changes might have a pronounced effect.

Case Va_LWC_10%_F had an applied temperature of -2°C over the course of the simulation; and an LWC variation as described by the upper plot in figure E.3. The first 10% of the simulation had the same conditions as the RefIS case. Thereafter there were four double-segments comprising around forty minutes simulation with LWC values $0.45g/m^3$, $0.37g/m^3$, $0.45g/m^3$, $0.37g/m^3$. It is conceivable that following the initial segment of $0.41g/m^3$, where the initial layer of ice would have been accreted; the surface conditions would have been well suited (in terms of surface temperature and roughness) for a slightly higher growth rate, whilst an increase of $0.04g/m^3$ would have a relatively low impact upon the overall freezing fraction. Consequently over that period it would be reasonable to observe a moderately greater amount of ice growth. At the beginning of segment 4 then, the ice accretion could have been expected to have more pronounced features that its RefIS counterpart. After segment 5 was complete the average LWC would be $0.41g/m^3$, but thinking sequentially, it can be seen that the ice accretion would not likely reflect this. Following the LWC values of $0.41g/m^3$, $0.45g/m^3$ and $0.45g/m^3$ in segments 1, 2 and 3; the greater collection efficiency of the more pronounced features would ensure that the proportion of water collected would be greater than it would at segment 4 of the RefIS encounter. Consequently it is understandable that after stage 5, and then again after stage 10, the resultant ice accretion would have been larger and hence, more intrusive, than the RefIS profile.

Case Va_LWC_10%_Half-Freq_F (see figure E.7) provokes similar thoughts to Va_LWC_10%_F above, by virtue of 4 segments of $0.45g/m^3$ after segment 1, and ahead of 4 segments of $0.37g/m^3$. Over segments 2, 3, 4, and 5 the WCR is is greater than that for RefIS by virtue of LWC; and after segments 6, 7, 8 and 9 the WCR is greater by virtue of the greater collection efficiency of the horn-protrusions; where these protrusions would have been more pronounced after segment 5 in comparison with the RefIS case. CFD data is not available

for this case, but its geometric parameters and the relationships provided for lift and drag coefficients in figure 8.1 allow approximation of $C_L = 0.143$ and $C_D = 0.076$ at $\alpha = 2.4°$, . In comparison with Va_LWC_10%_F this is less aerodynamically detrimental and is due to the less intrusive orientation of the upper horn. This difference in orientation might be related to the prolonged period with LWC = $0.45g/m^3$. Regardless the values estimated for C_L and C_D suggest a worse aerodynamic performance penalty for this profile than for the RefIS accretion profile.

Case Va_LWC_10%_Rise varies by virtue of a small rise in LWC from $0.37g/m^3$ to $0.45g/m^3$ over the course of the encounter simulation at a temperature of -2°C. It is possible to examine the input conditions for this case and consider the accretion behaviour as a compounding of near-optimum conditions. Many cases, including the reference case, reported runoff water at the beginning of the encounter. Were the goal to achieve a large ice accretion then runoff water would suggest sub-optimal conditions, with too much water. A reduction of LWC to $0.37g/m^3$ would therefore alleviate the quantity of runoff water. Over the course of the encounter, with the development of roughness, ridges and horns, the convective heat transfer would increase around such features, encouraging additional freezing. This, combined with the ever increasing LWC and WCR would result in ever increasing freezing at the specific location of the developing horn tips, with the greatest horn growth rate occurring in segment 10. Such a growth pattern would account for the additional $15mm$ growth to the upper horn thickness observed in comparison with RefIS.

Va_LWC_50%_F; Va_LWC_50%_B; Va_LWC_50%_Half-Freq_F and Va_LWC_50%_Half-Freq_B:

In section 7.1 it was explained that the profile measured for the ice accretion generated under Va_LWC_50%_F conditions (see figure E.5)) was not adequately representative of the uniform majority of the ice accretion. It was estimated that a more representative profile would have shown a far

greater similarity with the RefIS profile, and therefore would have been far less intrusive and aerodynamically detrimental than the profile recorded. In fact if this is the case, then the accretion generated under Va_LWC_50%_F conditions is far more comparable with the other ice accretions within this heading, where none of the Va_LWC_50%_B; Va_LWC_50%_Half-Freq_F and Va_LWC_50%_Half-Freq_B cases (see figures E.13, E.9 and E.15) produced accretion profiles that were hugely more intrusive than the RefIS profile. Of the three profiles, Va_LWC_50%_Half-Freq_B is slightly more intrusive and predicted to be slightly more aerodynamically detrimental than the RefIS profile; whilst both Va_LWC_50%_B and Va_LWC_50%_Half-Freq_F are in the sub-critical category, being less intrusive and less aerodynamically detrimental than the RefIS profile.

Common to each of these four ice accretions is the large value of the deviation from the mean LWC where the minimum and maximum values are $0.21g/m^3$ and $0.62g/m^3$ respectively. Considering again the theme of optimum icing conditions it is understandable that an early perturbation to either $0.21g/m^3$ or $0.62g/m^3$ would be a significant deviation. In the case of the lower LWC the generation of latent heat would be far less of an influence and freezing might be expected to occur more rapidly. In the case of the higher LWC freezing would be inhibited far more significantly because of the greater release of latent heat and the larger quantity of impinging water. Fluctuation between these two LWC values has not proved to generate any ice accretions that are hugely more damaging than the RefIS profile (discounting the non-uniform peak recorded for case Va_LWC_50%_F). During periods of high LWC, it seems that whilst there might be areas where there is a high growth rate; runback, runoff and evaporation may all be important losses (and all associated with a low freezing fraction) that affect the rate and distribution of ice growth and hence the thickness and orientation of the horns.

Va_LWC_50%_Double-Freq_F and Cluster:

In case Va_LWC_50%_F, whilst the non-uniform horn feature was discounted,

it is clearly necessary to consider why such features appear. These features are apparent for both cases Va_LWC_50%_Double-Freq_F and Cluster (see figures E.17 and E.31). The aerodynamic performance penalties associated with the profiles generated under these variable conditions suggest that they are less detrimental than the RefIS profile, being categorised as sub-critical. However the profiles utilised for CFD analysis represented only the uniform proportions of the ice growth and there was in fact, far more to these accretions.

As discussed above, conditions with very high values of LWC did not necessarily generate very intrusive ice accretions on the whole, but they did cause the appearance of spikes as introduced in section 7.1. These spikes appeared in random chordwise locations at differing points on the upper and lower leading edges, suggesting that there was a real volatility to the ice growth behaviour with these conditions. Whilst associated in these cases with high LWC, it should be recognised that this phenomenon is rather more likely resultant from a combination of warmer and wetter conditions, rather than just wetter conditions. Once formed these features have very high collection efficiencies, convective heat transfer and subsequent growth rates; and become dominant features of the ice accretions on which they form.

Aerodynamically, these features are important exactly because of their non-uniformity. Asymmetry of lift is acknowledged as a significant danger presented by aircraft icing, and the unique feature of ice growth behaviour observed with these cases could certainly contribute to such problems with stability and control.

Sin(θ); Sin(θ - 90°C); Sin(θ - 180°C) and Sin(θ - 270°C):

The four profiles generated under the conditions listed above demonstrate how simple changes to variation pattern have proven to yield notably different ice accretions (see figures E.31, E.33, E.35 and E.37). The largest & most intrusive and aerodynamically damaging ice accretion of these four

is that generated under Sin(θ) conditions. Here following initial growth at mean conditions, warmer temperatures for ten minutes led to slower growth; but growth that involved development of features similar to those in the Va_LWC_50%_Double-Freq_F and Cluster cases.

The subsequent temperature reduction beyond -2°C down to -3°C allowed these features to grow fast; and to grow to dominate the accretion to the extent that the final accretion had a huge upper horn. So intrusive was this horn that the profile recorded for this accretion was predicted to be the worst aerodynamically of all profiles but that generated under LWC (30%) Rise and Temperature Drop.

Cases Sin(θ - 90°C), Sin(θ - 180°C) and Sin(θ - 270°C) all provided results different to the Sin(θ) conditions. This is believed to be due to further differences in the changeable thermal environment, its effect on early ice accretion and the interdependence of both profile shape and thermal conditions as well as LWC.

Construct #1 and Construct #2:

The cases Construct #1 and Construct #2 (see E.39 and E.41) provide examples of how a significant drop in temperature might do little to make the ice accretion more intrusive.

The temperature variation in Construct #1 had a much colder period for segments 2 and 3. Following segment 1 conditions of 0.41g/m^3 and -2°C, colder conditions served purely to increase growth rates around the leading edge for a ten minute period. After that period an increase in temperature greatly reduced the potential growth rate, and reduced the opportunity for a severe compounding of icing potential that was observed in other cases.

Similarly a greater degree of runoff and runback water at the earlier, warmer stages of Construct #2 led to less severe early ice growth. However simply

having a lower temperature from segments 6 to 9 did not serve to sufficiently enhance the severity of the ice accretion to compensate for early loss of impinged water. This is essentially because at LWC = $0.41g/m^3$, reduced temperatures can only cause more rapid freezing of the impinging water, where droplets impinging at the upper and lower horns freeze earlier. Whilst this would result in a moderately greater growth rate (due to enhanced horn collection efficiency) it is unlikely to produce severe ice growth because there is no accompanying increase in LWC to take advantage of colder temperatures (-3.5°C and -4°C).

Essentially in these cases there was potential for significant ice accretion as a result of the colder temperatures. However enhanced growth rates required an accompanying increase in LWC, which was not present. Instead colder temperatures were more likely to bring transition to rime conditions, as is evident from the photograph in figure E.41.

LWC(B)/Sin(θ - 270°):

The profile that represents the ice accretion generated under LWC(B)/Sin(θ - 270°) conditions (see figure E.49) is an example of how a set of conditions designed to create an ice shape with low severity, can actually produce the opposite result.

The LWC and temperature variations were combined for this case to create a small non-intrusive ice accretion. The combinations of conditions were designed to diminish the opportunity for high growth rates to occur. To do so the large majority of high LWC segments were positioned at the warm ends of the simulation, and where the temperature was coldest (average temperature of -2.7°C) and the average LWC was low ($0.25g/m^3$). However whilst this did generate a relatively small ice accretion, the distribution of ice was such that the upper and lower horns had a very intrusive orientation. As a result this profile was categorised as super-critical, in recognition of its aerodynamic performance prediction. This case demonstrates how the input

conditions and the subsequent sequencing effects could lead to an accretion where the distribution of ice, rather than the quantity of ice, gives rise to enhanced severity.

LWC (30%) Rise and Temperature Drop:
Input conditions for this case are presented in figure E.51 along with details of the resultant accretion. Designed at the end of the experimental programme, it is fair to say that the conditions for case LWC (30%) Rise and Temperature Drop were deliberately optimised in an attempt to identify how severe an ice accretion could be attributed to the same average LWC and temperature conditions as the RefIS conditions. In doing so it was recognised that at some stage a warm temperature was necessary to allow for colder temperatures at other times. It was therefore felt appropriate to begin the encounter with very warm early segments combined with low LWC of $0.29g/m^3$. In doing so this period of less severe growth conditions and reduced ice formation was traded off against later conditions whose severity and growth rate would more than mitigate against earlier losses. This first segment was therefore intended to provide a smaller amount of freezing around the leading edge that would serve as the basis for further droplet capture and subsequent growth. In doing so the collection efficiency of roughnesses, protrusions, ridges and horns was expected to increase over the course of the encounter simultaneously with increasing LWC and reducing temperature; with this compounded combination of severity intended to result in a hugely severe ice accretion. This is a very good example of increasing water catch rate and reducing temperature combining to create a much more severe encounter than would be expected with constant conditions, as is illustrated by the profile in figure E.51.

Figure E.52 shows that the difference between the aerodynamic performance predictions is very large indeed. So large is the difference between the RefIS and LWC (30%) Rise and Temperature Drop profiles, that the aerodynamic drag coefficient predicted by CFD at $\alpha = 2.4°$ is 7.7 times the predicted value for the clean aerofoil and 3.8 times the same value for the RefIS profile

respectively.

8.2 Commercial Research - Addressing Flight Path Variability: Feedback from the Icing Community

Research conducted via questionnaire and discussions with industry showed that if variability could be shown to contribute to ice accretions that deviate significantly from the critical shape generated under conventional Appendix C conditions, in terms of shape and (more importantly) aerodynamic performance penalty; then this would be something the icing community may look to address.

The questionnaire results showed the majority of respondents to have a strong technical understanding of icing and an appropriate level of responsibility for icing related activities. Furthermore the array of organisations represented, and the activities they engage in were relevant to the questionnaire's subject matter. Respondents were asked if they would support or oppose a recommendation for variability should be incorporated into ground-based icing simulations, were the technical research to suggest it may be of benefit. Whilst none were wholly committal in their answers, none indicated any immediate opposition and many signalled their potential approval of such a measure.

One respondent from NASA made a pertinent comment, the essence of which was subsequently echoed in a discussion with a Civil Aviation Authority representative. This was that variability would have to be shown to have a significant enough impact to warrant attention on the basis that there could be an expected safety benefit, otherwise there was a risk that the attention and resources invested in addressing variability would be unnecessary. This conditional view is understandably cautious and strikes an excellent balance between (a) the need to protect the current safety approach & ensure

resources are directed appropriately, and (b) the need to address additional factors that might lead to enhanced safety measures. These statements made by NASA and the CAA, as as a government body and a regulator respectively, contrast somewhat to a comment from another respondent who was part of an aircraft manufacturing company who expressed an understandingly different perspective: "the way we choose the critical case today, whilst not completely rigorous, is okay and it is accepted by the airworthiness authorities, so any improvement would not give any cost benefit".

Another employee from an aircraft manufacturer expressed an alternate view, suggesting that large aircraft manufacturers might accept any recommendations quite readily because any requirement would have accompanying instructions for simulation activities, and additional tasks could be added to a test plan for numerical or experimental simulation.

Perhaps the most poignant sentiment came in discussions with an employee of the UK regulator, who raised the question of whether variability was something solely to be considered in relation to safety and efficiency of aircraft of the current generation; or whether it should be addressed as part of our continual technological development and advancement of knowledge. Should we debate the need to consider variability now or assume that an understanding will prove beneficial in the future, and that refining the process of simulation is ultimately a good and important thing to do?

Whilst this view is possibly the most sensible, similar thoughts were not forthcoming from others questioned. Other respondents, who work for aircraft manufacturers, suggested that they would be more inclined to support efforts to address variability were it to prove beneficial in other ways. Two areas that were raised in questionnaire responses and further discussions with icing colleagues were (a) reduction in ice protection system power requirements and (b) reduction in the time/cost associated with IPS design/development. These ideas will be explored further in the following sections.

8.3 Commercial Research - Potential for Improved Efficiency of Anti-Icing Systems[3]

The benefit of reducing the power usage of operating anti-icing systems is clear. Reducing the power required to operate in icing conditions would require less energy to be extracted from the engine for bleed-air and electrothermal anti-icing systems, lessening the penalty upon engine performance and fuel cost. Indeed if the cost attributable to 'de-icing' for Ryanair is approximately 0.26% of operating expenditure (Ryanair, 2007), and this figure is comparable for other, larger airlines who own or lease similar aircraft; then a reduction in the cost of ice protection becomes a far more significant amount. United Airlines for example, reported an operating expenditure for 2006 of over $17bn (UAL-Corporation, 2007), of which 0.26% is over $40m.

The potential to reduce the power requirements for bleed-air and electrothermal anti-icing systems are predicated on the possibility to regulate power delivery on the basis of the demand for thermal energy. To do so it is necessary to be able to define the demand for ice protection thermal energy and apply the minimum power required to ensure zero ice formation over the aerodynamic surfaces of the aircraft. Review of existing patent information discovered a system designed primarily for use on the inlet surfaces of helicopter engines. This anti-icing management system (Rumford and Norris, 1988) aimed to apply the required amount of heat by regulating the bled mass flow, using an electronic controller that specifies whether the anti-icing valve is open or closed. The valve is pulsated between open and closed positions with shorter periods at the open position for low bleed conditions and longer periods at the open position for high bleed conditions.

This device responds to "the presence of an ice producing condition" which

[3]Whilst this aspect of the research project addresses variability in reference to anti-icing systems, it is a separate piece of research from that discussed in section 8.1. Findings relate to relevant information from identified sources, supported by understanding of icing variability (rather than the specific development of critical ice shapes), associated effects and technologies.

is diagnosed by surface temperature measurements at the engine inlet. The system as described by Rumford and Norris (1988) applies greater quantities of bleed-air at -10°C than it does at just below 0°C and still more at -20°C. Whilst this is likely to provide sufficient heating to prevent the formation of ice it is also likely that heat is still wasted because the quantity of water in an icing cloud reduces as the temperature gets colder. Continuous maximum Appendix C conditions, for example, predicts [LWC, temperature] combinations of [0.63g/m^3, 0°C], [0.43g/m^3, -10°C] and [0.21g/m^3, -20°C] at an MVD of 20μm and standard horizontal extent. Therefore the icing severity is unlikely to worsen more and more as temperature decreases from 0°C. It is more likely that the icing severity will worsen as the combination of temperature and LWC approaches critical conditions for each region of interest, i.e. engine inlet, main wing, vertical tail. With continuing temperature decrease and reduction in LWC the severity of the conditions will reduce before the ice formation becomes fully rime.

A system of the type described by Rumford and Norris (1988), or an electrothermal ice protection system could be applied to aerodynamic surfaces where the energy usage were tailored to ensure zero ice accretion but with optimised power extraction. This could be done on the basis of measured icing severity, which would require measurements of outside air temperature and liquid water content. Measurement of cloud droplet size distribution would also be advantageous.

Accurate measurement of cloud water properties has historically been difficult. Several limitations in in-flight measurement of LWC were identified in chapter 3. These limitations would have the potential to reduce the value of such an innovation, if measurement of LWC was accurate to 20% at best. The heat supply at this level of accuracy would need to account for the measured level of LWC, plus the 20% uncertainty, plus a safety margin. In order for such an innovation to be successful, more accurate, robust technology for LWC measurement would be advantageous.

Limitations of different devices have been recognised in developing more advanced apparatus, (Emery and Kok, 2002), (Tan et al., 2004). Further design and development of such equipment has continued over recent years by several parties including Emery and Kok (2002), Tan et al. (2004), Hammond and Ivey (2005) and Lilie et al. (2005). These publications show that accurate determination of LWC is eminently more possible in both icing facilities and in-flight. The device described by Lilie et al. (2005) is specifically intended to be able to describe the severity of icing conditions based on LWC and droplet size. Lilie et al. (2005) state the exact application as a: "Flight deck icing severity indicator for general and commercial aircraft."

So if it is possible to diagnose in-flight LWC and MVD for aircraft which are already capable of measuring the outside air temperature accurately, then reliable measures of icing severity could be determined for different parts of the aircraft in real time. Were this the case then the ice protection systems could be tailored during design and development, using simulation and test techniques, to provide only that amount of power required to guarantee the surfaces remain ice free. In doing so the aircraft would provide the required safety margin whilst at the same time using less power and being ultimately more efficient and cost effective.

8.4 Commercial Research - Potential for Reduced Flight Testing in Icing Conditions

Responses to question 5 of the questionnaire suggest the total timescales and cost of an icing programme can be substantial, albeit not large in relation to an entire aircraft development programme. One responded estimated a total cost of an icing programme to be of the order of $30m for a wide-body airliner. Several respondents confirmed that the majority of this cost would be due to flight testing with artificial ice shapes, natural flight tests and wind tunnel tests. Reduction of natural flight tests by increased use of ground-

simulation techniques would be doubtless be welcome.

In order for this to occur, present numerical simulation techniques would have to improve to the point where certification authorities would accept their findings without subsequent validation with flight tests. Additionally, numerical simulation and icing tunnel simulation techniques may be expected to develop a capability in modelling flight-path variability. Certainly this would be expected if variability is recognised as an important factor in aircraft icing.

Habashi (2006) refers to recent advances in CFD techniques that "signal an inexorable march towards a virtual certification methodology for all types of aircraft, and simultaneously reduce the likelihood of ice-induced hazardous events in operation."

A more realistically achievable target in the short/medium term is the accepted use of codes like FENSAP-ICE as an increasing part of icing design and certification, and reducing proportions of flight testing. Perhaps then, if these codes are able to accurately model icing physics and airflow behaviour, it would be appropriate to consider the incorporation of flight-path variability.

Improvement of numerical ice accretion modelling is ongoing, second generation codes like Trajice2, Lewice3D and FENSAP-ICE all simulating icing scenarios on whole aircraft, in 3D, using RANS techniques for airflow solution. Forthcoming steps in their development include modelling of the water film, surface tension, and droplet splash/re-impingement. Airflow solution will also progress, with the application of unsteady RANS and unsteady DES (Detached Eddy Simulation) techniques, supported by ever greater computational power.

Modelling icing encounters in an icing tunnel is already at an advanced stage, and it was suggested by one survey respondent (who works for a government research institution providing icing tunnel facilities) that icing wind tunnels

could be upgraded to fit new requirements, i.e. the incorporation of variability. Indeed this was achieved as part of the present study. However icing tunnel simulation is at a disadvantage to numerical simulation in terms of modelling capability, as codes are unrestricted when it comes to full-scale simulations. This, along with the cost differential will most likely see numerical simulation become the method of choice once it is sufficiently capable.

For the moment the required level of modelling capability for certification authorities to accept numerical results without flight test validation is some way off. In the interim period, and as numerical modelling capabilities advance further, codes would be well placed for further research into the impact of variability, following on from the present study. This is further outlined in section 8.5 below. Further experimental research into the impact of variability and its incorporation in icing tunnels, also outlined in section 8.5, would provide the next step towards useful ground-based simulation of variable conditions.

8.5 Recommendations for Further Work

This research project is the first of its kind to address the influence of variability in any kind of comprehensive manner. Therefore it would be advisable to undertake follow-up research to independently (a) confirm or otherwise, the potential for flight-path variability to enhance the severity of ice accretions; (b) further investigate flight-path variability to identify potentially severe scenarios more definitively. These activities should be undertaken before any further consideration of incorporating variability takes place.

To perform (a) and (b) there is a scope for these activities to be undertaken, at least in part, at Cranfield University. Further research could form part or all of a doctoral project, or perhaps be well served as a suite of Masters projects. However, given the variations known to occur between results obtained from different icing tunnels, it may be sensible to replicate selected

experiments in other icing tunnels. Suitable candidates might be the Icing Research Wind Tunnel at GKN ATS Luton (UK) or the NASA Glenn IRT. Certainly any further investigations would benefit from wider collaboration within industry by having partners from organisations with appropriate expertise.

The engineering research described within this document involved the following:

- Knowledge of the icing atmosphere;
- Understanding of ice accretion physics;
- Understanding of the aerodynamics of iced aerofoils;
- Performing computational icing simulation;
- Design and execution of an experimental icing programme;
- Experimental wind-tunnel testing of an iced aerofoil;
- Development and application of CFD for experimentally generated ice accretions.

In any future project(s), the involvement of experts in each area would prove advantageous in comparison to the current project, where the above requirements were satisfied by very few people who had/gained a broad knowledge and/or capability in each area.

Further research could consult icing-specialist meteorologists, flight-test engineers and pilots to better identify (a) the kinds of variability that could be expected, and (b) the likelihood of occurrence of such types of variability. This would then allow the identification of severity associated with more realistic and more likely variable scenarios. Continuing with this line of thought a number of tasks might follow:

1. Meteorologists, flight-test engineers and pilots identify scenarios where flight-path variability present may warrant attention (e.g. 20 encounters).

2. Icing specialist designs one test to simulate each variable encounter, plus one to simulate the duration averaged conditions.

3. Icing tunnel A (e.g. CIRT) and icing tunnel B (e.g. GKN ATS Luton[4]) each simulate the constant-condition and variable-condition cases 1 - 8. Icing tunnel A simulates cases 9 - 14 and icing tunnel B simulates cases 15 - 20.

4. Icing tests involve video and still photography to visually examine the differences exhibited by the different cases. Applying different coloured dye to the water would also be advantageous in identifying the impact of different encounter segments.

5. Aerodynamic assessment could be useful to again assess the impact of the ice accretions on aerofoil performance.

Further to these activities, first and second generation icing codes could play a major part in this activity, helping identify the impact of variable conditions more comprehensively.

It would be possible to utilise a first generation code such as Trajice2 to rapidly assess combinations of conditions. This would require adaption of the programme to make it capable of reading a set of input parameters that describe a variable sequence; of automatic execution of the code in a stepwise manner sufficient to model large quantities of ice growth & changeable icing conditions; and of smoothing any significant surface discontinuities that would cause divergence of the solution. It is possible, however, that this would be of limited value as such codes are restricted in their prediction of glaze ice accretions. Any more sophisticated use than described above might

[4]The Cranfield and GKN ATS tunnels would be suitable given their similar working section dimensions.

reduce accuracy further, lessening the validity of any results. Then again, were such a programme capable of assessing hundreds of cases[5] and identifying those where significant mass is calculated, then those cases could be selected for further, more in-depth analysis. Such in-depth analysis would then allow more accurate ice shape prediction.

A second generation code like ICECREMO or FENSAP-ICE could also be of great value to any further investigation. Either following on from, or instead of using first generation codes as described above, second generation codes could give a favourable balance between accuracy and the number of cases that can be run. These second generation codes solve the RANS equations instead of incompressible, potential flow solution of first generation codes and would give a more accurate answer but would require a longer solution time. This time could be substantially reduced if the codes were adapted for two-dimensional modelling.

The value of icing codes to this analysis is advantageous over experiment in one important respect. This is because the programme would be able to provide information about the case at the intermediate stages; like proportions of runback water, heat transfer coefficients, horn growth rate etc. Such information would be very valuable, provided there were an appropriate way to post-process, present and interpret it.

[5]With Trajice2 an engineer can perform a 10-stage icing encounter in around an hour, with over 90% of the time devoted to file management and surface smoothing in between calculations, both of which could be automated.

Chapter 9

Conclusions

In undertaking this project a comprehensive programme of technical research was undertaken, into: the impact of flight-path variability of icing conditions upon the ice accretion process; subsequent ice accretion profiles & the associated aerodynamic penalty; and any potential consequences of addressing variable conditions for industry. The primary motivation for the research project was that consideration of flight-path variability could assist preventative efforts towards flight safety in icing conditions.

The technical programme generated multiple accretions using constant icing conditions that were defined from Appendix C, and conditions that were variable, but had equivalent duration-averaged conditions. Variability was assessed using temperature variation, LWC variation, and a combination of LWC/temperature variation. A CFD technique was developed and utilised for aerodynamic assessment of 24 of the experimentally iced aerofoils (one profile was not analysed, the CFD data for another could not be used).

Upon ranking these profiles by drag coefficient at an angle of attack of 2.4°, 12 of the 24 profiles were categorised as more aerodynamically damaging than the RefIS profile[1], and 11 of the 24 were categorised as being less aerodynamically damaging. A further breakdown using C_L and C_D curves for

[1]The ice accretion profile representing the constant-conditions case

each variable profile placed 6 profiles in the sub-critical category, 6 in the near-critical category, 6 in the super-critical category and 5 in the super-critical$^+$ category. The terms sub-critical, near-critical, super-critical and super-critical$^+$ describe less aerodynamically damaging, similarly damaging, more damaging and very much more damaging profiles respectively.

The most aerodynamically damaging ice accretions were characterised by an upper horn thickness & horn orientation that combine to make a very intrusive upper surface protrusion. The least damaging profile was predicted to have $C_L = 0.254$ and $C_D = 0.029$ at $\alpha = 2.4°$. The RefIS profile was predicted to have $C_L = 0.185$ and $C_D = 0.067$ at $\alpha = 2.4°$. The most damaging profile was predicted to have C_L = -0.152 and $C_D = 0.136$ at $\alpha = 2.4°$. These values suggest that simulated variability can have large favourable and adverse impacts upon aerodynamic penalty. The adverse impact is considered sufficient to warrant further research into the impact of flight-path variability of icing conditions upon ice accretions.

An additional investigation using Trajice2 showed how different combinations and sequences of LWC and temperature, at different stages of glaze ice growth, could lead to enhanced or reduced icing severity. It also showed that particular encounter sequences could be near the optimum values for severe ice growth, or conversely, they could involve excessive losses like runoff and poor opportunities for severe ice growth. Several factors in the ice growth process were identified as important in respect of variable scenarios: roughness growth & location; local thermal environment; runback/runoff water; collection efficiency development; water catch rate; conditions conducive to spikes that develop into large 3D features; and, inter-cycle and/or residual ice.

Of the conditions generated, smaller variations (LWC $\pm$10%, T $\pm 1°C$) often proved more conducive to severe ice growth. Since critical conditions are selected from a finite dataset (Appendix C), that describes combinations of LWC, temperature and droplet size that have been shown to occur at the

same time, they provide an initial guess for optimum icing conditions. It is believed that such relatively small perturbations about those critical conditions, caused by flight-path variability, can cause more severe encounters. Larger variations (LWC $\pm 50\%$, T $\pm 2.5°C$) seemed less conducive to severe ice growth, presumably because larger deviations introduce scope for low growth rates, high runback/runoff or evaporative losses.

Commercial research undertaken in the form of a questionnaire, with later discussions with industry representatives, confirmed that the icing community would look to address flight-path variability of icing conditions, were there evidence of a substantial impact that warrants attention on the basis that there could be an expected safety benefit. On the basis of the technical research, as a initial study, there is preliminary evidence that would suggest such attention is warranted. Recommendations for further attention follow shortly.

Questionnaire respondents also suggested that variability may be considered advantageous if there were opportunities to reduce the operational & design/development costs, most likely in the areas of IPS power requirements & natural flight testing respectively.

Further to these suggestions, additional research revealed existing and emerging technologies that, combined, may have the potential to determine in-flight icing severity and inform the power regulation for anti-icing, making a more efficient system. At this stage, the most apparent obstacle to such an innovation is the lack of a proven icing-severity measurement device that is both accurate and robust. Nevertheless, active design and development of enhanced instrumentation is ongoing, and may result in sufficiently improved devices.

On the suggestion of reduced natural flight-testing, alternative methods of determining the impact of icing on aircraft are not presently sufficient for this to be possible. In the much longer term this seems like a realistic goal,

and the incorporation of variability into icing codes and tunnels could well be desirable in this regard. In the short term, application of variability to tunnels and codes may be best served as tools for further research into the impact of variability on critical conditions.

In summary:

1. The technical programme demonstrated that flight-path variability of icing conditions has the potential to enhance the severity of icing conditions and the aerodynamic penalty of the resultant ice accretion.

2. Of the conditions generated, smaller variations often proved more conducive to severe ice growth. This is believed to be because 'critical' Appendix C conditions are relatively close to optimum, and small deviations produce the opportunity for sequencing of compounded conditions that enhance severity.

3. Questionnaire responses confirmed that the icing community would look to address flight-path variability of icing conditions, were there evidence of a substantial impact that warrants attention on the basis that there could be an expected safety benefit.

4. Existing and emerging technologies may have the potential to determine variable in-flight icing severity and inform the power regulation of anti-icing systems, making a more efficient system. This will first require development of more accurate and robust LWC measurement systems.

5. Though a realistic possibility in the long term, alternative methods of determining the impact of icing on aircraft are not presently sufficient to replace natural flight-testing.

The following are recommendations for further work and follow-up research:

- Independently confirm or otherwise, the potential for flight-path variability to enhance the severity of ice accretions.

- Undertake further simulations, modelling more realistic icing encounters to more definitively identify potentially severe scenarios.
- Further experimental studies should better utilise video and still photography to visually examine the differences exhibited by the ice growth process.
- Apply coloured dye to the spray cloud to identify the impact of different encounter segments and associated growth behaviour.
- Employ 1st & 2nd generation icing codes to more rapidly assess combinations of conditions within variable sequences in 2D & 3D.

This page has been left intentionally blank.

References

Abbott, I. and Von Doenhoff, A. (1959). *Theory of Wing Sections*. Dover Publications, Inc.

Addy, H., Broeren, A., Zoeckler, J., and Lee, S. (2003). A wind tunnel study of icing effects on a business jet airfoil. In *41st AIAA Aerospace Science Meeting and Exhibition, Reno, Nevada*.

Anderson, D. and Ruff, G. (1997). Scaling methods for simulating aircraft in-flight icing encounters. Technical report, NASA-TM-107538.

Anderson, D. and Tsao, J. (2003). Evaluation and validation of the messinger freezing fraction. In *41st AIAA Aerospace Sciences Meeting and Exhibition*.

Badcock, K., Richards, B., and Woodgate, M. (2000). Elements of computational fluid dynamics on block structured grids using implicit solvers. *Progress in Aerospace Sciences*, 36:351–392.

Barley, S. (2007). Evaluation of small scale icing tunnel test results. In *SAE Aircraft and Engine Icing International Conference 2007*.

Boer, J. and Van Hengst, J. (1991). Certification of fokker 50 and fokker 100 for operation in icing conditions. In *29th AIAA Aerospace Sciences Meeting, Reno, Nevada*.

Bussoletti, J. (1994). Cfd calibration and validation: The challenges of correlating computational model results with test data. In *18th AIAA Aerospace Ground Testing Conference, Colorado Springs, Colorado*.

Campbell, S., Broeren, A., and Bragg, M. (2007). Aircraft performance sensitivity to icing cloud conditions. In *45th AIAA Aerospace Sciences Meeting and Exhibition.*

Chi, X., Li, Y., Chen, H., Addy, H., Choo, Y., and shih, T.-P. (2005). A comparative study using cfd to predict iced airfoil aerodynamics. In *43rd AIAA Aerospace Sciences Meeting and Exhibition, Reno, Nevada.*

Chi, X., Williams, B., Crist, N., Kreeger, R., Hindman, R., and Shih, T.-P. (2006). 2-d and 3-d cfd simulations of clean and iced wings. In *44th AIAA Aerospace Sciences Meeting and Exhibition, Reno, Nevada.*

Chi, X., Zhu, B., Shih, T.-I., Slater, J., Addy, H., and Choo, Y. (2002). Computing aerodynamic performance of a 2d iced airfoil: Blocking topology and grid generation. In *40th AIAA Aerospace Sciences Meeting and Exhibition, Reno, Nevada.*

Chi, X., Zhu, B., Shih, T.-P., Addy, H., and Choo, Y. (2004). Cfd analysis of the aerodynamics of a business-jet airfoil with leading-edge ice accretion. In *42nd AIAA Aerospace Sciences Meeting and Exhibition, Reno, Nevada.*

Chung, J. and Addy, H. (2000). A numerical evaluation of icing effects on a natural laminar flow airfoil. In *38th AIAA Aerospace Sciences Meeting and Exhibition, Reno, Nevada.*

Chung, J., Reehorst, A., Choo, Y., Potapczuk, M., and Slater, J. (2000). Navier-stokes analysis of flowfield characteristics of an ice-contaminated aircraft wing. *Journal of Aircraft*, 37:947–959.

Clifford-Law (2007). Making a 110-million dollar crash settlement fly. Company Website.

Cosentino, G. (2007). Cfd to flight: Some recent success stories of x-plane design to flight test at the nasa dryden flight research center. Technical report, NASA.

Cox&Co (2007). Low power ice protection systems. Company Website.

Dafa' Alla, A. (2002). Ice effect on the aerodynamic characteristics of aerofoils. In *20th AIAA Applied Aerodynamics Conference, St. Louis, Missouri.*

Dunn, T., Loth, E., and Bragg, M. (1999). Computational investigation of simulated large-droplet ice shapes on airfoil aerodynamics. *Journal of Aircraft*, 36:836–843.

Edwards, C. (2000). Calibration of the reference velocity in the test section of the low speed wind tunnel at the aeronautical and maritime research laboratory. Technical report, Sefence, Science and Technology Organisation.

Emery, E. and Kok, G. (2002). Icing sensor probe. Technical report, NASA/TM-2002-211368.

ESDU-77021 (1977). Properties of a standard atmosphere. Technical report, Engineering and Science Data Unit.

FAA (2000). Report of the 12a working group on determination of critical ice shapes for the certification of aircraft. Technical report, U.S. Department of Transportation.

Flight-Ice (2007). Flight ice, inc. home page. Company Website.

Gent, R. (1990). Trajice2 - a combined water droplet trajectory and ice accretion prediction program for aerofoils. Technical report, Royal Aerospace Establishment.

Goodrich-Anti-Ice (2007). Ice protection systems. Company Website.

Goodrich-De-Ice (2007). De-icing systems. Company Website.

Guo, Z., Hirano, T., and Kirk, R. (2005). Application of cfd analysis for rotating machinery - part i: Hydrodynamic, hydrostatic bearings and squeeze film damper. *Journal of Engineering for Gas Turbines and Power*, 127:445 – 451.

Habashi, W. (2006). Toward virtual certification of in-flight icing: A pacing item for cfd. In *Fifth International Conference on Engineering Computational Technology, University of Las Palmas de Gran Canaria, Canary Islands.*

Hammond, D. and Ivey, P. (2005). Development of a mass flux probe for application in an icing wind tunnel - review report. Technical report, Cranfield University.

Hammond, D., Luxford, G., and Ivey, P. (2003). The cranfield university icing tunnel. In *40th AIAA Aerospace Sciences Meeting and Exhibition, Reno, Nevada.*

Hindman, R., Crist, N., Williams, B., Chi, X., Choo, Y., and Shih, T.-P. (2006). Q3d-wing: Validation of a modern lifting-line method for application to clean and iced wings. In *44th AIAA Aerospace Sciences Meeting and Exhibition.*

Hoffmann, H. (1989). Cloudphysical parameters' dependance on height above cloud base in different clouds. *Journal of Atmospheric Physics*, 41:247–254.

Hoffmann, H. and Roth, R. (1990). A documentation of vertical and horizontal aircraft soundings of icing relevant cloudphysical parameters. In *AGARD Conference Proceedings No. 480, Propulsion and Energetics Panel, 76h Symposium, Brussels, Belgium.*

Howard, G. (2008). Personal communication.

Ide, R. (1999). Comparison of liquid water content measurement techniques in an icing tunnel. Technical report, NASA.

Inc., F. (2006). *Fluent 6.3 User's Guide.* Ansys Fluent Inc., Sheffield, UK, 6.3 edition.

Isaac, G., Ayers, J., M., B., Bissonnette, L., Bernstein, B., Cober, S., Driedger, N., Evans, W., Fabry, F., Glazer, A., Gultepe, I., Hallett, J.,

Hudak, D., Korolev, A., Marcotte, D., Minnis, P., Murray, J., Nguyen, L., Ratvasky, T., Reehorst, A., Reid, J., P., R., Scheider, T., Sheppard, B., Strapp, J., and Wolde, M. (2005). First results from the alliance icing research study ii. In *43rd AIAA Aerospace Sciences Meeting and Exhibition, Reno, Nevada.*

Jameson, A. and Kostinski, A. (2000). The effect of stochastic cloud structure on the icing process. *Journal of the Atmospheric Sciences.*, 57:2883–2891.

Jeck, R. (1994). Other ways to characterize the icing atmosphere. In *32nd Aerospace Sciences Meeting and Exhibition, Reno, Nevada.*

Jones, A. and Lewis, W. (1949). Recommended values of meteorological factors to be considered in the design of aircraft ice-prevention equipment. Technical report, NACA-TN-1855.

Kline, D. (1949). Investigation of meteorological conditions associated with aircraft icing in layer-type clouds. Technical report, NACA-TN-1793.

Kline, D. and Walker, J. (1951). Meteorological analysis of icing conditions encountered in low-altitude stratiform clouds. Technical report, NACA-TN-2306.

Koenig, G., Ryerson, C., and Larsson, J. (2003). Effect of variable lwc on ice shape in the nasa-grc irt. In *41st AIAA Aerospace Sciences Meeting and Exhibition, Reno, Nevada.*

Kostinski, A. and Jameson, A. (1997). Fluctuation properties of precipitation. part i: On deviations of single-size drop counts from the poisson distribution. *Journal of the Atmospheric Sciences*, 54:2174–2186.

Kreeger, R., Baez, M., Braun, D., Schilling, H., and Vickerman, M. (2007). Smaggice 2.0: Additional capabilities for interactive grid generation of iced aerofoils. In *45th AIAA Aerospace Sciences Meeting and Exhibition.*

Lear, C. (2007). Personal communication. Personal Communication.

Lee, S., Ratvasky, T., Thacker, M., and Barnhart, B. (2005). Geometry and reynolds-number scaling on an iced business-jet wing. Technical report, NASA.

Levy, D., Zickuhr, T., Vassberg, J., Agrawal, S., Wahls, R., Pirzadeh, S., and Hemsch, M. (2002). Summary of data from the first aiaa cfd drag prediction workshop. In *40th AIAA Aerospace Sciences Meeting, Reno, Nevada*.

Lewis, W. (1947). Icing properties of noncyclonic winter stratus clouds. Technical report, NACA-TN-1391.

Lewis, W. and Begrun, N. (1952). A probability analysis of the meteorological factors conducive to aircraft icing in the united states. Technical report, NACA-TN-2738.

Li, Y., Shock, R., Zhang, R., Chen, H., and Shih, T.-P. (2005). Simulation of flow over an iced airfoil by using a lattice-boltzmann method. In *43rd AIAA Aerospace Sciences Meeting and Exhibition.*

Lilie, L., Emery, E., Strapp, J., and Emery, J. (2005). A multiwire hot-wire device for measurement of icing severity, total water content, and dropet diameter. In *43rd AIAA Aerospace Sciences Meeting and Exhibition*.

Ludlum, F. (1958). The hail problem. *Nubila.*, 1:12–96.

Makkonen, L. (1981). Estimating intensity of atmospheric ice accretion on stationary structures. *Journal of Applied Meteorology*, 20:595–600.

Messinger, B. (1953). Equilibrium temperature of an unheated icing surface as a function of air speed. *Journal of the Atmospheric Sciences.*, 20:29–42.

Miller, D., Potapczuk, M., and Langhals, T. (2005). Preliminary investigation of ice shape sensitivity to parameter variations. In *43rd AIAA Aerospace Sciences Meeting and Exhibition, Reno, Nevada.*

Miller, D., Potapczuk, M., and Langhals, T. (2006). Additional investigations of ice shape sensitivity to parameter variations. In *44th AIAA Aerospace Sciences Meeting and Exhibition.*

Miller, D., Ratvasky, T., Bernstein, B., McDonough, F., and Strapp, J. (1998). Nasa/faa/ncar supercooled large droplet icing flight research: Summary of winter 96-97 flight operations. In *36th AIAA Aerospace Sciences Meeting and Exhibition, Reno, Nevada.*

Norris, R., Rumford, K., and Youd, D. (1989). Method of operating anti-icing valve (us patent 4852343). Technical report, United States Patent and Trademark Office.

NTSB (1996). Aircraft accident report: In-flight icing encounter and loss of control; simmons airlines, d.b.a. american eagle flight 4184 avions de transport regional (atr) model 72-212, n401am, roselawn indiana; october 31, 1994. Technical report, National Transportation Safety Board.

NTSB (1998). Aircraft accident report, in-flight icing encounter and uncontrolled collision with terrain: Comair flight 3272 embraer emb-120rt, n265ca monroe, michigan, january 9, 1997. Technical report, National Transportation Safety Board/AAR/98-04.

Ogretim, E., Huebsch, W., and Shinn, A. (2006). Aircraft ice accretion prediction based on neural networks. *Journal of Aircraft*, 43:233–240.

Olsen, P. (1998). Icing analysis, flight test and certification of the gulfstream gv business jet. In *36th AIAA Aerospace Sciences Meeting and Exhibition, Reno, Nevada.*

Pan, J. and Loth, E. (2003). Effect of airfoil geometry on performance with simulated ice accretions, volume 2: Numerical investigation. Technical report, Federal Aviation Administration.

Pan, J. and Loth, E. (2004). Detached eddy simulations for airfoil with ice shapes. In *42nd AIAA Aerospace Sciences Meeting and Exhibition, Reno, Nevada.*

Papadakis, M., Gile Laflin, B., Youssef, G., , and Ratvasky, T. (2001). Aerodynamic scaling experiments with simulated ice accretions. In *39th AIAA Aerospace Sciences Meeting and Exhibition, Reno, Nevada.*

Parkins, D. (2007). Developing critical ice shapes for use in aircraft development and certification. In *Proceedings of the 45th AIAA Aerospace Sciences Meeting and Exhibition, Reno, Nevada.*

Penny+Giles (2007). Ice and snow systems. Website.

Politovich, M. (1998). Forecasting aviation icing: Icing type and severity. University Corporation for Atmospheric Research Website.

Politovich, M. (2000). Predicting rime or glaze growth on airfoils. *Journal of Aircraft.*, 37:117–121.

Potapczuk, M., Gent, R., and Guffond, D. (1997). *Review, Validation and Extension of Ice Accretion Prediction Codes*, chapter 5, pages 5–1 to 5–14. Advisory Group for Aerospace Research & Development.

QuickMBA (2008). Questionnaire design. Website.

Rae, W. and Pope, A. (1984). *Low-Speed Wind Tunnel Testing*, chapter 6 (Wind Tunnel Boundary Corrections), page 344 to 444. John Wiley & Sons.

Ragni, a., Esposito, B., Marrazzo, M., Belluci, M., and Vecchione, L. (2005). Calibration of the cira iwt in the high speed configuration. In *43rd AIAA Aerospace Sciences Meeting and Exhibition, Reno, Nevada.*

Rumford, K. and Norris, R. (1988). Anti-icing management system. Technical report, United States Patent and Trademark Office.

Rumsey, C., Rivers, S., and Morrison, J. (2004). Study of cfd variation on transport configurations from the second drag-prediction workshop. In *42nd AIAA Aerospace Sciences Meeting and Exhibition, Reno, Nevada.*

Ryanair (2007). Ryanair holdings plc annual report. Annual Report Pursuant to Section 13 or 15(d) of the Securities Exchange Act of 1934.

Ryerson, C., Koenig, G., Melloh, R., Meese, D., Reehorst, A., and Miller, D. (2001). Spatial analysis of great lakes regional icing cloud liquid water content. In *39th AIAA Aerospace Sciences Meeting and Exhibtion, Reno, Nevada.*

Saeed, F. and Paraschivoiu, I. (2003). Optimization of a hot-air anti-icing system. In *41st AIAA Aerospace Sciences Meeting and Exhibition, Reno, Nevada.*

Schumann, T. (1938). The theory of hailstone formation. *The Quarterly Journal of the Royal Meteorological Society.*, 64:3–21.

Stallabrass, J. (1978). An appriasal of the single rotating cylinder method of liquid water content measurement. Technical report, Canadian Natianal Research Council.

Stollery, J. and Dyer, D. (1988). The flight performance of an rpv compared with wind tunnel and theoretical (cfd) results. In *16th International Congress of Aerospace Sciences.*

Strapp, J., Oldenburg, J., Ide, R., Lilie, L., Oleskiw, M., Leone, G., Bacic, S., Voukovic, Z., Miller, D., and Emery, E. (2003). Wind tunnel measurements of the response of hot-wire liquid water content instruments to large droplets. *Journal of Atmospheric and Oceanic Technology*, 20:791–806.

Tai, T. (2000). *Single-Block Body-Conforming Structured Grid for Complex Geometries.*, pages 91–100. ISGG.

Tan, S., Papdakis, M., and Muthuswamy, S. (2004). Development of a total liquid water content probe. In *42nd AIAA Aerospace Sciences Meeting and Exhibition, Reno, Nevada.*

Thompson, C. (2007). Personal communication. Personal Communication.

Thompson, D. and Soni, B. (2002). Automated geometric modeling and grid generation for airfoils with ice accretions. In *40th AIAA Aerospace Sciences Meeting and Exhibition, Reno, Nevada.*

Trebble, W. (1985). Low-speed wind-tunnel tests on the x-rae 2 unmanned aircraft in the rae 24ft wind-tunnel. Technical report, RAE-TM-Aero 2048.

Trebble, W. (1986). Aerodynamics of unmanned aircraft at full-scale in the rae 24ft wind tunnel. Technical report, RAE-TM-Aero 2081.

UAL-Corporation (2007). United airlines annual report. Annual Report Pursuant to Section 13 or 15(d) of the Securities Exchange Act of 1934.

Valenzuela, D. and Shrivastava, P. (2002). Interview as a method for qualitative research. Presentation.

Vickerman, M., Choo, Y., Schilling, H., Braun, D., Baez, M., and Cotton, B. (2005). Smaggice: Further progress in software for gridding 2d iced aerofoils. In *43rd AIAA Aerospace Sciences Meeting and Exhibition, Reno, Nevada.*

Wagner, B., Hammond, D., Van Hengst, J., Gent, R., Kind, R., Jeck, R., Seubert, B., King, R., Feo, A., Golia, C., Shah, A., Potapczuk, M., Guffond, D., Carbonaro, M., Ozgen, S., and Feo, A. (1997). Ice accretion simulation. Technical report, AGARD (NATO).

Wells, P. (2006). Future engines - ice protection implications. Presentation.

Whalen, E., Broeren, A., Bragg, M., and Lee, S. (2005). Characteristics of runback ice accretions on airfoils and their aerodynamic effects. In *43rd Aerospace Science Meeting and Exhibition, Reno, Nevada.*

Woodgate, M., Badcock, K., and Richards, B. (1999). A parallel 3d fully implicit unsteady multiblock cfd code implemented on a beowulf cluster. In *Parallel Computational Fluid Dynamics.*

Woodgate, M., Badcock, K., and Richards, B. (2000). A parallel 3d fully implicit unsteady multiblock cfd code implemented on a beowulf cluster. In *Parallel Computational Fluid Dynamics*.

Yeoman, K. (1989). Selection of the critical icing/flight case for an unprotected airfoil. In *Proceedings of the 27th AIAA Aerospace Sciences Meeting, Reno, Nevada.*

Yeoman, K. (1994). Efficiency of a bleed air powered inlet icing protective system. In *32nd Aerospace Sciences Meeting and Exhibition, Reno, Nevada*.

Zhu, B., Chi, X., Shih, T.-P., and Slater, J. (2002). Computational aerodynamic performance of 2d iced airfoils: Blocking strategy and convergence rate. In *20th AIAA Applied Aerodynamics Conference, St. Louis, Missouri.*

Zhu, B., Chi, X., Shih, T.-P., Slater, J., Addy, H., and Choo, Y. (2003). Computing aerodynamic performance of 2-d iced airfoils with structured grids. In *41st AIAA Aerospace Sciences Meeting and Exhibition, Reno, Nevada.*

This page has been left intentionally blank.

Appendix A

The Icing Community

Organisations represented at the 2007 SAE Aircraft & Engine Icing International Conference:

- Air Accidents Investigation Branch;
- National Transportation Safety Board;
- Boeing Commercial Airplanes;
- European Aviation Safety Agency;
- Transport Canada;
- Federal Aviation Administration;
- UK Civil Aviation Authority;
- General Electric Company;
- Sino Swearingen Aircraft Co.;
- Cessna Aircraft Co.;
- Bombardier Aerospace;
- Eurocopter France;
- Continental Airlines Inc.;

- APS Aviation Inc.;
- BAE Systems;
- Dow Chemical Canada;
- National Defense Headquarters;
- Anti-Icing Materials International Laboratory;
- Airbus SAS;
- National Center for Atmospheric Research;
- Radiant Aviation Services;
- MISCO Products;
- MDA Space Missions;
- Dan-Ice A/S;
- Oslo Lufthaven AS;
- Lufthansa EFM;
- Nordic Aero AB;
- Multiconsult;
- Norwegian Water Technology Centre;
- Battelle Memorial Institute;
- Michigan Technological University;
- Swedish Civil Aviation Authority;
- NASA John Glenn Research Center;
- Embraer-Empresa Brasileira Aero SA;
- ATR Corp.;

- University of Illinois at Urbana-Champaign;
- Trebor Systems Inc.;
- Newmerical Technologies Inc.;
- Instituti Nacioanal de Tecnica Aeroespace;
- Iowa State University;
- ONERA;
- Qinetiq;
- Cougar Helicopters;
- Sikorsky Aircraft Corp.;
- Bell Helicopter Textron Inc.;
- Pall Europe, Ltd.;
- CIRA;
- McGill University;
- Dassault Aviation;
- Beijing University;
- Iberespacio;
- EA International;
- Wichita State University;
- Cox & Co. Inc.;
- Kanagawa Institute of Technology;
- Moritz Corp.;
- Kelly Aerospace Thermal Systems;

- ICON;
- Goodrich Sensor Systems;
- Honeywell;
- Cranfield University;
- Nagoya Aerospace Systems;
- Mitsubishi Heavy Industries, Ltd.;
- ASRC Aerospace;
- GKN Aerospace;
- Environment Canada;
- Universitat Hannover;
- Leading Edge Atmospherics;
- VTT;
- Norwegian Meteorological Institute;
- Meteo-France;
- Finnish Meteorological Institute;
- US Army Corps of Engineers;
- Institute for Aerospace Research NRC.

Appendix B

Commercial Survey Results

QUESTION 1(a)	How would you classify the operations of the organisation you work for?																			Specific Comments
	Academically Based Research	Airframe Manufacturer	Airframe Systems/ Component Supplier/	Airline	Engine Manufacturer	Government Research Body	Helicopter Manufacturer	Provision of Experimental Facilities	Provision of Numerical Simulation Facilities	Regulatory	Technological Consultancy	Other								
Respondent 1		■																		
Respondent 2		■																		
Respondent 3	■												Used to work for manufacturing but was still a researcher							
Respondent 4	■																			
Respondent 5			■					■		■			IPS design and manufacture. CAA/FAA approval of facilities							
Respondent 6		■																		
Respondent 7					■															
Respondent 8										■			Government authority							
Respondent 9							■						Bell Helicopter							
Respondent 10						■		■												
Respondent 11	■																			
Respondent 12	■																			
Respondent 13					■															
Respondent 14			■										Supplier of IPS's (tier 1)							
Respondent 15					■															
Respondent 16						■							ONERA							
Respondent 17		■	■																	
Respondent 18						■														
Respondent 19			■																	
Respondent 20						■							Some fundamental research is condicted at times. We do applied icing research, and certification of de-icing systems							

Figure B.1: Commercial Survey Question 1(a).

QUESTION 1(b)	
	Your Background: How did you become involved in icing related work?
Respondent 1	My first job in 1994 was in the icing group in DRA (now Qinetiq). I have stayed in icing related jobs ever since then.
Respondent 2	I have been a systems engineer since 1995, mostly with pneumatics, environmental control and anti-ice. I have been involved with the prediction of wing ice shapes since January 1995.
Respondent 3	Had been working in strength of materials and my employers wanted to know how best to break ice off aircraft.
Respondent 4	Was asked for modelling by test center.
Respondent 5	Started in this business as an apprentice. The site has worked in the research of aircraft since 1947. An ice protection business has developed since that time. I started in the manufacturing development of such systems e.g. Concorde and went on into engineering design and managing the icing wind tunnel.
Respondent 6	Participation in development of the ice protection systems on BAE ATP.
Respondent 7	I was first involved in icing related work as a compressor designer. I need to design blades to withstand ice impact from ice coming from upstream of the IP compressor. I 'm now involved with the Trent 1000 anti-icing rig.
Respondent 8	Hazard! Owing to the fact that the civil aircraft anti-ice system is supplied by the ECS bleed air system. I was also previously an ECS qualification specialist.
Respondent 9	Design and certification of BAC1-11 (1987) and B727QF (1990) with RR Tay 650 engines. Qualification of the V22 Tiltrotor Ice Protection System (1990 and 1993). Design and Certification of BA609 Tiltrotor Ice Protection Systems (Present).
Respondent 10	Just working within the Icing Test Laboratory of my company.
Respondent 11	Through a research project on modelling high-speed droplets.
Respondent 12	I studied Applied Mathematics. In particular Numerical Analysis and Differential Equations.
Respondent 13	---
Respondent 14	Company - Propeller de-icing controllers (1990) as a Dowty Propellers supplier. Developed power control technologies and consortium. Various attempts to break into electro-thermal de-ice systems; now the supplier of Boeing 787 wing ice protection systems. I have had various involvement over 16 years in the above.
Respondent 15	Thermal analysis of engine structures.
Respondent 16	I always work on icing.
Respondent 17	Job opportunity.
Respondent 18	Graduate student research.
Respondent 19	Liquid ice protection system manufacturer.
Respondent 20	Transferred to the icing branch at NASA in 1994 and have been here ever since doing thermal ice protection testing, icing instrumentation testing and development, and flight research to characterize the SLD icing environment in our Twin Otter.

Figure B.2: Commercial Survey Question 1(b).

QUESTION 1(c)	Categories describing level of familiarity with the field				Reason for choice (optional)
	None	Basic	Intermediate	Extensive	
Respondent 1					Extensive in most aspects (ice shape prediction, ice effects), intermediate in others (e.g. meteorology, some aspects of system design).
Respondent 2					Extensive in system design, intermediate in ice shape prediction, ice effects.
Respondent 3					There is a lot on the aerodynamic, systems and meteorological side I am pretty hazy on.
Respondent 4					
Respondent 5					Many years experience of designing/testing/manufacturing and certification of ice protection systems for a wide range of aircraft types. Also applies to our other product line of windscreens to some extent.
Respondent 6					
Respondent 7					My involvement gave me basic knowledge of where the ice physically forms on the aircraft and exists within the flight envelope. I have not got much knowledge of how it forms, how the surface affects the formation of ice and so on.
Respondent 8					
Respondent 9					There is always more to learn ....
Respondent 10					
Respondent 11					I have worked in icing for 3 years now including a stint in industry looking at modelling various aspects of the field. I don't have much experience on the experimental side however.
Respondent 12					Interesting project related to applied mathematics and aerospace.
Respondent 13					
Respondent 14					Basic knowledge with intermediate knowledge of electro-thermal anti/de-ice systems.
Respondent 15					
Respondent 16					
Respondent 17					
Respondent 18					
Respondent 19					
Respondent 20					12 years research in a variety of icing research tasks

Figure B.3: Commercial Survey Question 1(c).

QUESTION 2	Which does your role most closely resemble?				Specific Comments
	Engineer	Project Engineer	Project Manager	Programme Manager	
Respondent 1					I cover various Airbus projects, including aircraft developments and research projects (e.g. Project Manager for ICECREMO 2).
Respondent 2					Group leader of wing ice protection at Airbus
Respondent 3					It's a bit specialised so you end up doing jobs at many levels for a bit of time here and there
Respondent 4					(actually not fully adapted to academic research)
Respondent 5					Current role is design/technology lead. I have a roving role in all these areas as a senior manager in the business
Respondent 6					Responsible for design, development & test analysis of Nimrod MRA4 ice & rain protection systems.
Respondent 7					I don't perform the technical tasks but lead to ensure tasks are completed.
Respondent 8					
Respondent 9					Most projects include icing.
Respondent 10					
Respondent 11					
Respondent 12					Technical work involving engineering and mathematics
Respondent 13					
Respondent 14					Responsibly technically for various programmes
Respondent 15					
Respondent 16					Different projects but all in icing
Respondent 17					
Respondent 18					
Respondent 19					
Respondent 20					I also wear the project engineer hat at times.
For the purposes of the survey, an engineer completes technical work including icing tasks					
For the purposes of the survey, a project engineer has responsibility for completion of a number of technical tasks and takes a lead role in their completion					
For the purposes of the survey, a project manager is responsible for a number of different projects at one time, where one could involve aircraft icing.					
For the purposes of the survey, a programme manager is responsible for an entire programme, e.g. the design and manufacture of an IPS for a customer.					

Figure B.4: Commercial Survey Question 2.

QUESTION 3

	Weighting of role and responsibilities					Specific Comments
	Technical Matters	Project Resources	Project Scheduling	Project Cost	Programme Management	
Respondent 1	78%	10%	5%	5%	2%	
Respondent 2	40%	10%	10%	10%	20%	
Respondent 3	50%	12%	12%	12%	12%	
Respondent 4	60%	10%	10%	10%	10%	
Respondent 5	50%	10%	10%	10%	20%	
Respondent 6	85%	5%	5%	0%	5%	
Respondent 7	35%	5%	20%	20%	20%	
Respondent 8	95%	0%	5%	0%	0%	
Respondent 9	70%	10%	10%	10%	0%	
Respondent 10	10%	20%	20%	20%	30%	
Respondent 11	90%	10%	0%	0%	0%	
Respondent 12	60%	20%	20%	0%	0%	
Respondent 13	20%	20%	10%	40%	10%	
Respondent 14	75%	10%	5%	5%	5%	
Respondent 15	90%	0%	10%	0%	0%	
Respondent 16	20%	30%	10%	20%	20%	
Respondent 17	60%	0%	20%	15%	5%	
Respondent 18	91%	3%	3%	3%	0%	
Respondent 19	40%	10%	10%	20%	20%	
Respondent 20	80%	5%	10%	5%	0%	

Figure B.5: Commercial Survey Question 3.

QUESTION 4	What icing related activities does your organisation regularly engage in?										
	Use of Appendix C and flight profile to ascertain likely icing conditions	Numerical ice accretion simulation	Numerical aerodynamic analysis	Experimental ice accretion simulation	Experimental aerodynamic analysis	Artificial flight testing	Natural flight testing	Research into icing (e.g. processes, physics, technologies)	Development of prediction and design tools	Specific Comments
Respondent 1										Core task; Core task; Core task; Core task.
Respondent 2										
Respondent 3										Generally a starting point; Few bits & pieces - to support research; Reasonably extensive; Not directly; With colleagues in AMAC (uni department).
Respondent 4										
Respondent 5										Regularly; Have specialists; Not a regular activity as this is usually under the control of the Type Certificate holder/certifier; Icing wind tunnel - specific to project or hired to third party competitors; But only to basic levels as the wind tunnel has no force measuring equipment or aerodynamic measuring ability; Icing wind tunnel; Support to customer/type certificate holder icing flight testing; Not a large sector of work for us but is done for third party customers and academic institutions or as part of a Dti or EU funded programme; With colleagues in AMAC (uni department).
Respondent 6										
Respondent 7										
Respondent 8										
Respondent 9										
Respondent 10										

Figure B.6: Commercial Survey Question 4 part 1.

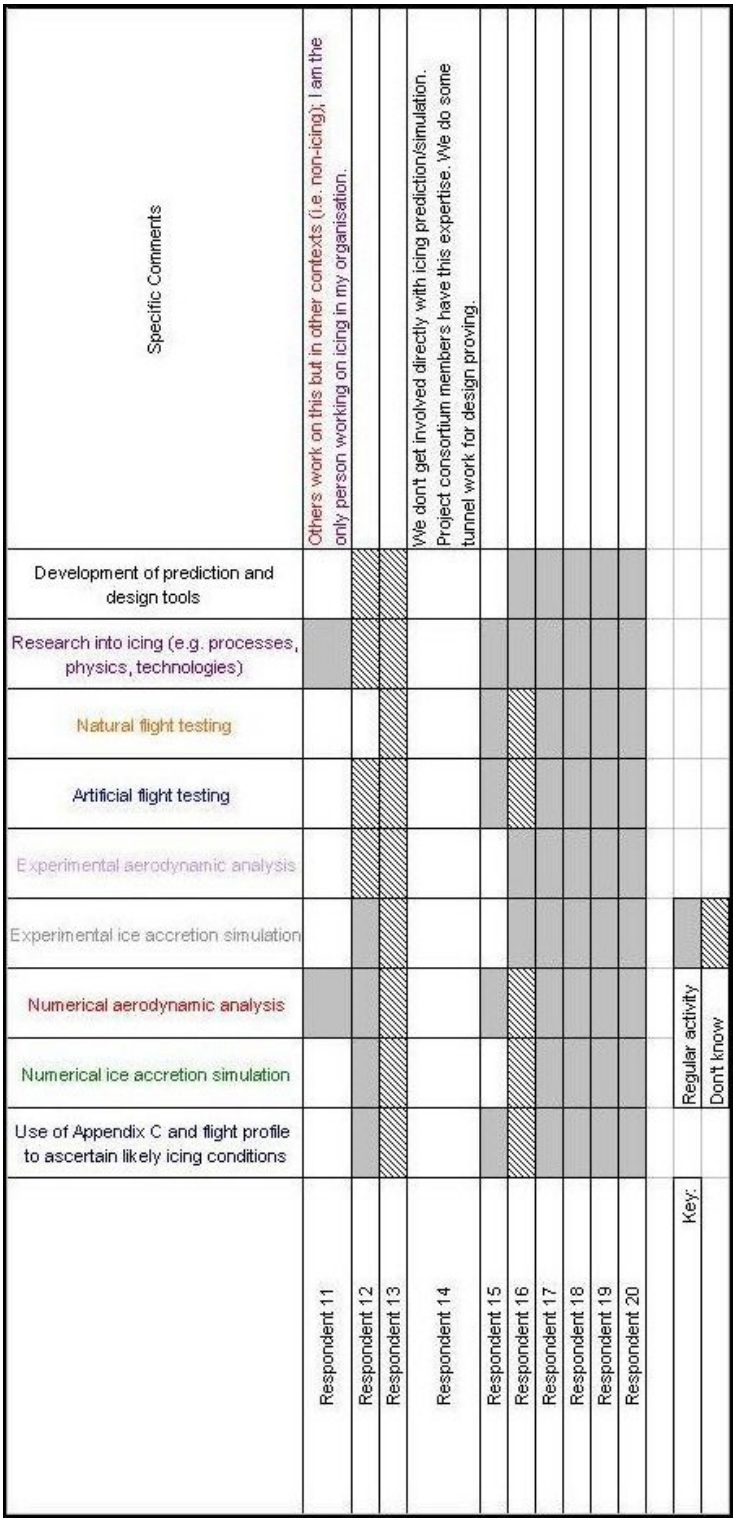

Figure B.7: Commercial Survey Question 4 part 2.

QUESTION 5(a)	How long might a typical icing programme take to complete (weeks/months)?	
	Answer	Specific Comments
Respondent 1	About 5 yrs	The 'icing programme' effectively runs in parallel with the overall aircraft development programme. It starts out with a very preliminary estimate of ice protection requirments and energy requirements during the feasibility phase, is gradually refined throughout the development phases and finishes with natural icing flight tests and artificial ice shape flight tests which are normally done just before the aircraft is certified.
Respondent 2	About 5 yrs	As above - same company
Respondent 3	0.5-2 yrs	6 months or so to do a ground test campaign or a chunk of a/c design support. 2 years initial design to certification
Respondent 4	Months	
Respondent 5	1-3 yrs	Depends entirely on the aircraft/project type and how complicated. It's very rare for a certified system to be less than a year simply due to the length of time the calculations/trials and design evolution take.
Respondent 6	3-4.5 yrs	2-3 years system design, 12-18 months testing.
Respondent 7	9 mths	First time running this kind of test, majority of time to design and make a rig that is representable to engine geometry and flow.
Respondent 8	At least 2 yrs	
Respondent 9	4-5 yrs	Initial design - 6mths, Component qualification - 18mths, SOF icing tunnel tests - 6mths; natural icing - 2 winters
Respondent 10		
Respondent 11	2-3 yrs	
Respondent 12	2 yrs	
Respondent 13	10 mths	
Respondent 14	36 mths	This is the complete project cycle from preliminary design to start of the production. Actual icing work is approximately 6/8 mths within the programme
Respondent 15	~~3 years~~ 1 year	
Respondent 16	Mths/yrs	
Respondent 17	10 mths	6 months design, 4 months flight test + certification
Respondent 18	Wks to yrs	
Respondent 19	0.5-1.0 yr	For a small G.A. aircraft
Respondent 20	Months	

Figure B.8: Commercial Survey Question 5(a).

QUESTION 5(b)	Do you consider an icing programme to be resource intensive (engineer time, equipment, software)	
	Answer	Specific Comments
Respondent 1	Yes	It requires prediction software (for ice shapes and ice protection modelling), wind tunnel testing, ground test rigs, sometimes icing tunnel tests, CFD, flight testing and knowledgeable personnel throughout the programme.
Respondent 2	Yes	As above - same company
Respondent 3	Not especially	Relatively small number of specialists, if all goes well.
Respondent 4		
Respondent 5	Yes	Depends (as of today) on having highly skilled staff at all stages. Even the best ice prediction software outputs require considerable interpretation and subsequent confirmation testing. The development of an ice protection system impinges on many other aspects of the vehicle being protected, e.g. structural/power generation/control and distribution, performance required and likely theatre of use.
Respondent 6	Yes	Engineer time
Respondent 7		As (a), majority of work is desgin and make of the rig. The actual initial analysis is to define the rig geometry from the existing engine geometry. And the final analysis is to record the icing during the test. Again, not something too resource intensive.
Respondent 8	Yes	
Respondent 9	Yes	
Respondent 10		
Respondent 11		No more than any other project area
Respondent 12	Yes	
Respondent 13	Yes	Engineer time
Respondent 14		Engineering (internal) - 18 man months, Equipment/tunnel etc - approx 7% programme cost, Software/subcontract (external) - approx 18 man months
Respondent 15	Yes	Engineer time
Respondent 16	Yes	
Respondent 17	Yes	
Respondent 18	Yes	
Respondent 19	Yes	Fairly
Respondent 20	Yes	It can involve experimental and analytical methods thereby being quite multi-disciplinary. Experimental methods also require instrumentation, and fabrication support. If an icing facility is involved, those support personnel will be required to operate the facility.

Figure B.9: Commercial Survey Question 5(b).

QUESTION 5(c)	Is an icing programme significantly expensive as a proportion of total cost of a project that will incorporate icing work?	
	Answer	Specific Comments
Respondent 1	Yes	Perhaps not large as a proportion of the whole development programme, but is still very significant. I've got no idea what the cost is, but I would guess it would be about £20M for icing related activities for an aircraft development programme. Personnel costs would be £5M, as a rough order of magnitude. The other costs would be mainly wind tunnel and flight testing.
Respondent 2	Yes	As above - same company
Respondent 3	Yes	On occasion
Respondent 4		
Respondent 5	No	Not really, which is why software and experts are difficult to justify due to poor utilisation hours. However the ability to make such calculations and predicitons is vital at the early stages and is the spring board for the whole programme.
Respondent 6	No	Probably not as a proportion of the total project cost. The most significant aspect in terms of cost is artificial ice shape testing and natural icing trials.
Respondent 7	Don't know	Not sure of the cost of a project incorporating icing work.
Respondent 8	Yes	An AIS development is comparatively much more expensive to quality than an ECX (x3)
Respondent 9	Yes	The entire aircraft certification has to be revisited to account for effects of icing, normal and failed systems and development of flight limitations.
Respondent 10		
Respondent 11		
Respondent 12	Probably not	
Respondent 13	Yes	
Respondent 14	Yes	
Respondent 15	Yes	
Respondent 16		Full cost on icing (?)
Respondent 17	Yes	Yes, if we consider possible regulation changes
Respondent 18	Yes	Icing is 100% of project
Respondent 19	Varies	
Respondent 20	Can't answer	this one! I'm thinking this question would be most relevant to an aircraft de-ice/anti-ice certification test. For this type of activity, I don't know what percentage of the de-icing system certification would constitute relative to the total aircraft cost.

Figure B.10: Commercial Survey Question 5(c).

QUESTION 6(a)	If a more comprehensive, more accurate simulation methodology for predicting 'critical' ice growth was suggested, would you support it considering potential time and cost implications for the design and certification process, and for your organisation?	
	Answer	Specific Comments
Respondent 1	Maybe	
Respondent 2	Maybe	
Respondent 3	Yes	
Respondent 4	---	I am involved in simulation and find it most important
Respondent 5	Yes	
Respondent 6	Yes	
Respondent 7	Yes	
Respondent 8	Yes	
Respondent 9	Likely	
Respondent 10	Yes	
Respondent 11	Don't know	
Respondent 12	Yes	
Respondent 13	Yes	
Respondent 14	Yes	
Respondent 15	Yes	
Respondent 16	Yes	
Respondent 17	Yes	
Respondent 18	Yes	
Respondent 19	Don't know	
Respondent 20	Don't know	

Figure B.11: Commercial Survey Question 6(a).

QUESTION 6(b)	If a suggested simulation methodology provided better information for design of ice protection systems and associated power requirements, would this significantly effect your answer to (a)?	
	Answer	Specific Comments on answer to (b)
Respondent 1	Maybe	The most significant cost benefits would come from reducing wind tunnel testing and flight testing. It is unlikely that in the foreseeable that we could delete natural icing flight testing for validating the icing code results or for checking the functionality of the ice protection system. Wind tunnel costs could be reduced if CFD was reliable for predicting CLmax with ice shapes, but that's very challenging. A way to predict better the critical ice shapes is unlikely to give cost benefits. I think the way we choose the critical case today, whilst not completely rigorous, is okay and it is accepted by the airworthiness authorities, so any improvement would not give any cost benefit. Better methods for predicting the system's performance would certainly help to improve the design of the system, which may not save costs (unless it meant not having to do an experiment), but would contribute towards a more effective aircraft.
Respondent 2	Maybe	As above - same company
Respondent 3	Don't know	There are still some significant unknowns in the real life cloud conditions & and I would be cautious of reliance on any one source of data on the effect of icing in practice.
Respondent 4		I am involved in simulatio and find it most important.
Respondent 5	No	Both are needed and are complimentary to each other.
Respondent 6	Yes	I would be more inclined to support (a) if (b) was likely to reduce ice protection system power requirements and design/development time.
Respondent 7	Yes	Assuming the protection systems mean the prevention of ice build up, (a) become not relevant although, I will argue you cannot prevent ice build up until you can predict ice growth. Assuming the protection systems mean to divert, break down or make some physical change to prevent damage from ice, then it's passive protection system. I will still interesting in (a) to prevent root cause - ice forming in the first place.
Respondent 8	No	As qualification of AIS requires to figure out the most accurelly, performances and liability of the system, combining simulation methodologies and flight tests is necessary to cross check efficiency. As design of the AIS is not part of my field of work a simulation methodology which is dedicated to such a subject is not my concern.
Respondent 9	No	Material and established knowledge is readily available to some extent to design and size system at the component level however integration of all systems at the aircraft level to evaluate performance and aircraft qualities is essential at predicting 'critical' ice growth vs power requirements.
Respondent 10	No	The icing wind tunnel could be upgraded to fit new requirements.

Figure B.12: Commercial Survey Question 6(b) part 1.

QUESTION 6(b)	If a suggested simulation methodology provided better information for design of ice protection systems and associated power requirements, would this significantly effect your answer to (a)?	
	Answer	Specific Comments on answer to (b)
Respondent 11	Don't know	
Respondent 12	No	Simulations can approach the actual problems that icing involves, it is only a question of time that computers are going to be developed enough to avoid errors and improve accuracy. Because I work with simulation, this will not be affected.
Respondent 13	Yes	
Respondent 14	No	Assume that (a) would lead to better understanding. Therefore (b) is part of (a). Cost would be an issue and (a) would need to demonstrate benefits.
Respondent 15	No	
Respondent 16	No	Independent problems (failure cases)
Respondent 17	Yes	Provided that this simulation methodology will be approved by AA's, the potential benefit would be significant.
Respondent 18	Yes	
Respondent 19	Yes	Reasonably satisfied with present method
Respondent 20	Don't know	I think answers to (a) and (b) somewhat depend on what the more accurate simulation methodology is, and its potential improvement in the state of the art relative to what exists now.

Figure B.13: Commercial Survey Question 6(b) part 2.

Appendix C

Assessment of CFD Predictions by Experiment

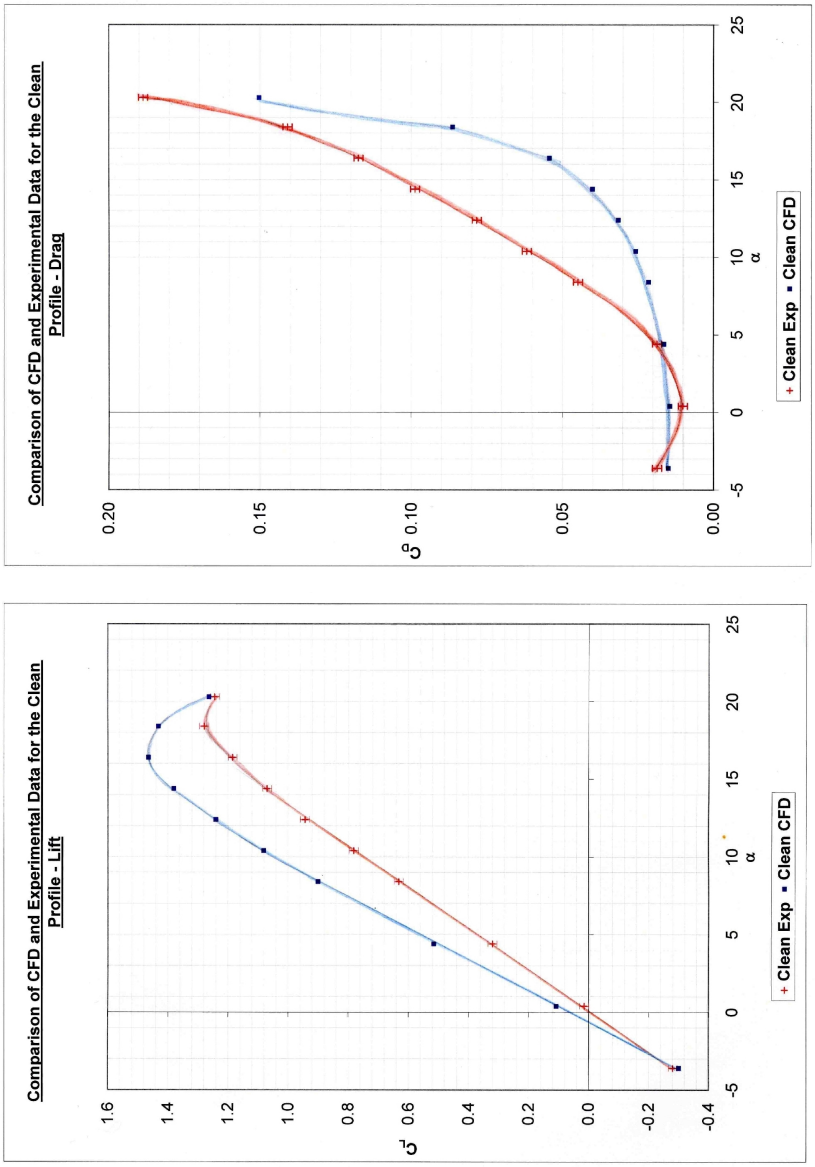

Figure C.1: C_L and C_D versus α from experiment, and CFD for the clean aerofoil.

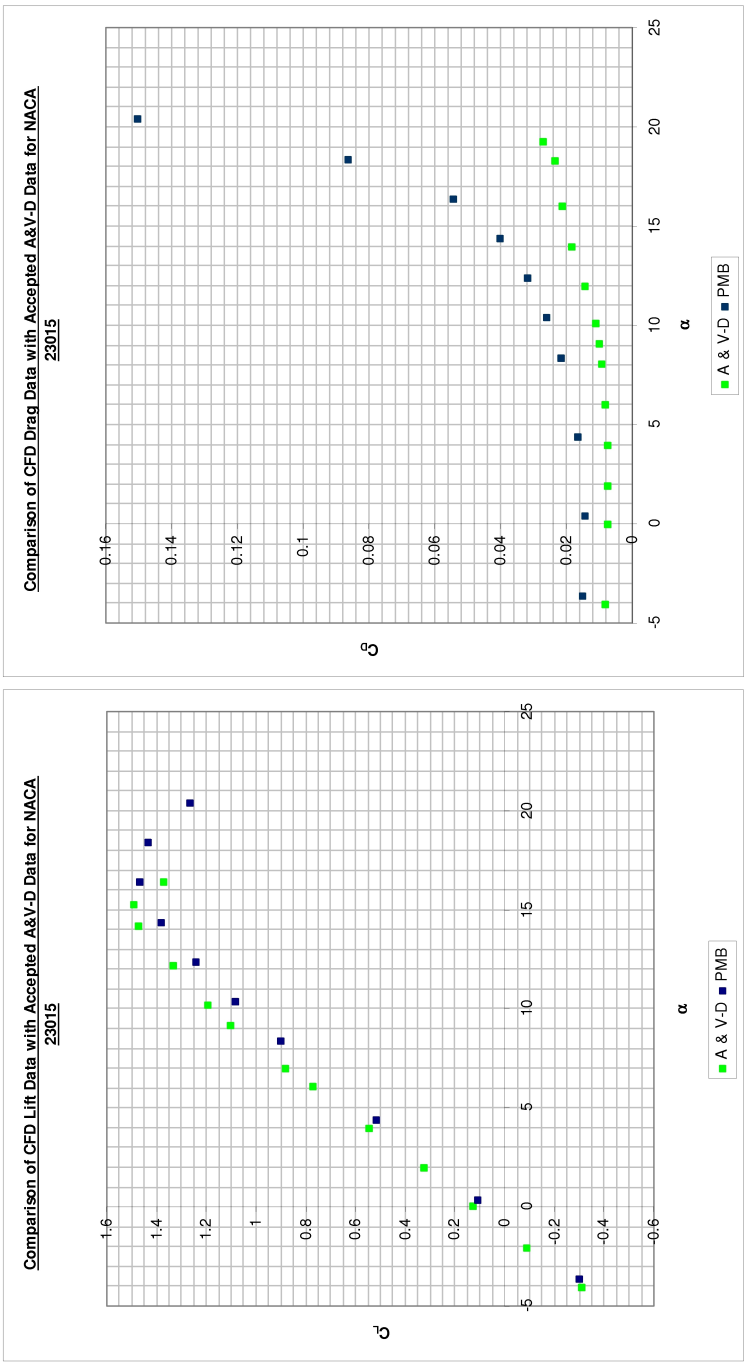

Figure C.2: C_L and C_D versus α from CFD and from Abbott and Von Doenhoff (1959) for the clean aerofoil.

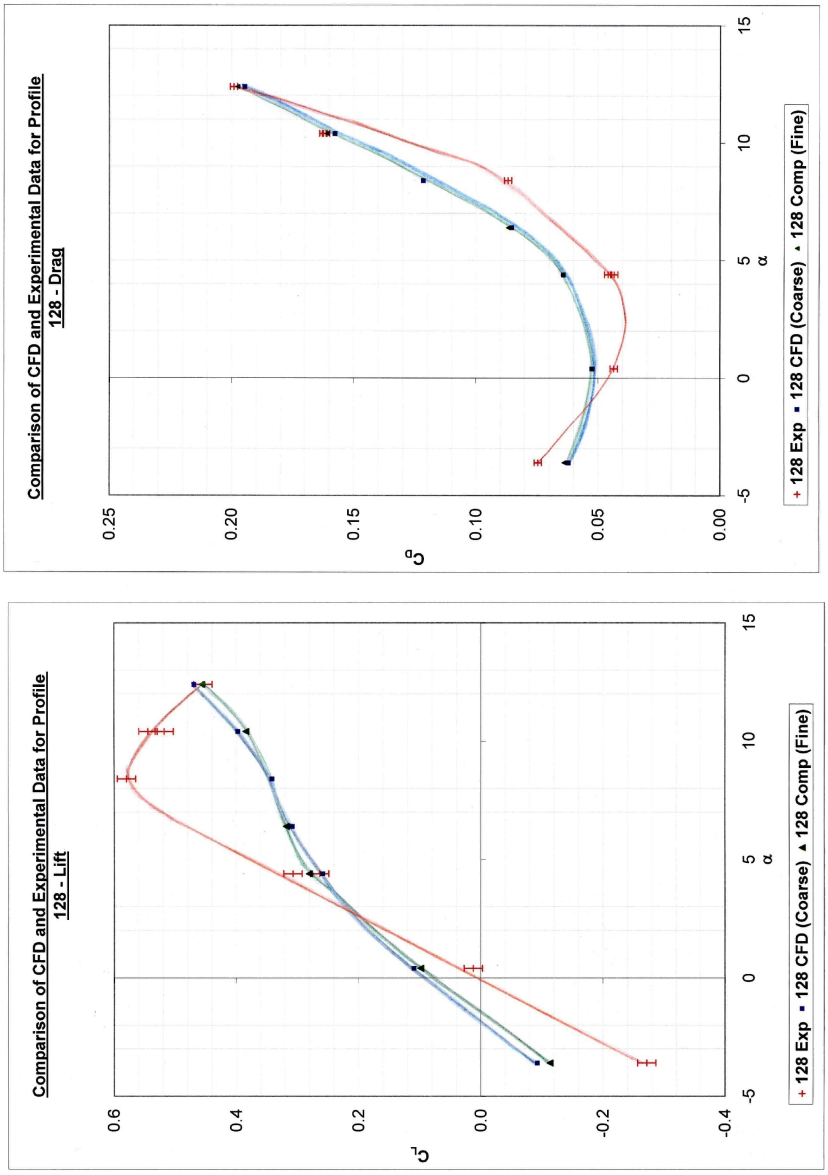

Figure C.3: C_L and C_D versus α from experiment, coarse grid CFD and fine grid CFD for profile 128.

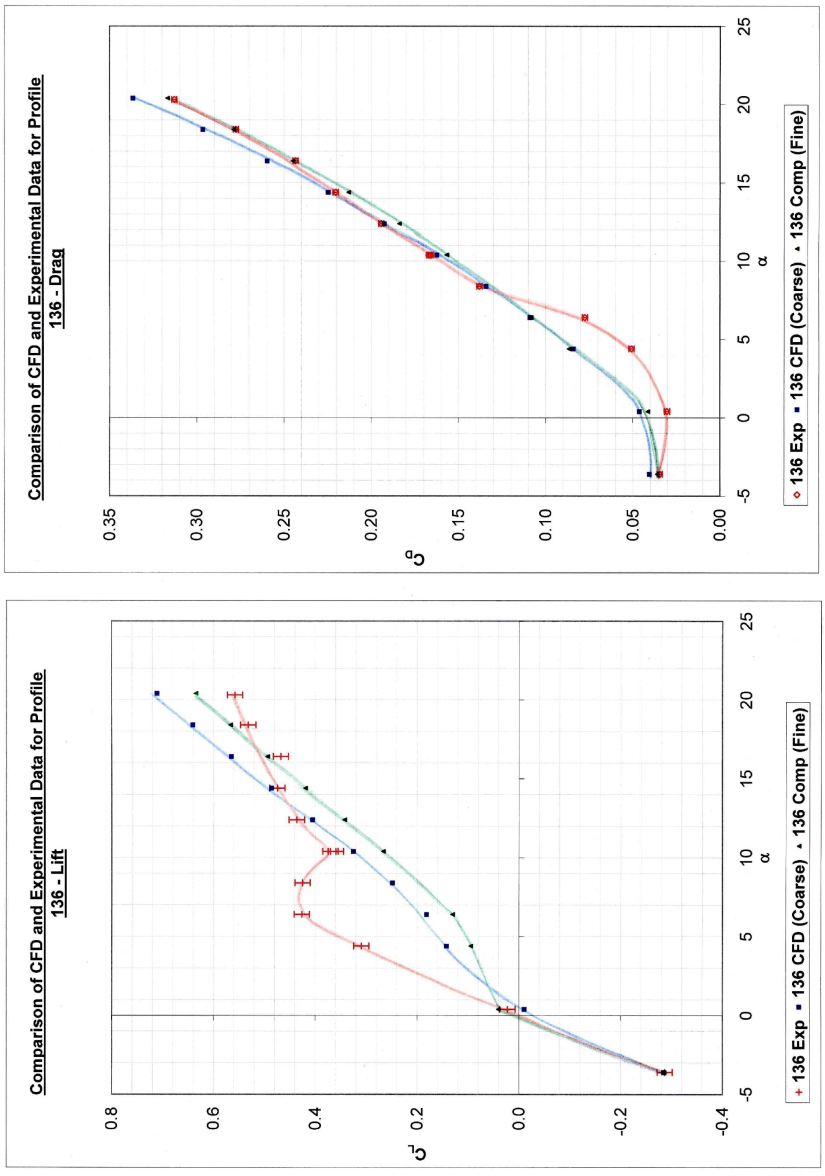

Figure C.4: C_L and C_D versus α from experiment, coarse grid CFD and fine grid CFD for profile 136.

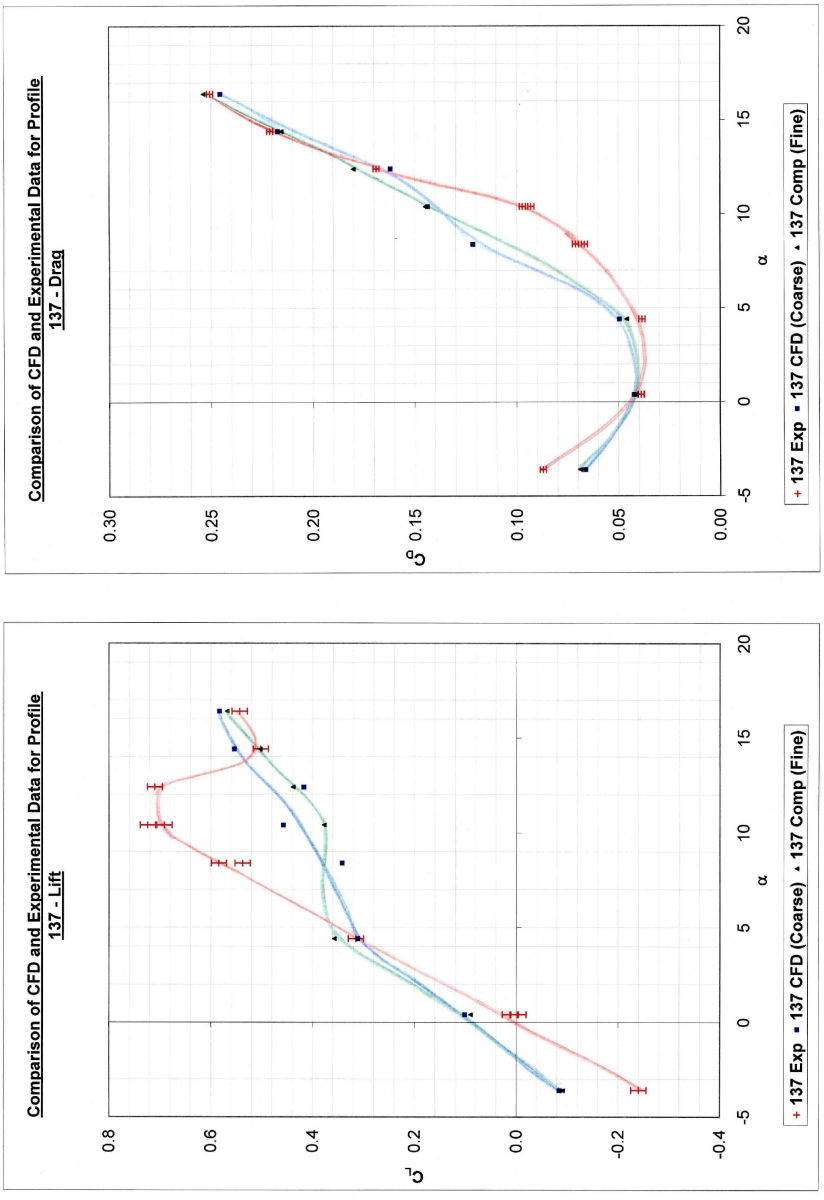

Figure C.5: C_L and C_D versus α from experiment, coarse grid CFD and fine grid CFD for profile 137.

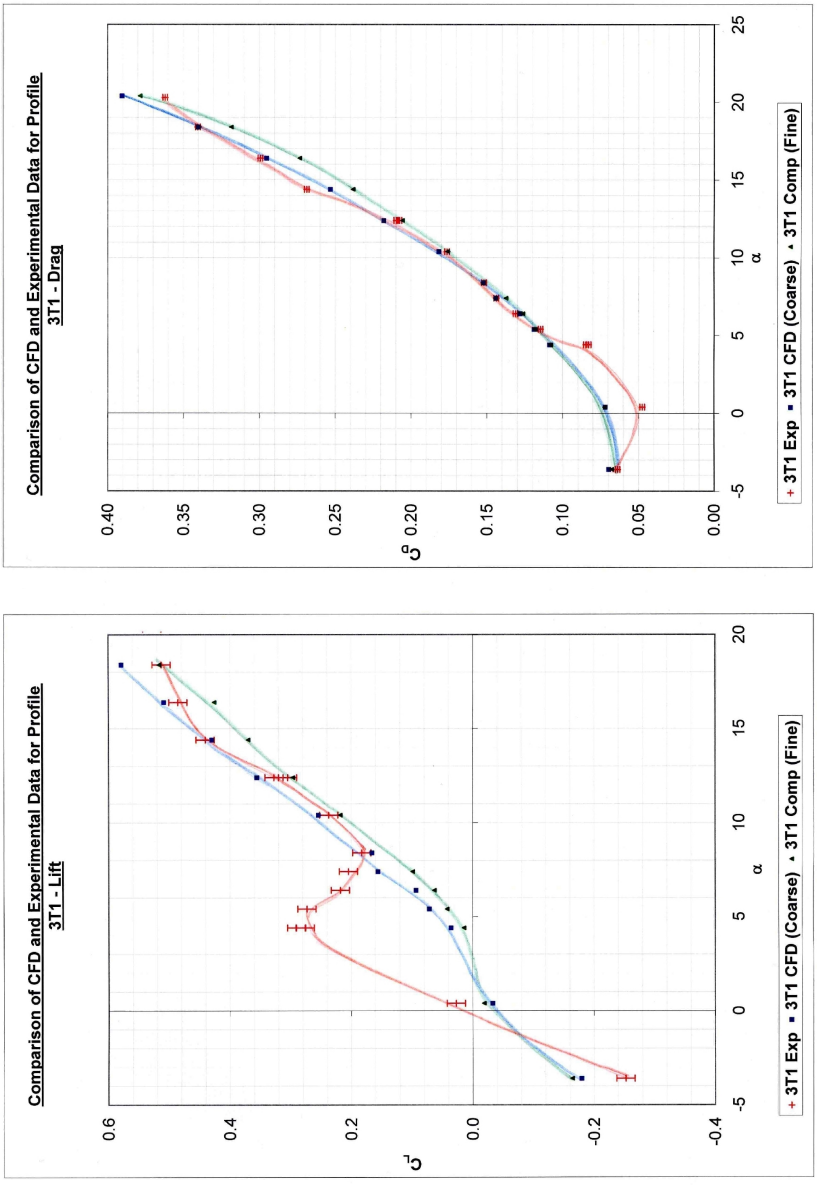

Figure C.6: C_L and C_D versus α from experiment, coarse grid CFD and fine grid CFD for profile 3T1.

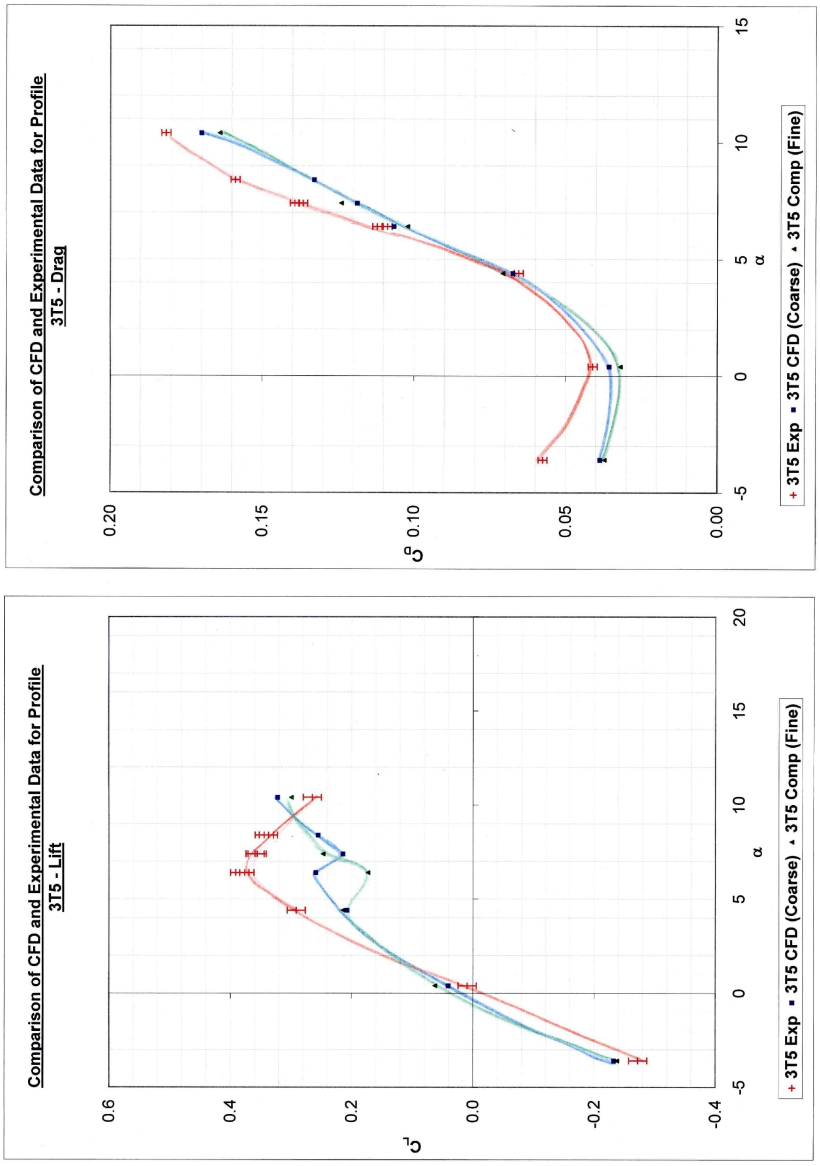

Figure C.7: C_L and C_D versus α from experiment, coarse grid CFD and fine grid CFD for profile 3T5.

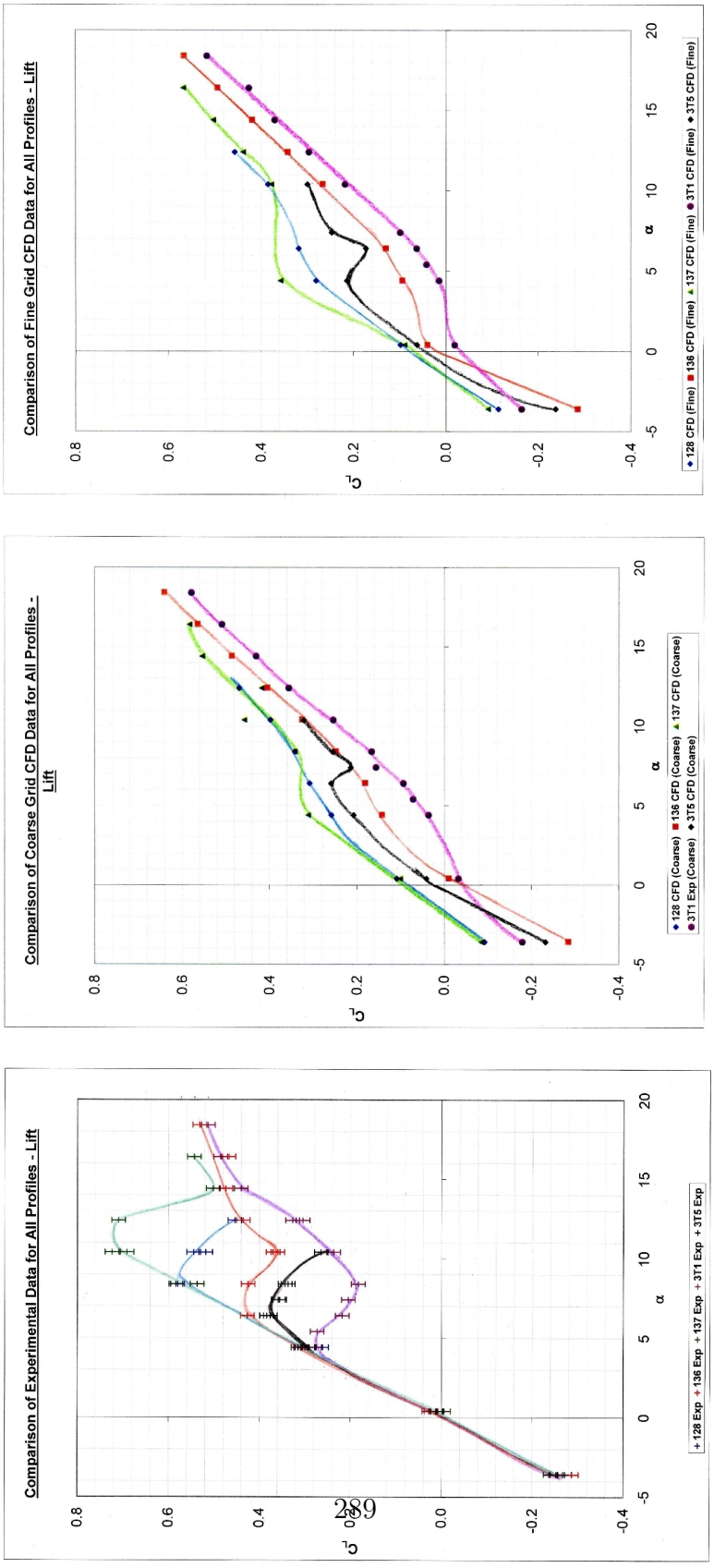

Figure C.8: C_L versus α from experiment, coarse grid CFD and fine grid CFD for all iced profiles.

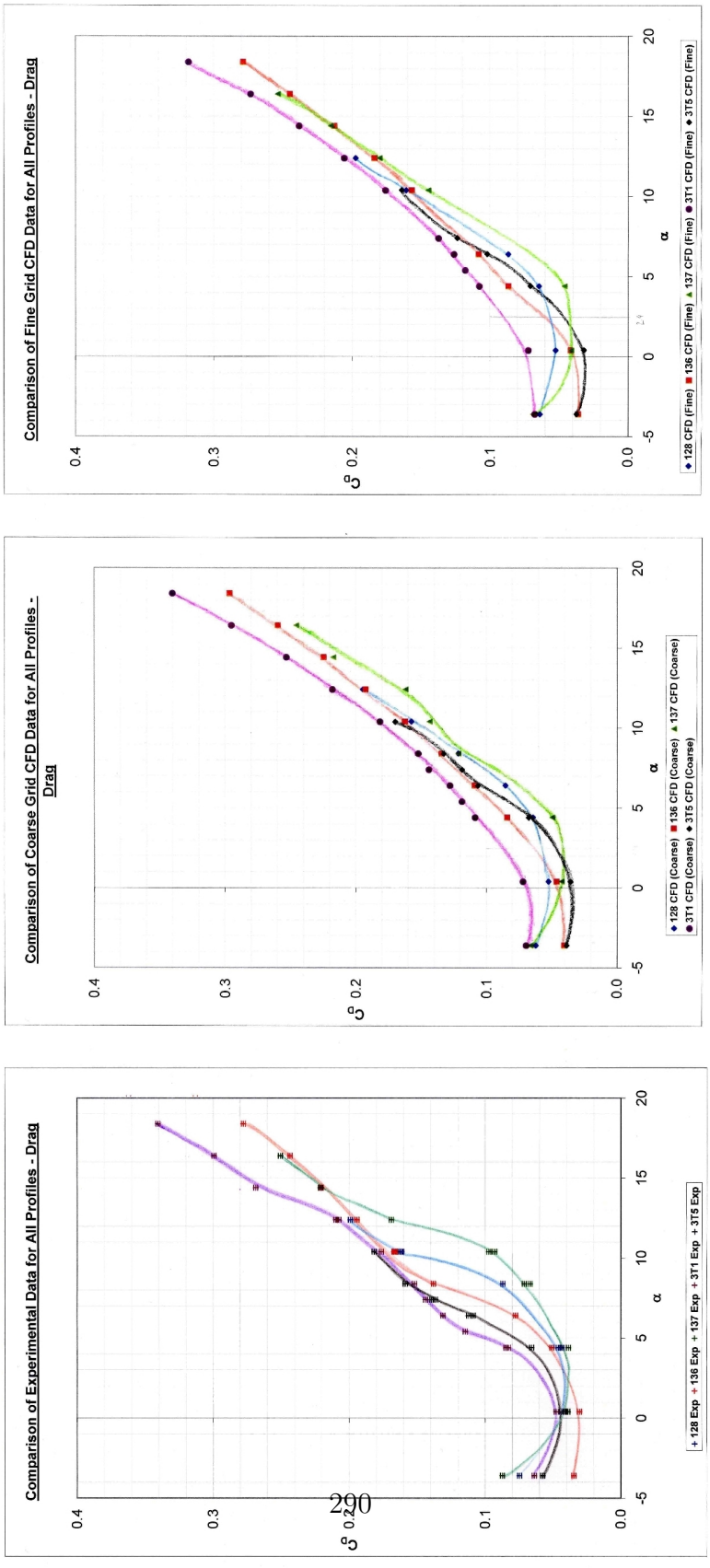

Figure C.9: C_D versus α from experiment, coarse grid CFD and fine grid CFD for all iced profiles.

Figure C.10: Spreadsheet helping ascertain the trend agreement shown in figure C.9 for drag coefficient.

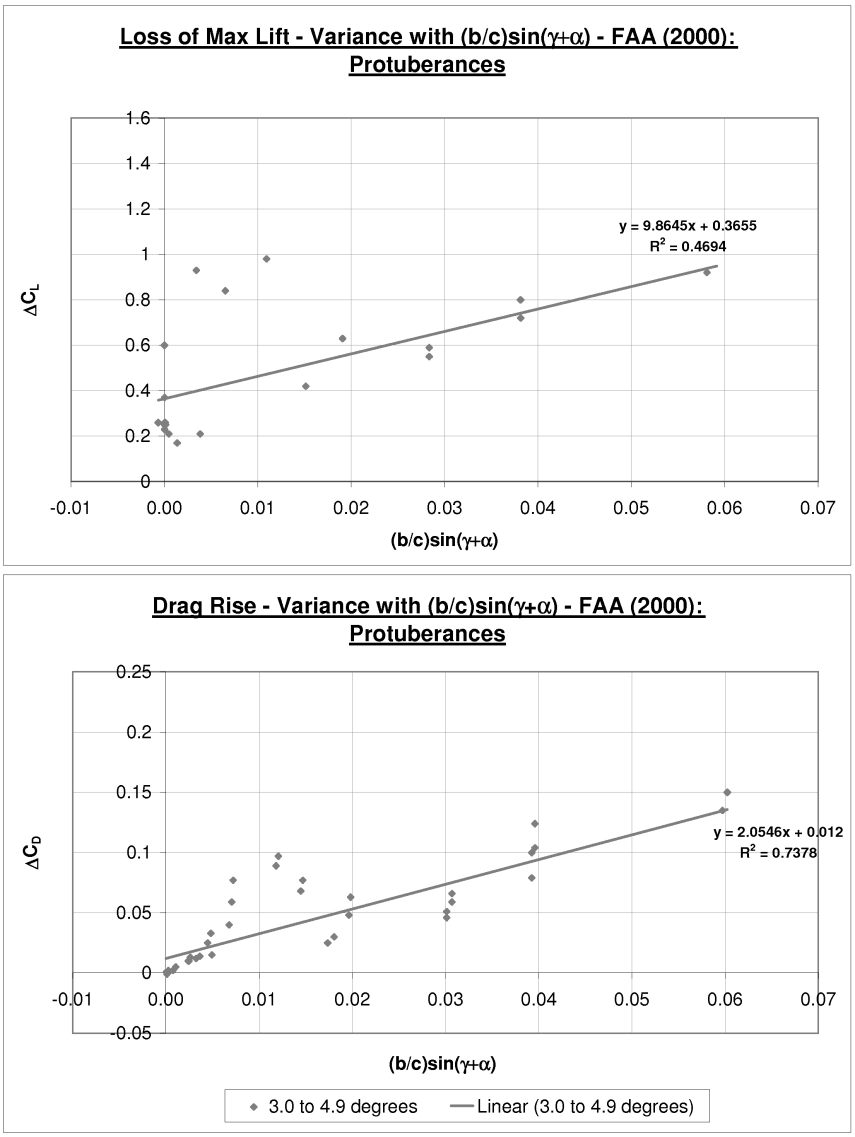

Figure C.11: Application of linear regression to selected wind tunnel data. Lift loss and drag rise for simulation of upper surface glaze horn.

Appendix D

Experimentally Iced Aerofoils - Grid Generation Example

Note: figures for this example are presented at the end of the appendix.

1. Digitised coordinates[1] were substituted into an ICEMCFD geometry file (a . tin file). The file was created by opening an ICEMCFD project and creating one coordinate (0, 0, 0) before saving and closing. This created a file with the required .tin structure that could be modified to hold any number of coordinates in place of (0, 0, 0). Coordinates for the ice profile and clean aerofoil were included in the .tin file and the file was modified with either Excel in Windows or Nedit in Linux. Saving this file and opening it in ICEMCFD produced a set of points which for P1-29 is shown in figure D.1. Once within ICEMCFD, it was possible (and often necessary) to identify coordinates as those that would either be used to create the profile geometry or discarded. In figures D.1 and D.2 a number of points were discarded. This was either because they were part of the clean leading edge and were not required, or because their removal was necessary to ensure the resultant edge was free of features that would prevent successful grid generation. This operation is similar to the smoothing of the profile geometry mentioned in the literature. It is important to highlight that whilst some modification

[1]Note the unit for the coordinates was the millimetre (mm).

has been made to the geometry during this step, it is minimal. This can be seen in comparing the profile points in figure D.2 and the curve in figure D.3.

2. The points selected to represent the profile geometry were used to create a set of curves that would become the reference geometry for the creation of the grid. Generally there would be one curve for the trailing edge of the aerofoil and one each for the clean upper and lower surfaces. The number of curves used to describe the iced profile itself was dependent upon the main features of the geometry and the surface roughness. A minimum of five curves would likely be used for the ice profile itself. However once created the curves for the ice profile or for the ice profile plus clean upper and lower surfaces could be concatenated into one curve.

3. Points and curves also needed to be made for the far-field. The domain extended some ten metres aft of the leading edge of the profile downstream and five metres in the upstream direction. The distance from the aerofoil to the far-field was also five metres in the y-direction.

4. Once the curves for the profile and the far-field were created the next step was to create the the two-dimensional surface. This was done by making one surface from the four far-field curves, and using the profile curves to remove the profile shape from this surface. The remaining profile surface was then deleted.

5. With creation of 2D geometry complete the next step was to start creation of blocking topology (see figures D.4 and D.5. The initial block was created before the splitting procedure that creates the aerofoil block and edges was performed. Key vertices whose position was to be fixed on profile points (i.e. at the trailing edge) or far-field points were associated with those points. Other vertices were then associated with the appropriate curves (the curves where they were to be located) before edges themselves were associated with curves. Finally the faces

(made up of four edge-splits) created at this stage were associated with the two-dimensional surface that had been created.

6. Figure D.6 showS how a large number of splits can be used to ensure the profile-edge is discretised appropriately to ensure adequate representation of the profile geometry. Figure D.7 shows how those splits propagate into the far field.

7. Once the profile-edge was split into an adequate number of smaller edges and the newly created vertices were located onto the curve with which they were associated; a split were introduced that created the wrap-around blocks for modelling the boundary layer. Another two splits were created further away from the surface. This created a blocking structure where there were sufficient blocks and vertices to allow shaping of the block topology both at the surface and moving away from the surface. The resultant blocking is presented in figures D.8 and D.9.

8. The remaining steps in 2D allowed creation of a high quality mesh by setting the nodal distributions on edges and assessing and improving the quality of the cells using the angle and volume parameters. Blocks were modified mainly by moving vertices.

9. With the grid completed (see blocking in figure D.10 in two dimensions) all that remained was to convert it to 3D. Figure D.11 shows the profile surface created by copying curves and points by $480mm$ in the z-direction, creating appropriate spanwise curves and making surfaces thereafter. This was also done using far-field curves and points to make the far-field surface. The two-dimensional surface created already (that represented the fluid domain to be modelled) was also copied to the new spanwise location. Thus the three-dimensional geometry was complete.

10. The grid was translated into 3D by $480mm$ to create a 3D blocking topology as shown in figure D.12. The faces representing the profile

surface, the far-field and the symmetrical spanwise surfaces of the domain were associated with the appropriate surfaces.

11. The mesh was created under meshing options as a structured Multiblock grid before being exported to .grd format using the Multiblock-info option. The final grid is shown is figure D.13.

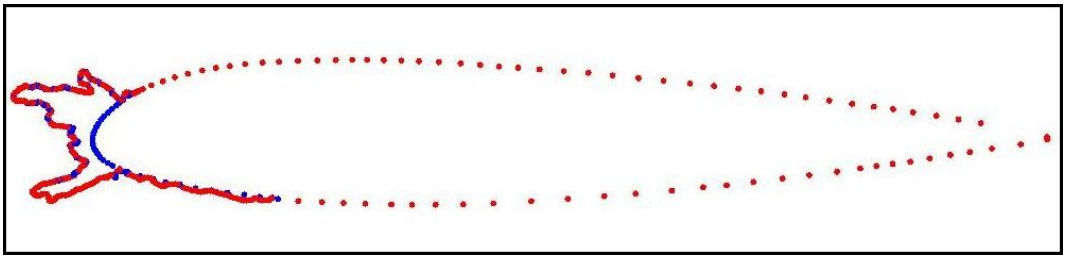

Figure D.1: Digitised coordinates imported into ICEMCFD for geometry creation.

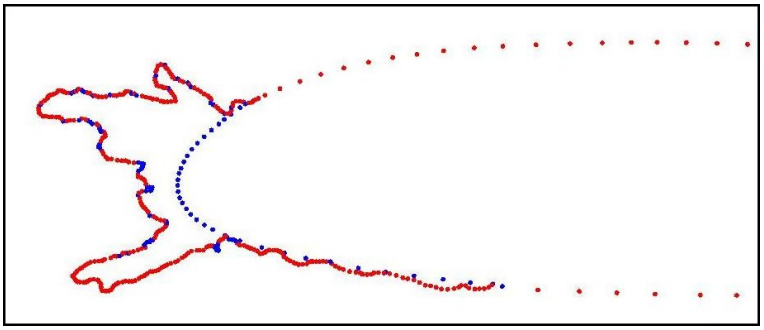

Figure D.2: Profile coordinates in ICEMCFD. Red coordinates were selected to be used to make the geometry, blue coordinates were discarded.

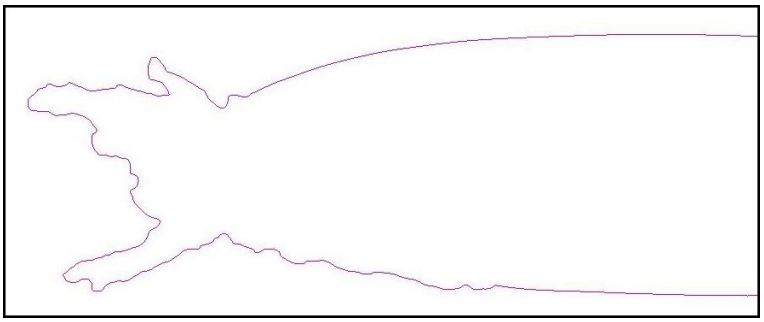

Figure D.3: Curve(s) representing the profile of the iced aerofoil, created using the red coordinates in figure D.2.

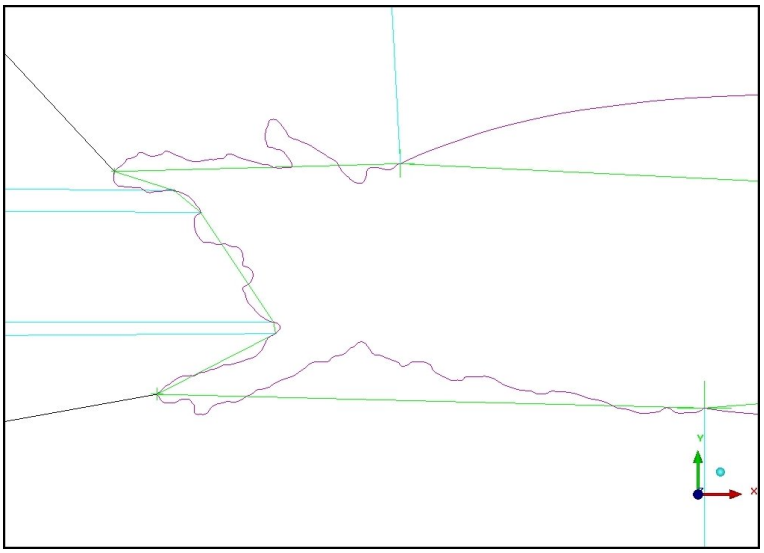

Figure D.4: Early splits to profile edges intended to fit the block topology to the profile geometry.

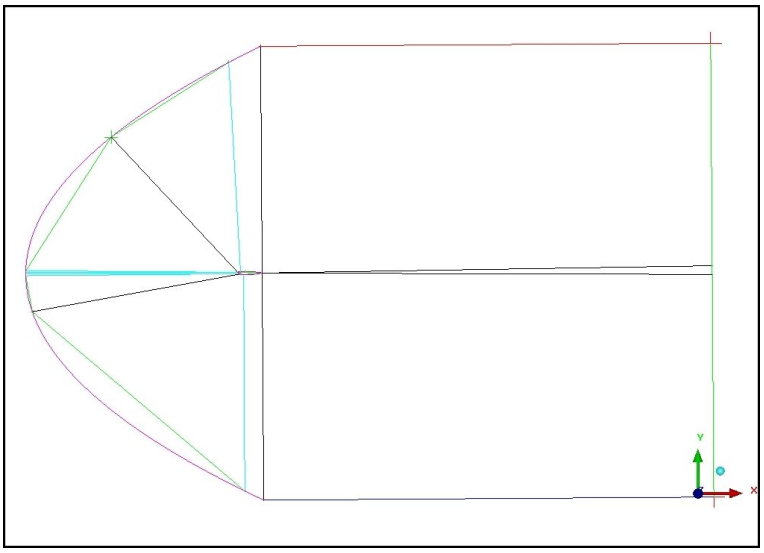

Figure D.5: Effect of splits made at the profile edge on the rest of the domain.

Figure D.6: Image showing the splitting of the profile edge at a later stage.

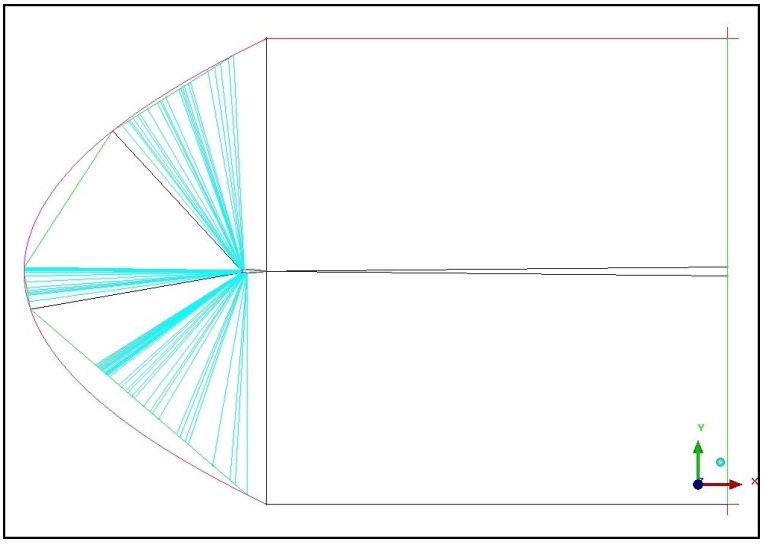

Figure D.7: Image showing the splits from figure D.6 propgating into the whole domain.

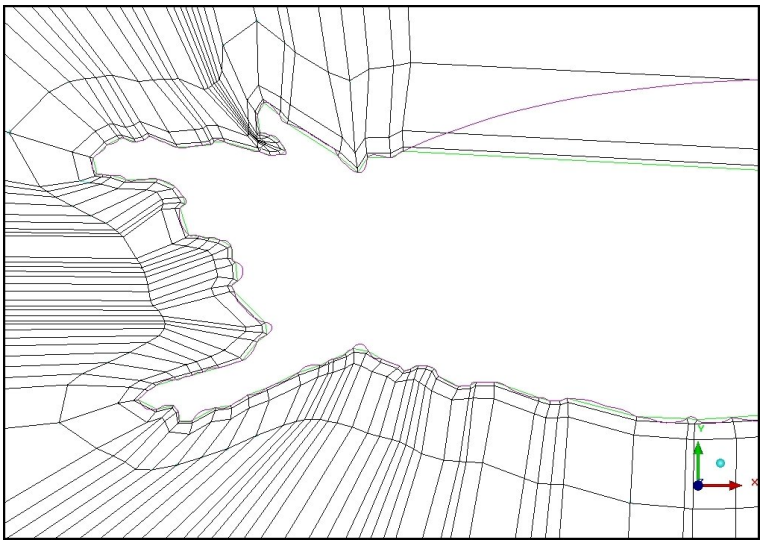

Figure D.8: Image showing completed splitting of the profile-edge and splits moving into the fluid, creating the boundary layer blocking and further layers in the near-field.

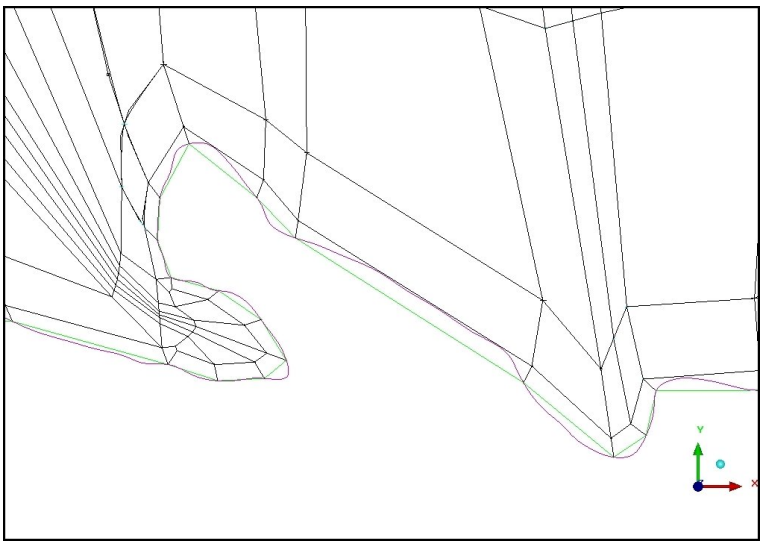

Figure D.9: Close shot of figure D.8 showing the intricate blocking structure required at the fluid surface.

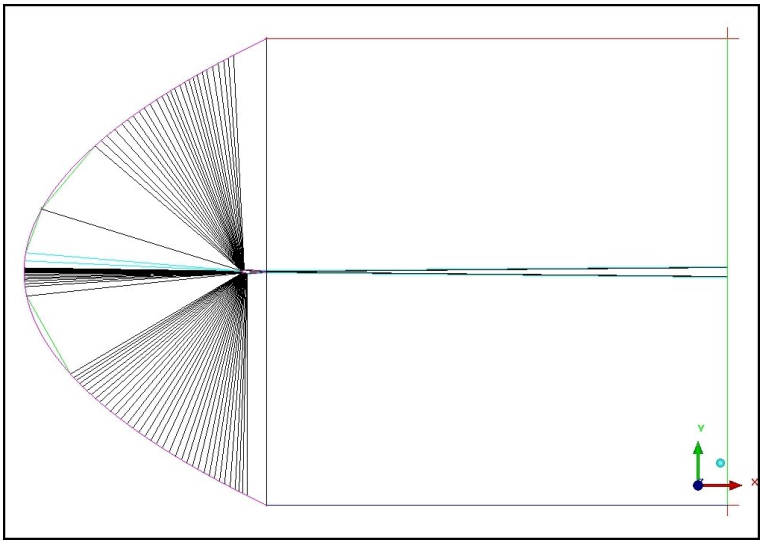

Figure D.10: Image of the completed 2D blocking, with edges placed appropriately around the far-field for smoothness in cell distribution.

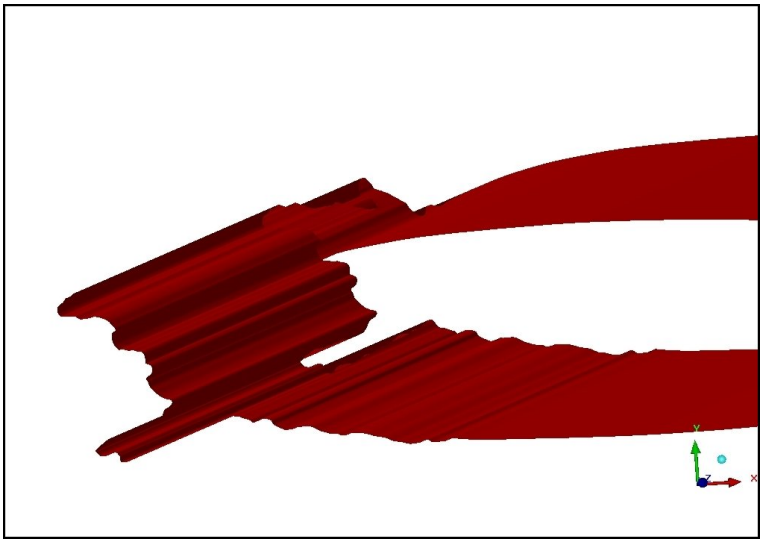

Figure D.11: The iced profile in 3D.

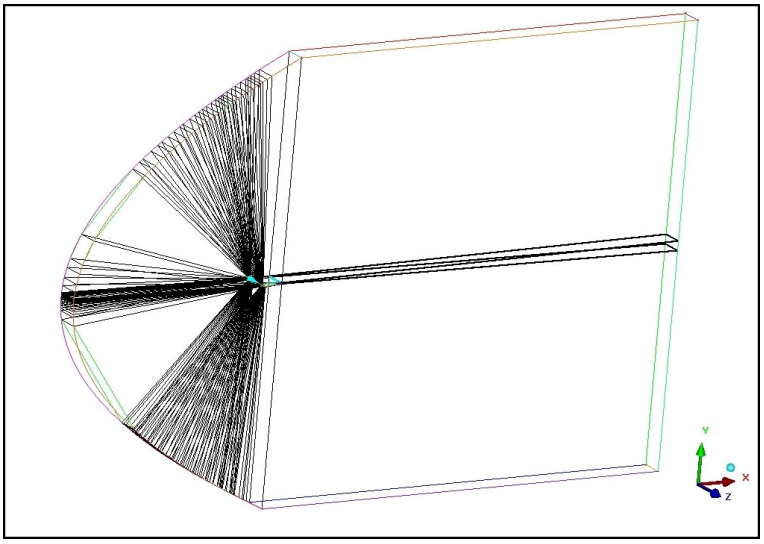

Figure D.12: The completed blocking topology extruded into three dimensions.

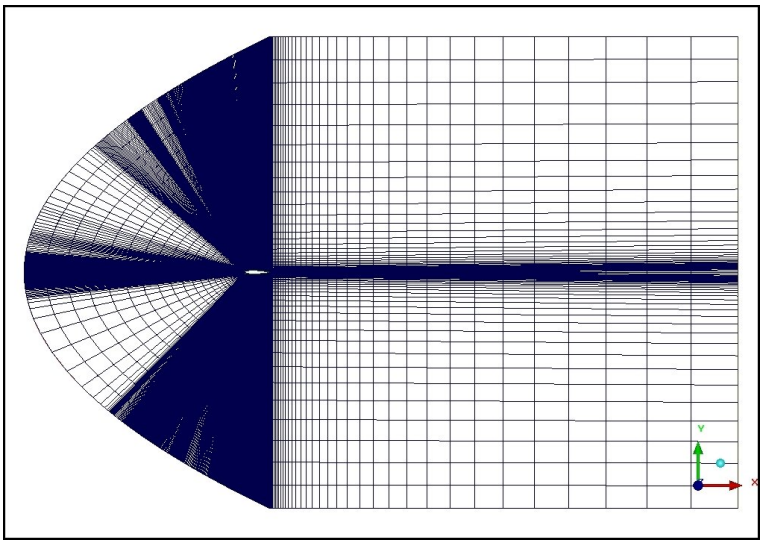

Figure D.13: The completed grid.

Appendix E

Full Condensed Ice Accretion and CFD Prediction Results

This section contains two pages of condensed yet comprehensive results for each icing scenario undertaken as part of the technical investigation. Information about the icing simulation is presented the first of the two pages (the left-hand page); being input conditions, resultant profile, photograph, measured geometric parameters and notes taken during the simulation. Information about the aerodynamic assessment is presented on the second of the two pages (the right-hand page); namely an image of the grid generated, lift and drag predictions varying with angle of attack (in comparison with the reference profile) and any comments specific to the CFD predictions for that ice profile.

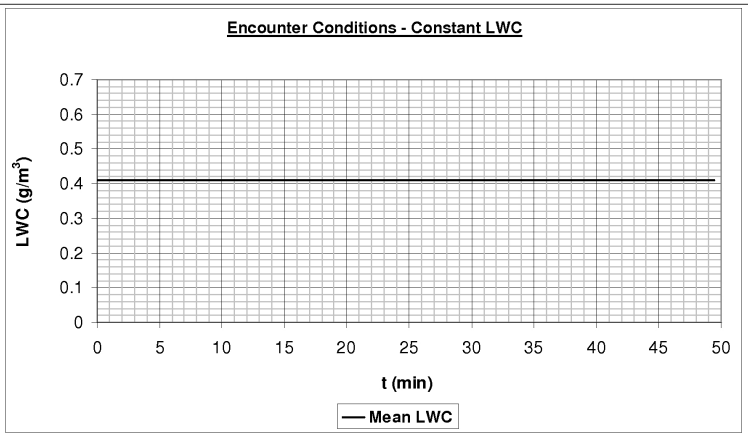

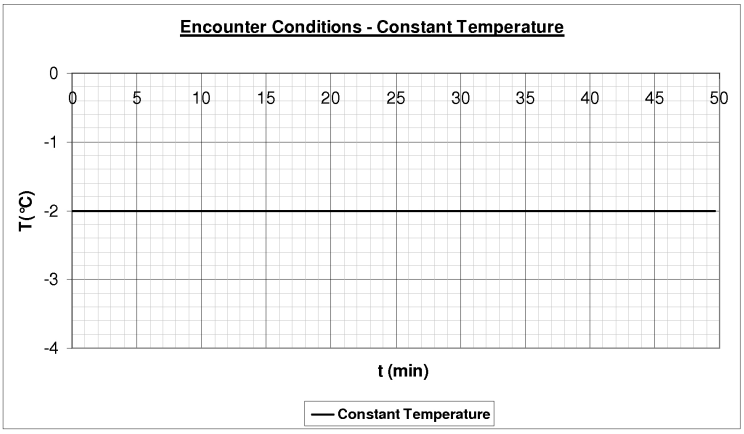

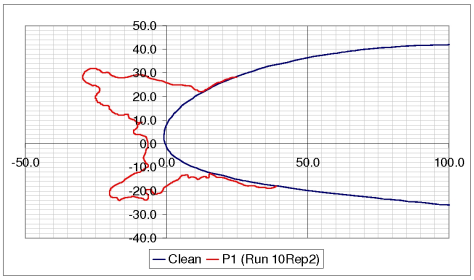

Run No.	Desc^{n} Code	h_{upper}	Θ_{upper}	Φ_{upper}	L_{upper}	h_{lower}	Θ_{lower}	Φ_{lower}	L_{lower}	t_{c-l}
P1-10Rep2	Co_LWC&T	36.50	48.75	32.50	23.00	28.50	-48.50	-41.00	38.00	7.00
---	*ReflS*	*36.00*	*46.58*	*30.58*	*24.17*	*28.17*	*-53.00*	*-43.17*	*53.67*	*7.33*
---	*StDev*	*1.32*	*2.40*	*4.45*	*2.93*	*0.58*	*5.07*	*2.02*	*14.15*	*2.02*

Figure E.1: Encounter P1-10Rep2 - Ice accretion simulation information.

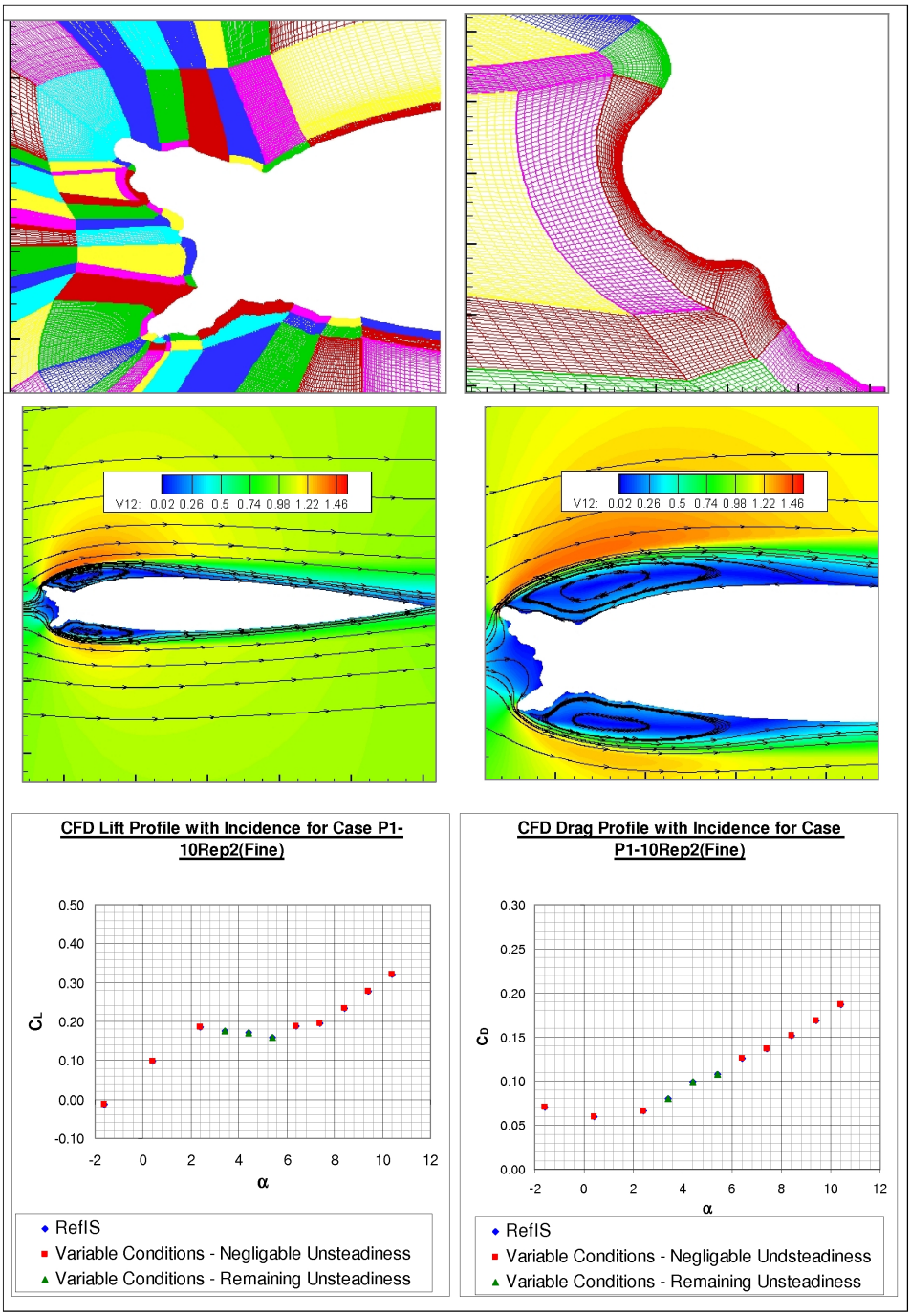

Figure E.2: Encounter P1-10Rep2 - CFD simulation information.

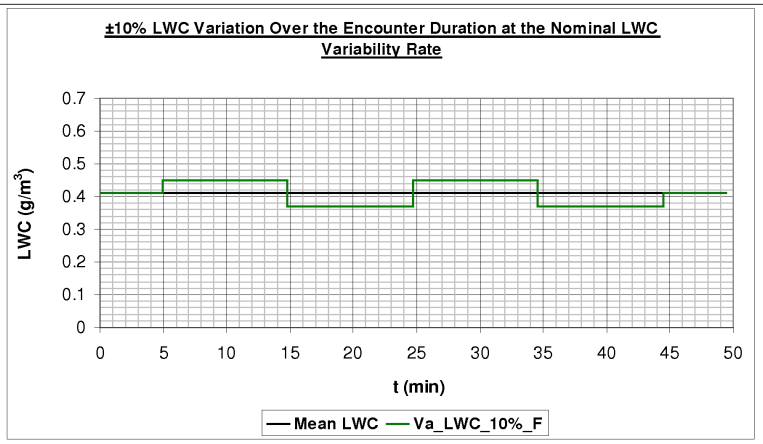

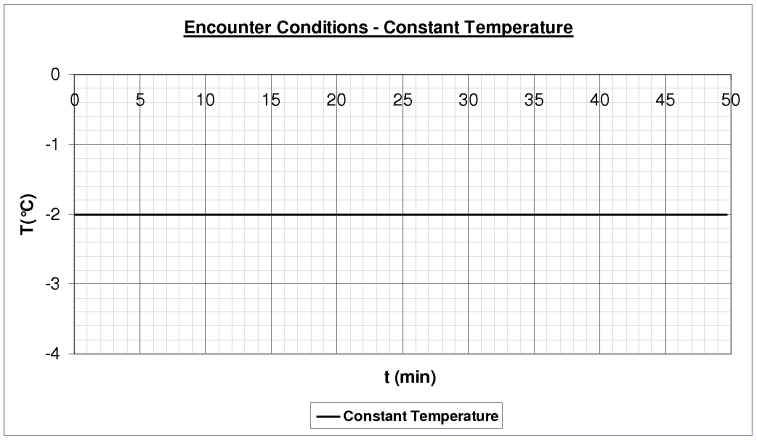

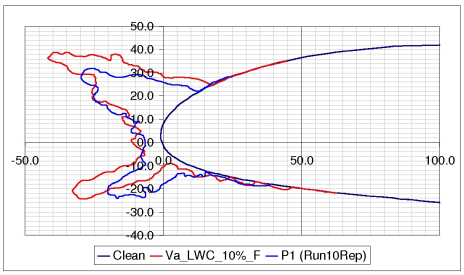

Run No.	Desc^{n} Code	h_{upper}	Θ_{upper}	Φ_{upper}	L_{upper}	h_{lower}	Θ_{lower}	Φ_{lower}	L_{lower}	t_{c-l}
P1-11Rep	Va_LWC_10%_F	50.00	43.25	32.00	17.00	38.00	-33.00	-27.25	46.00	12.00
---	*RefIS*	*36.00*	*46.58*	*30.58*	*24.17*	*28.17*	*-53.00*	*-43.17*	*53.67*	*7.33*
---	*StDev*	*1.32*	*2.40*	4.45	*2.93*	*0.58*	*5.07*	2.02	*14.15*	*2.02*

Figure E.3: Encounter Va_LWC_10%_F - Ice accretion simulation information.

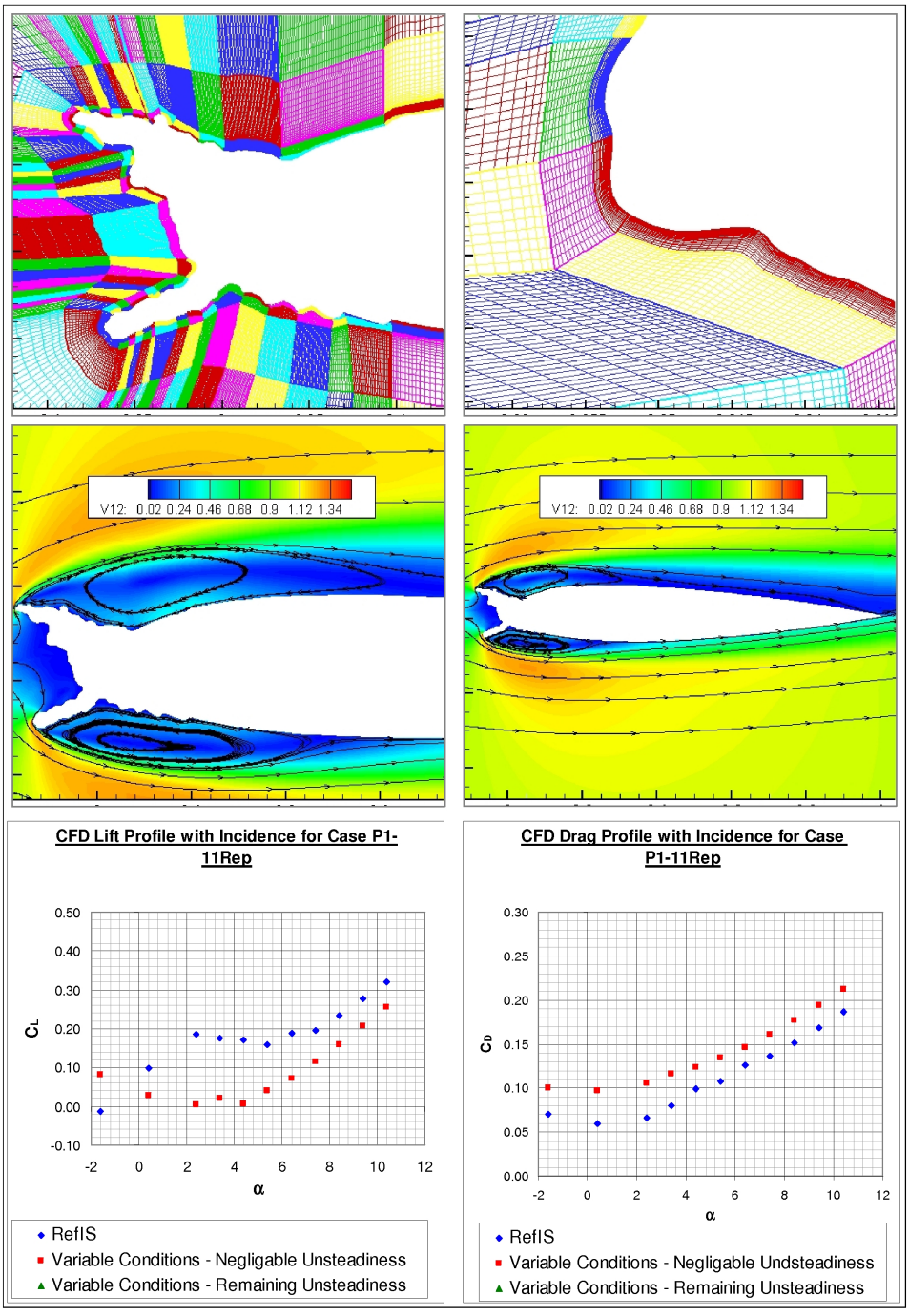

Figure E.4: Encounter Va_LWC_10%_F - CFD simulation information.

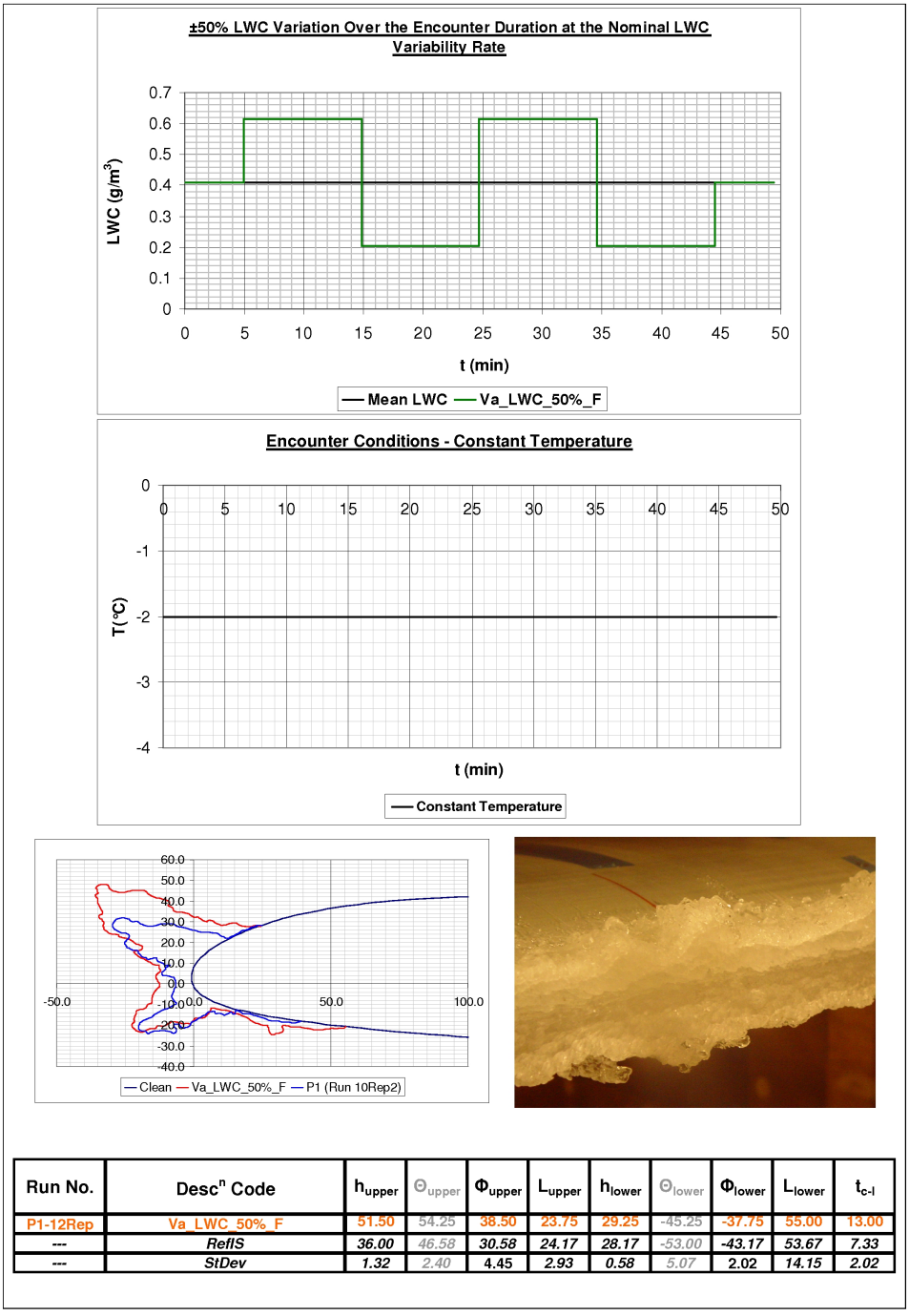

Run No.	Desc^{n} Code	h_{upper}	Θ_{upper}	Φ_{upper}	L_{upper}	h_{lower}	Θ_{lower}	Φ_{lower}	L_{lower}	t_{c-l}
P1-12Rep	Va_LWC_50%_F	51.50	54.25	38.50	23.75	29.25	-45.25	-37.75	55.00	13.00
---	*RefIS*	*36.00*	*46.58*	*30.58*	*24.17*	*28.17*	*-53.00*	*-43.17*	*53.67*	*7.33*
---	*StDev*	*1.32*	*2.40*	4.45	*2.93*	*0.58*	*5.07*	2.02	*14.15*	*2.02*

Figure E.5: Encounter Va_LWC_50%_F - Ice accretion simulation information.

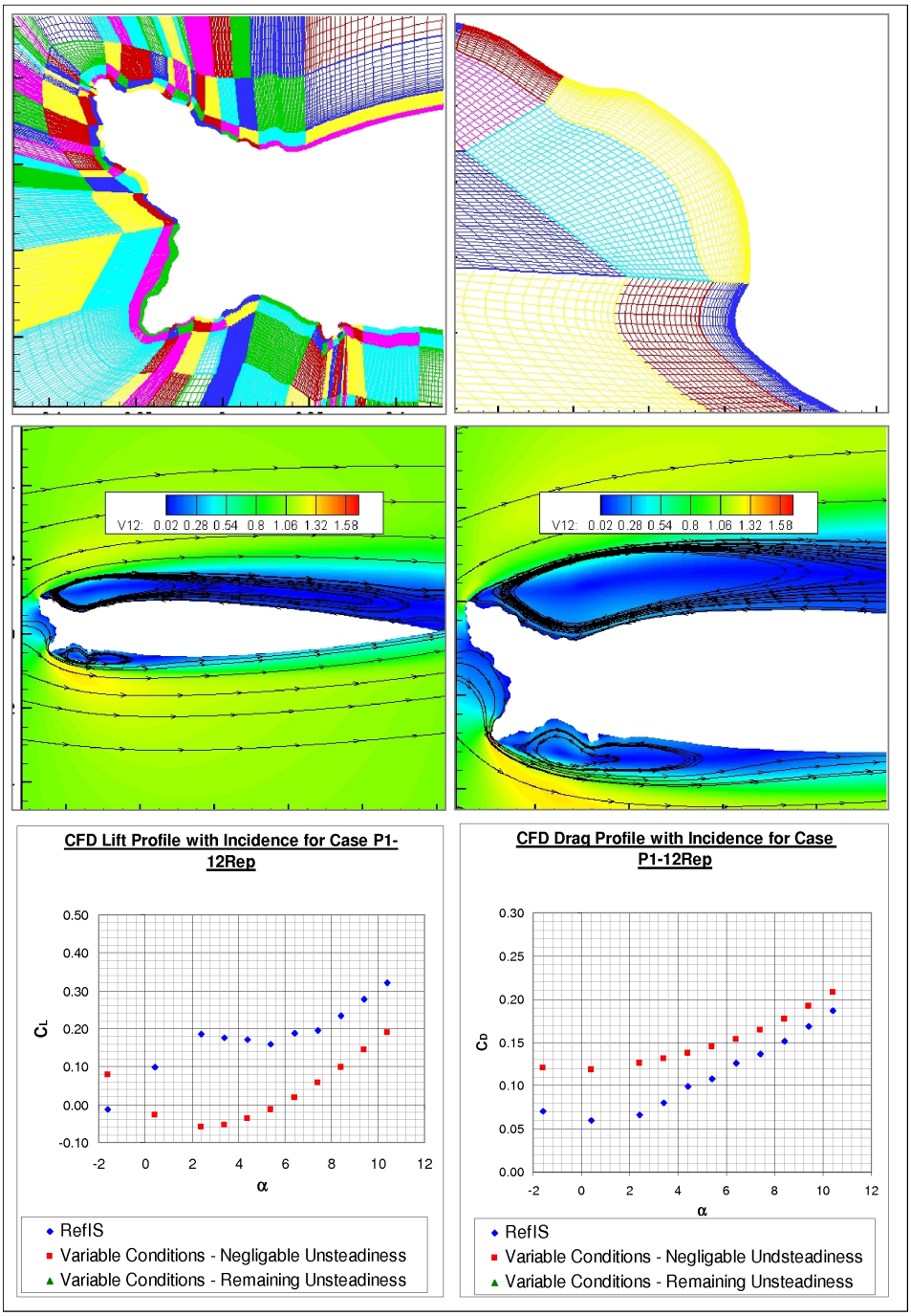

Figure E.6: Encounter Va_LWC_50%_F - CFD simulation information.

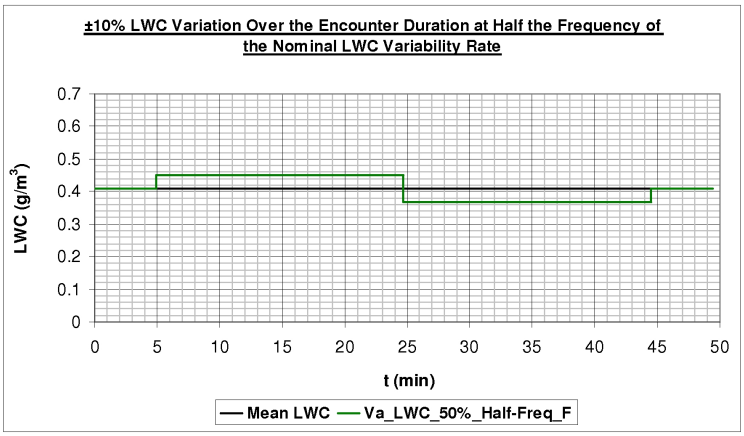

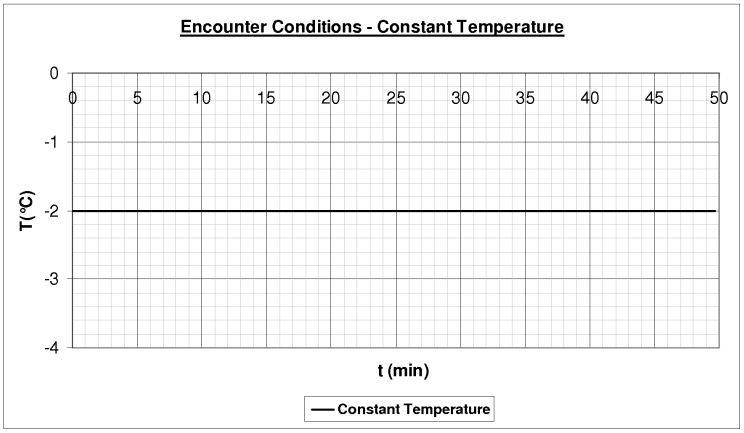

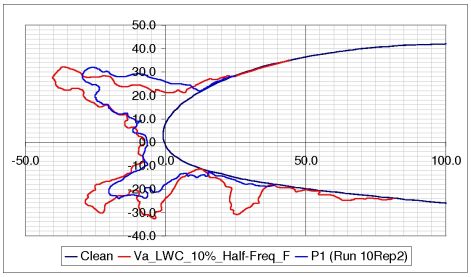

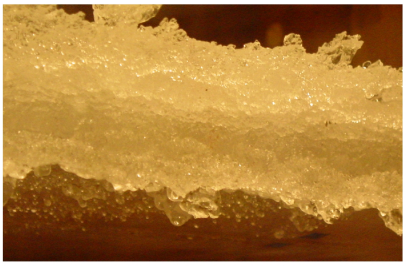

Run No.	Desc^{n} Code	h_{upper}	Θ_{upper}	Φ_{upper}	L_{upper}	h_{lower}	Θ_{lower}	Φ_{lower}	L_{lower}	t_{c-l}
P1-27	Va_LWC_10%_Half-Freq_F	45.00	33.50	24.00	22.75	38.00	-42.00	-39.50	80.00	8.00
---	*RefIS*	*36.00*	*46.58*	*30.58*	*24.17*	*28.17*	*-53.00*	*-43.17*	*53.67*	*7.33*
---	*StDev*	*1.32*	*2.40*	4.45	*2.93*	*0.58*	*5.07*	2.02	*14.15*	*2.02*

Figure E.7: Encounter Va_LWC_10%_Half-Freq_F - Ice accretion simulation information.

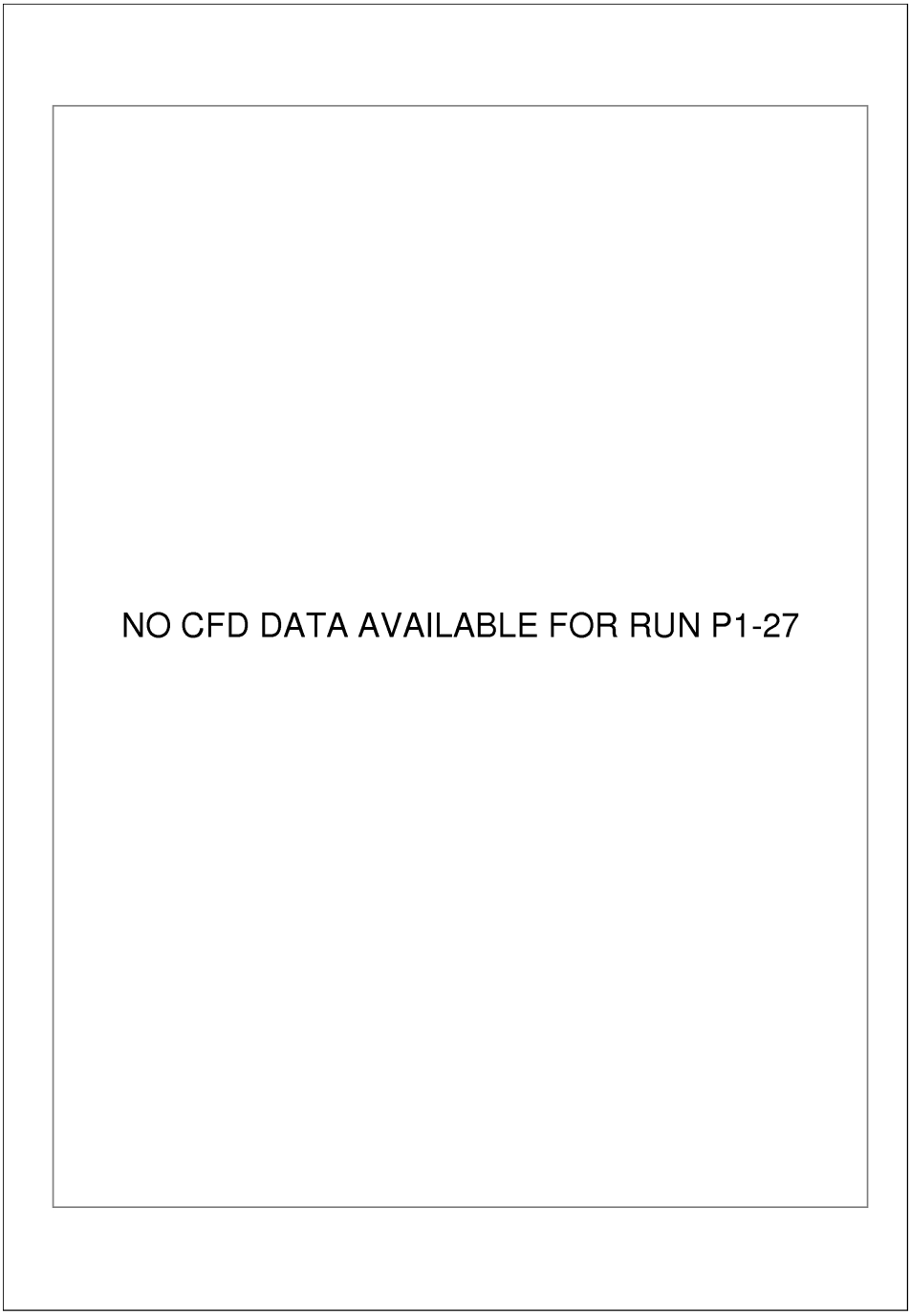

Figure E.8: Encounter Va_LWC_10%_Half-Freq_F - CFD simulation information.

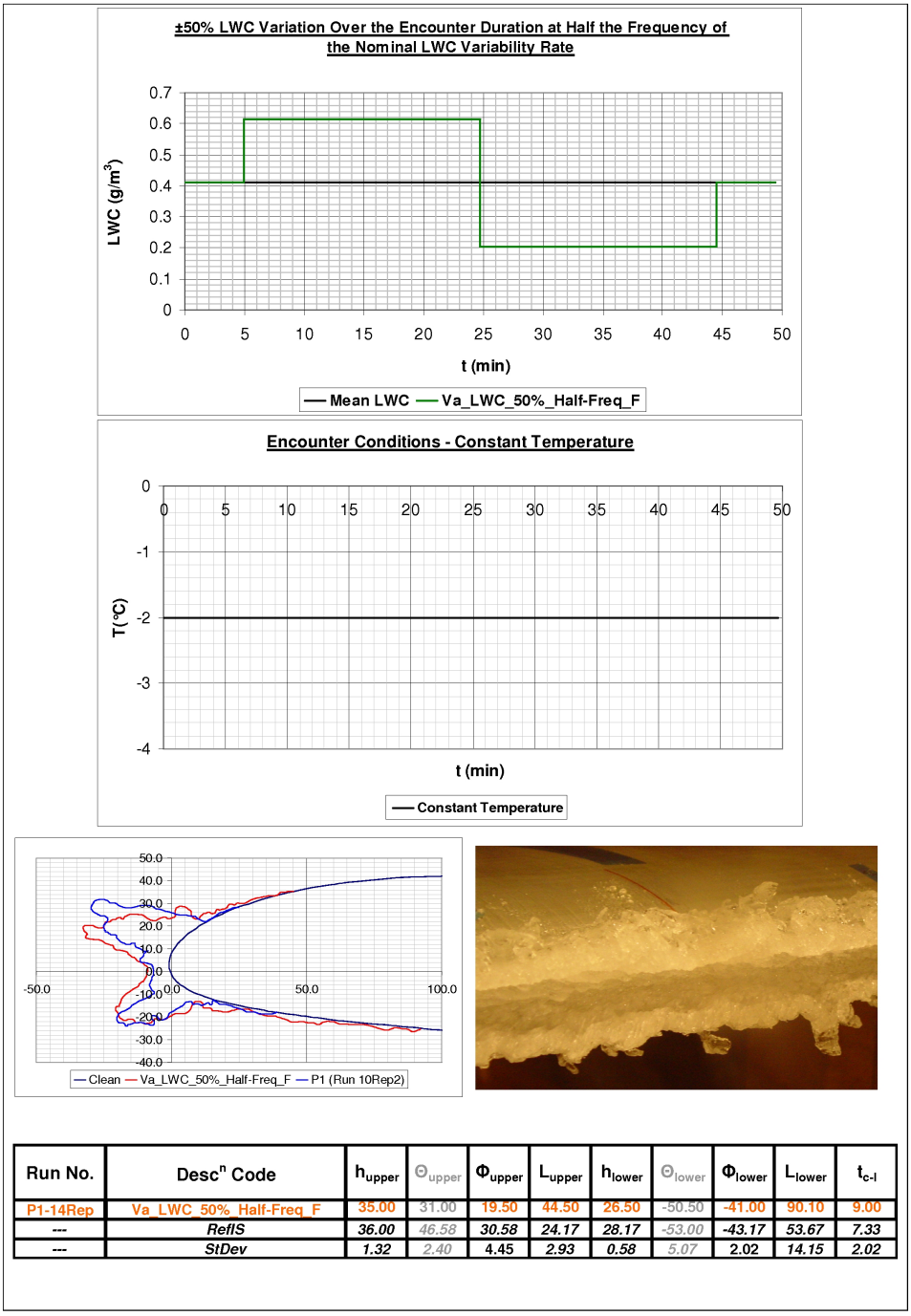

Run No.	Descⁿ Code	h_{upper}	Θ_{upper}	Φ_{upper}	L_{upper}	h_{lower}	Θ_{lower}	Φ_{lower}	L_{lower}	t_{c-l}
P1-14Rep	Va_LWC_50%_Half-Freq_F	35.00	31.00	19.50	44.50	26.50	-50.50	-41.00	90.10	9.00
---	*RefIS*	*36.00*	*46.58*	*30.58*	*24.17*	*28.17*	*-53.00*	*-43.17*	*53.67*	*7.33*
---	*StDev*	*1.32*	*2.40*	4.45	*2.93*	*0.58*	*5.07*	2.02	*14.15*	*2.02*

Figure E.9: Encounter Va_LWC_50%_Half-Freq_F - Ice accretion simulation information.

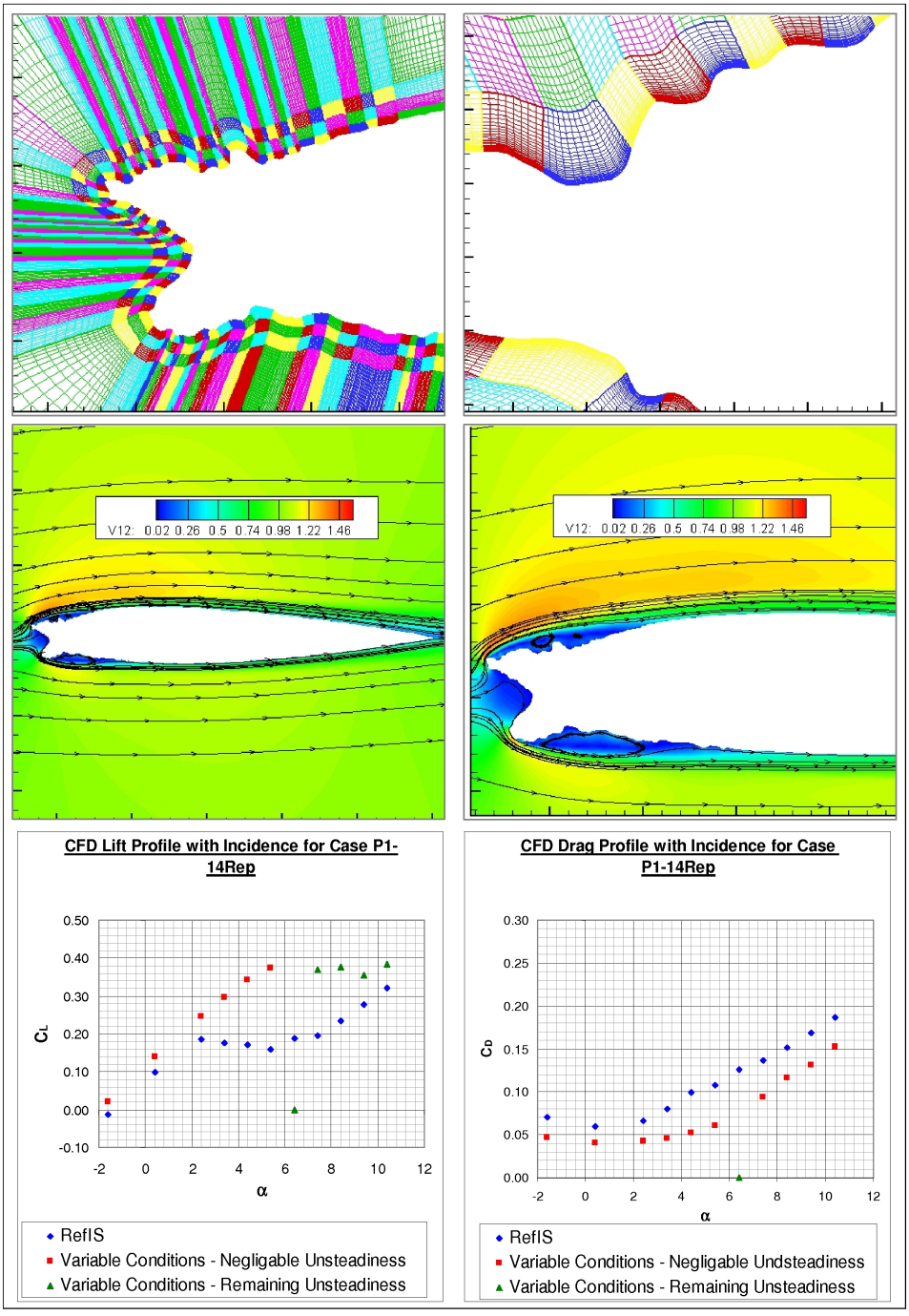

Figure E.10: Encounter Va_LWC_50%_Half-Freq_F - CFD simulation information.

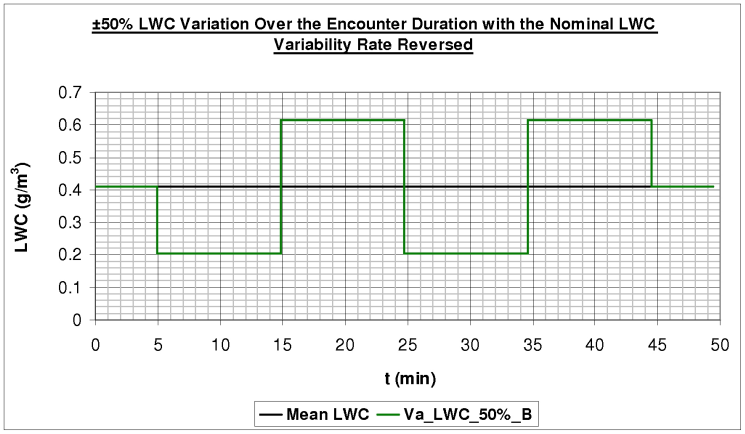

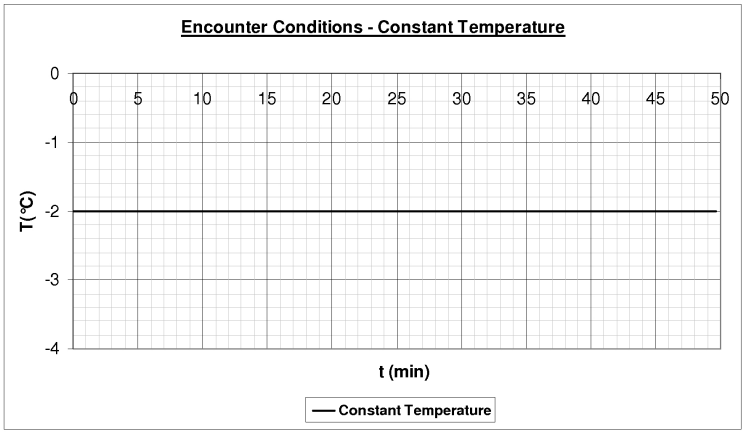

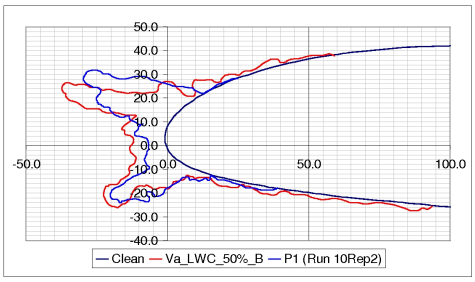

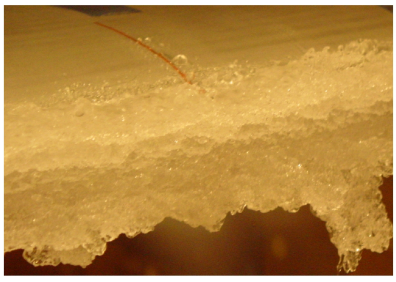

Run No.	Desc^{n} Code	h_{upper}	Θ_{upper}	Φ_{upper}	L_{upper}	h_{lower}	Θ_{lower}	Φ_{lower}	L_{lower}	t_{c-l}
P1-13Rep	Va_LWC_50%_B	41.00	34.50	26.25	58.50	30.50	-50.50	-42.00	93.25	13.25
---	*RefIS*	*36.00*	*46.58*	*30.58*	*24.17*	*28.17*	*-48.83*	*-43.17*	*53.67*	*7.33*
---	*StDev*	*1.32*	*2.40*	4.45	*2.93*	*0.58*	*3.01*	2.02	*14.15*	*2.02*

Figure E.11: Encounter Va_LWC_50%_B - Ice accretion simulation information.

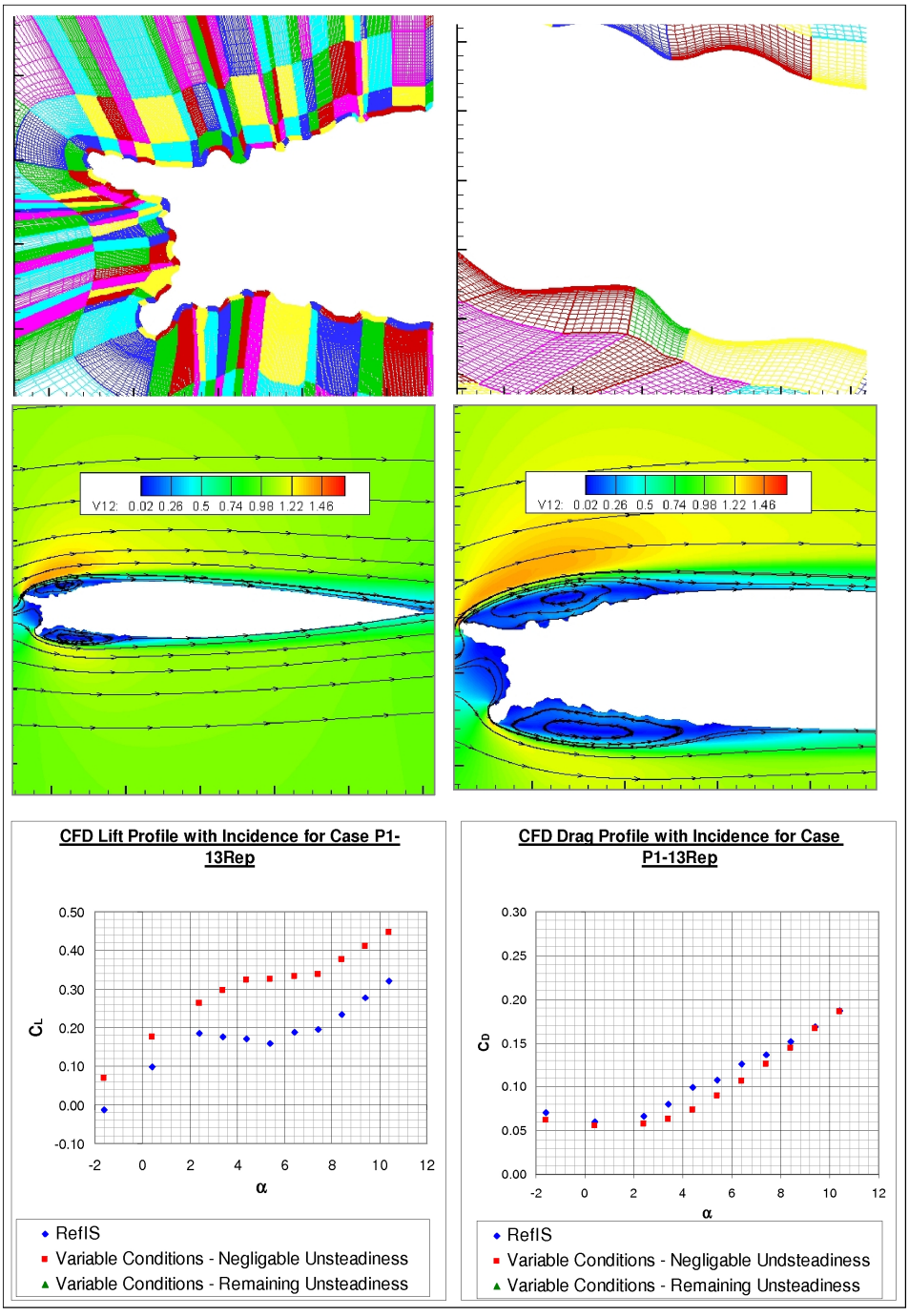

Figure E.12: Encounter Va_LWC_50%_B - CFD simulation information.

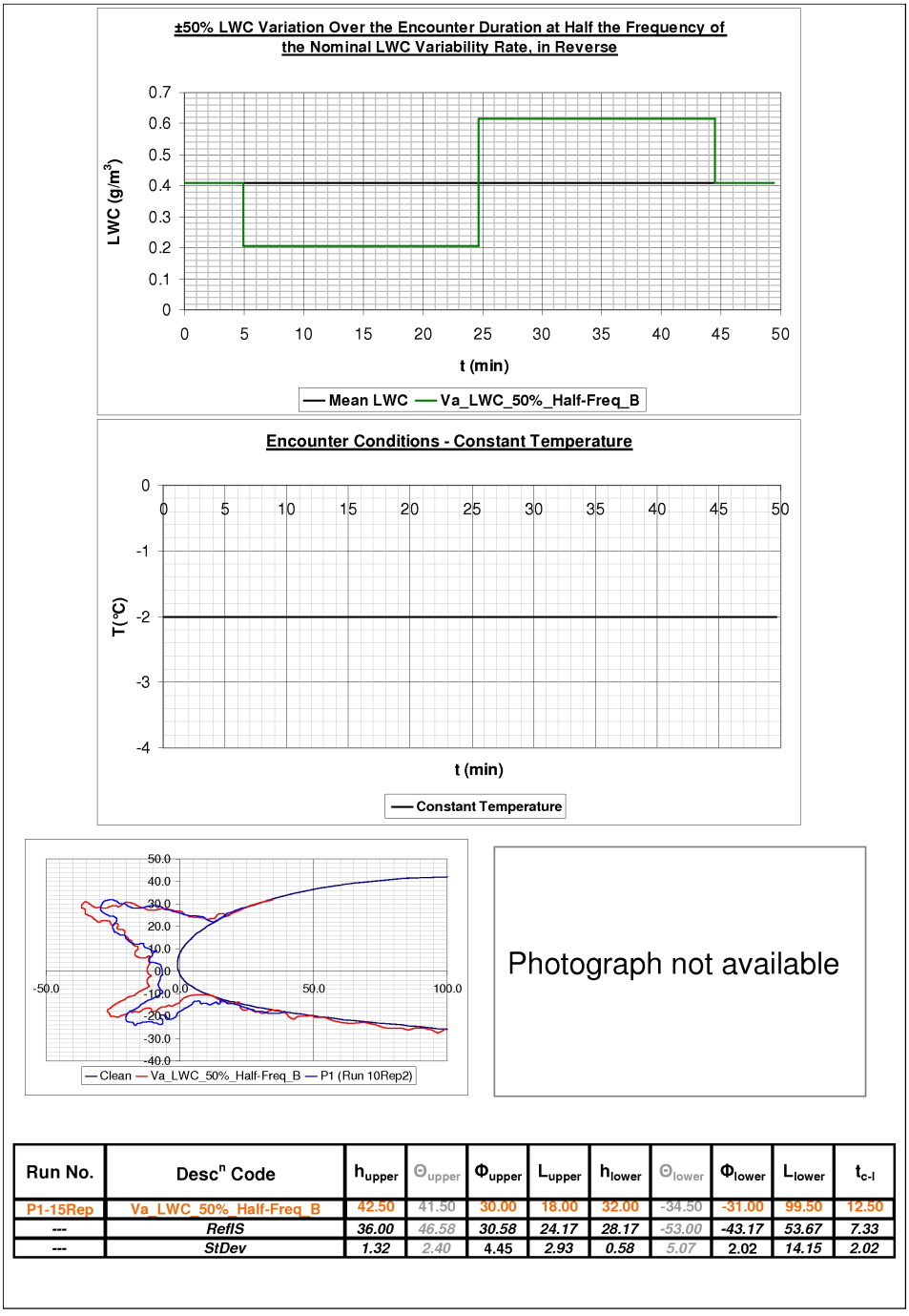

Run No.	Desc^{n} Code	h_{upper}	Θ_{upper}	Φ_{upper}	L_{upper}	h_{lower}	Θ_{lower}	Φ_{lower}	L_{lower}	t_{c-l}
P1-15Rep	Va_LWC_50%_Half-Freq_B	42.50	41.50	30.00	18.00	32.00	-34.50	-31.00	99.50	12.50
---	*RefIS*	*36.00*	*46.58*	*30.58*	*24.17*	*28.17*	*-53.00*	*-43.17*	*53.67*	*7.33*
---	*StDev*	*1.32*	*2.40*	4.45	*2.93*	*0.58*	*5.07*	2.02	*14.15*	*2.02*

Figure E.13: Encounter Va_LWC_50%_Half-Freq_B - Ice accretion simulation information.

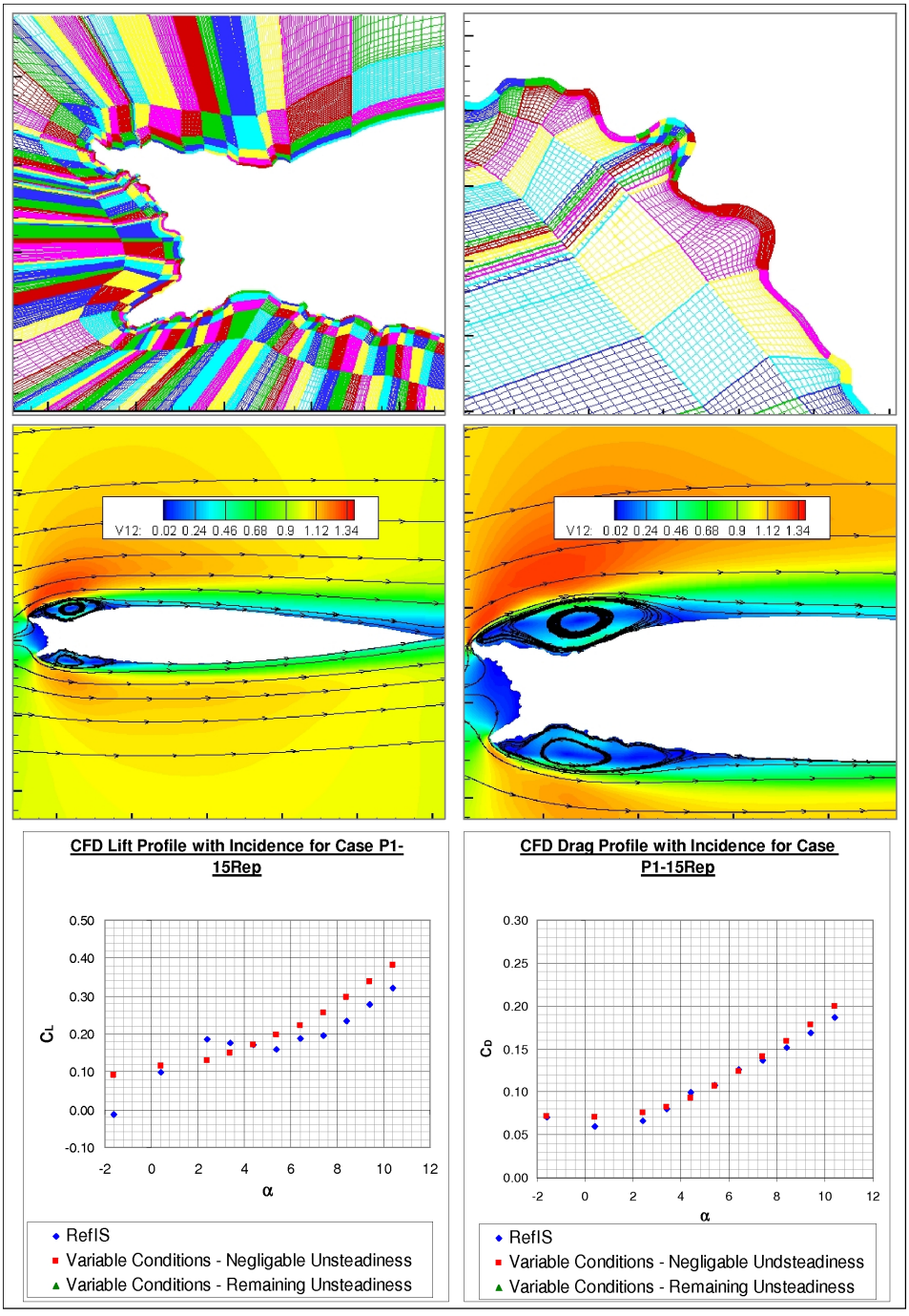

Figure E.14: Encounter Va_LWC_50%_Half-Freq_B - CFD simulation information.

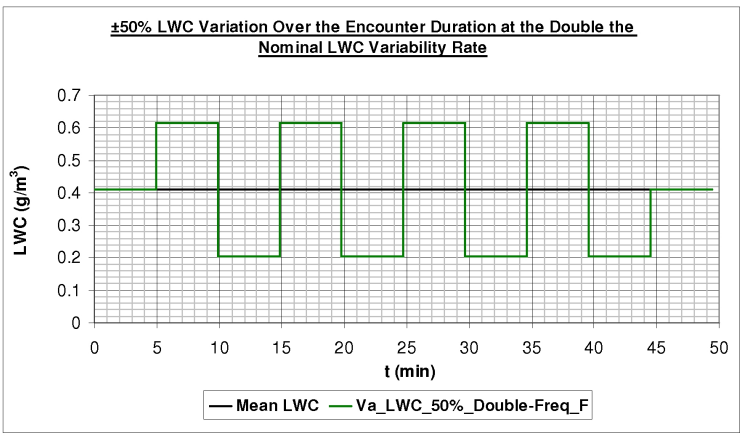

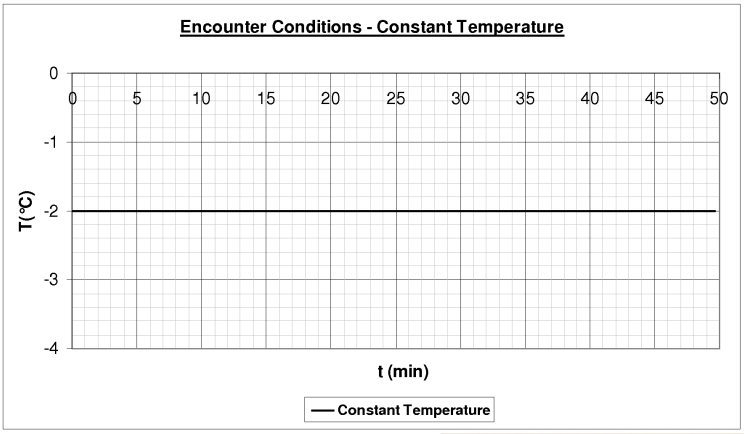

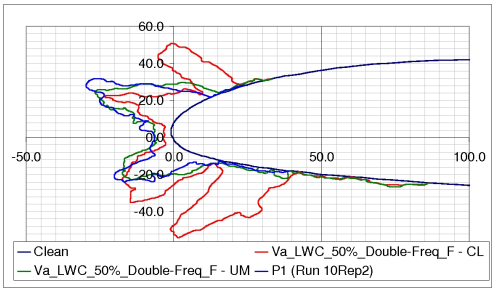

Run No.	Desc^{n} Code	h_{upper}	Θ_{upper}	Φ_{upper}	L_{upper}	h_{lower}	Θ_{lower}	Φ_{lower}	L_{lower}	t_{c-l}
P1-25(CL)	Va_LWC_50%_Double-Freq_F	33.00	88.25	56.25	85.00	44.50	-91.25	-71.75	32.50	3.00
P1-25(UM)	Va_LWC_50%_Double-Freq_F	31.50	44.00	29.50	85.00	29.00	-50.25	-44.00	32.50	6.50
---	*RefIS*	*36.00*	*46.58*	*30.58*	*24.17*	*28.17*	*-53.00*	*-43.17*	*53.67*	*7.33*
---	*StDev*	*1.32*	*2.40*	4.45	*2.93*	*0.58*	*5.07*	2.02	*14.15*	*2.02*

Figure E.15: Encounter Va_LWC_50%_Double-Freq_F - Ice accretion simulation information.

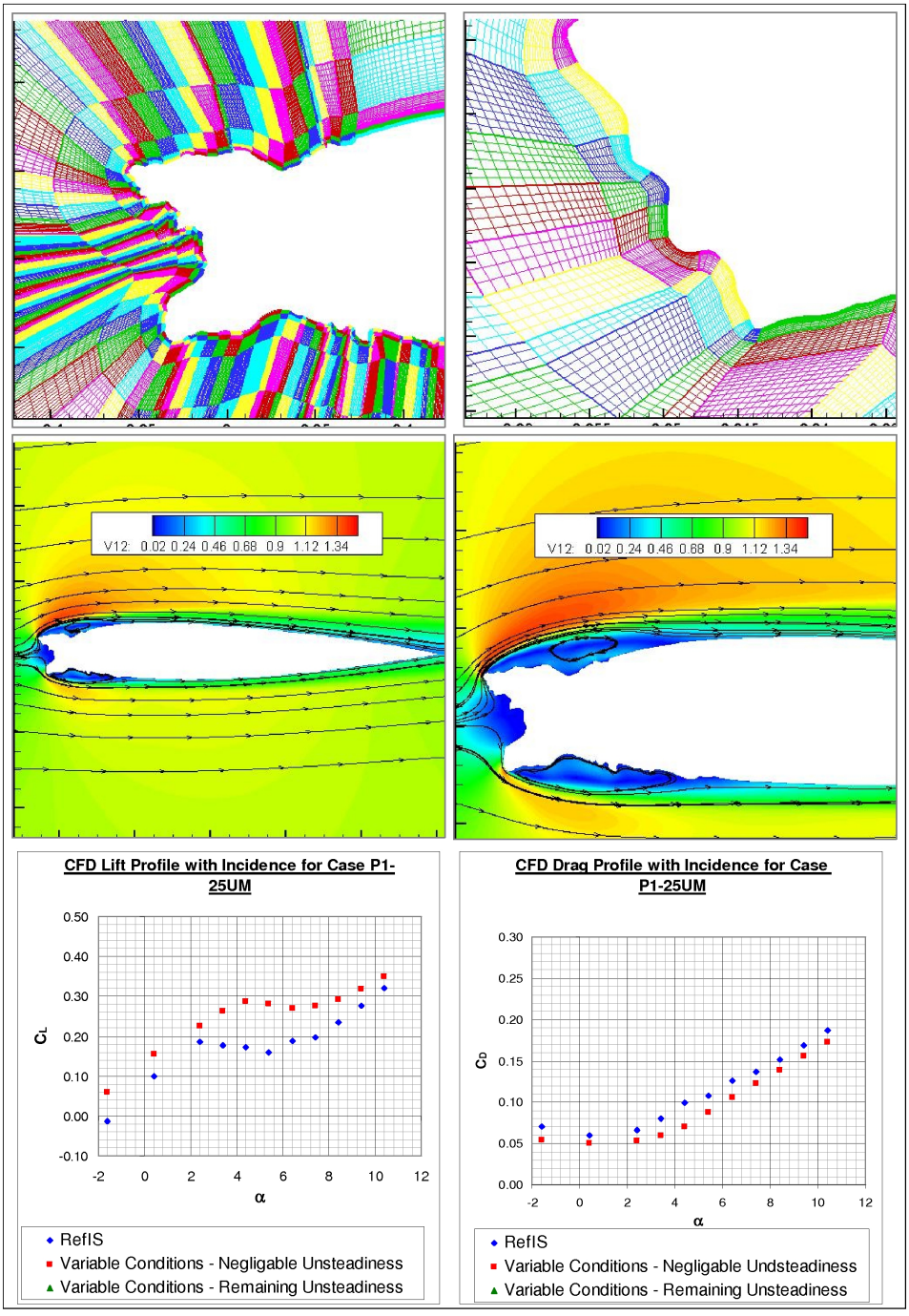

Figure E.16: Encounter Va_LWC_50%_Double-Freq_F - CFD simulation information.

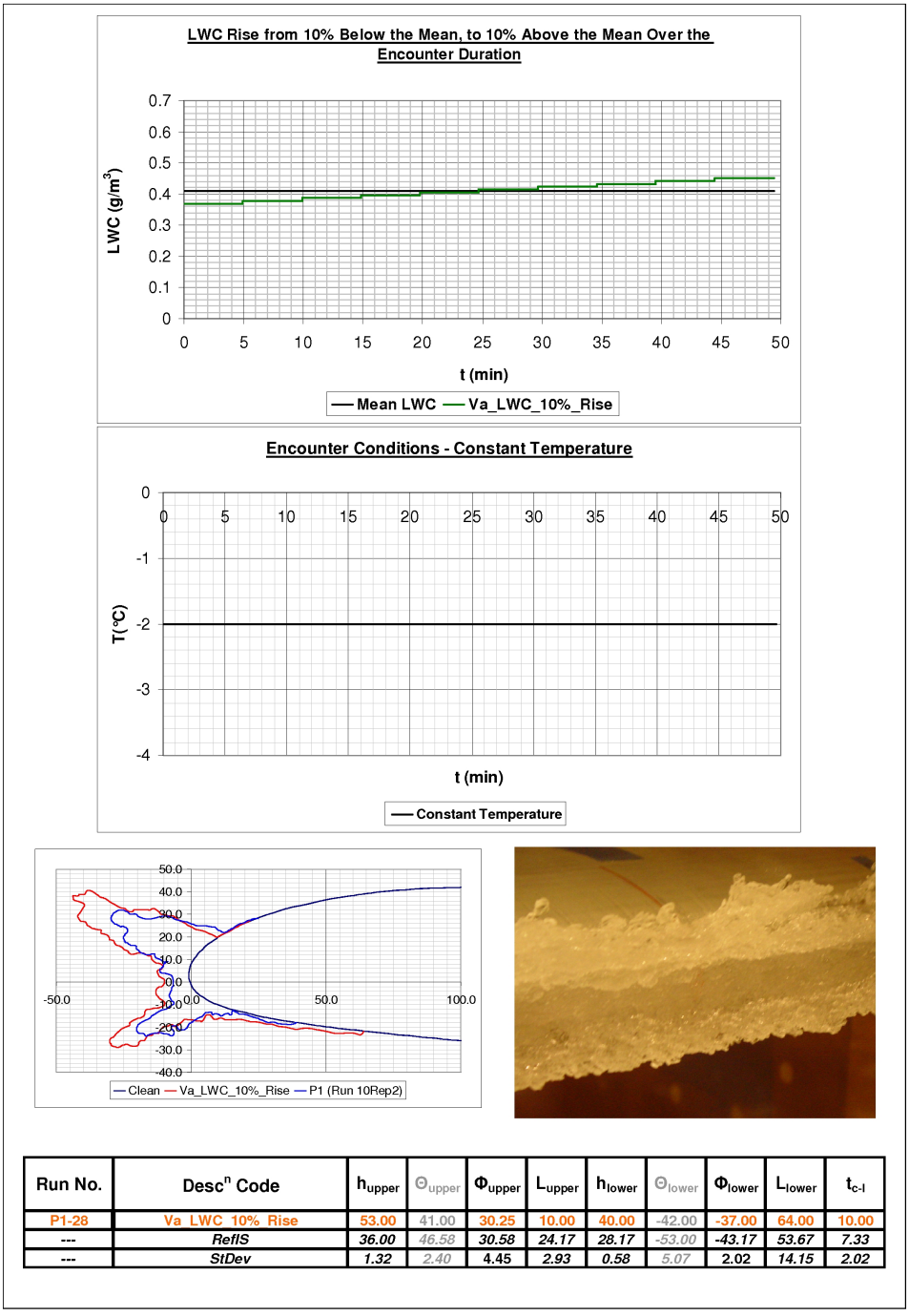

Run No.	Desc^{n} Code	h_{upper}	Θ_{upper}	Φ_{upper}	L_{upper}	h_{lower}	Θ_{lower}	Φ_{lower}	L_{lower}	$t_{c\text{-}l}$
P1-28	Va_LWC_10%_Rise	53.00	41.00	30.25	10.00	40.00	-42.00	-37.00	64.00	10.00
---	*RefIS*	*36.00*	*46.58*	*30.58*	*24.17*	*28.17*	*-53.00*	*-43.17*	*53.67*	*7.33*
---	*StDev*	*1.32*	*2.40*	4.45	*2.93*	*0.58*	*5.07*	2.02	*14.15*	*2.02*

Figure E.17: Encounter Va_LWC_10%_Rise - Ice accretion simulation information.

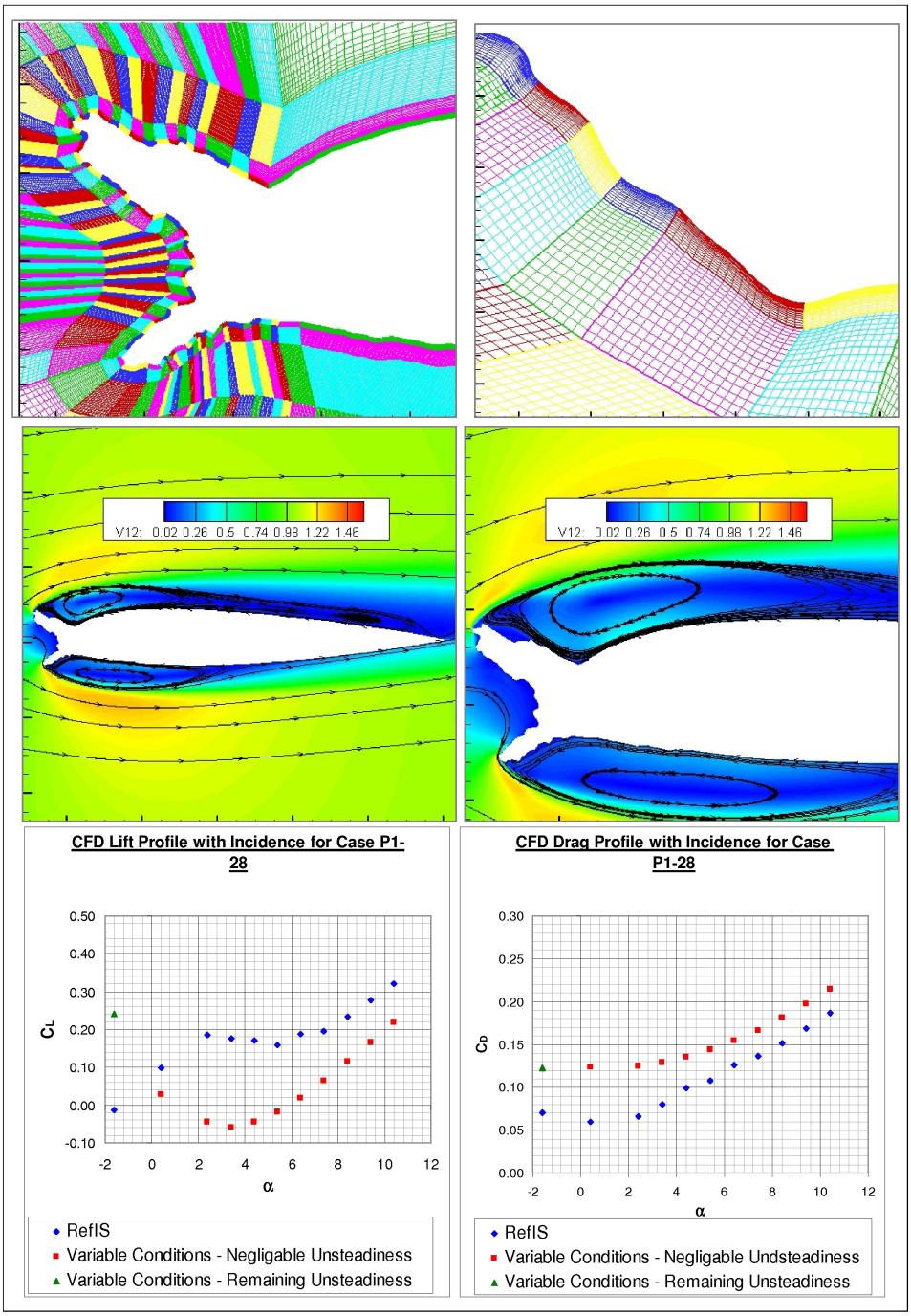

Figure E.18: Encounter Va_LWC_10%_Rise - CFD simulation information.

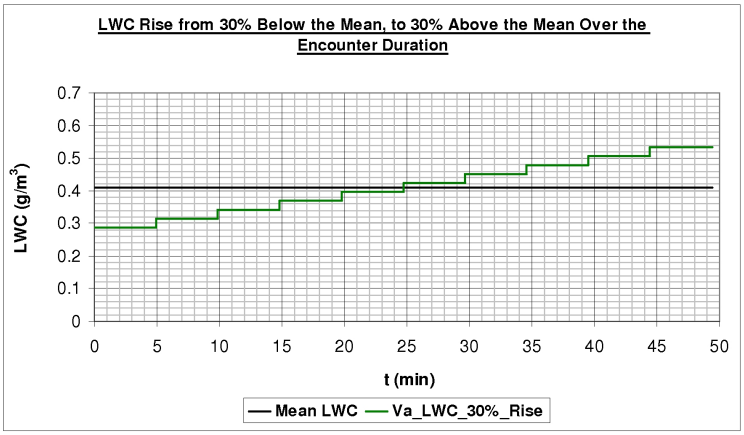

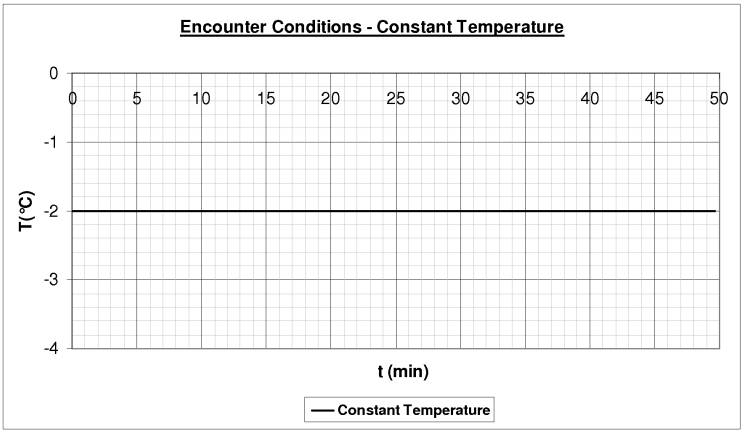

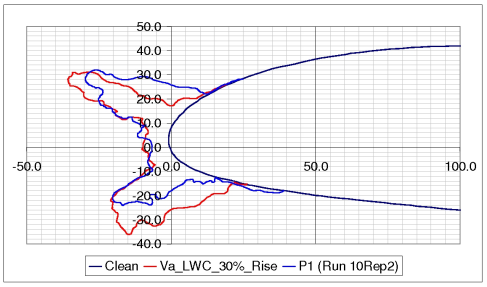

Run No.	Desc^{n} Code	h_{upper}	Θ_{upper}	Φ_{upper}	L_{upper}	h_{lower}	Θ_{lower}	Φ_{lower}	L_{lower}	t_{c-l}
P1-18Rep	Va_LWC_30%_Rise	41.00	42.75	30.00	20.00	35.00	-67.50	-57.75	25.50	10.00
---	*RefIS*	*36.00*	*46.58*	*30.58*	*24.17*	*28.17*	*-53.00*	*-43.17*	*53.67*	*7.33*
---	*StDev*	*1.32*	*2.40*	4.45	*2.93*	*0.58*	*5.07*	2.02	*14.15*	*2.02*

Figure E.19: Encounter Va_LWC_30%_Rise - Ice accretion simulation information.

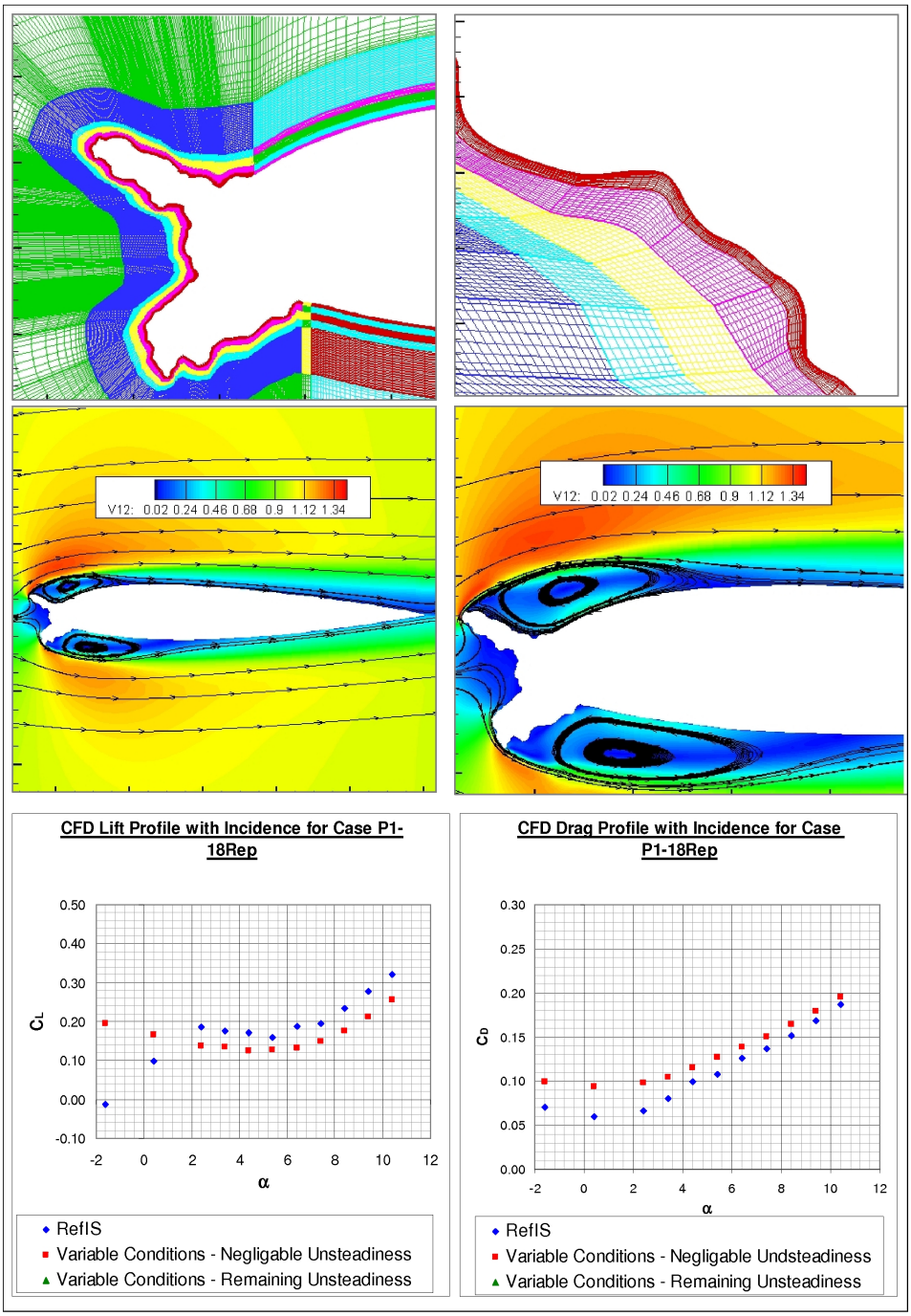

Figure E.20: Encounter Va_LWC_30%_Rise - CFD simulation information.

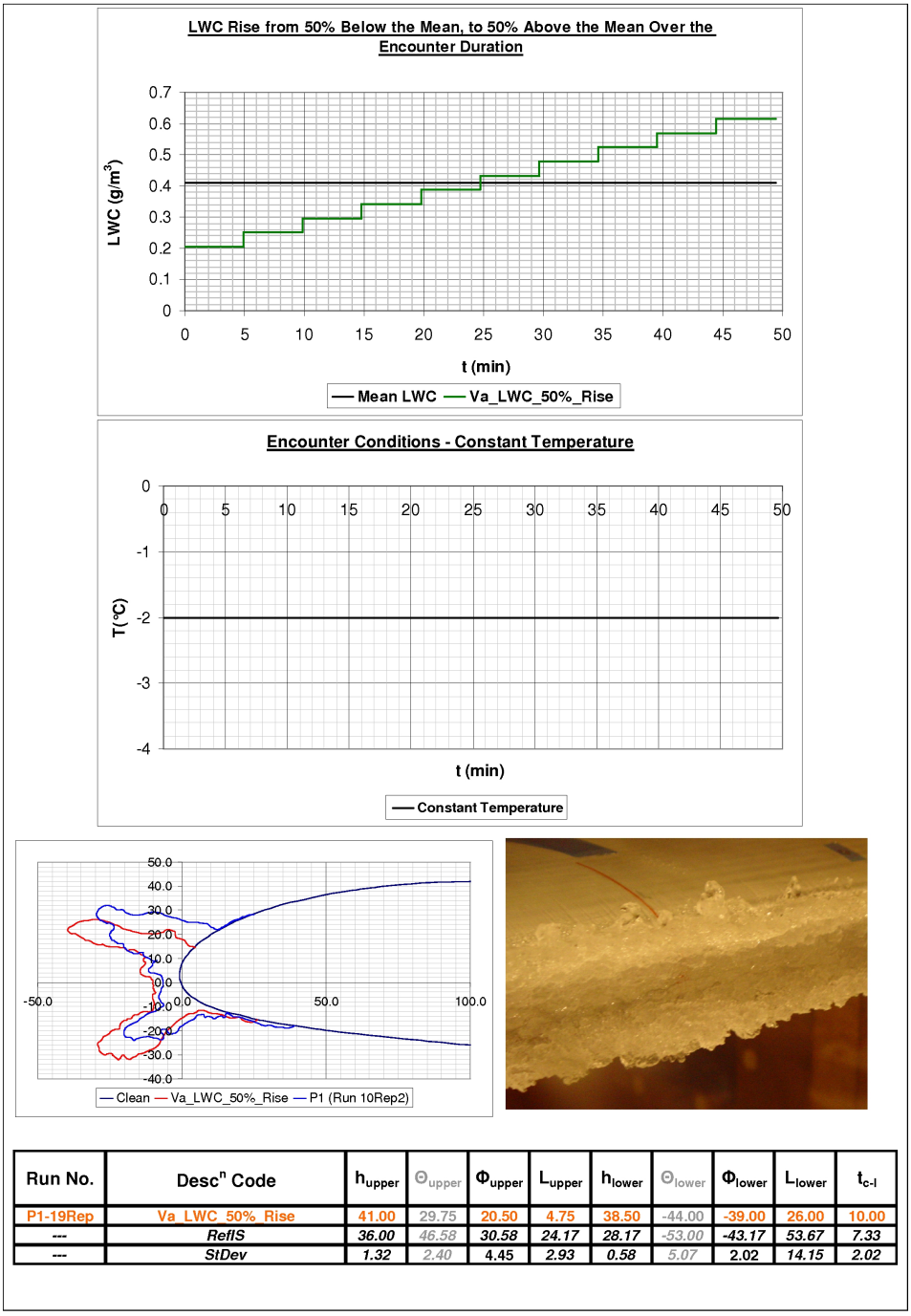

Run No.	Desc^{n} Code	h_{upper}	Θ_{upper}	Φ_{upper}	L_{upper}	h_{lower}	Θ_{lower}	Φ_{lower}	L_{lower}	t_{c-l}
P1-19Rep	Va_LWC_50%_Rise	41.00	29.75	20.50	4.75	38.50	-44.00	-39.00	26.00	10.00
---	*RefIS*	*36.00*	*46.58*	*30.58*	*24.17*	*28.17*	*-53.00*	*-43.17*	*53.67*	*7.33*
---	*StDev*	*1.32*	*2.40*	4.45	*2.93*	*0.58*	*5.07*	2.02	*14.15*	*2.02*

Figure E.21: Encounter Va_LWC_50%_Rise - Ice accretion simulation information.

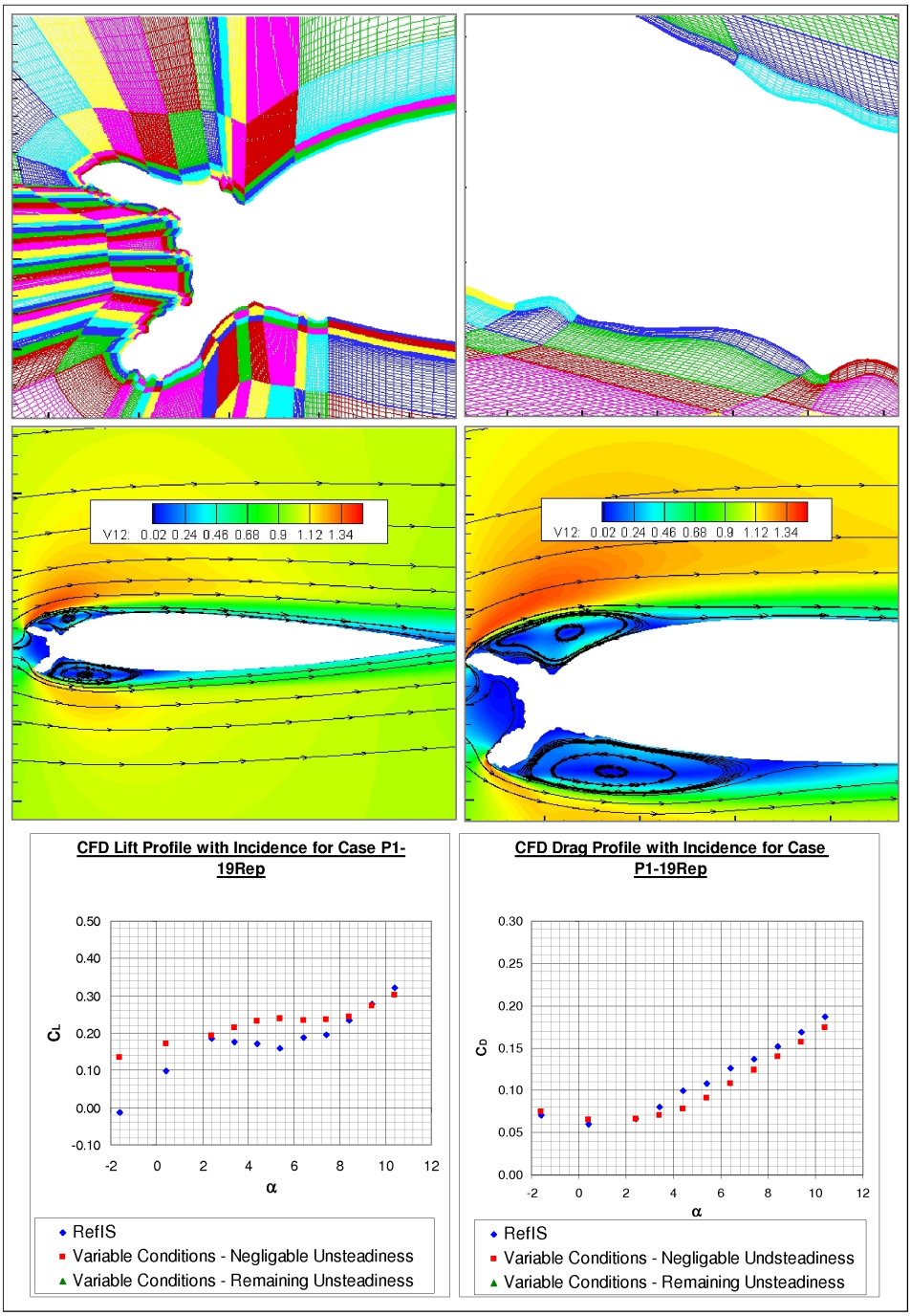

Figure E.22: Encounter Va_LWC_50%_Rise - CFD simulation information.

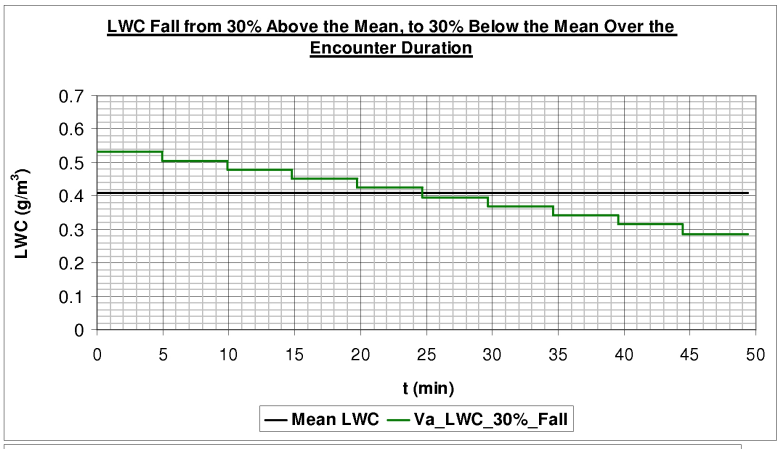

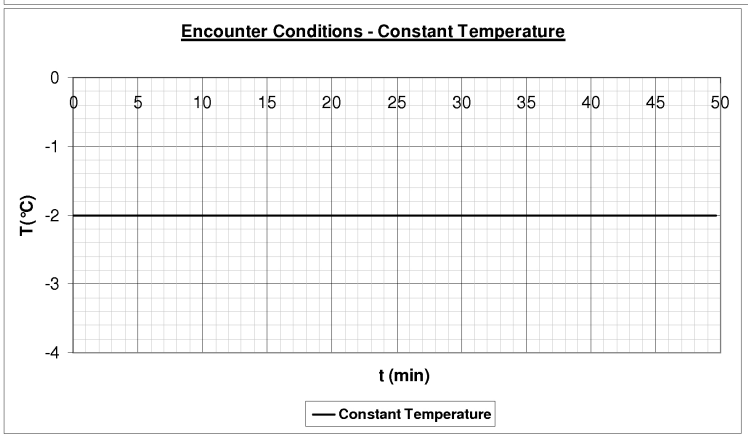

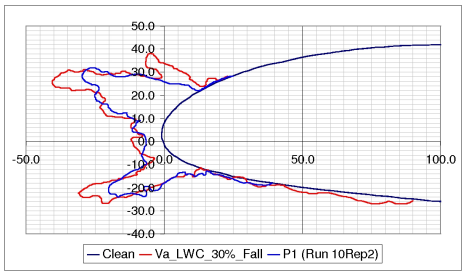

Run No.	Desc^{n} Code	h_{upper}	Θ_{upper}	Φ_{upper}	L_{upper}	h_{lower}	Θ_{lower}	Φ_{lower}	L_{lower}	t_{c-l}
P1-29	Va_LWC_30%_Fall	44.00	33.00	23.25	22.00	38.00	-39.00	-35.25	91.00	12.00
---	*RefIS*	*36.00*	*46.58*	*30.58*	*24.17*	*28.17*	*-53.00*	*-43.17*	*53.67*	*7.33*
---	*StDev*	*1.32*	*2.40*	4.45	*2.93*	*0.58*	*5.07*	2.02	*14.15*	*2.02*

Figure E.23: Encounter Va_LWC_30%_Fall - Ice accretion simulation information.

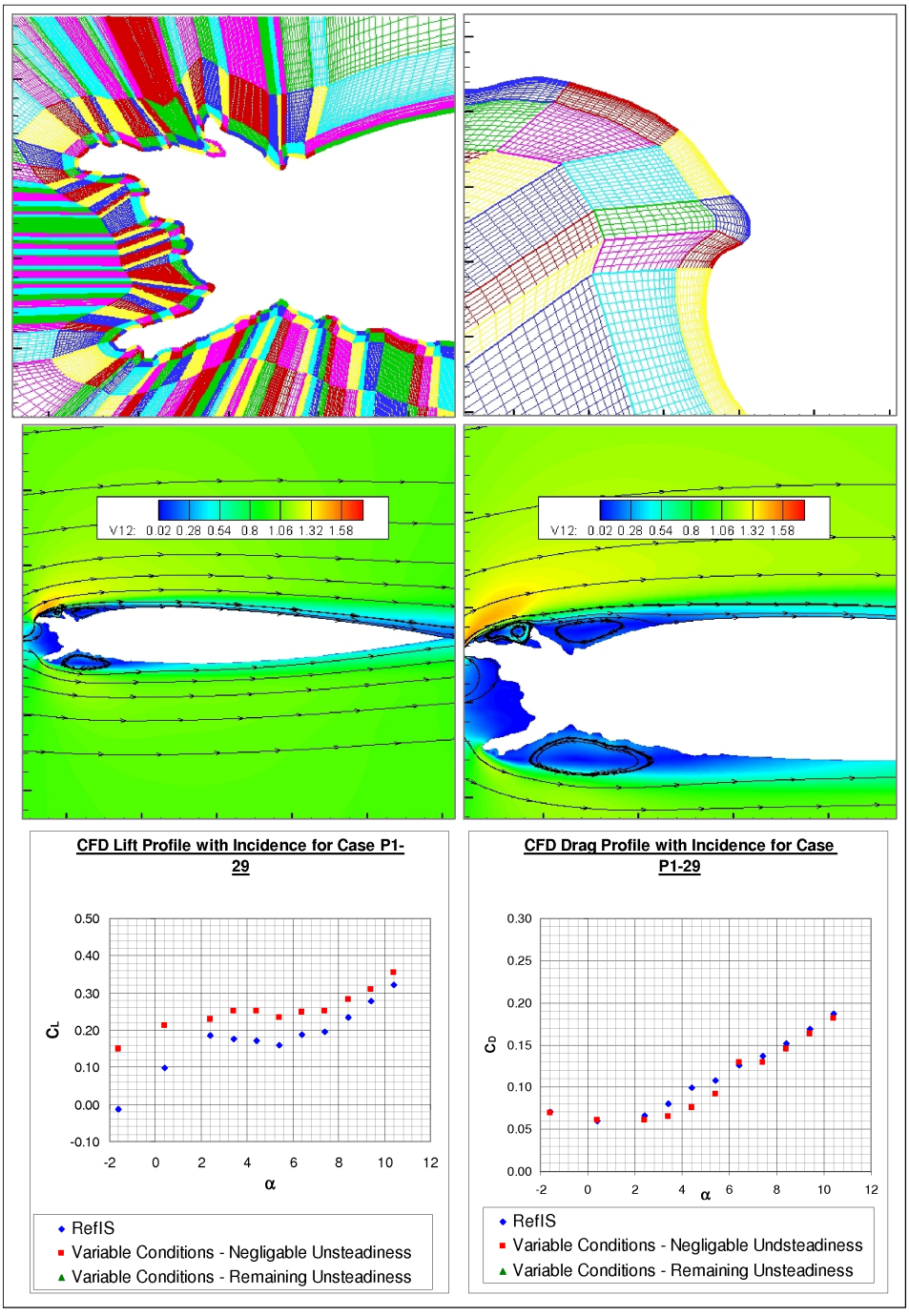

Figure E.24: Encounter Va_LWC_30%_Fall - CFD simulation information.

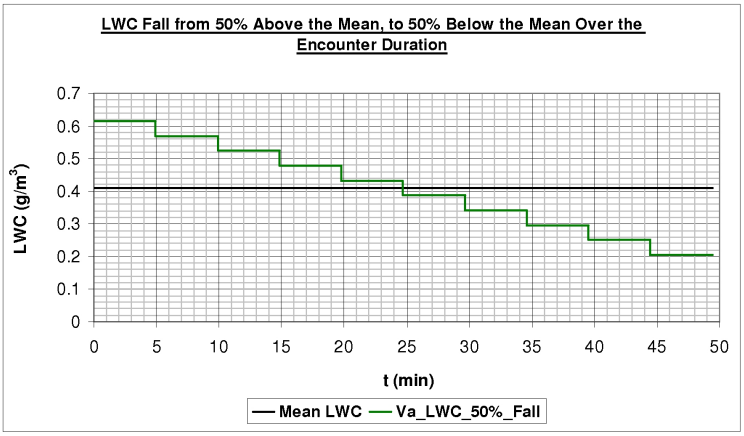

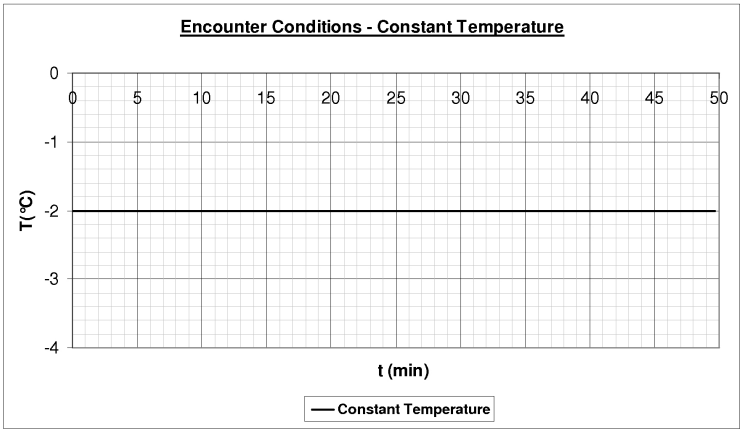

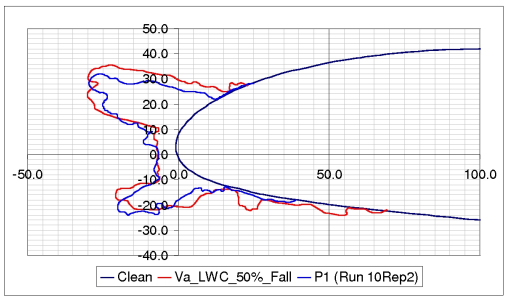

Run No.	Desc^{n} Code	h_{upper}	Θ_{upper}	Φ_{upper}	L_{upper}	h_{lower}	Θ_{lower}	Φ_{lower}	L_{lower}	t_{c-l}
P1-23Rep	Va_LWC_50%_Fall	37.50	47.00	33.00	22.00	27.00	-42.00	-35.25	68.75	7.00
---	*RefIS*	*36.00*	*46.58*	*30.58*	*24.17*	*28.17*	*-53.00*	*-43.17*	*53.67*	*7.33*
---	*StDev*	*1.32*	*2.40*	4.45	*2.93*	*0.58*	*5.07*	2.02	*14.15*	*2.02*

Figure E.25: Encounter Va_LWC_50%_Fall - Ice accretion simulation information.

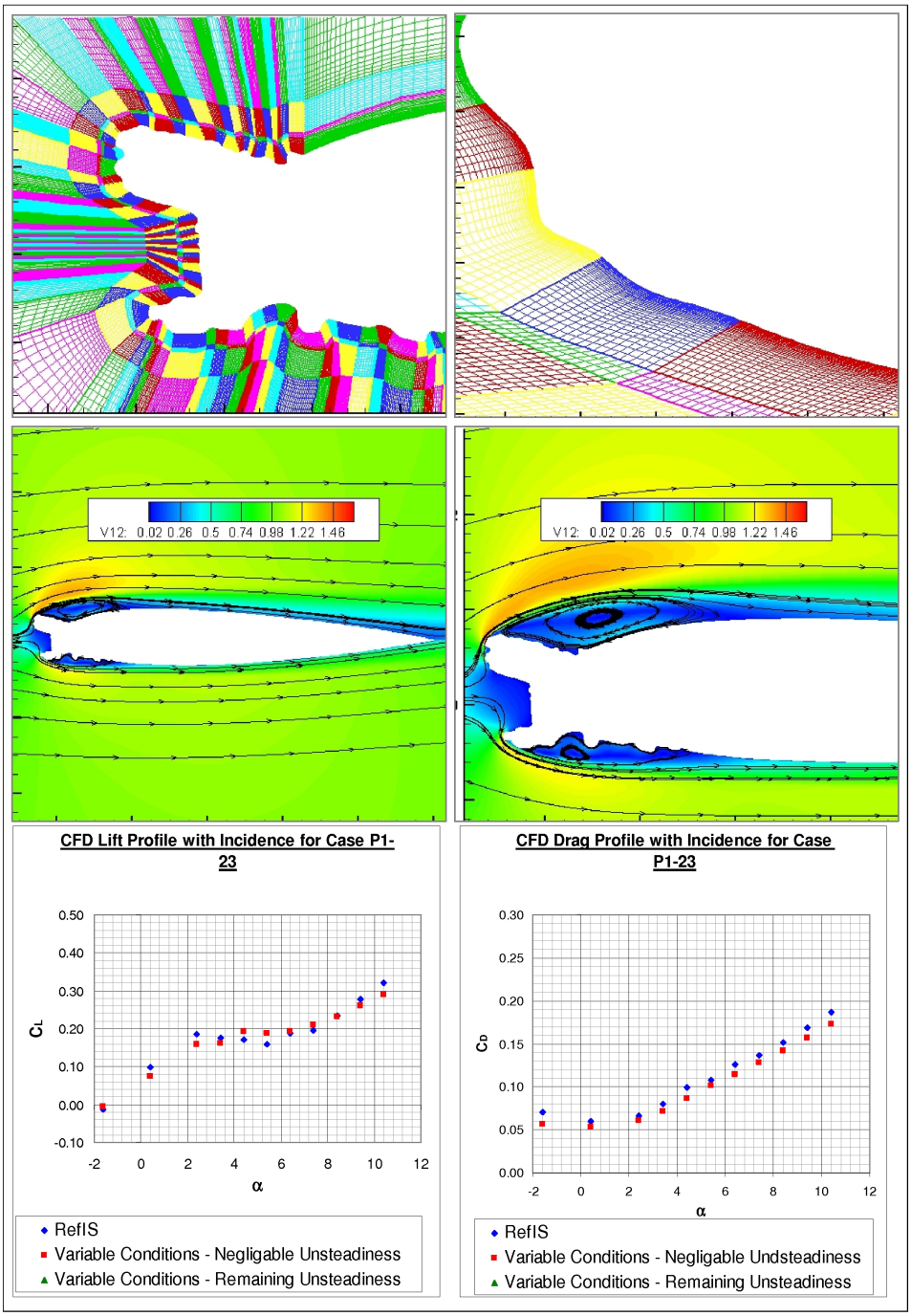

Figure E.26: Encounter Va_LWC_50%_Fall - CFD simulation information.

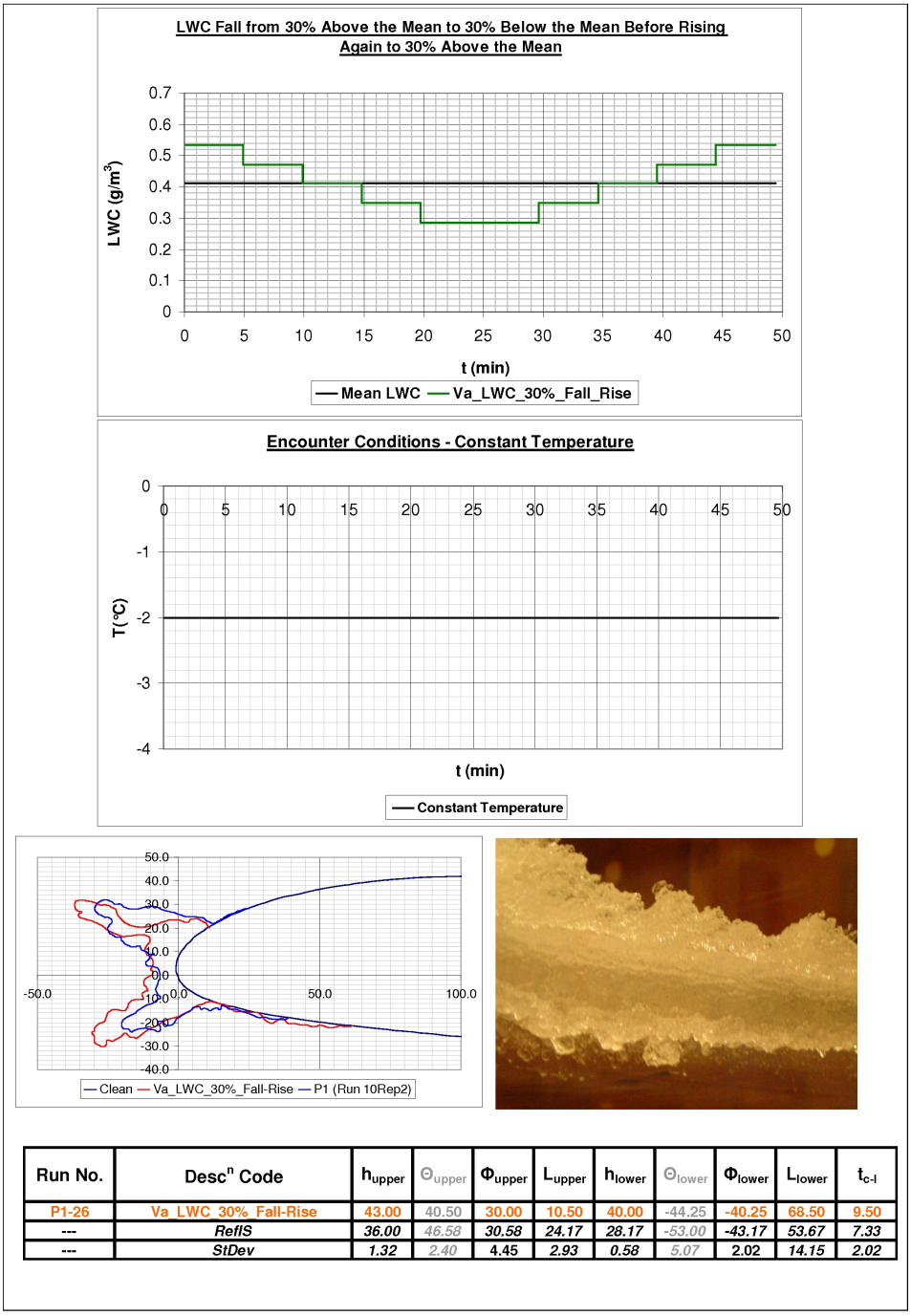

Run No.	Desc^{n} Code	h_{upper}	Θ_{upper}	Φ_{upper}	L_{upper}	h_{lower}	Θ_{lower}	Φ_{lower}	L_{lower}	t_{c-l}
P1-26	Va_LWC_30%_Fall-Rise	43.00	40.50	30.00	10.50	40.00	-44.25	-40.25	68.50	9.50
---	*RefIS*	*36.00*	*46.58*	*30.58*	*24.17*	*28.17*	*-53.00*	*-43.17*	*53.67*	*7.33*
---	*StDev*	*1.32*	*2.40*	4.45	*2.93*	*0.58*	*5.07*	2.02	*14.15*	*2.02*

Figure E.27: Encounter Va_LWC_30%_Fall-Rise - Ice accretion simulation information.

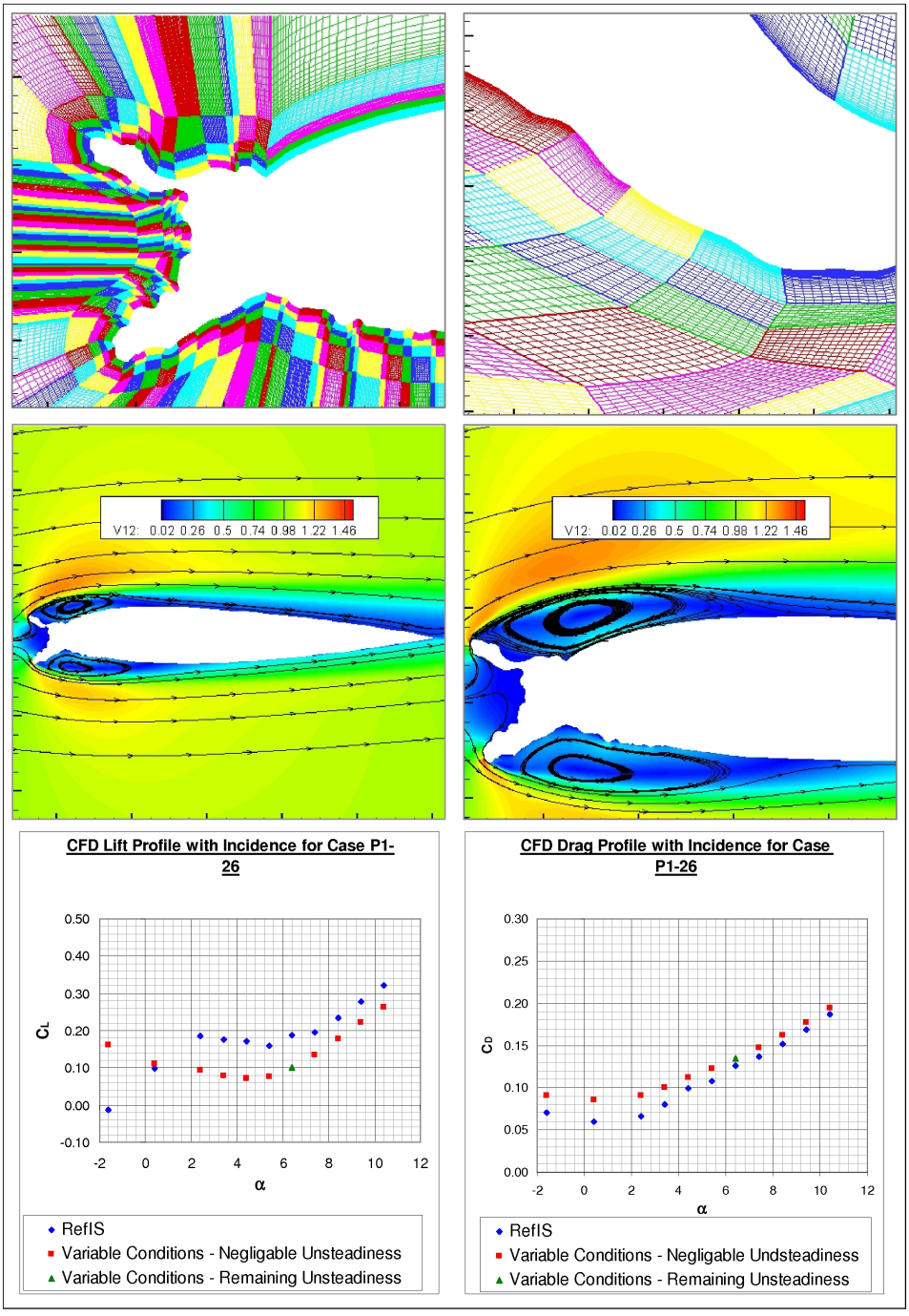

Figure E.28: Encounter Va_LWC_30%_Fall-Rise - CFD simulation information.

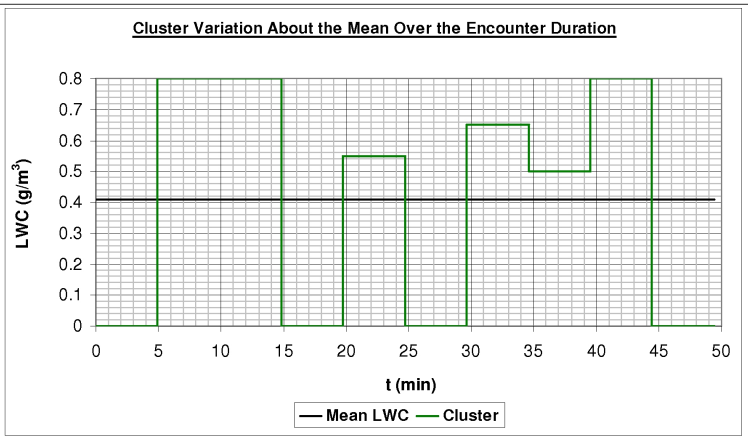

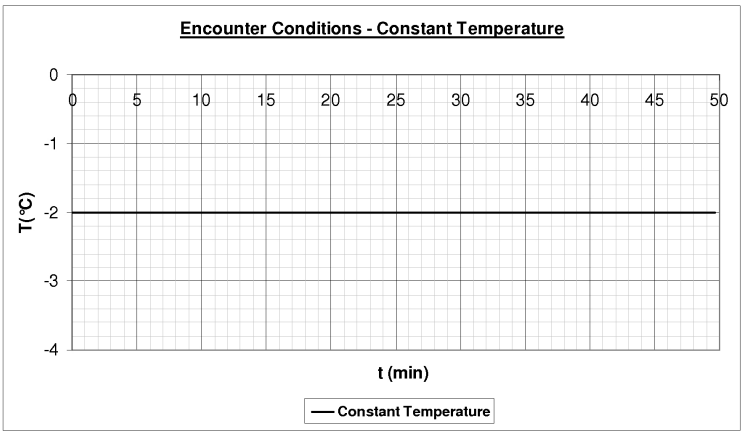

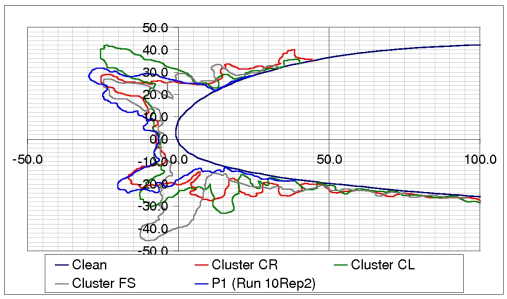

Run No.	Desc^{n} Code	h_{upper}	Θ_{upper}	Φ_{upper}	L_{upper}	h_{lower}	Θ_{lower}	Φ_{lower}	L_{lower}	$t_{c\text{-}l}$
P1-24Rep	Cluster (CR)	32.50	49.00	31.50	43.50	23.50	-51.00	-42.50	112.50	7.50
P1-24Rep	Cluster (CL)	40.00	59.50	40.00	40.00	27.50	-72.50	-60.00	104.50	6.50
P1-24Rep	Cluster (FS)	31.50	46.50	30.00	34.00	40.50	-76.00	-64.00	95.50	7.00
---	*RefIS*	*36.00*	*46.58*	*30.58*	*24.17*	*28.17*	*-53.00*	*-43.17*	*53.67*	*7.33*
---	*StDev*	*1.32*	*2.40*	4.45	*2.93*	*0.58*	*5.07*	2.02	*14.15*	*2.02*

Figure E.29: Encounter Cluster - Ice accretion simulation information.

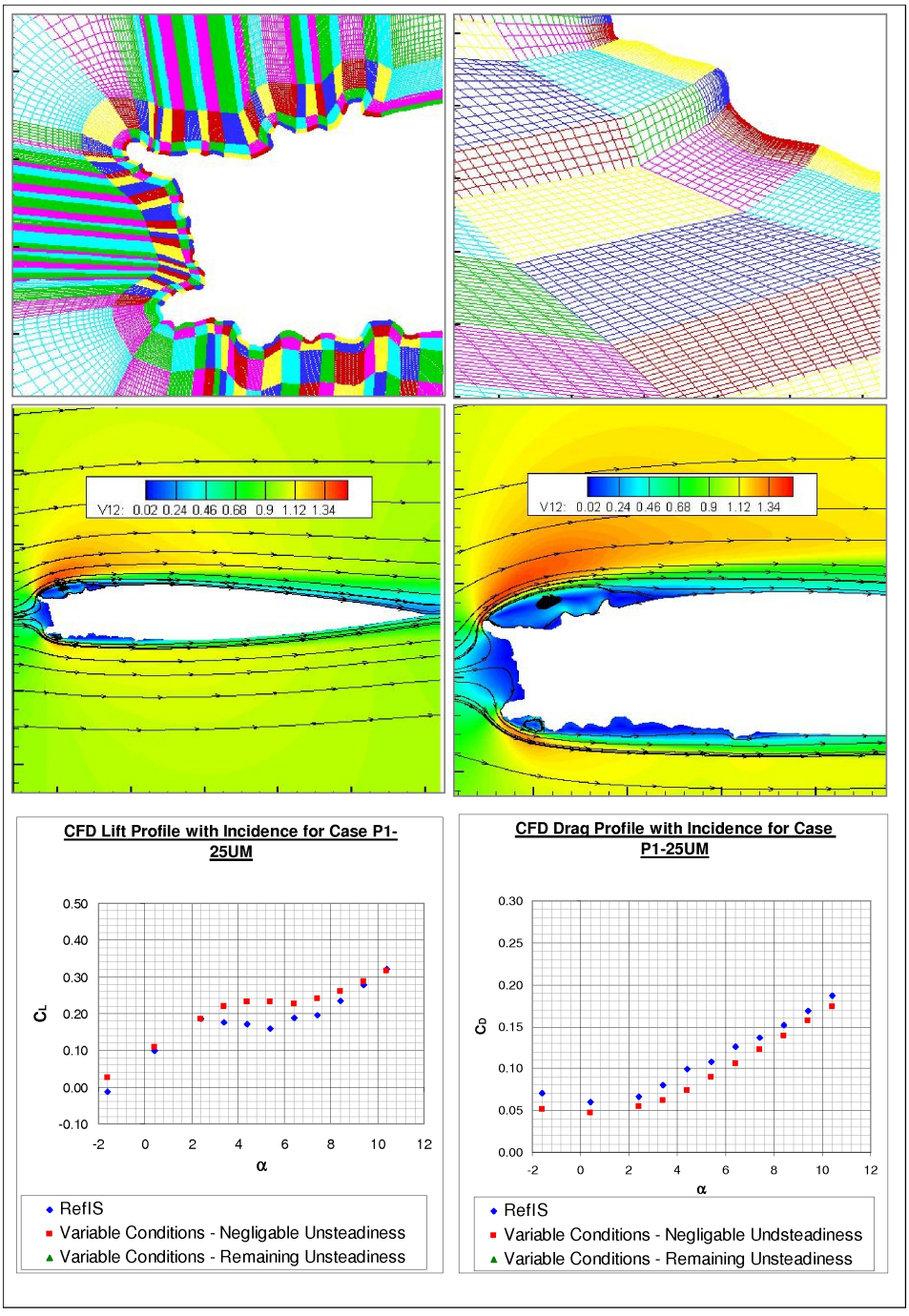

Figure E.30: Encounter Cluster - CFD simulation information.

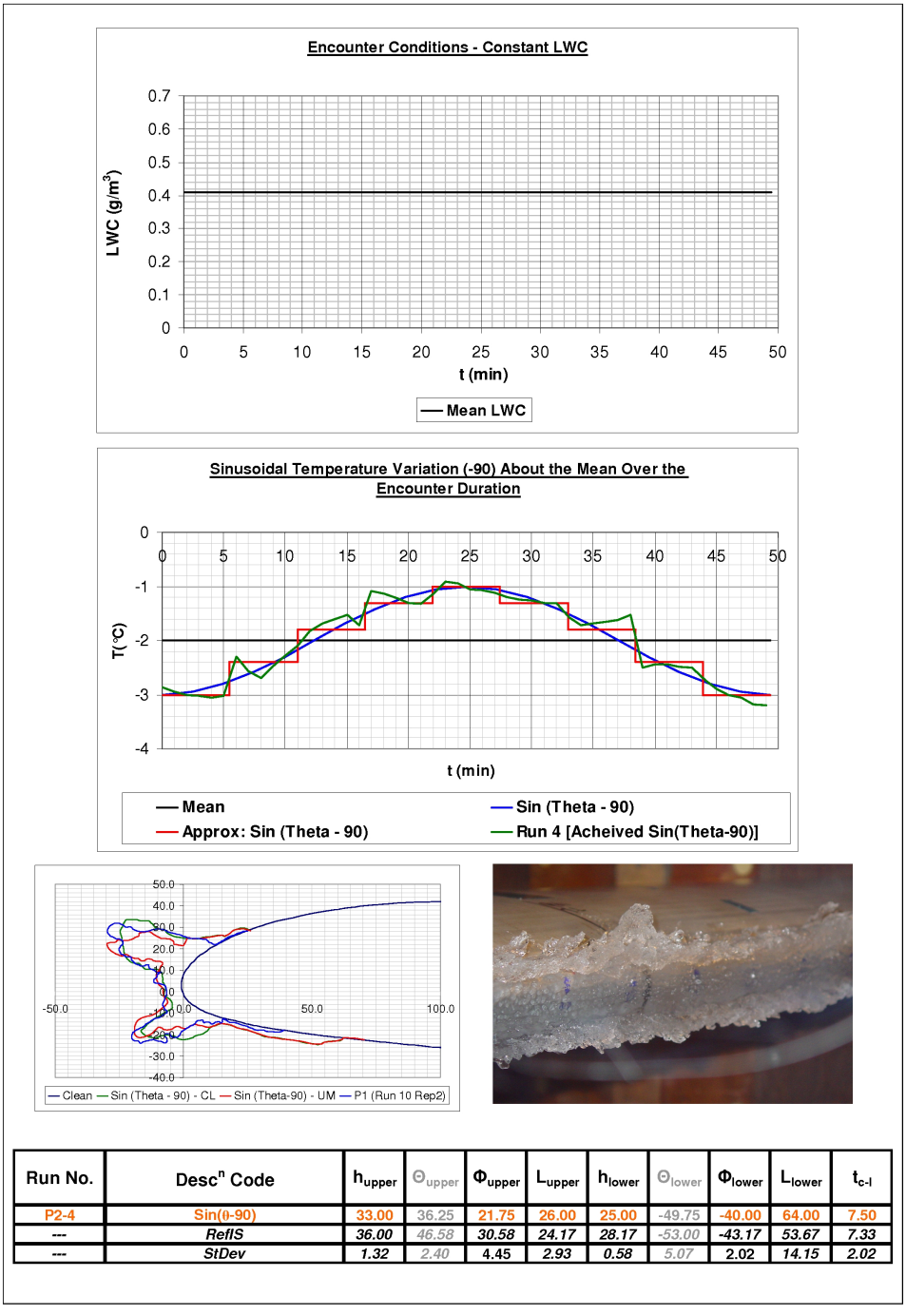

Run No.	Desc^{n} Code	h_{upper}	Θ_{upper}	Φ_{upper}	L_{upper}	h_{lower}	Θ_{lower}	Φ_{lower}	L_{lower}	t_{c-l}
P2-4	Sin(θ-90)	33.00	36.25	21.75	26.00	25.00	-49.75	-40.00	64.00	7.50
---	*RefIS*	*36.00*	*46.58*	*30.58*	*24.17*	*28.17*	*-53.00*	*-43.17*	*53.67*	*7.33*
---	*StDev*	*1.32*	*2.40*	4.45	*2.93*	*0.58*	*5.07*	2.02	*14.15*	*2.02*

Figure E.31: Encounter Sin(θ - 90°) - Ice accretion simulation information.

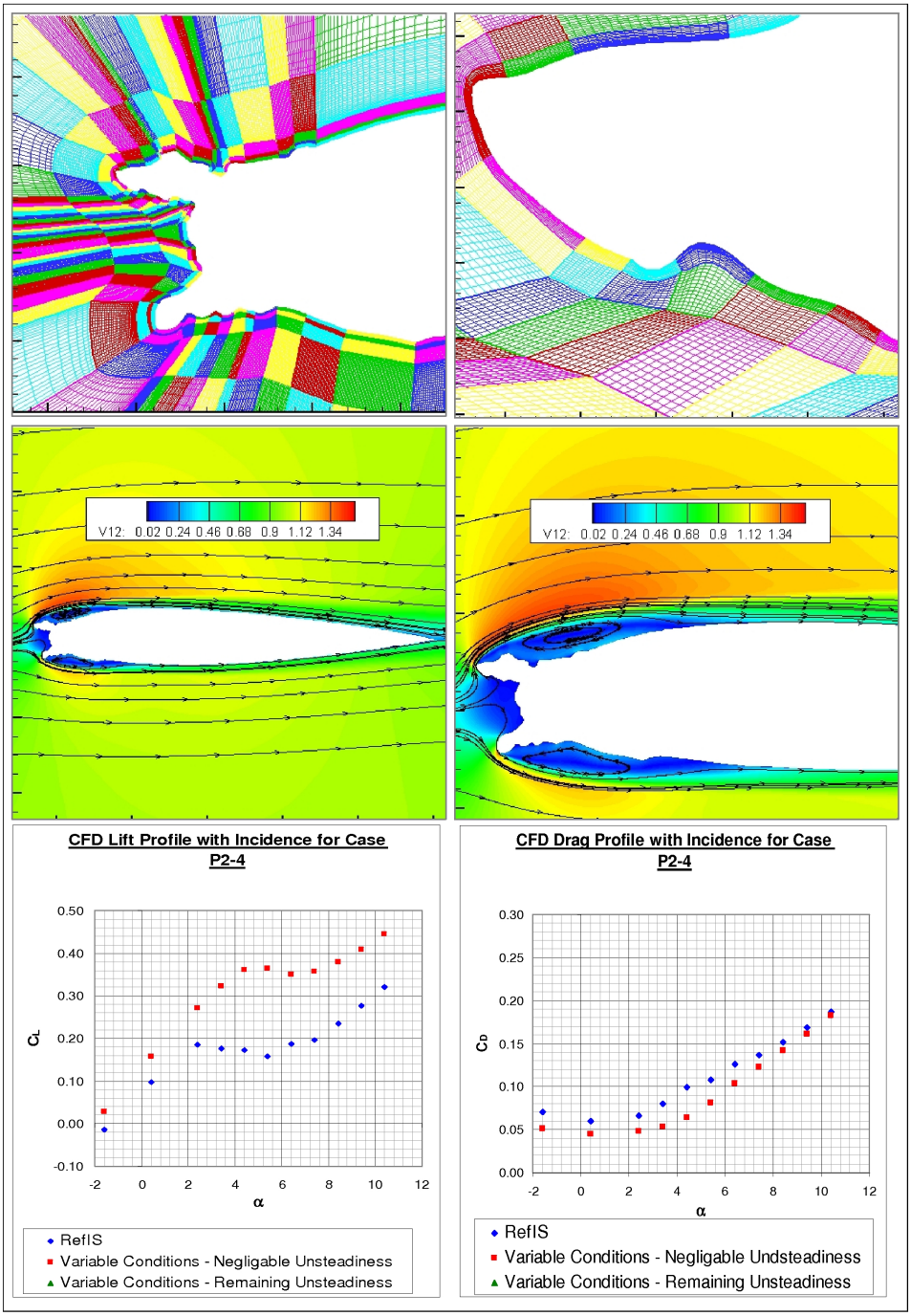

Figure E.32: Encounter Sin(θ - 90°) - CFD simulation information.

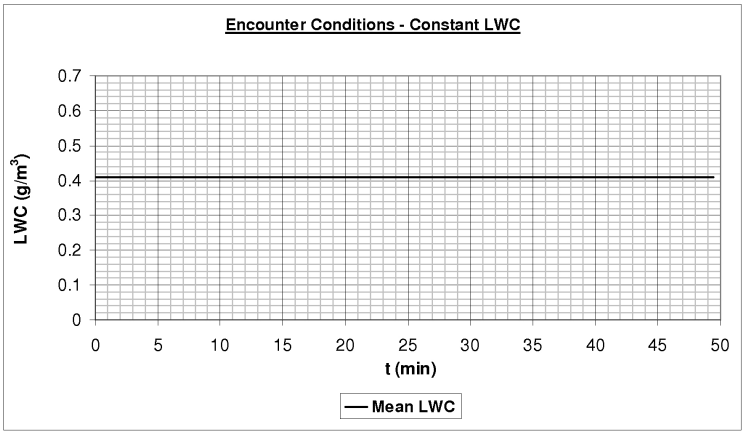

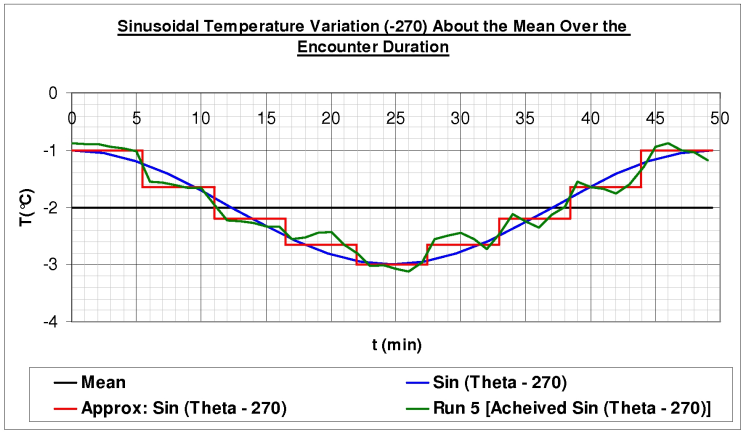

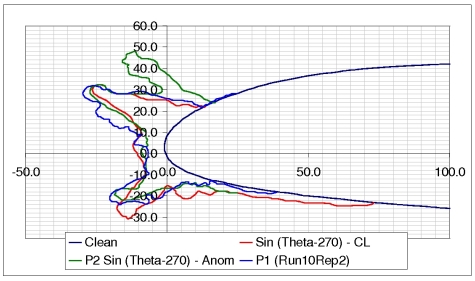

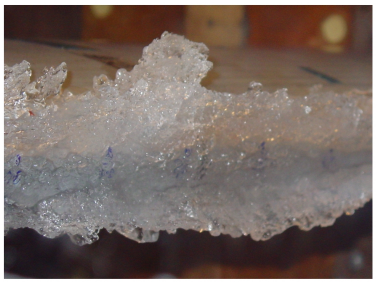

Run No.	Desc^{n} Code	h_{upper}	Θ_{upper}	Φ_{upper}	L_{upper}	h_{lower}	Θ_{lower}	Φ_{lower}	L_{lower}	$t_{c\text{-}l}$
P2-5	Sin(θ-270)	34.50	50.50	33.00	13.00	30.00	-61.75	-51.25	73.00	9.00
---	*RefIS*	*36.00*	*46.58*	*30.58*	*24.17*	*28.17*	*-53.00*	*-43.17*	*53.67*	*7.33*
---	*StDev*	*1.32*	*2.40*	4.45	*2.93*	*0.58*	*5.07*	2.02	*14.15*	*2.02*

Figure E.33: Encounter Sin(θ - 270°) - Ice accretion simulation information.

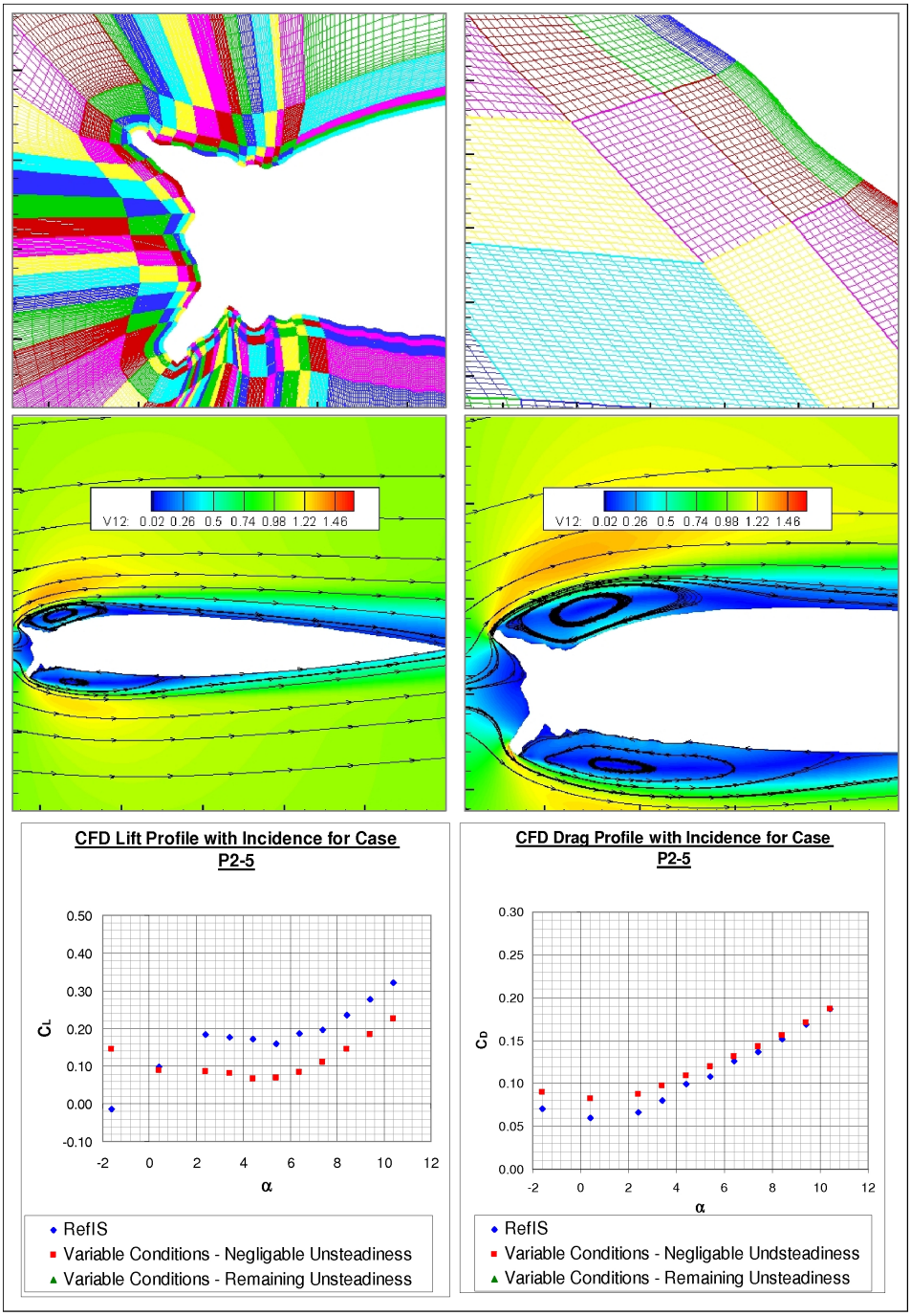

Figure E.34: Encounter Sin(θ - 270°) - CFD simulation information.

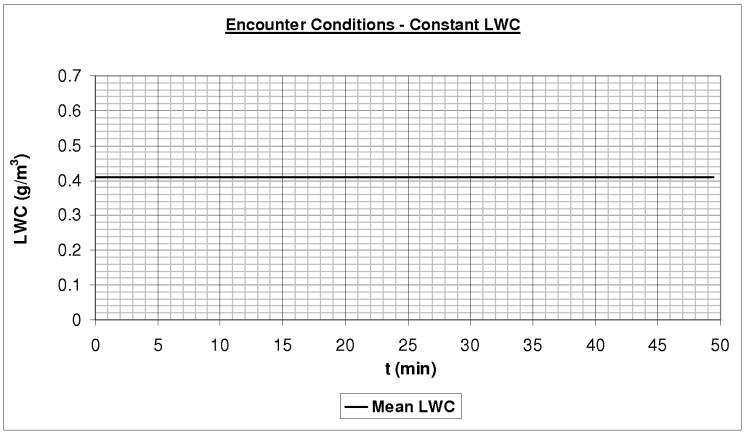

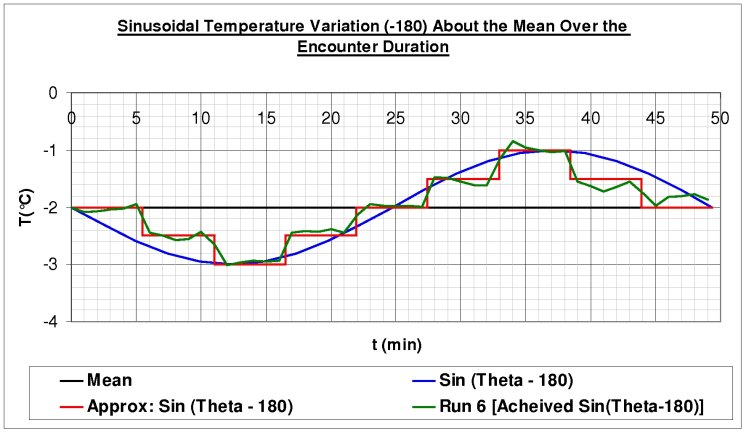

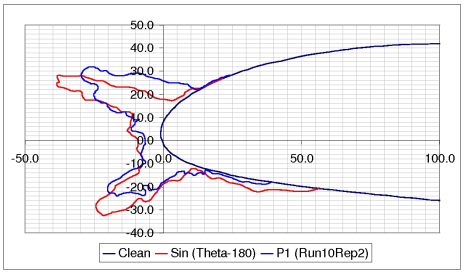

Run No.	Desc^{n} Code	h_{upper}	Θ_{upper}	Φ_{upper}	L_{upper}	h_{lower}	Θ_{lower}	Φ_{lower}	L_{lower}	t_{c-l}
P2-6	Sin(θ-180)	43.00	37.00	25.00	20.00	37.00	-55.00	-46.50	56.50	9.50
---	*RefIS*	*36.00*	*46.58*	*30.58*	*24.17*	*28.17*	*-53.00*	*-43.17*	*53.67*	*7.33*
---	*StDev*	*1.32*	*2.40*	4.45	*2.93*	*0.58*	*5.07*	2.02	*14.15*	*2.02*

Figure E.35: Encounter Sin(θ - 180°) - Ice accretion simulation information.

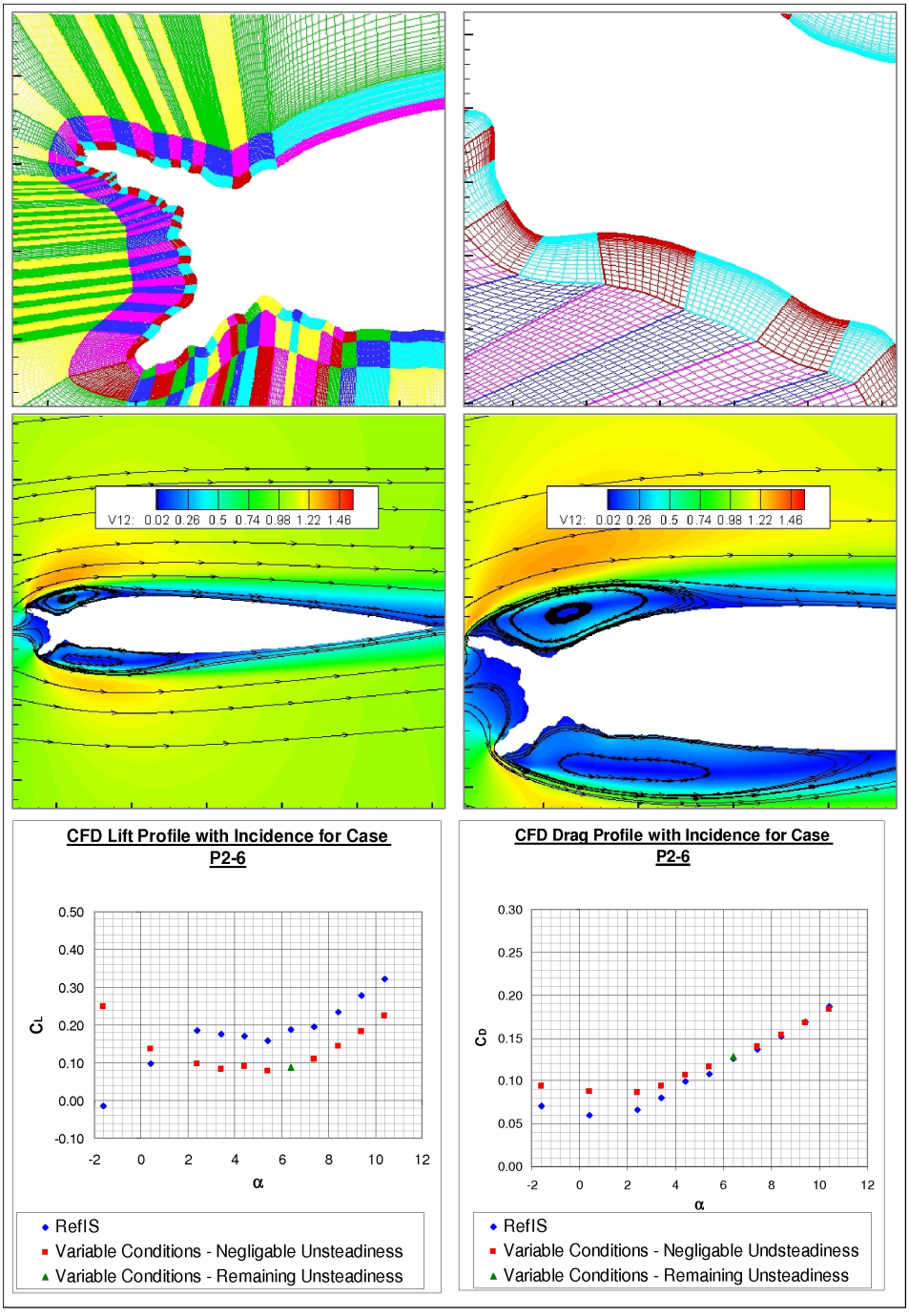

Figure E.36: Encounter Sin(θ - 180°C) - CFD simulation information.

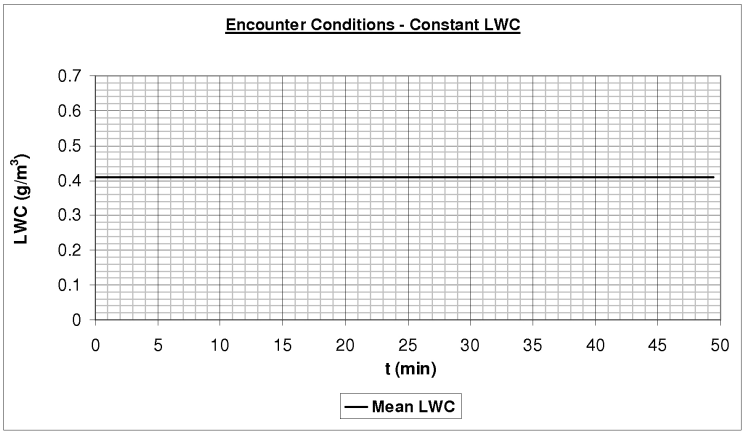

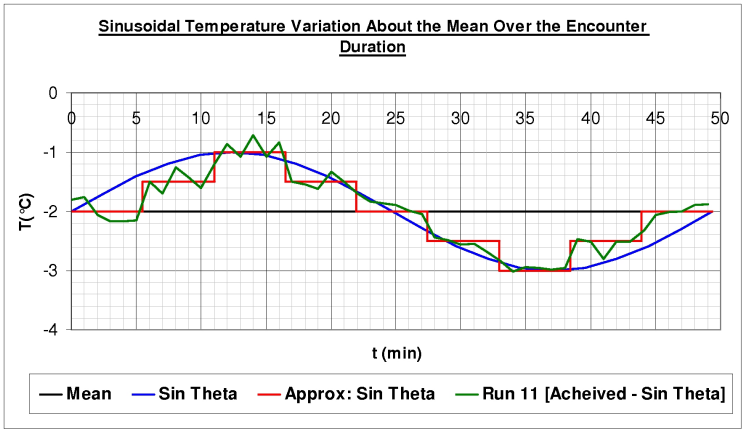

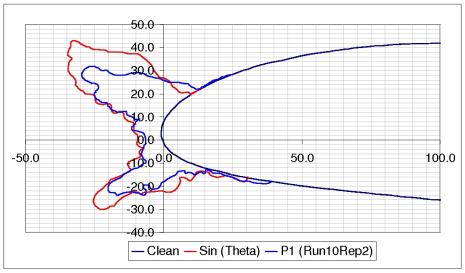

Run No.	Desc^{n} Code	h_{upper}	Θ_{upper}	Φ_{upper}	L_{upper}	h_{lower}	Θ_{lower}	Φ_{lower}	L_{lower}	$t_{c\text{-}l}$
P2-11	Sin(θ)	46.50	53.50	38.00	10.00	35.00	-50.50	-43.25	30.00	9.50
---	*RefIS*	*36.00*	*46.58*	*30.58*	*24.17*	*28.17*	*-53.00*	*-43.17*	*53.67*	*7.33*
---	*StDev*	*1.32*	*2.40*	4.45	*2.93*	*0.58*	*5.07*	2.02	*14.15*	*2.02*

Figure E.37: Encounter Sin(θ) - Ice accretion simulation information.

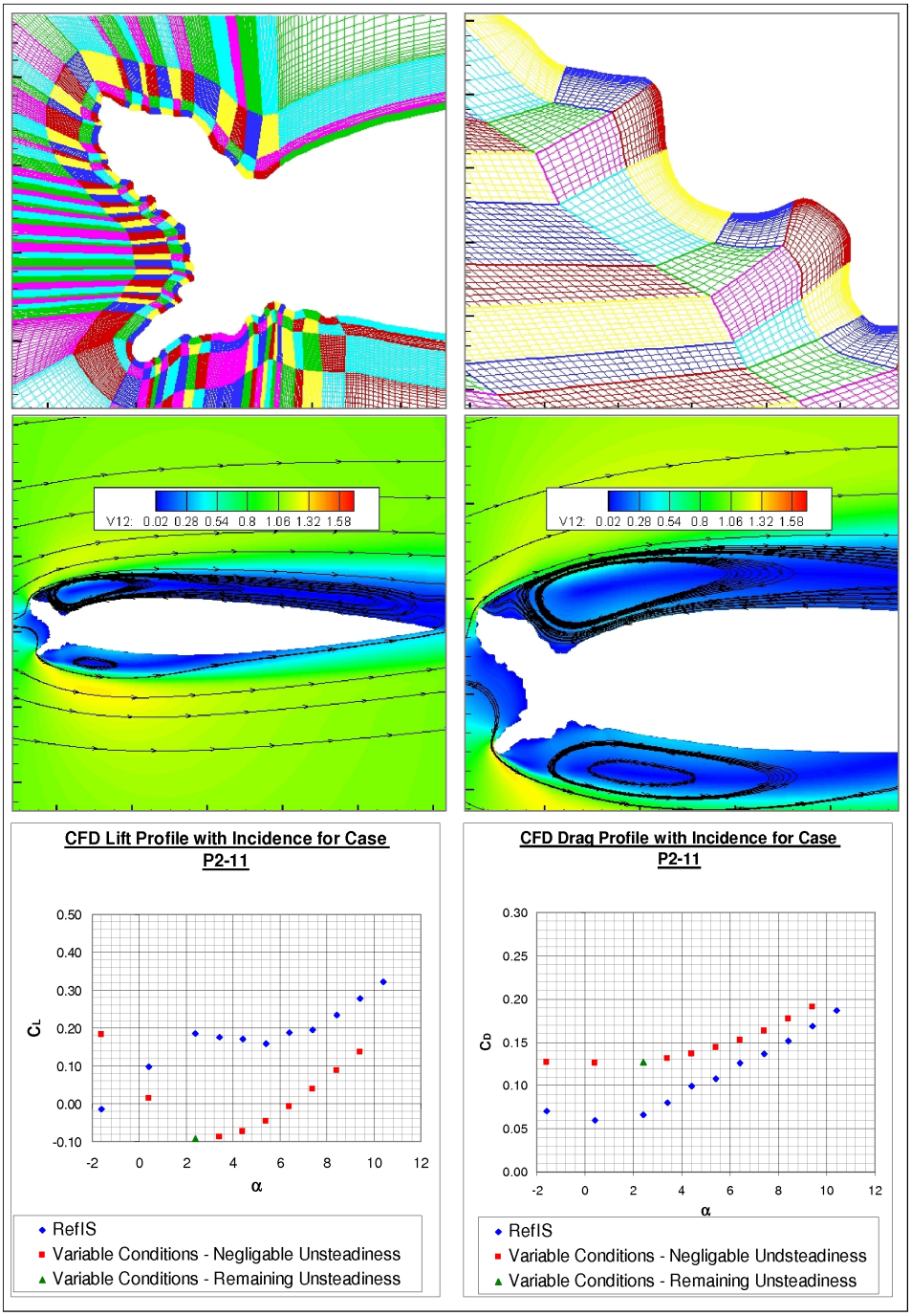

Figure E.38: Encounter Sin(θ) - CFD simulation information.

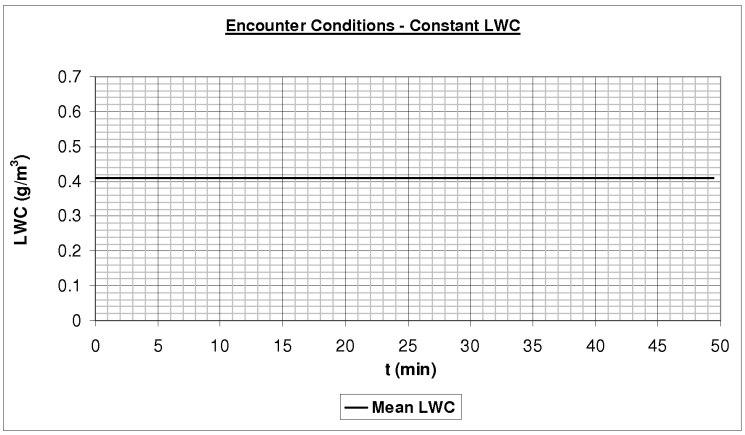

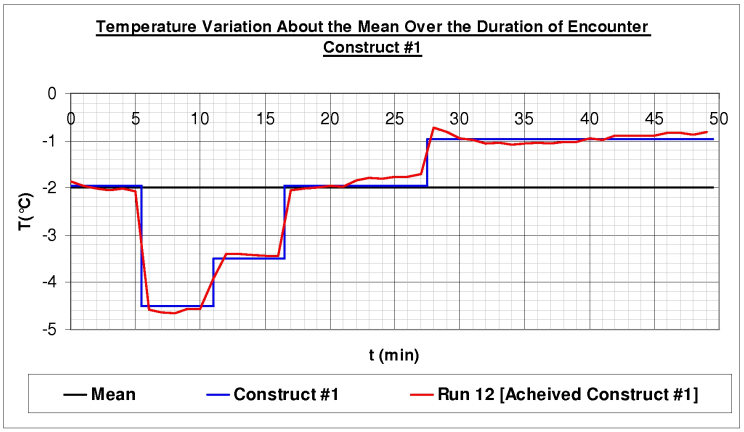

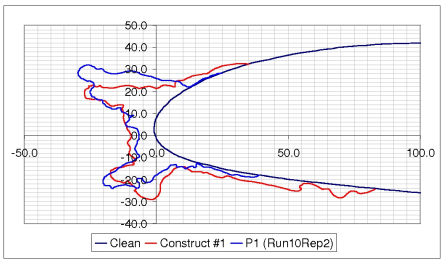

Run No.	Desc^{n} Code	h_{upper}	Θ_{upper}	Φ_{upper}	L_{upper}	h_{lower}	Θ_{lower}	Φ_{lower}	L_{lower}	t_{c-l}
P2-12	Temp Construct #1	30.00	36.50	23.00	35.00	22.00	-86.00	-64.50	82.50	8.50
---	*RefIS*	*36.00*	*46.58*	*30.58*	*24.17*	*28.17*	*-53.00*	*-43.17*	*53.67*	*7.33*
---	*StDev*	*1.32*	*2.40*	4.45	*2.93*	*0.58*	*5.07*	2.02	*14.15*	*2.02*

Figure E.39: Encounter Construct #1 - Ice accretion simulation information.

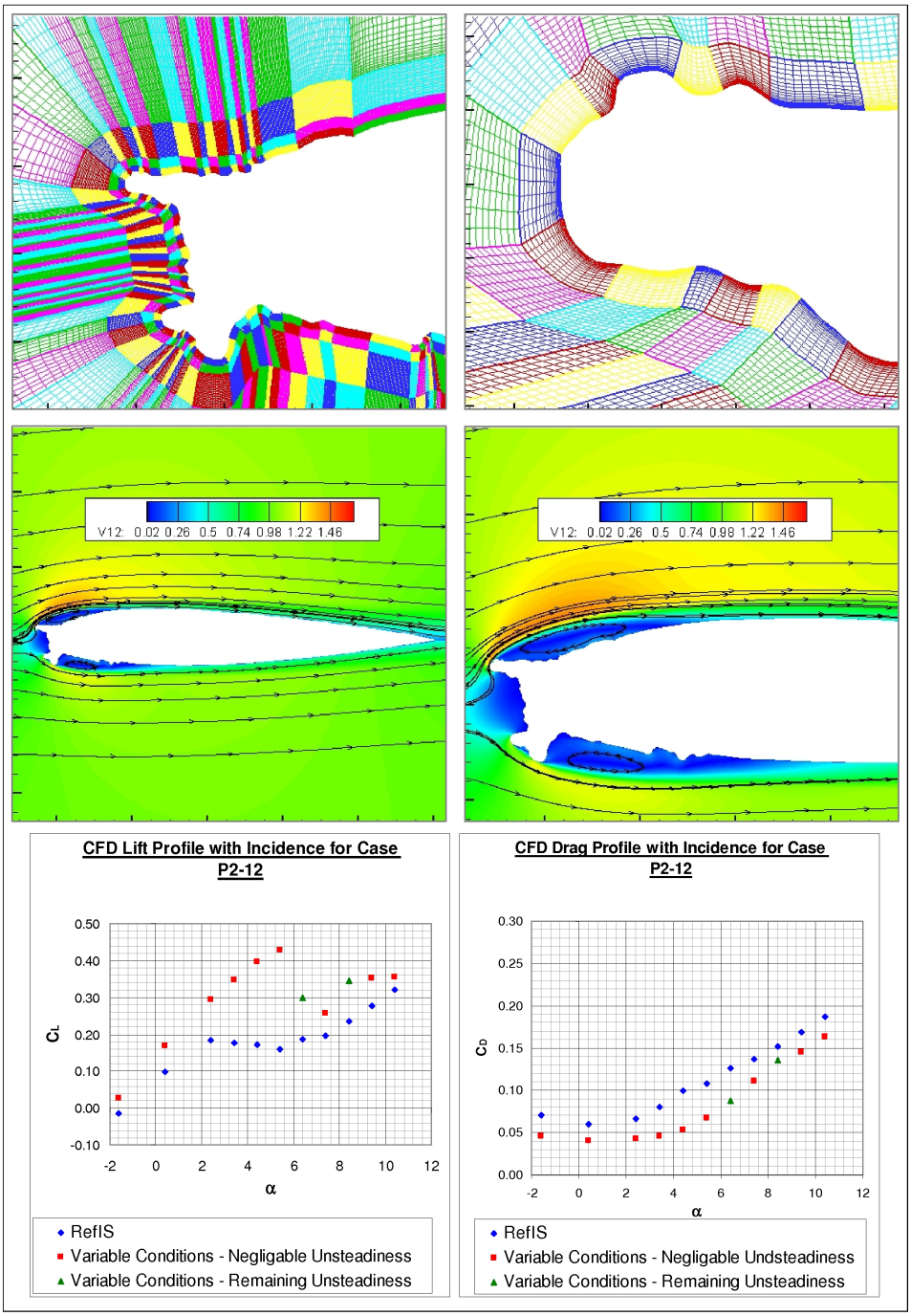

Figure E.40: Encounter Construct #1 - CFD simulation information.

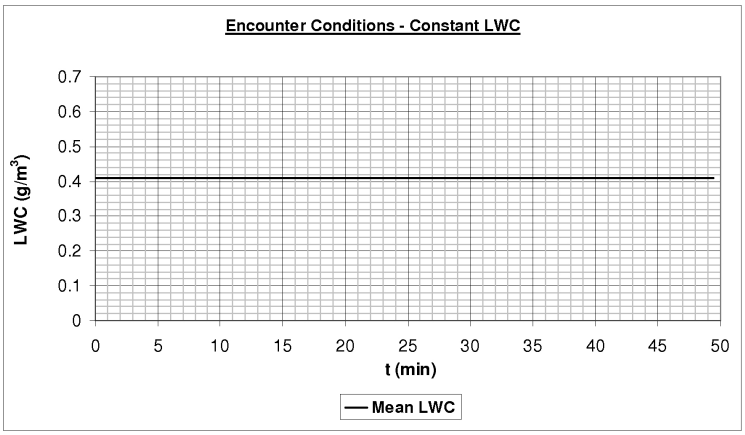

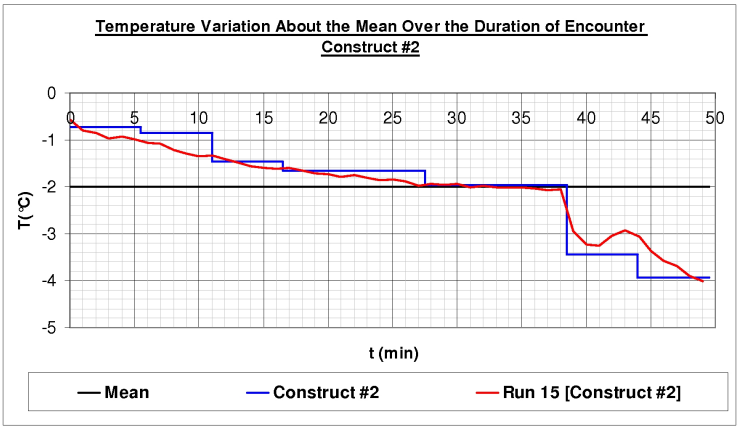

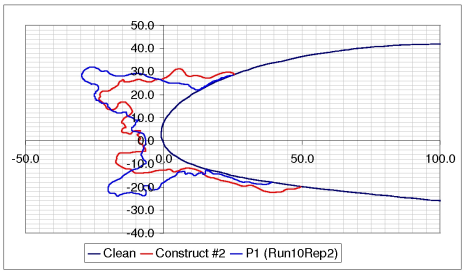

Run No.	Desc^{n} Code	h_{upper}	Θ_{upper}	Φ_{upper}	L_{upper}	h_{lower}	Θ_{lower}	Φ_{lower}	L_{lower}	t_{c-l}
P2-15	Temp Construct #2	24.50	38.25	20.25	26.00	19.00	-30.50	-27.75	50.00	9.00
---	*RefIS*	*36.00*	*46.58*	*30.58*	*24.17*	*28.17*	*-53.00*	*-43.17*	*53.67*	*7.33*
---	*StDev*	*1.32*	*2.40*	4.45	*2.93*	*0.58*	*5.07*	2.02	*14.15*	*2.02*

Figure E.41: Encounter Construct #2 - Ice accretion simulation information.

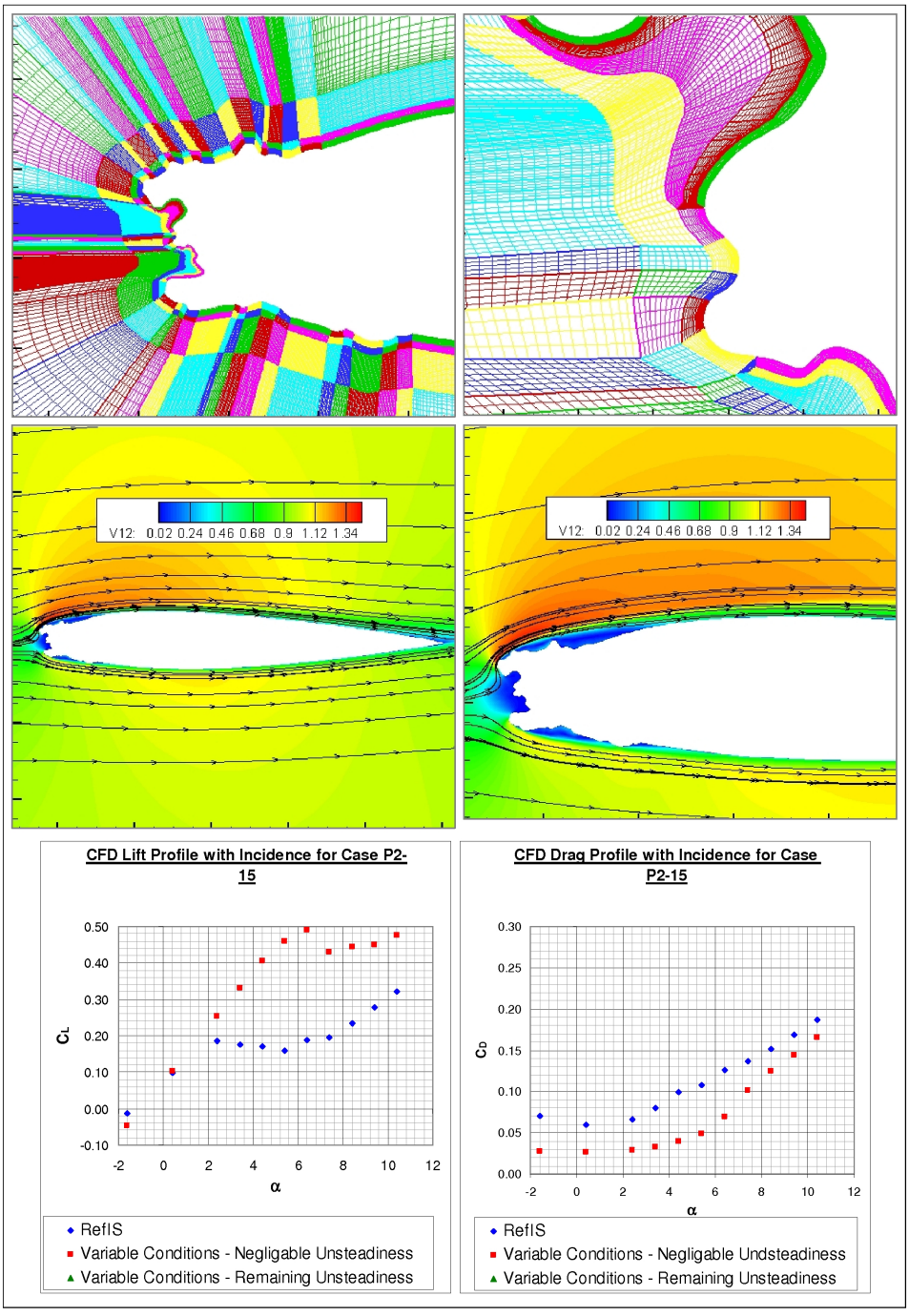

Figure E.42: Encounter Construct #2 - CFD simulation information.

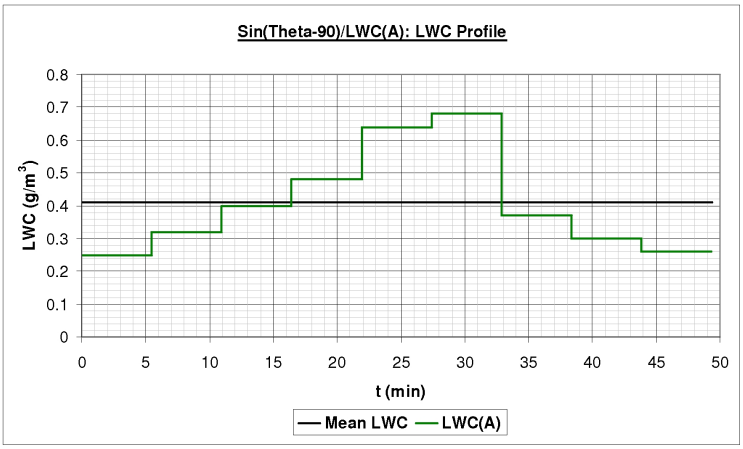

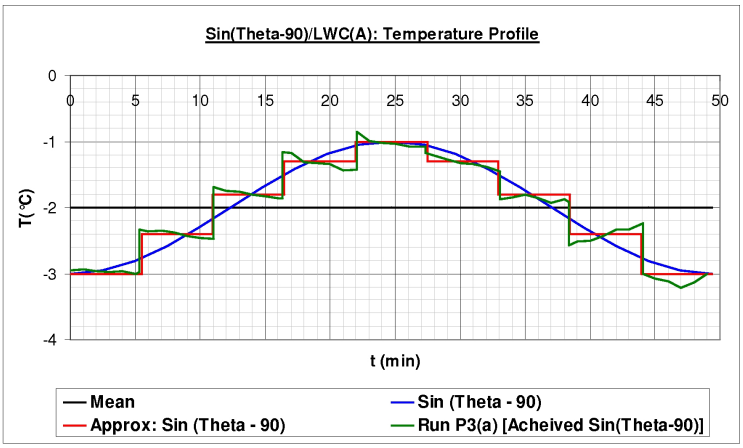

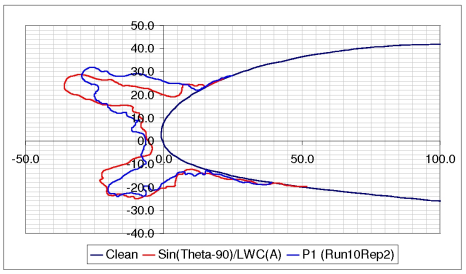

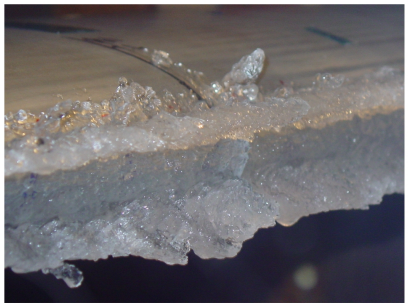

Run No.	Desc^{n} Code	h_{upper}	Θ_{upper}	Φ_{upper}	L_{upper}	h_{lower}	Θ_{lower}	Φ_{lower}	L_{lower}	t_{c-l}
P3-a	Sin(Theta-90)/LWC(A)	40.00	35.00	21.25	15.00	29.00	-50.00	-39.00	54.00	6.00
---	*RefIS*	*36.00*	*46.58*	*30.58*	*24.17*	*28.17*	*-53.00*	*-43.17*	*53.67*	*7.33*
---	*StDev*	*1.32*	*2.40*	4.45	*2.93*	*0.58*	*5.07*	2.02	*14.15*	*2.02*

Figure E.43: Encounter LWC(A)/Sin(θ - 90°) - Ice accretion simulation information.

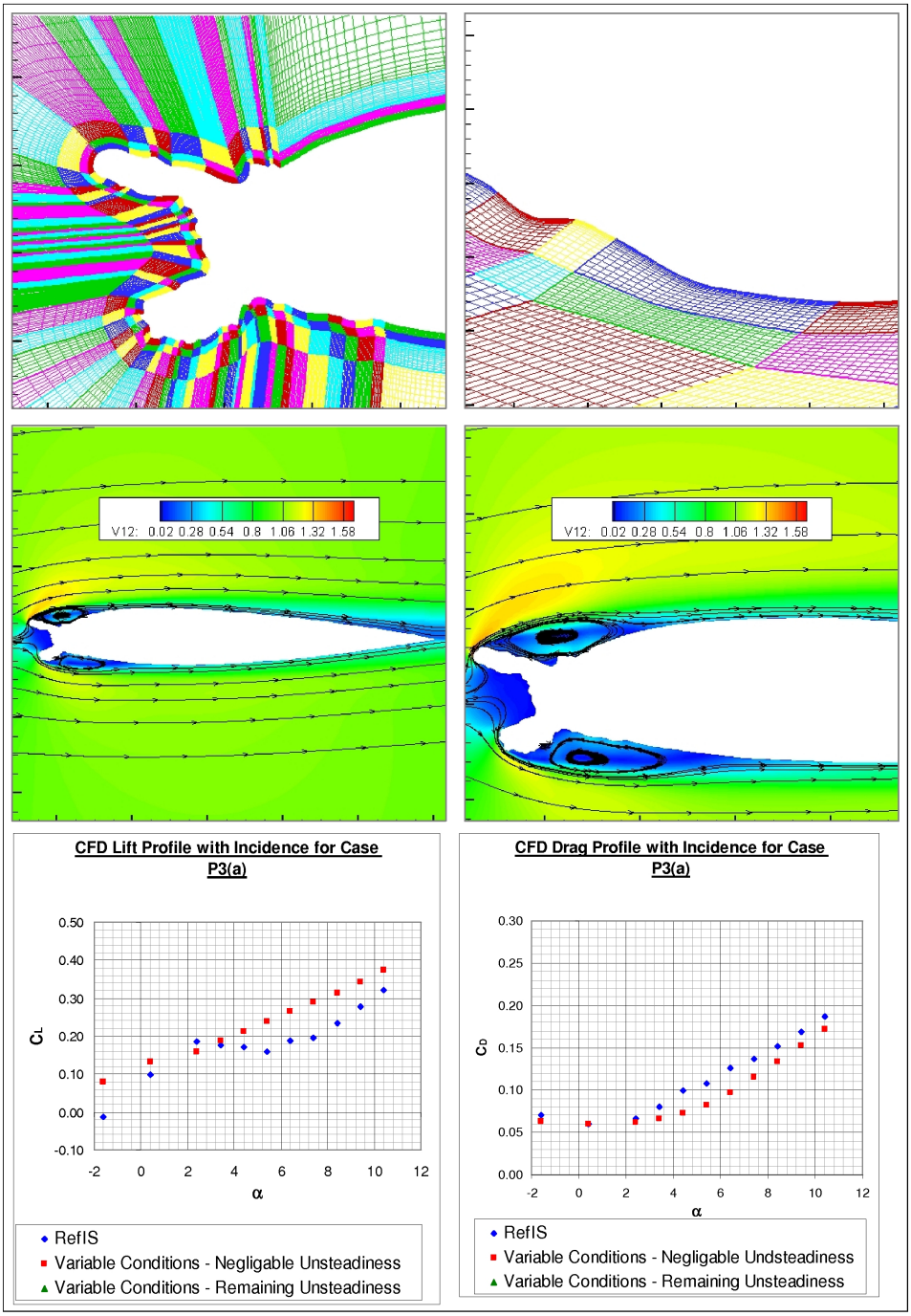

Figure E.44: Encounter LWC(A)/Sin(θ - 90°) - CFD simulation information.

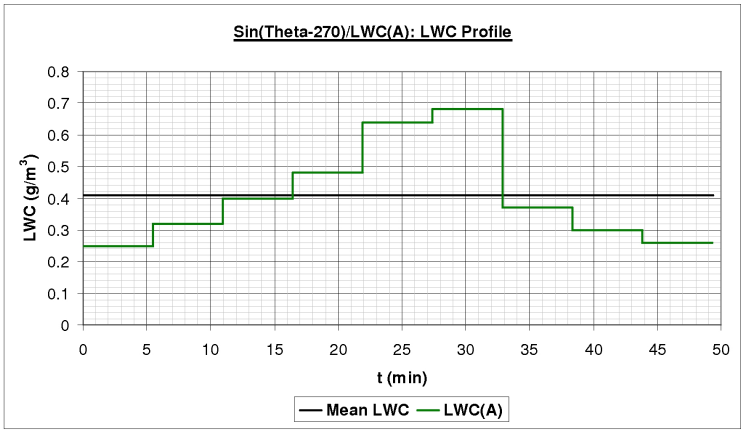

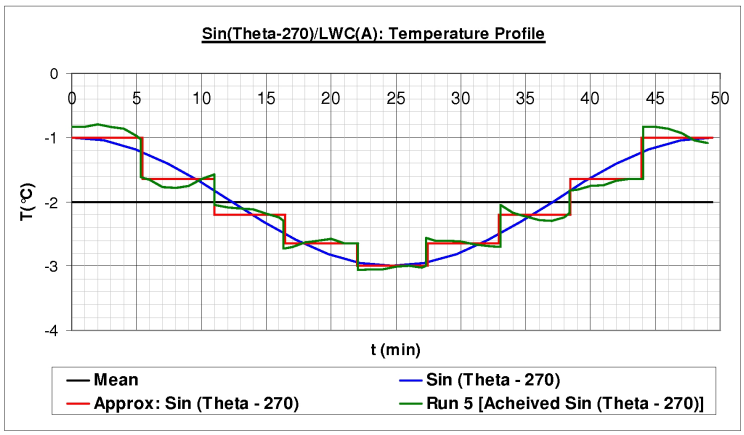

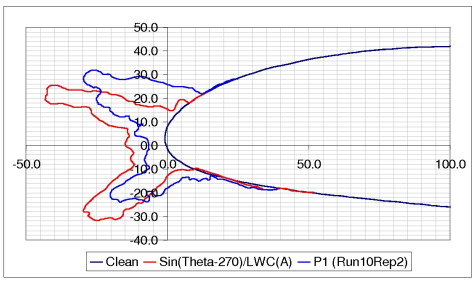

Run No.	Desc^{n} Code	h_{upper}	Θ_{upper}	Φ_{upper}	L_{upper}	h_{lower}	Θ_{lower}	Φ_{lower}	L_{lower}	t_{c-l}
P3-b	Sin(Theta-270)/LWC(A)	45.00	30.00	20.00	7.50	39.50	-40.25	-37.75	10.00	15.00
---	*RefIS*	*36.83*	*46.17*	*31.08*	*23.50*	*28.67*	*-53.00*	*-43.33*	*48.67*	*8.50*
---	*StDev*	*0.29*	*3.09*	3.59	*1.80*	*1.26*	*5.07*	2.25	*9.88*	*1.32*

Figure E.45: Encounter LWC(A)/Sin(θ - 270°) - Ice accretion simulation information.

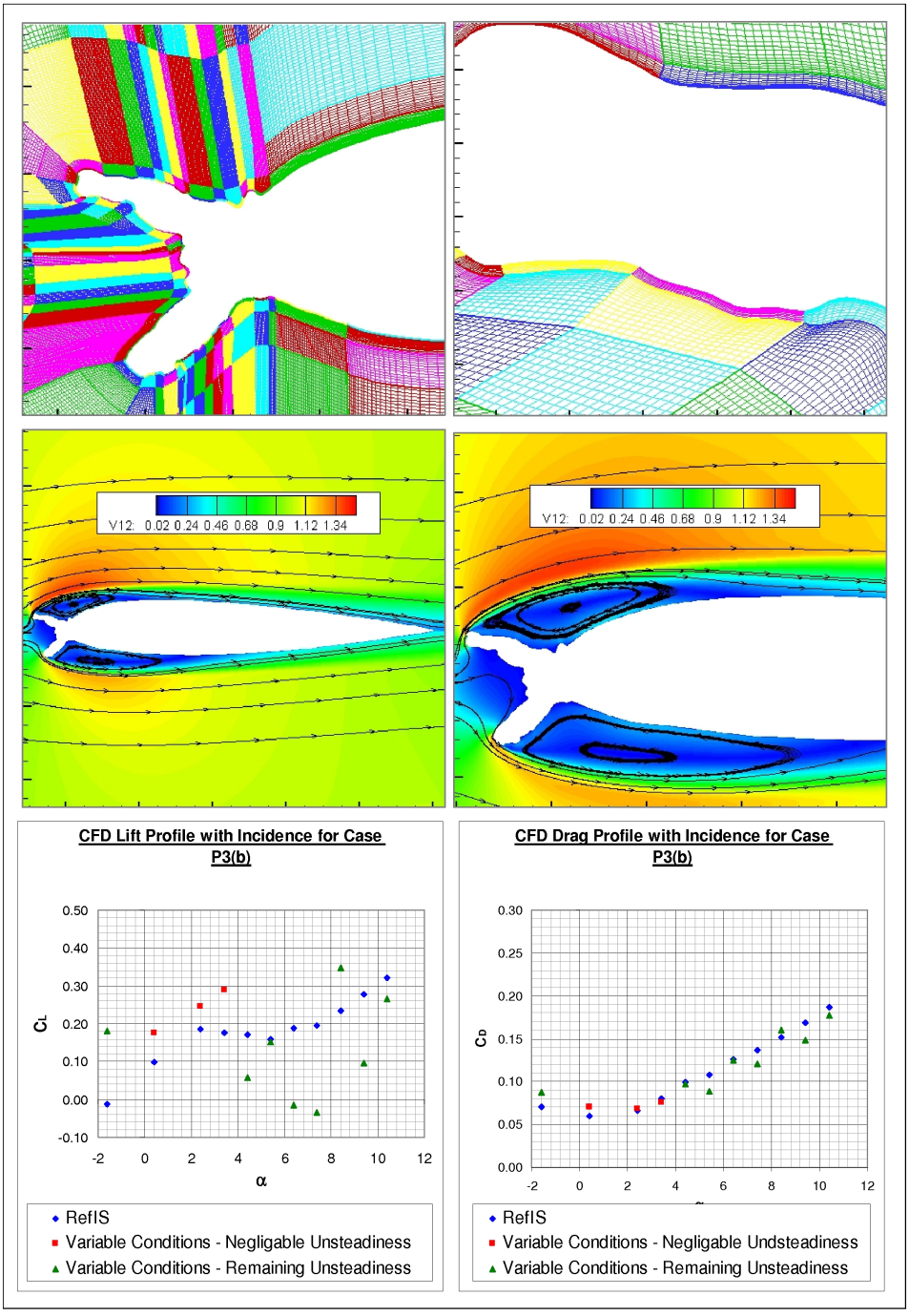

Figure E.46: Encounter LWC(A)/Sin(θ - 270°) - CFD simulation information.

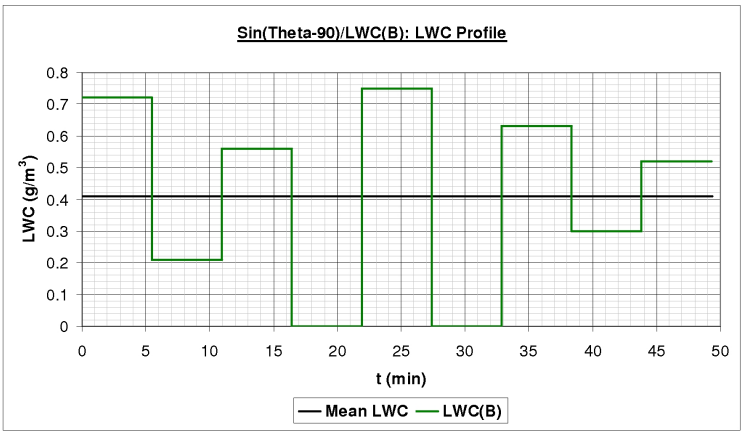

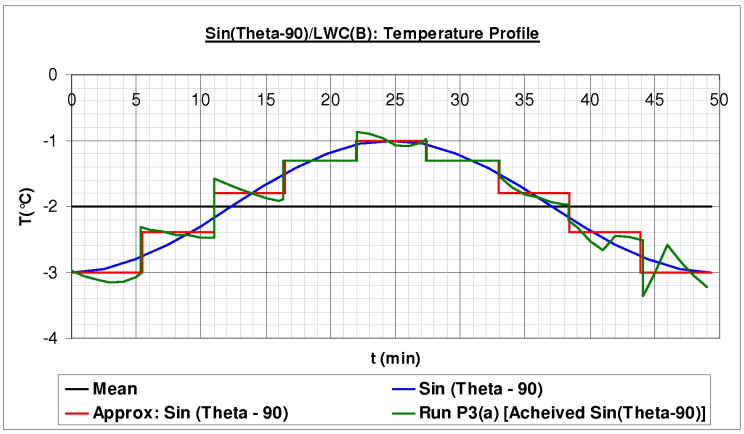

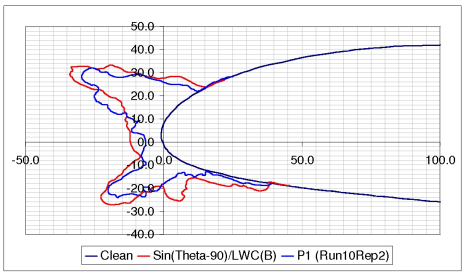

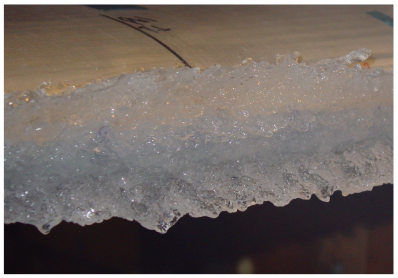

Run No.	Desc^{n} Code	h_{upper}	Θ_{upper}	Φ_{upper}	L_{upper}	h_{lower}	Θ_{lower}	Φ_{lower}	L_{lower}	t_{c-l}
P3-c	Sin(Theta-90)/LWC(B)	41.00	44.25	31.75	15.50	31.50	-47.00	-43.25	38.00	12.00
---	*RefIS*	*36.00*	*46.58*	*30.58*	*24.17*	*28.17*	*-53.00*	*-43.17*	*53.67*	*7.33*
---	*StDev*	*1.32*	*2.40*	4.45	*2.93*	*0.58*	*5.07*	2.02	*14.15*	*2.02*

Figure E.47: Encounter LWC(B)/Sin(θ - 90°) - Ice accretion simulation information.

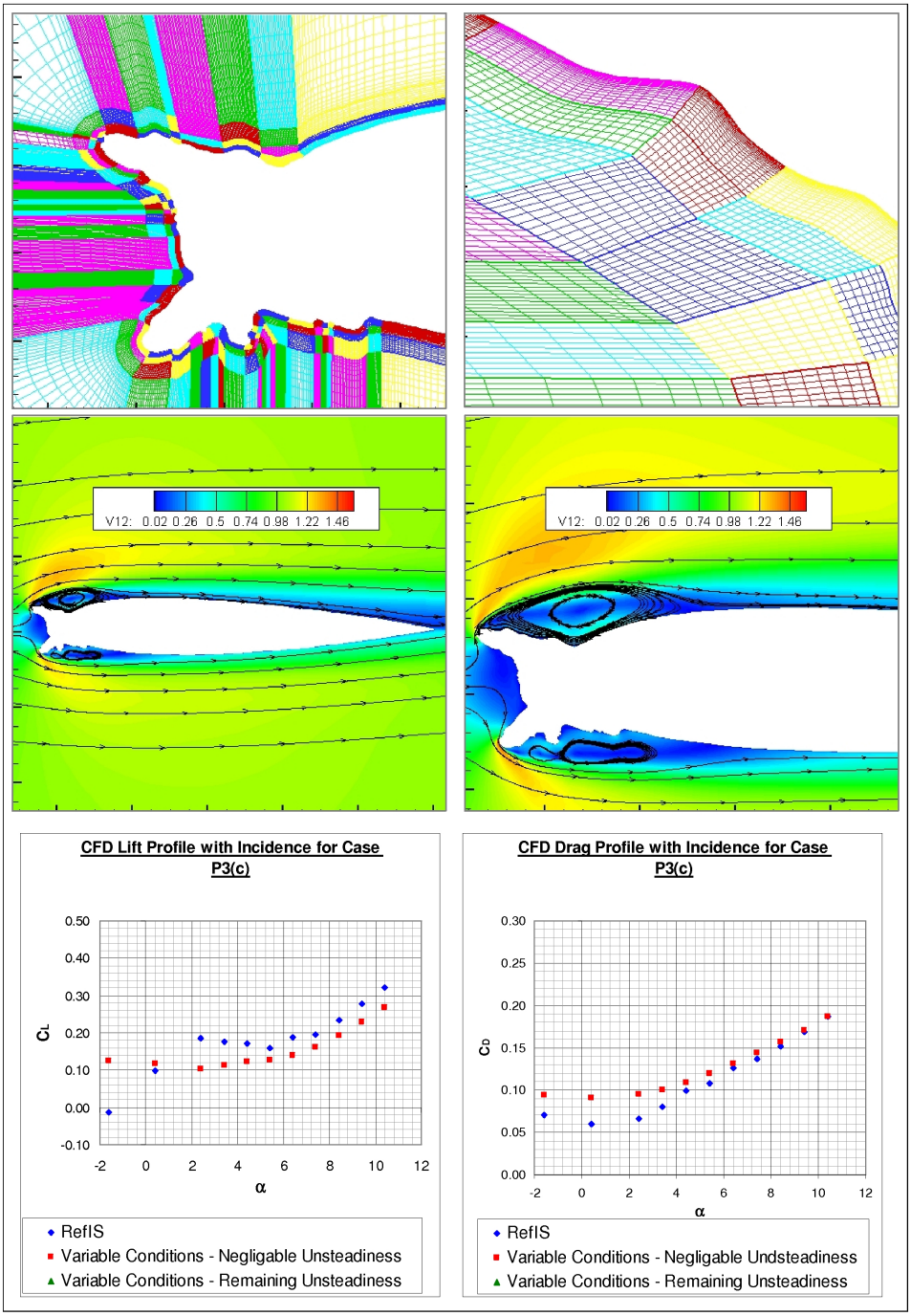

Figure E.48: Encounter LWC(B)/Sin(θ - 90°) - CFD simulation information.

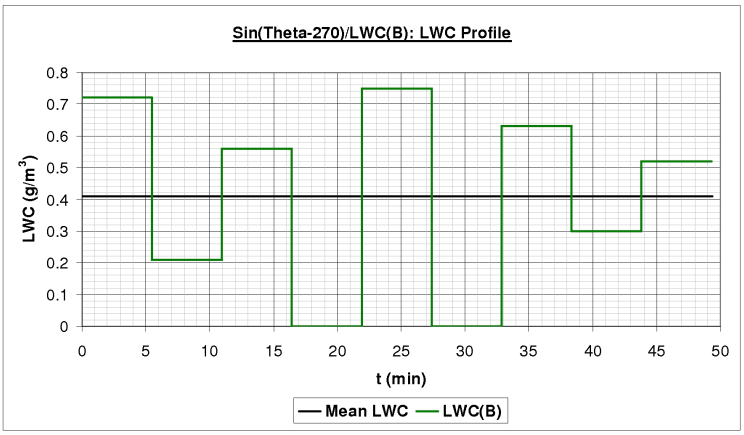

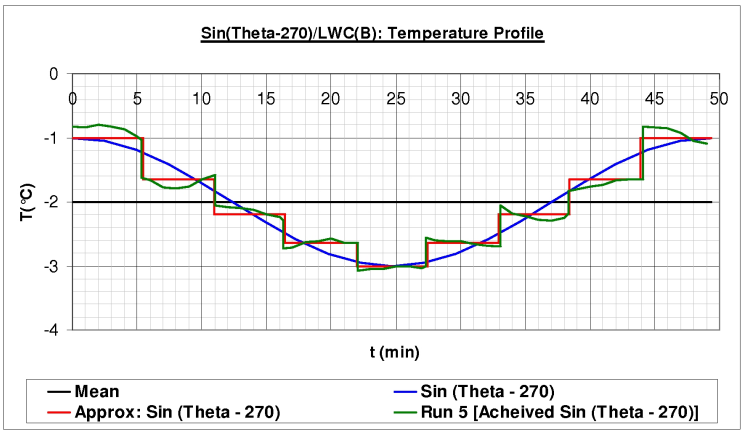

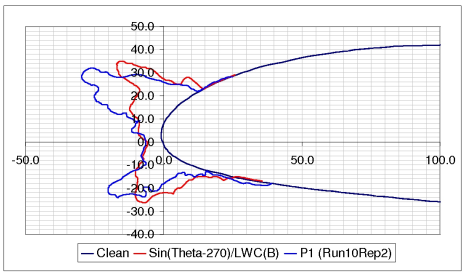

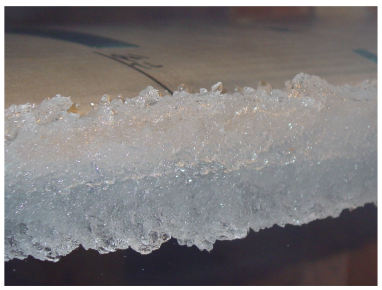

Run No.	Desc^{n} Code	h_{upper}	Θ_{upper}	Φ_{upper}	L_{upper}	h_{lower}	Θ_{lower}	Φ_{lower}	L_{lower}	t_{c-l}
P3-d	Sin(Theta-270)/LWC(B)	28.00	65.25	44.25	14.00	22.50	-65.75	-53.75	25.50	6.00
---	*RefIS*	*36.00*	*46.58*	*30.58*	*24.17*	*28.17*	*-53.00*	*-43.17*	*53.67*	*7.33*
---	*StDev*	*1.32*	*2.40*	4.45	*2.93*	*0.58*	*5.07*	2.02	*14.15*	*2.02*

Figure E.49: Encounter LWC(B)/Sin(θ - 270°) - Ice accretion simulation information.

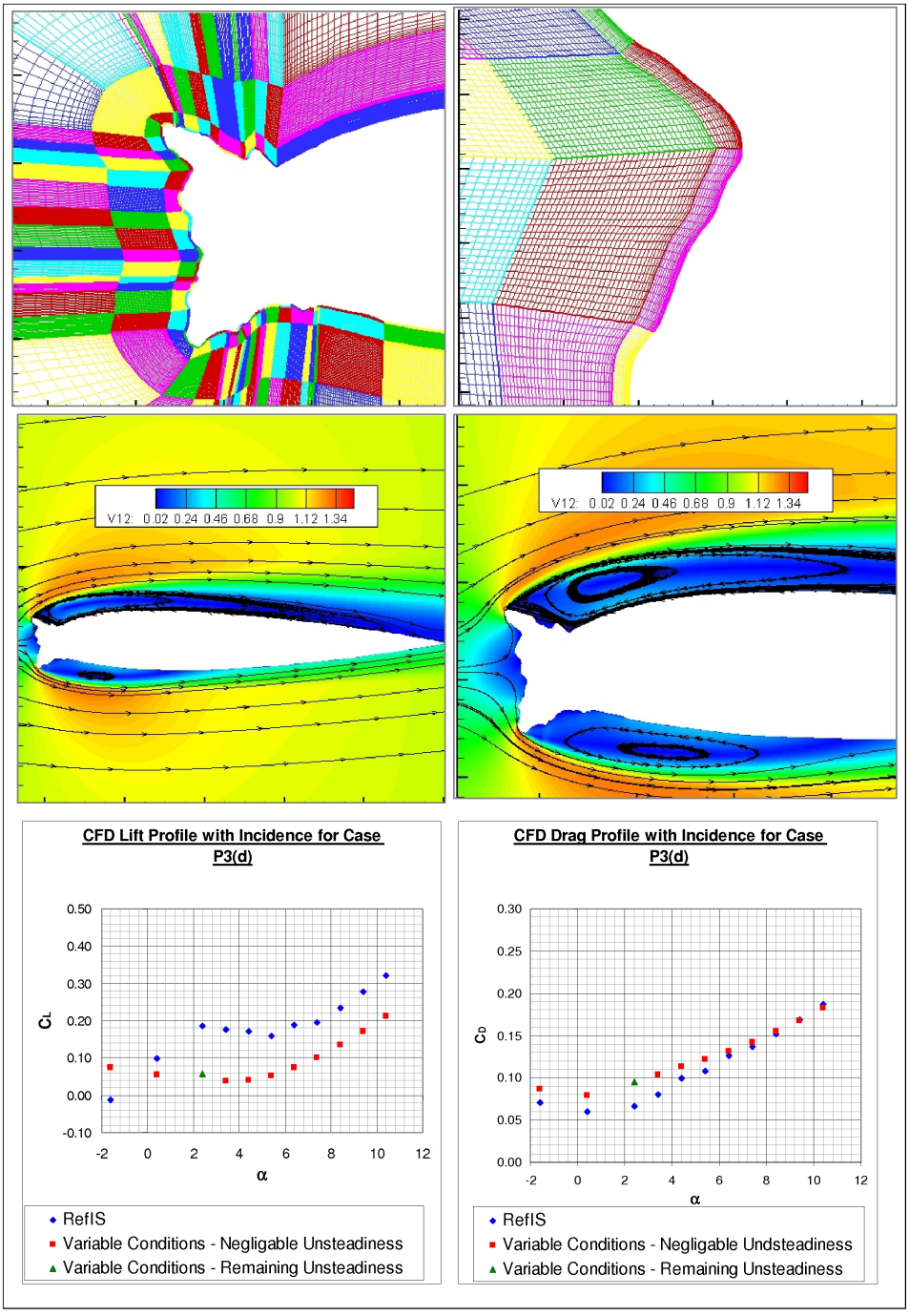

Figure E.50: Encounter LWC(B)/Sin(θ - 270°) - CFD simulation information.

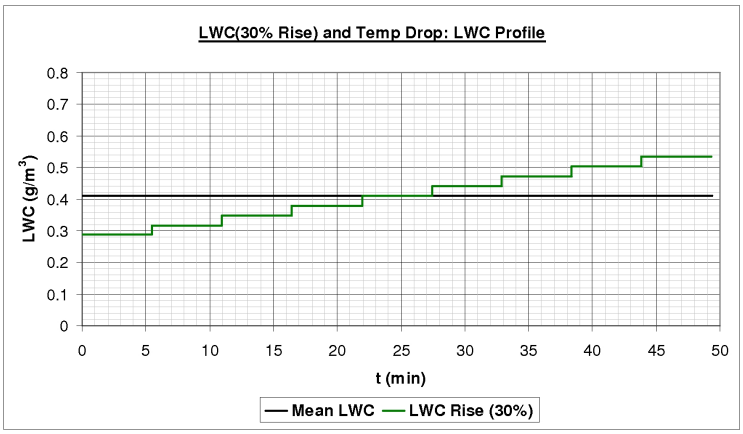

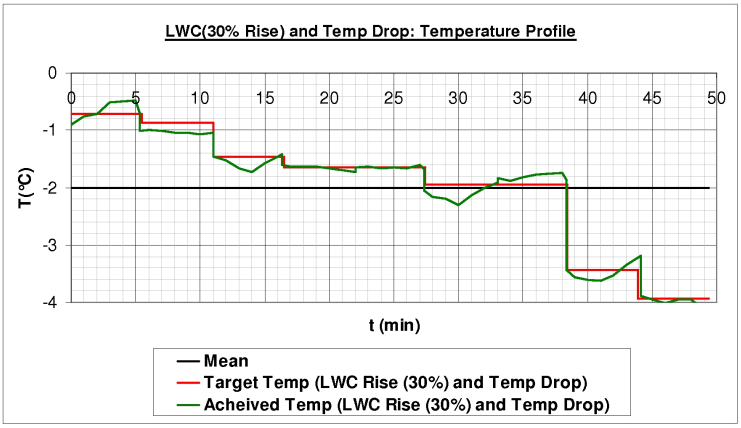

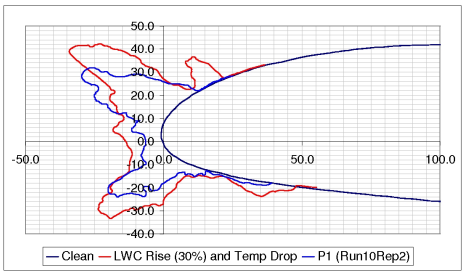

Run No.	Desc^{n} Code	h_{upper}	Θ_{upper}	Φ_{upper}	L_{upper}	h_{lower}	Θ_{lower}	Φ_{lower}	L_{lower}	t_{c-l}
P3-e	LWC(30% Rise) and Temp Drop	46.00	50.00	35.00	21.50	35.50	-60.25	-50.00	47.50	14.00
---	*RefIS*	*36.00*	*46.58*	*30.58*	*24.17*	*28.17*	*-53.00*	*-43.17*	*53.67*	*7.33*
---	*StDev*	*1.32*	*2.40*	4.45	*2.93*	*0.58*	*5.07*	2.02	*14.15*	*2.02*

Figure E.51: Encounter LWC (30%) Rise and Temp Drop - Ice accretion simulation information.

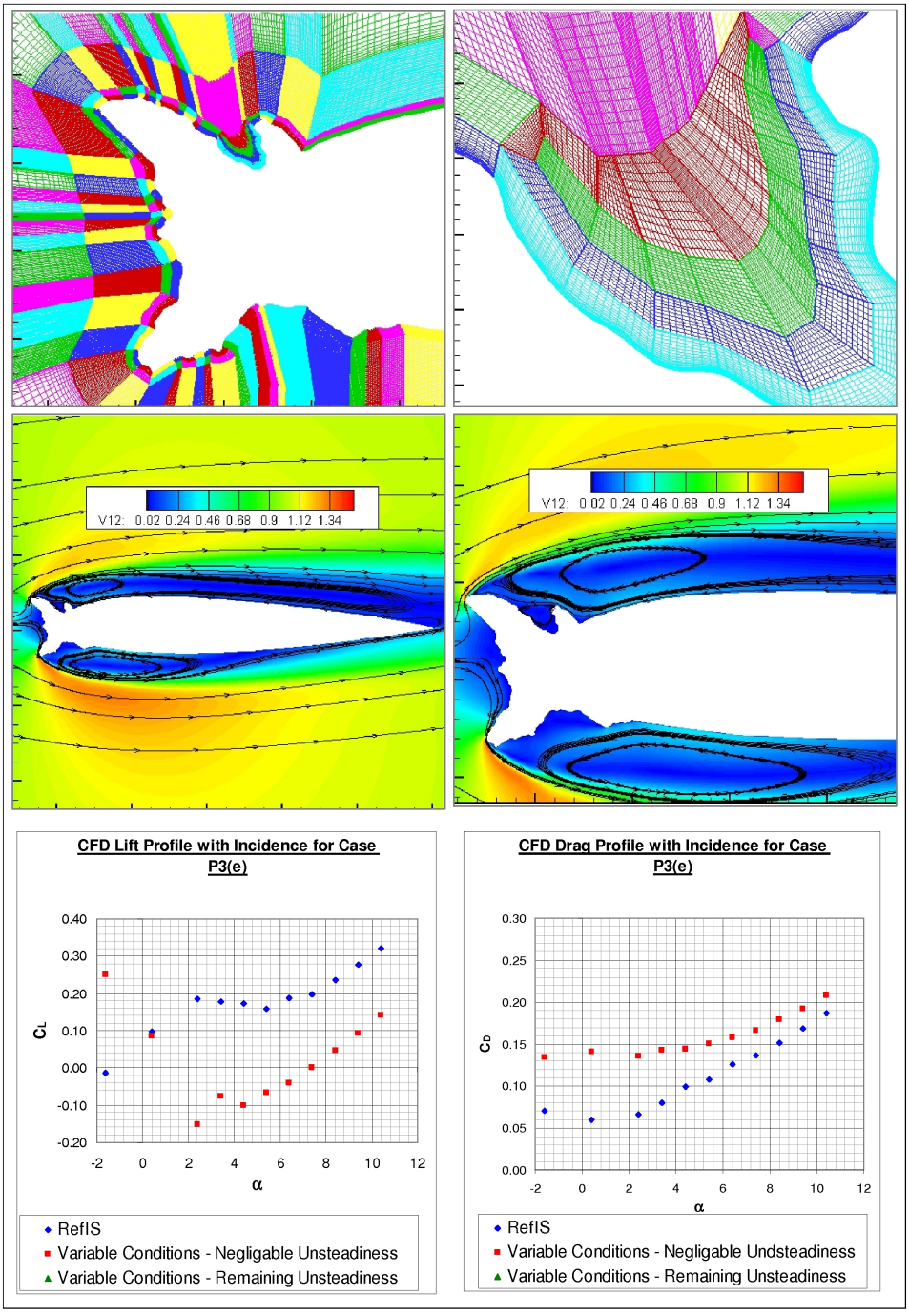

Figure E.52: Encounter LWC (30%) Rise and Temp Drop - CFD simulation information.